ELASTIC-PLASTIC ANALYSIS OF

COMPLETE STRUCTURES WITH SHEAR

WALLS AND FRAMES

BY

TUNCER CELIK

A THESIS SUBMITTED FOR THE DEGREE

OF DOCTOR OF PHILOSOPHY

DEPARTMENT OF CIVIL ENGINEERING

THE UNIVERSITY OF ASTON IN BIRMINGHAM

JULY 1977

ELASTIC-PLASTIC ANALYSIS OF COMPLETE

STRUCTURES WITH SHEAR WALLS AND FRAMES

BY

TUNCER CELIK

A THESIS SUBMITTED FOR THE DEGREE OF

DOCTOR OF PHILOSOPHY

Department of Civil Engineering

The University of Aston in Birmingham

1977

SYNOPSIS

This thesis aims at producing general computer methods for the failure
load analysis of structures. It is divided into two parts. In the first
part, three methods are proposed for the failure load analysis of plane
frames using the theorems of structural variation. The first method
is for the piecewise linear elastic-plastic analysis of frames in
which the plastic hinges are represented by infinitely small members with
zero flexural rigidity. A single elastic analysis is utilised to trace
the full load-deflection behaviour of a frame and its derivatives.

The second method deals with frames with nonlinear moment-curvature
relationship. Again a single elastic analysis is utilised to trace the
load-deflection behaviour up to and including failure. This method is
also applicable to the strain hardening analysis of steel frames. The
third method, which is iterative, is developed for the non-linear analysis
of reinforced concrete frames under proportional or non-proportional
loads.

The second part deals with the failure load analysis of complete structures
with parallel frames and a grillage of shear walls and slabs. This
ignores translations normal to the wind direction and rotation about
an axis parallel to it. The lateral buckling of homogeneous rectangular
panels, the interaction of torsion and shear in deep reinforced concrete
panels, and the corresponding failure criteria are investigated. The
frames and the grillage are separated and the loads transmitted to are
calculated. To verify the theoretical work, 16 structural models were
tested. In these steel or reinforced concrete frames and reinforced
concrete shear walls were either included or excluded. The results of the
analysis of a series of four storey and six storey practical structures
are reported and conclusions are drawn.

Key words (Failure load, Complete Structures, frames, Nonlinear moment-
          curvature, Concrete).

THE AUTHOR

The author graduated from the Civil Engineering Department of the Faculty of Civil Engineering and Architecture, Karadeniz Technical University, Trabzon-Turkey, in 1970. For the following two years he was employed as an Assistant Lecturer in the same department. He was then awarded a state scholarship to study for the degree of Ph.D. The work presented in this thesis has been carried out since 1973 in a full time course under the supervision of Professor K.I. Majid.

No part of this thesis has been submitted in support of an application for another degree or qualification.

<div align="center">CONTENTS</div> <div align="right">Page</div>

NOTATION

A	area of a member
$\underline{A}$	displacement transformation matrix
A,B,C	parameters in Chapter 5
A_f	flange area of a universal section
A_s	area of steel in a layer
A_w	web area of a universal section (in Chapter 3)
A_w	area of a stirrup (Chapter 5)
a	spacing of horizontal layers in a reinforced concrete cross section (Chapter 5)
a_1, a_2	distances from a reference axis (Chapter 5)
$\underline{a}, \underline{a}_n$	horizontal deflection matrices of a grillage due to shear wall loading (Chapter 4)
$\alpha, \beta, \eta, \zeta, \gamma$	parameters in Chapter 5
δA	variation in area
α	variation ratio (Chapters 2 and 3)
$\alpha_L, \alpha_b, \alpha_r, \alpha_{mt}, \alpha_{sy}$	inclinations
b	breadth of a section
β_1, β_2	concrete stress block parameters (Chapter 3)
C	compressive force
$\underline{C}$	unit load matrix
d, d_1, d', d'', d''' etc.	depths
E	modulus of elasticity
E_c	modulus of elasticity for concrete
E_s	modulus of elasticity for steel
δE	variation in the modulus of elasticity
$(EI)_i$	initial flexural rigidity
$(EI)_c$	flexural rigidity of a cracked section
$(EI)_u$	flexural rigidity after yielding takes place in the reinforcement

EI_{xx}, EI_{yy}	major and minor axis flexural rigidities
ε	strain
ε_s	strain in steel
ε_k	strain at the kth layer
ε_u	ultimate strain of steel
ε_y	yield strain of steel
ε_{cu}	ultimate strain of concrete
$\underline{F}, \underline{F}_n$	influence coefficient matrices of frames
F_1, F_2, F_3 etc	forces carried by layers of longitudinal reinforcement
F_y	yield force carried by a layer of reinforcement
F_u	ultimate force carried by a layer of reinforcement
$F, F^1, \delta, \phi, \zeta, \eta, \eta^1, \alpha$	parameters in Chapter 4
$\underline{f}$	vector of horizontal forces transmitted of frames
f_c	compressive stress in concrete
f_{cu}	crushing strength of concrete
f_{ct}	tensile strength of concrete
f_{ii}, f_{ji}	axial forces in members i and j due to unit loads acting axially to member i
f_u	ultimate stress in steel
ϕ	curvature
ϕ_c, ϕ_y, ϕ_u	curvatures at cracking, yielding and the ultimate stage
ψ_k	new displacement of joint k in a pin jointed structure
ψ_{vq}	new displacement of joint q in v direction
G	shear modulus of elasticity
$\underline{G}, \underline{G}_n$	influence coefficient matrices of grillage
$\underline{GJ}$	torsional stiffness
$\underline{g}$	vector of horizontal forces transmitted to the grillage

h	equivalent cantilever of a plastic hinge
I	second moment of area of a member
I'	new second moment of area of a member
δI	variation in the second moment of area
I_G	gross second moment of area of a reinforced concrete section
$\underline{K}$	overall stiffness matrix
$\underline{K}_{HH}, \underline{K}_{DH}, \underline{K}_{HD}, \underline{K}_{DD}$	submatrices of the overall stiffness matrix (Chapter 1)
$\underline{K}'$	modified stiffness matrix (Chapter 1)
$\underline{k}$	member stiffness matrix
"k"	strain hardening factor
$\bar{k}, \bar{m}$	parameters in Chapter 3
L	length of a member
$\underline{L}$	applied load matrix
$[\underline{L}\ \underline{C}]$	compound load matrix
$\underline{L}_H$	vector of the known external loads (Chapter 1)
L_L, L_r	lever arms of the left hand and the right hand side vertical stirrup legs
ℓ_{ijk}	load applied at junction ij, at stage k
$\lambda, \lambda_1 . \lambda_1^k, \lambda_{FL}, \lambda_{GB}, \lambda_{GC}$ etc.	load factors
$\Delta\lambda$	increment in the load factor
M	bending moment
$\underline{M}$	bending moment matrix
$\underline{MA}$	actual bending moment matrix
$\underline{M}_D$	vector of unknown bending moments on inactive hinges (Chapter 1)
M_E	equivalent moment
M_b	in-plane bending moment
M_c, M_y, M_u	cracking moment, yielding moment and ultimate moment (Chapter 3)

$\bar{M}_{bi}, \bar{M}_{ti}$ bending moment and torque calculated for a unit increment in the load factor

M_t torsional moment

M_{ij}, M_{ji} first and second end moments of member ij

M_p^k fully plastic moment of member k

M_{yzcr}, M_{Eyz} critical in plane bending moment for the lateral buckling

M_{ult} ultimate bending moment carrying capacity

M_{tult}, M_{tult}^s ultimate torque carrying capacities

M_k, μ_k bending moments on member k, in single curvature due to external loads and unit loading at its ends

M_{vq}, μ_{vq} first or second end moments on member q due to external loads and unit loading

M'_{vq} new first or second end moment on member q due to external loads

$\bar{m}$ total number of reinforcement layers in a reinforced concrete cross section

m_p, ℓ_p direction cosines

DM   matrix of discontinuity moments on a moment-curvature diagram

dM   increment in the fully plastic moment of a section due to strain hardening

$\underline{P}$ vector of member forces (Chapters 2,3)

$\underline{P}'$ vector of new member forces (Chapters 2,3)

$\underline{\bar{P}}$ axial force matrix

$\underline{PA}$ actual force matrix

P_q, p_q shear forces on member q due to external loads and unit loading

P'_q new axial force on member q due to external loads

$\underline{P}$ vector of horizontal loads acting on frame-slab junctions of a complete structure

P_{ij} axial force in member ij

P_i, P_j axial forces in members i and j

π_i, π_j	new axial forces in members i and j
$r_{\alpha k}$	variation factor for member k
r_α	variation factor matrix
ρ	radius of curvature
S_{ij}	shear force in member ij
S_q, s_q	shear forces in member q due to external loadings and unit loading
SPR	spread of plasticity rate
S_y	in plane shear force
S_{yult}, S^s_{yult}	ultimate shear force carrying capacities
$\bar{S}_{yi}$	shear force calculated for a unit increment of load factor
S'_q	new shear force of member q due to external loads
s	spacing of stirrups
σ	direct stress
$\sigma_{max}, \sigma_{min}$	principal stresses
σ_y, σ_y'	yield stress, effective yield stress
σ_{wy}	yield stress of stirrups
T	tensile force
T_E	total tensile force carried by elastic layers of reinforcement
T_u	total tensile force carried by yielded layers of reinforcement
t	thickness of a section
t'	distance between side reinforcement
$\bar{t}$	width of compression zone in a skew failure mechanism
τ, τ_{max}	shear stress, maximum shear stress
τ_t	shear stress due to torque
τ_s	shear stress due to shear force

τ_R	resultant shear stress
σ_i, σ_j	first and second end rotations of a member
σ_H	rotation of a plastic hinge H
$\underline{\sigma}_D$	known rotation of inactive hinges
V_L, V_r	vertical forces carried by left hand side and right hand side exposed stirrup legs (Chapter 5)
v	relative sway of a member
$\underline{v}$	vector of vertical loads
$\underline{w}$	vector of horizontal forces acting on shear walls
$\underline{X}$	joint displacement matrix
$\underline{XA}$	actual displacement matrix
$\underline{X}_H$	unknown joint displacement (Chapter 1)
x	depth of neutral axis
x_{vq}, x_{vq}	displacements of joint q in v direction due to external loads and unit loading
Z_e	gross elastic modulus of a reinforced concrete section
$\underline{z}$	displacement matrix of a member in local co-ordinates
z_b, z_b'	elastic modules of a section
z_t	elastic torsion medulus of a section

CHAPTER 1

INTRODUCTION AND A REVIEW OF PUBLISHED WORK

1.a. General Introduction:

In recent years, rapid development in digital computers made it possible to study the actual behaviour of frames up to and including failure in a rational manner. Up to date methods are available to deal not only with the elastic behaviour of frames but also with nonlinearities due to axial forces or material properties.

The developments to cope with reinforced concrete structures has been relatively slow because of the complex nature of the material. This is in spite of the fact that reinforced concrete is being widely used in construction. There is, therefore, a need to develop a method for the analysis of reinforced concrete structures which is equally advanced as those for steel structures.

It is possible in certain cases to analyse complete structures by simplifying them into sub-components such as beams and columns and use existing methods to analyse these components. Such a simplification can lead to erroneous results particularly if these are considered as isolated entities. Hence the need for dealing with the entire complete structure as an integral unit. To do this it may be possible to use the finite element method in conjunction with the matrix displacement method. This however leads to the solution of a large number of equations which is uneconomical. The computing cost becomes especially high when a failure load analysis, dealing with nonlinearities is required. Therefore some rational and fairly inexpensive methods are in demand.

This thesis deals with two distinct types of problem. The first is the non-linear analysis of plane frames which may be

either reinforced concrete or steel. In the case of reinforced concrete frames non-linearity due to moment-curvature is taken into consideration. In steel frames, the elastic-plastic analysis with strain hardening is considered. In both cases, the non-linear effects of axial forces may or may not be included.

The second problem is the failure analysis of complete structures consisting of frames, shear walls and slabs. Details of experimental work on the latter problem are given and comparison is made with analytical results.

1.b. Analysis of Frames:

1.b.1 Steel Frames:

Livesley[25,26] was one of the first to apply the computer to the problems of structural analysis using matrix displacement method. This method gives the relationship between the externally applied loads and the resulting joint displacements in the form:

$$\underline{L} = \underline{K}\,\underline{X} \qquad\qquad 1.1$$

Here $\underline{L}$, $\underline{K}$ and $\underline{X}$ are the applied load matrix, the overall stiffness matrix and the resulting joint displacements respectively. The matrices $\underline{L}$ and $\underline{K}$ are known for a given frame, while the joint displacements $\underline{X}$ are to be determined. Livesley introduced the effects of axial loads when using equations (1.1) by using the stability ϕ functions, to modify the member stiffnesses. These functions depend upon the axial load and the Euler load of a member and have the value of unity when the axial load in a member is zero. As the axial forces are initially unknown, Livesley used an iterative technique for the non-linear elastic analysis of frames subject to a given set of external loads. In this technique, equations (1.1) were repeatedly solved until the axial

loads were reliable.

The failure load analysis of frames was a subject of considerable research by Wood[69] who described the actual failure load of a steel frame as a function of its deteriorated critical load after various plastic hinges had developed in a frame. By considering instability, Wood found that failure took place when the stiffness of a frame is completely lost. This could happen even before the development of a mechanism. The plastic theory was thus proved to be marginally unsafe even for the analysis of frames.

Realising this fact, Horne[11] took the advantage of strain hardening to compensate for instability. In doing so, Horne pointed out that the increase of bending moment at a plastic hinge, above the full plastic moment, Mp, can be expressed as

$$d\,M = \frac{EI}{Kh}\,\theta_H \qquad\qquad 1.2$$

where, EI is the initial flexural rigidity of the member, θ_H is the hinge rotation, h is the equivalent cantilever of the hinge and "k" is an experimental factor. This increment in the bending moment causes plasticity to spread in the vicinity of a plastic hinge. Horne included this increment and an approximate second order effect of axial loads into the virtual work equations, in order to find the value of "k" which is necessary to compensate the losses in the load carrying capacity. However further research[27,12] showed that this idea could only be useful for small structures where axial forces are insignificant.

Considering this fact, the focus of interest was concentrated on the elastic-plastic theory. The elastic-plastic failure load was studied by Majid[28], Jennings and others. Jennings and Majid[29]

produced a general elastic-plastic analysis program. They
modified the stiffness equations given by Livesley, to include
the presence of real and plastic hinges. They also introduced
the effect of axial loads in reducing the plastic hinge moments
of members. As a result of this study, they obtained the load-
deflection curves of frames up to and including failure, under
proportional loads.

Using the computer program developed by Jennings and Majid,
Davies[15,30] studied the effect of plastic hinges becoming
inactive and then active again at different stages of loading.
Equations (1.1) was partitioned by Davies to become

$$
\begin{bmatrix} L_H \\ \\ M_D \end{bmatrix} = \begin{bmatrix} K_{HH} & K_{HD} \\ \\ K_{DH} & K_{DD} \end{bmatrix} \begin{bmatrix} X_H \\ \\ \theta_D \end{bmatrix} \qquad 1.3
$$

where L_H is the vector of known external loads, K_{HH}, K_{DH}, K_{HD},
K_{DD} are the sub matrices obtained from the overall stiffness
matrix K. θ_D is the known rotations of the hinges that had
become inactive and M_D is the vector of unknown bending moments
at the inactive hinges. The unknown joint displacements X_H were
then obtained from

$$
X_H = K_{HH}^{-1} [L_H - K_{HD} \theta_D] \qquad 1.4
$$

Having obtained the unknown vector X_H, the unknown bending moments
M_D were obtained as

$$
M_D = K_{DH} X_H + K_{DD} X_D \qquad 1.5
$$

The evaluation of other member forces P_H was carried out in the
usual way described by Jennings and Majid. Davies also used
equation (1.2) to deal with the strain hardening effect. The
incremental moment of equation (1.2) was added to the fully plastic
moment value appearing in the load matrix L and rearranged equations

appears both in the load and the displacement vectors) into the displacement vector $\underline{X}$. Therefore the diagonal element of each row of matrix $\underline{K}$, corresponding to a hinge H took the form

$$K'_{HH} = K_{HH} + (\frac{EI}{"k"h})_H \qquad 1.6$$

The modified stiffness matrix was expressed as $\underline{K}'$. The displacements were then expressed as:

$$\underline{X} = [\underline{K}']^{-1} \underline{L} \qquad 1.7$$

The displacement and the load vectors then remained unchanged. Davies employed a linear extrapolation or inter_polation process to predict the load factor λ, at which the next plastic hinge would form. Since the effect of axial loads were taken into account and the equivalent cantilevers for the plastic hinges were changing, Davies repeated the solution of equations (1.7) until two successive predictions of λ were within a specified tolerance.

The size of the program used by Jennings and Majid was considerably large, because they employed full matrix operations in order to solve the stiffness equations for the unknown displacements. Therefore their program was limited to medium size structures. To overcome this limitation, Majid and Anderson[20] modified the elastic-plastic analysis program[29]. The rows and the columns of matrix $\underline{K}$ corresponding to real or plastic hinges were placed immediately after the rows and columns corresponding to the related joints. The stiffness matrix was constructed as a unidimensional array in a compact form and the solution of the stiffness equations was carried out using the technique suggested by Jennings[72]. The diagonal elements of $\underline{K}$ were addressed in an "address sequence" array. Only the elements of each row between the first non zero element and that on the leading diagonal were

stored. Therefore only the elements on or to one side of the leading diagonal were stored.

Anderson[21] later grouped the hinges in a member around the lowest numbered joint to which the member is connected. Hence the half band widths corresponding to the hinge contributions to the stiffness matrix were kept as narrow as possible.

The variation of bending moment with increasing load factor λ was assumed to be linear[28,29]. In the iteration towards a reduced plastic moment Mp was kept constant during one cycle of iteration. The load factor at which the bending moment at a section reached Mp was predicted by extrapolation. It was pointed out that when Mp $\cong$ m_2 numerical inaccuracies would take place. To rectify this, it was suggested that the load factor for the next hinge should be predicted by the linear extrapolation:

$$\lambda = \frac{\lambda_2 - \lambda_1}{m_2 - m_1} M_p + \frac{\lambda_1 m_2 - \lambda_2 m_1}{m_2 - m_1} \qquad 1.8$$

where; λ_1, m_1 and λ_2, m_2 are the load factors and bending moments at previous and current iterations respectively. In this thesis, this formula is also employed in the failure load analysis of reinforced concrete frames. However the value of Mp is replaced by the value of the "critical moments" M_{cr} on the moment-curvature diagram of the section. These are points of discontinuity on the diagram.

The program of Majid and Anderson was later modified by Majid and Önen[31,32] to include the effect of composite action between reinforced concrete floor slabs and steel beams. The composite action moment in a section in which the concrete was in compression was calculated in a manner suggested by Holmes and Majed[33].

1.c. The Theorems of Structural Variation:

In 1973, Majid and Elliott[1] gave the basic relationships between the old and the new member forces and deflections of a pinjointed structure, when the area of one or more of its members were varied or removed. These relationships were proposed as "The theorems of structural variation".

1 - The first theorem of structural variation predicted the new member forces in the structure when the area of a member i was altered from A_i by an amount of δA_i. This gave the force π_i in a changing member i as:

$$\pi_i = P_i \, (1+\alpha)/(1+\alpha f_{ii}) \qquad\qquad 1.9$$

where $\alpha = -\delta A_i/A_i$ and P_i is the force in i before altering it and f_{ii} is the force in i due to unit external force acting on i. The force in any other member j was given as:

$$\pi_j = P_j + r_{\alpha i} \, f_{ji} \qquad\qquad 1.10$$

where f_{ji} is the force in j due to the above unit force and $r_{\alpha i} = \dfrac{\alpha P_i}{1+\alpha f_{ii}}$ was defined as the variation factor of member i.

2 - The second theorem predicted the new deflection ψ_k at a joint k as:

$$\psi_k = X_k + r_{\alpha i} \, X_{ki} \qquad\qquad 1.11$$

where X_k is the old deflection and X_{ki} is the deflection at k due to the unit force in i.

3 - The third theorem dealt with structures in which member areas all changed proportionally and predicted the new deflections $\underline{X}^*$ as:

$$\underline{X}^* = \frac{1}{1+\alpha} \, \underline{X} \qquad\qquad 1.12$$

These theorems were later extended by Saka[3], who proved that they are also valid for rigidly jointed frames. Saka found it

necessary to apply the theorems to each end of a member which is being changed or removed. More details of these theorems and the work of Saka will be given in chapter 2, since these are employed by the author here in this thesis to carry out the elastic-plastic and the nonlinear moment-curvature analyses of plane frames.

1.d Analysis of Reinforced Concrete Frames:

The need for a rational analysis to explore the behaviour of reinforced concrete frames was realised by early investigators such as Glanville and Thomas[34]. Tests carried out by these indicated that continuous beams and portal frames experienced a redistribution of bending moment as failure was approached. It was therefore suggested that these structures had some ductility. This point was taken up by Baker[35,36] who investigated this redistribution of bending moments and developed the ultimate load theory for the design of reinforced concrete frames. Baker assumed a simple elastic-plastic moment-curvature relationship which was defined by the initial flexural rigidity $(EI)i$ of the section, its ultimate moment of resistance and its limited capacity for plastic rotation. The ultimate load was defined as the load at which a sufficient number of plastic hinges form to render the frame "statically determinate". The slope-deflection equations were used to predict the hinge locations and the rotation of each hinge was calculated from the virtual work equations by a trial and error procedure. An appropriate relaxation technique was used to check the deflections and crack widths. Although this method defined the ultimate load of a given structure, it was laborious and no provision was made for the frame instability.

Baker later dealt with the ultimate load design of concrete

frames[37]. By considering each loading case in turn, a sufficient number of hinges were inserted into the frame to make it statically determinate. These hinges were assumed to be subject to the moment of resistance of the sections. The positions of the hinges and the values of the hinge rotations were detected in the same manner as in reference (36). These were then adjusted until, for a specified load factor at failure, a satisfactory solution together with a corresponding design was obtained. The final design was selected in which each section was strong enough to withstand all the load cases. This method was an advancement to the previous one but again laborious. Further developments in it (38), prompted the European Committee for reinforced concrete (CEB) to initiate an extensive program of tests. This was to study the flexural behaviour of reinforced concrete members to obtain safe limiting values of hinge rotations, hinge moments and other parameters involved. The results of this investigation were published as the "limit design philosophy" (39).

The flexural behaviour of reinforced concrete members was also investigated by Monnier[18]. He carried out a series of tests and observed that the moment-curvature diagram of a reinforced concrete section was linear up to a stage at which the cracking started. The curve, then, gradually bent and became reasonably linear again, until the tensile reinforcement yielded. After this point a gradual flattening took place and the section failed at a finite value of curvature. For an under reinforced beam, Monnier empirically expressed the value of the flexural rigidity (EI)c at the crack stage, in terms of the percentage of tensile reinforcement r, the thickness of the section t and the effective depth of the

section d_1, as follows:

$$(EI)_c = (-2.5 \ r^2 + 13.9 \ r - 1.1) \ bd_1^3 \ x \ 10^3 \ kgf \ cm^2 \qquad 1.13$$

This equation is employed by the author, in constructing the moment-curvature diagrams of the reinforced concrete sections.

Beside the hand methods described above, efforts have been made to provide a computer method for the analysis of reinforced concrete structures. Cranston[40] for instance, attempted to develop ultimate design procedures upto and beyond the maximum load. This was done using the suggestions of reference (38). It was concluded that a reinforced concrete section showed a further reserve of strength even after the first crushing of concrete. It was thus suggested that plastic hinge rotations were, in many cases, greater than those previously considered reasonable. Cranston described the behaviour of reinforced concrete sections in terms of moment-curvature (M-C) relationships. The deflected shape and the rotational discontinuities of a frame were calculated after reducing it to a statically determinate one by insertion of a sufficient number of hinges. By iteration and numerical integration, the actual deflected shape was found as the one that gave zero hinge discontinuities. Cranston, tested this method by a series of experiments, performed on portal frames and concluded that this method predicted the failure loads with reasonable accuracy. Cranston calculated the plastic hinge moment of a section using the compressive stress distribution in concrete, given empirically by Hognestad et al[17]. He developed an eccentrically loaded specimen and a test method which permit the flexural stress distribution to be measured. Complete information regarding the flexural stress distribution, including stress-strain

graphs with a descending curve beyond the maximum stress, was reported for various water/cement ratios. Details of this distribution will be given in chapter 3, since it is also employed in this thesis to calculate the ultimate moment of resistance and the ultimate curvature of reinforced concrete sections.

Cranston's method was able to deal with any shape of (M-C) diagrams. However the method was rather complex and applicable only to frames of a limited size. No provision was made by Cranston to obtain the full load-deflection history of the frame and the instability effect of axial loads was again neglected.

Cranston[19] later proposed a computer method for determining the relation between the axial load, the moment and the curvature of members. A numerical integration technique was used to determine the moment-curvature relationship of a section for various values of the axial load. The interaction curve between the ultimate axial load and the ultimate moment was then obtained by plotting the ultimate moment values of each M-C curve against the corresponding axial load. This was also laborious and perhaps a more refined empirical formulae would be more useful for practical purposes.

The effect of instability in tall reinforced concrete sway frames was studied by Baker[41], Naddus and Yu[42]. The latter two suggested that if a thorough analysis was to be obtained, this effect must be allowed for. They pointed out that, even though Baker's design method[36] was extended to allow for instability, no attention was paid to the sequence of plastic hinge formation.

Chin[43] proposed a computer method for the non-linear analysis of plane frames subject to proportional loading with members having arbitrary M-C relationships. These were

considered to be functions of the bending moments only. The matrix displacement method was utilised throughout this analysis. At the first step, a set of trial displacements were used to calculate the forces required to maintain equilibrium. If this was not achieved, the trial displacements were corrected using the stiffness properties of the structure. The process was then repeated for other loads. Chin, analysed the frames tested by Cranston[40] and achieved good agreements with those obtained by Cranston. Chin's method was simpler than that of Cranston and required less computer time. Again the instability effect of axial loads was ignored throughout.

Deeble[16] described an incremental approach to trace the full load-deflection history of reinforced concrete frames in which the moment-curvature diagrams were approximated by a series of successive straight lines. Deeble analysed a frame under small increments of the load factor and added the resulting member forces and deflections to those due to the previous increments. Each time this was done, the flexural rigidity of a member was adjusted to the slope of the M-C diagram corresponding to the moments developed in that member. Deeble noticed a divergence in his results and suggested that smaller increments in the loading might reduce this to a tolerable level. Deeble subdivided the members and assumed that the bending moment on each submember was constant and equal to the larger of the two end moments. This subdivision increased the computational effort considerably.

Deeble also tried to adopt the analysis program of Majid and Anderson[20] for the analysis of reinforced concrete frames.

Piecewise linear M-C diagrams and subdivision of members were used once again. The full effect of axial forces on the stability of the frame was taken into account and the frame was analysed until a stipulated tolerance was satisfied. Once this was done, the process was repeated for the prediction of the next critical point in the M-C diagram. As a critical point was reached in a member, its flexural rigidity was adjusted to the slope of the next transition region on its M-C graph. However no allowance was made to preserve the forces and deflections present in the frame just before a critical point was reached. Therefore equilibrium was never satisfied.

Cakiroglu and Cetmeli[10] applied a modified unit force method to handle any type of nonlinearity. This included nonlinear stress-strain and M-C diagrams as well as the effect of axial loads. They derived the compatibility equations of a frame in nonlinear forms and applied the Newton-Ralpson method for the solution. The approach was general but not fully automatic. This was due to the necessity of deriving the compatibility equations, manually, in a mathematically explicit form. Such an analysis can only be carried out for a given set of loads.

Corradi et al[22] applied the "imposed rotations" method in conjunction with the finite element approach and an over relaxation technique to analyse reinforced concrete frames under a given load factor. This approach was anologous to that of Baker[36]. The full effect of axial loads on stability and the M-C diagrams were taken into account. Corradi analysed a six storey, single bay reinforced concrete frame for a given set of external loads, and compared their results with those obtained linearly. No comparison was made with any of the existing methods. It was implied that

even if this method could be extended to trace the full load-deflection history it would be restricted to proportional loads only. The numerical techniques (Beale's quadratic programming algorithm and linear complementary problem solution by systematic over relaxation), involved in the analysis, made the method complicated and computationally expensive.

1.e. A Historical Review of three dimensional Analysis of Structures :-

Since the computer became widely applicable to the problems of structural engineering, a considerable amount of research has been diverted in to the overall behaviour of structures. Work in this direction was encouraged by the well known fact that the lateral stability of a structure can be most efficiently provided by means of shear walls or cores. These can efficiently withstand the applied lateral forces.

Theoretically, the finite element method (44,45) was considered as a good tool to explore the overall behaviour of a complete structure of any shape. However, this method is computationally expensive. To reduce cost, some simplified methods have also been proposed for various specific type of structures.

The pioneering work in this field was carried out by Whitney[46] on the design of blast resistant structures. Further research was then carried out on shear walls [47,48,49,50,51], on coupled shear walls[52,53,5...] and also on shear wall-frame interaction[55,56,57,58,59,60]. The effect of cladding on the load-carrying capacity of steel structures was also studied by Bryan and El-dakhani[61,62], and Majid[28]. A brief review of the works related to the type of structures considered in this thesis is given here.

Clough et al[63] used the wide column anology for structures consisting of skeletal frames and wall-frame systems. This ignored

the in-plane bending of the slabs and the overall rotational stiffness
of a structure. The stiffness matrix of each frame was reduced to a
condensed form to cater for lateral displacements only. These
condensed stiffness matrices were then superposed to form the overall
stiffness matrix of the structure. The load vector consisted of the
applied wind forces and the lateral equivalent of the vertical and
rotational forces. Having calculated the common lateral displacements,
the vertical and the rotational displacements of the frames were
obtained by back substitution. This treatment was a simulation
of the three dimensional behaviour of a structure in two dimensions.
An analysis of a 20 storey structure showed that neglecting axial
deformations led to errors of about 20% in some of the columns.
Because the overall rotations of a structure were ignored, this method
was only applicable to symmetrical structures under symmetrical loads.

A method was proposed by Winokur and Gluck[58] for the analysis of
non-symmetrical structures. This used a matrix displacement approach
in which the relative lateral stiffness matrices of individual bracings
were obtained separately. Ignoring the in-plane bending of the slabs
the deflected shape of the structure was represented by the displacements
of an arbitrary point at each floor level. Horizontal displacements
parallel and normal to the wind direction and the rotation about a
vertical axis passing through the shear centre were considered. The
overall stiffness matrix of the structure was then constructed from
the contributions of each individual bracing component corresponding to
the assumed displacements. Once the deflected shape was found, the
member forces were obtained by back substitution. This method
was attractive particularly because it covered a large range of structures
while using a relatively small number of equations. However, the
concept of a 'shear centre,' proposed by the method, which was based

on the relative lateral stiffness of the bracings, at each floor level, was invalid, except when the bracings deflected colinearly.

Goldberg[64] proposed a method for the analysis of a type of structure consisting of parallel shear walls and frames. This ignored the axial deformations of the beams, the columns and the wide column effect. It was assumed that the slabs in the structure were pinned to the shear walls and the frames. Therefore, only the equilibrium of the lateral forces at the frame-slab and slab-shear wall junctions were satisfied. A maxtrix displacement approach was employed to solve for lateral displacements of the junctions. Two symmetrical ten storey and twenty storey structures, with side walls and seven intermediate frames were analysed by Goldberg. These showed that the bending of the slabs had an insignificant effect on the lateral deflections. It was found that the distribution of shear forces differed considerably from frame to frame. It was also shown that the effect of shear deformations in the walls and the slabs was significant and had to be taken into account.

Majid and Williamson[44,45] used a sparse matrix method[65] to develop a finite element analysis for structures consisting of prismatic members and plate elements subject to in-plane and out of plane forces. The effects of bending, torsion and cross coupling were taken into consideration. A series of experiments were carried out on two and three storey plane frames with shear wall cladding to study the effect of shear walls on the stiffness of bare frames. A pitched roof shed[28,61,62] was also analysed and the effect of sheeting on the load-carrying capacity of frames was demonstrated.

Majid and Croxton[66,67] later, developed a method for the linear analysis of complete structures consisting of a grillage of solid walls and floor slabs, stiffened against the horizontal displacements, by the action of parallel frames. The grillage and the frames were analysed separately under the action of a system of unit horizontal forces and their influence coefficients were determined. These components were then reassembled and horizontal equilibrium and compatibility conditions were satisfied at the slab-frame junctions. The parts of horizontal forces transmitted to the slabs and to the frames were thus calculated. Each of the frames and the grillage were then analysed under their own share of loads. The matrix displacement method was used in determining the influence coefficients and the forces and the deflections of each sub structure. In this approach the shear walls and the slabs were assumed to be deep beams and the effect of shear deformations were taken into account. Each grillage joint was assumed to have three degrees of freedom. These were the sway in the wind direction and rotations about the vertical and horizontal axes normal to the direction of the wind. A typical structure which was dealt with is shown in figure 1.1 together with the sign convension and the loads transmitted to the grillage and to the frames. The vector of wind load $\underline{P}$ was divided into two vectors $\underline{g}$ and $\underline{f}$ transmitted to the grillage and to the frames respectively. The horizontal equilibrium and compatibility equations for the frame-slab junctions were then expressed as:

$$\underline{P} = \underline{g} + \underline{f} \qquad\qquad 1.14$$

and

$$\underline{G}\,\underline{g} + \underline{a} = \underline{F}\,\underline{f} \qquad\qquad 1.15$$

where $\underline{G}$ and $\underline{F}$ are the influence coefficient matrices of the grillage and the frames and $\underline{a}$ is the horizontal deflection vector of the
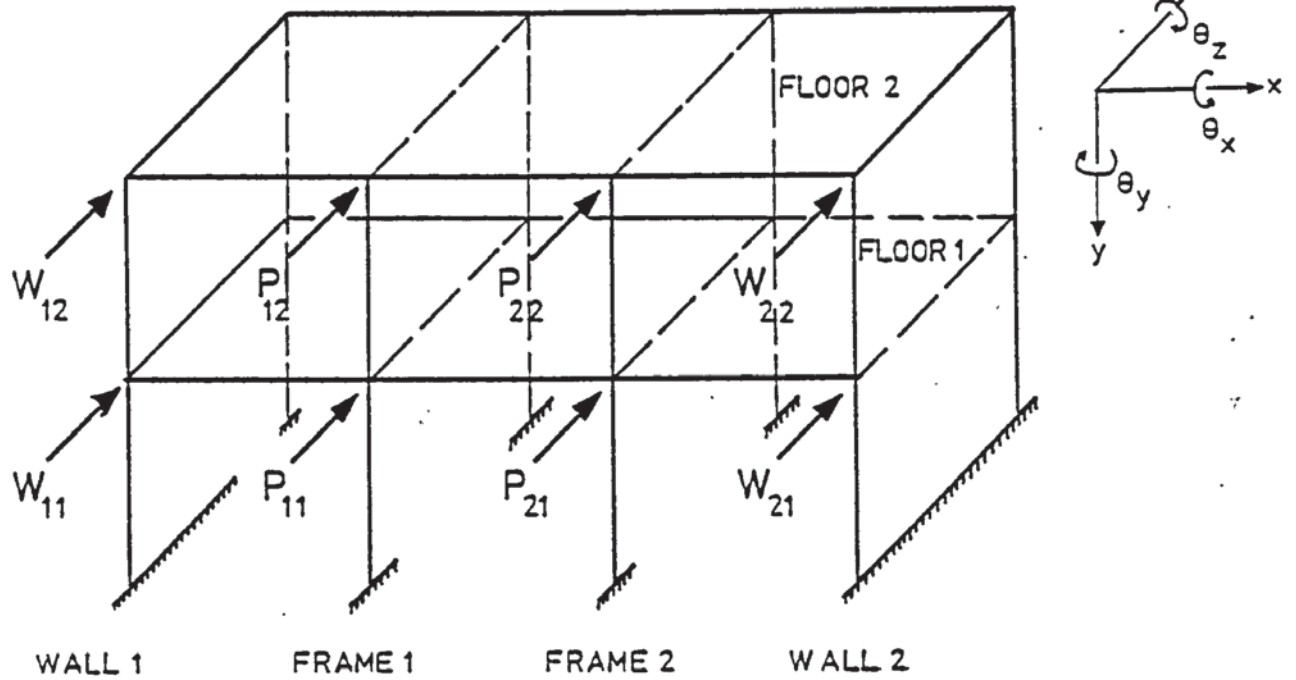
a–Structure and loading
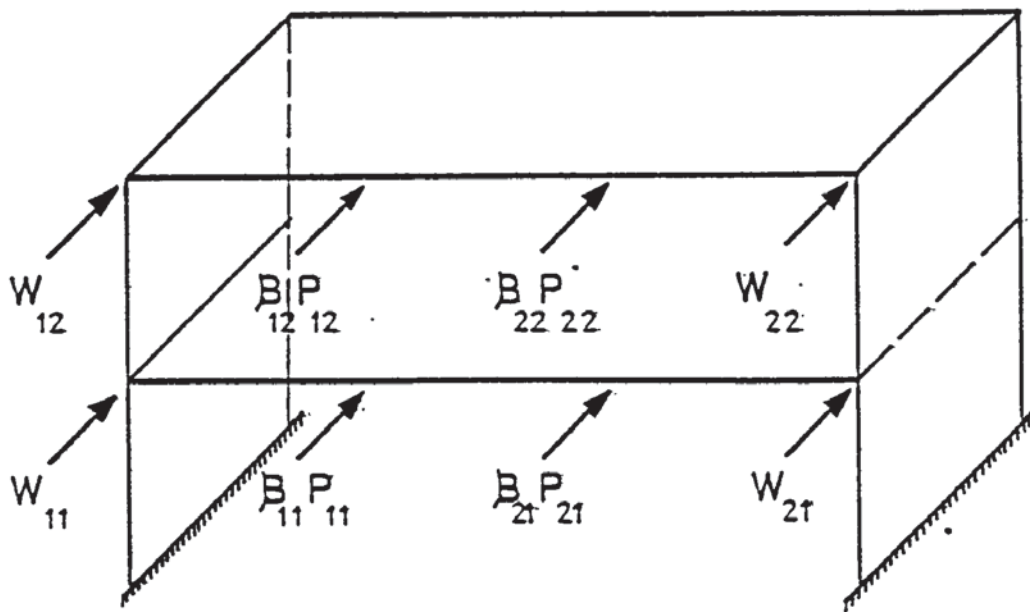
b–Loads transmitted to the grillage
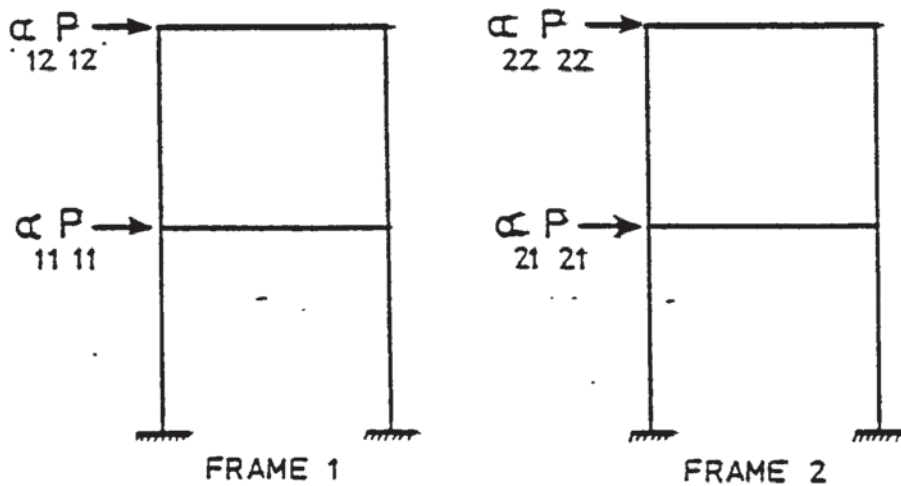
c Loads transmitted to the frames

FIGURE 1.1: A COMPLETE STRUCTURE

grillage due to the loads $\underline{w}$ acting on the shear walls. For the structure given in figure 1.1 these matrices are of the following forms:

a- The matrix G:

$$\begin{bmatrix} G_{11'11} & & & \\ G_{21'11} & G_{21,21} & \text{SYMMETRICAL} & \\ G_{12,11} & G_{12,21} & G_{12,12} & \\ G_{22,11} & G_{22,21} & G_{22,12} & G_{22,22} \end{bmatrix} \begin{array}{l} \text{Floor 1} \\ \\ \\ \text{Floor 2} \end{array} \qquad \cdots 1.16$$

Where, $G_{12,21}$, for example is the horizontal deflection of junction 1,2 due to a unit horizontal force acting at junction 2,1.

b- The vector $\underline{a}$:

$$\underline{a} = \{a_{11} \quad a_{21} \quad a_{12} \quad a_{22}\} \qquad \cdots 1.17$$

where a_{21} is the horizontal deflection of junction 2,1 due to the loads acting on the shear walls.

c- The matrix $\underline{F}$:

$$\underline{F} = \begin{bmatrix} F_{11'11} & & & \\ 0 & F_{21'21} & \text{SYMMETRICAL} & \\ F_{12,11} & 0 & F_{12,12} & \\ 0 & F_{22,21} & 0 & F_{22,22} \end{bmatrix} \begin{array}{l} \text{Floor 1} \\ \\ \\ \text{Floor 2} \end{array} \qquad \cdots. 1.18$$

Frame	Frame	Frame	Frame
1	2	1	2

ı

Writing equations (1.14) and (1.15) together, Majid and Croxton
obtained the loads transmitted to the frames and to the grillage as
follows:

$$\underline{f} = (\underline{G}+\underline{F})^{-1}(\underline{G}\ \underline{P}+\underline{a}) \qquad\qquad 1.19$$

and

$$\underline{g} = \underline{P} - \underline{f} \qquad\qquad 1.20$$

Majid and Croxton verified this method by tests carried out on a
two storey model structure, consisting of shear walls and slabs made
out of perspex and three intermediate frames made out of steel. The
method was further verified by the analysis of a 10 storey structure
reported by Goldberg[64]. The limitations of the method were that the
structures that could be considered consisted of parallel shear walls
and frames. Each frame and grillage should at least show some
amount of stiffness against lateral loads.

Croxton[67] later modified this method and considered the complete
structure as a grillage, laterally restrained by the frames. The
matrix displacement method was used to determine the lateral stiffness
of the individual frames by partitioning and condensation of their
overall stiffness matrices. The stiffness matrix of the complete
structure was then formed by superimposing the lateral frame stiffnesses
on to the stiffness matrix of the grillage. The joint displacements
and member forces of the grillage were obtained directly and the
analyses of the frames were completed by back substitution.

Majid and Önen[31,32,68] developed the lineal approach of Majid and
Croxton to analyse complete structures up to and including failure.
The elastic-plastic analysis method of Majid and Anderson[20] was used
in the individual analysis of each steel frame. The grillage system was
assumed to be sufficiently strong to maintain its initial stiffness

throughout the loading procedure.

After the first separation of the lateral loads Majid and Önen considered each individual frame in turn and analysed it under the factored loads to predict the load factor at which the next plastic hinge would possibly form in a frame. The lowest load factor was selected and a plastic hinge was inserted into the corresponding frame. This caused a reduction in the relative stiffness of the frame. Therefore more loads were transmitted to the other frames and to the grillage. The frame influence coefficient matrix F was reconstructed while the grillage influence coefficient matrix G remained unaltered. The influence coefficient equations were solved again and the new parts of the lateral loads transmitted to each individual component were calculated. Again each frame was analysed under its own new share of loads and further plastic hinges were detected until failure took place in one of the frames. Full effect of axial loads were considered. The effect of composite action between the floors and the beams was also considered. The method was tested by experiments on one and two storey model structures with steel frames and perspex grillage. The results were found to be satisfactory for one storey structures but not for two storey structures. These latter ones were reported to have failed due to buckling and cracking of the shear walls and the floor slabs. Some practical structures were also analysed and it was concluded that the presence of shear walls increased the load-carrying capacities of these structures drastically. Part of the work in this thesis is a continuation and development of this field.

1.e. Lateral Buckling of structural members

The phenomenon of lateral buckling has been studied by various investigators. The basic differential equations for the lateral

buckling were derived by Timoshenko[89], Michell[90] and a solution
was proposed for the problem of a simply supported beam subjected to
equal and opposite end moments. Beside various authors, Horne[73]
and Salvadori[74], studied the lateral buckling of eccentrically
loaded columns under unequal terminal moments. For an I section, Horne
used energy equations together with successive approximations in
conjunction with a Fourier analysis. This was concerned with the
elastic case and assumed that the members are initially free from
imperfections. The second moment of area about the major axis of the
section was assumed to be considerably greater than that about the
minor axis and the curvature in the weak plane was ignored. The
ends of the member were assumed to be simply supported, therefore the
effect of end restraints was ignored. The warping rigidity of the
section was considered as one of the parameters. The method was
applicable to any cross section with double symmetry. For the case when
the axial force was zero, a simplified equation was given for the
critical value of the maximum end moment Myzcr which caused lateral
instability as:

$$M_{yzcr} = (F + \gamma F_1) M_{Eyz}^2 \qquad\qquad 1.21$$

where F and F_1 are the parameters tabulated by Horne for various ratios
of end moments, γ is the warping rigidity factor and M_{Eyz} is the value
of the elastic critical moment derived by Timoshenko [89] for the
case when the end moments are equal and opposite. An approximate equation
was also given for the interaction of this moment and the axial force.
This made the method practically acceptable.

Trahair[75] studied the effects of symmetrical elastic end restraints on the lateral buckling of symmetrically loaded I beams. He employed the energy method given by Timoshenko[89] and carried out the analyses by a digital computer. A variety of symmetrical load cases and end restraints were dealt with for various values of warping rigidity. The results of the analyses were given in the following form:

$$M_{yzer} = \delta\sqrt{EI_{yy}\,GJ}\,/\,L \qquad\qquad 1.22$$

Here EI_{yy}, is the minor axis flexural rigidity; GJ is the torsional rigidity; L is the length of the member; δ is the parameter tabulated by Trahair, which depends on the end restraints, warping rigidity and load cases.

Massey[76] dealt with simply supported reinforced concrete beams under equal and opposite end moments. Here it was assumed that the major axis flexural rigidity was very large and, therefore, the displacements in the weak plane were small. The minor axis flexural rigidity, the torsional rigidity and the warping rigidity were expressed in terms of dimensions of the cross section and the stress-strain diagrams of steel and concrete respectively. The theory was testified by a series of experiments and the results were in reasonable agreement with the theory.

Netercot and Rockey[77] tried to develop a unified approach to consider separate pieces of work carried out on different aspects of lateral buckling. These simplified the existing equations, so that

they may be used for design purposes. A recent work in this field was produced by Vacharajittipan and Trahair[78] to deal with the lateral buckling of frames. The differential equations for in plane bending and flexural-torsional buckling were obtained, together with the boundary, compatibility conditions and warping and joint equilibrium equations. The finite integral method was utilised for the solutions of the above equations by a fully computerised approach.

1.f. Failure of Reinforced Concrete Sections under the combined
     action of Bending, Shear and Torsion:-

Work in this field was directed primarily towards predicting the strength of members. Hoegnestad[91] discussed the fundamental concepts in the ultimate load design of reinforced concrete members and derived the general equations for the possible failure modes. Kani[92], on the other hand, studied the failure of large (deep) reinforced concrete beams under the combined action of bending and shear. From the experiments carried out, it was observed that the relative beam strength decreased considerably as the beam depth increased. It was concluded that the safety factors derived from the tests of small beams are not realistic and might be even dangerous. The main cause of the deterioration of the beam strength was claimed to be the prematurely developed diagonal cracks, which were merely due to the shear force.

Neville et al[93] developed an analytical method for the calculation of the flexure-shear strength of reinforced concrete deep beams. The effect of shear force on failure was taken into account in deriving the equations for the failure load.

The investigators, studying the interaction of torsion with bending and shear followed two different approaches known as the truss analogy and the skew bending theory. The method of truss analogy was presented by Reusch[94] and was later expanded by Lampert[95], Elfren[83] and others to include the combined effects of torsion and bending.

Early work on the interaction of bending torsion and shear by using the skew bending theory was carried out by Gvosdev and Lessing[86] and others[82,85,87]. They studied the equilibrium conditions and tried to derive expressions for external and internal energy for observed skew failure mechanisms.

Elfren, Karlson and Losberg[88] applied the skew bending theory to study the general interaction of bending, torsion and shear in a simple and rational way. They first studied the equilibrium equations for the special case of bending and torsion only. They reported that their results were in agreement with what has been developed previously with the skew bending theory and with the truss analogy. The effect of the shear force was then taken into account in deriving the equilibrium equations for a general skew failure surface. This assumed that the compression centre of the section was at the level of top horizontal stirrup legs for the mode in which the compression zone is in the top of the cross section. The dowel action of the longitudinal reinforcement which was placed at the bottom and at the top of the cross section was ignored. It was also assumed that the stirrups are completely yielded at the stage of failure and the concrete in the compression zone did not sustain any shear stress. The inclination of the cracks were related to the torsion and shear acting on the member. In this manner an interaction equation was expressed in terms of the ratios of the applied bending, torsion and shear to the ultimate values of each respectively. For the mode in which the compression zone is placed in the

top of the beam the interaction equation was given in the following
form:

$$\frac{M}{M_{ult}} + (\frac{M_t}{M_{tult}})^2 + \frac{S_y}{S_{yult}} = 1 \qquad 1.23$$

where M, M_t and S_y are the bending moment, the torque and the shear
force acting on the member. M_{ult}, M_{tult} and S_{yult} are, on the other hand,
the ultimate bending moment, torque and shear force carrying
capacities respectively. These were given as:

$$M_{ult} = -2 A_{1b}\sigma_{1by}h'$$

$$M_{tult} = 2b'h' \frac{Aw\sigma wy}{s} \sqrt{\frac{2A1b\sigma 1by}{b'+h'} \frac{s}{Aw\sigma wy}} \qquad 1.24$$

$$S_{yult} = 2h' \frac{Aw\sigma wy}{s} \sqrt{\frac{2A1b\sigma\ 1by}{h'} \frac{s}{Aw\sigma wy}}$$

Here, $Aw\sigma wy$ is the yield force carried by a stirrup leg; $2A1b\sigma 1by$ is the
force carried by the tensile reinforcement; s is the spacing of the stirrups
b' is the distance between the vertical legs of a stirrup and h' is the
distance between the tensile and compressive reinforcements. It was
reported that the available test results supported their method; however
more tests were needed for further justification. To develop this
method, the depth of the neutral axis had to be determined in a more
rational way. A similar approach is employed in this thesis to derive
the interaction equations of bending, shear and torsion for deep,
multilayered reinforced concrete panels.

1.g. The Scope of the presented Work:-

The work presented in this thesis can be divided into two parts.

The first part is an investigation into the behaviour of plane frames in order to present a simple and versatile method, to deal with the nonlinearities due to various effects and to analyse such frames up to a given load factor or upto and including failure. The application of the theorems of structural variation to the elastic-plastic analysis of steel frames is studied in chapter 2. The concept of 'the compensating loads' is derived from these theorems. These are defined as the loads necessary to be applied on a frame in order to maintain the initial state of forces and deflections, when the flexural rigidity of a member is altered or when a member is removed. A piecewise linear elastic-plastic analysis method which only makes use of a unique linear elastic analysis, is proposed. Using the theorems of structural variation, it is also shown that an elastic-plastic analysis of a derivative frame, obtained by removing or altering some members of a ground frame, can be carried out by using a single initial elastic analysis of the ground frame.

In chapter 3 the nonlinear material properties are expressed in terms of moment-curvature (M-C) diagrams and the theorems of structural variation are again used in a nonlinear M-C analysis procedure. This procedure is also applied to the analysis of steel frames with strain hardening. In the second part of this chapter, the nonlinear M-C properties of reinforced concrete members are presented by trilinear M-C diagrams. The compensating loads are then used to develop a rigorous failure load analysis for reinforced concrete-frames. This procedure takes the nonlinear material properties and the effect of non-proportionally increasing loading into account as well as the second order effect of axial loads. The reliability of the proposed methods are

checked by a number of examples and the problems encountered, are discussed.

In the second part of this thesis, the failure of complete structures with shear walls, slabs and bare frames is studied. A method of analysis is given in chapter 4 to obtain the load-deflection diagram of a complete structure upto and including failure. The structure may be made out of reinforced concrete or steel frames together with shear walls and slabs made out of reinforced concrete or any homogenous material. Lateral buckling prior to failure and cracking of panels are taken into consideration. Plastic hinges in steel frames and critical stiffness changes in reinforced concrete frames are also included. The frames and the grillage of shear walls and slabs are first treated separately with their own share of the applied loads. These are calculated from the compatibility conditions at the frame-slab junctions. Since the effects mentioned above cause major stiffness changes, the loads transmitted to each component of the structure vary throughout the loading process. Therefore special care is taken to calculate the actual values of these transmitted loads as each critical change takes place in the structure. Lateral buckling of panels is then studied and an approximate method is proposed to calculate the critical bending moments which cause lateral instability. Since practical structures do not fail due to buckling of slabs, the approximation proposed is rather crude but sufficient to analyse Onen's frames that failed by the buckling of perspex slabs. Cracking of brittle, homogenous panels under the combined action of bending, torsion and shear is also considered in this chapter and the proposed failure criteria are discussed. Chapter 5 is spared for the failure of deep reinforced concrete panels under the

combined action of bending, torsion and shear. The skew bending theory is employed to derive the interaction equations at failure. The location of the neutral axis along the failure surface is studied and a method is proposed to calculate its depth. The validity of this method is verified by the experimental data obtained from the tests. The effect of the depth of the neutral axis to the ultimate failure load of a complete structure is then studied and its significance is revealed. Under the light of these studies, some modifications in the process described in chapter 4 are given. The validity of the interaction equation are then checked by experimental data.

The computer program developed for the nonlinear analysis of plane frames by means of the structural variation theory and the program developed for the failure load analysis of complete structures are presented in chapter 6.

The first program is able to carry out the following types of analysis of frames:

1 - Linear elastic analysis

2 - Nonlinear elastic analysis

3 - Piecewise linear elastic-plastic analysis

4 - Piecewise linear elastic-plastic analysis of a derivative frame by using the initial solution of the ground frame, from which the derivative frame is obtained.

5 - Nonlinear moment-curvature analysis.

The failure load analysis program can handle any kind of complete structure consisting of parallel steel or reinforced concrete frames . and shear walls and slabs made out of reinforced concrete or out of a homogenous material. The effect of inactive hinges and the composite action of slabs and beams are also taken into account. This program is also able to carry out the failure load analysis of a plane frame or grillage repeatedly.

In chapter 7, the experiments carried out on the model structures with reinforced concrete grillage, with or without refinroced concrete or steel frames are described.

Comparison of the theoretical and the analytical results is then given in chapter 8. This chapter also includes the results of the analyses of four storey and six storey practical structures for which results obtained by Önen are available for comparison.

General conclusions concerning the validity of the proposed methods are drawn in chapter 9 and suggestions are made for future research.

CHAPTER 2

APPLICATION OF THE THEOREMS OF STRUCTURAL

VARIATION IN THE ELASTIC-PLASTIC ANALYSIS

2.a. Introduction:-

The basic principles of the theorems of structural variation
were first outlined by Majid and Elliott[1,2,6]. They dealt with
the changes in the forces and deflections of pin jointed structures
due to changes in the areas of their members., and suggested that
these theorems can be extended to cover all kinds of structures.
Later, Saka[3] extended them to cover rigidly jointed plane frames,
and studied the effect of changes in the second moment of areas on
the forces and deflections of these frames.

In this chapter, the basic principle of these theorems is
first used to obtain the load vector to be applied to a structure
to preserve the member forces and deformations when the flexural
rigidity EI of a member.changes. The application of the theorems
is then simplified to cover the case of members in single curvature.
Once this is done, it becomes possible to predict the forces and
deflections in a frame when it develops hinges or when hinges are
inserted. This enables the use of the theorems to carry out the
elastic-plastic analysis of plane frames.

2.b. The compensating loads:-

Consider a member of a frame, shown in figure (2.1), for
which the member forces are:

$$
\begin{bmatrix} S_{ij} \\ M_{ij} \\ M_{ji} \end{bmatrix} = \begin{bmatrix} \dfrac{12EI}{L^3} & -\dfrac{6EI}{L^2} & -\dfrac{6EI}{L^2} \\ -\dfrac{6EI}{L^2} & \dfrac{4EI}{L} & \dfrac{2EI}{L} \\ -\dfrac{6EI}{L^2} & \dfrac{2EI}{L} & \dfrac{4EI}{L} \end{bmatrix} \begin{bmatrix} v \\ \theta_i \\ \theta_j \end{bmatrix} \qquad 2.1
$$

$$\underline{P} \qquad\qquad \underline{K} \qquad\qquad \underline{Z}$$

a- Deflection of a member

$S_{ji} = S_{ij}$

M_{ji}

M_{ij}

$S_{ij} = -\dfrac{M_{ij} + M_{ij}}{L}$
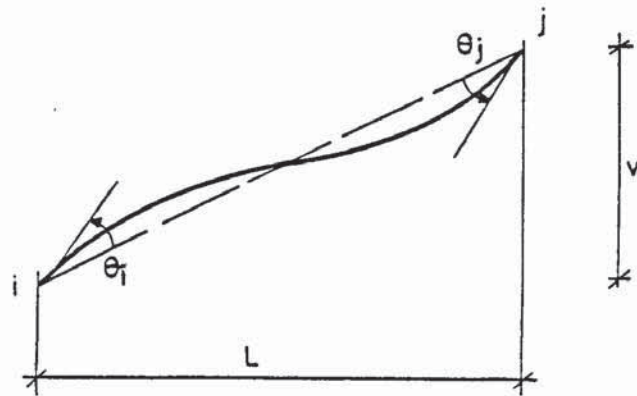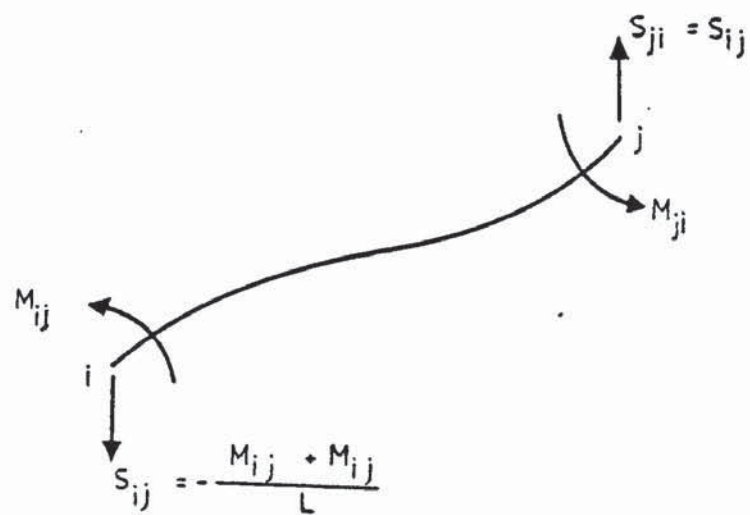
b- Forces on a member

FIGURE 2.1: FORCES AND DEFLECTIONS ON A MEMBER

where S_{ij} is the shear force and M_{ij} and M_{ji} are the bending moments at the ends i and j respectively. The variables v, θ_i and θ_j are the sway and the rotations. The modulus of elasticity is E, the second moment of area is I and L is the length of the member.

If I is now reduced to a value I' by an amount δI, then

$$I' = I - \delta I \qquad \qquad 2.2$$

Defining $\qquad \qquad \alpha = -\delta I/I, \qquad \qquad 2.3$

it follows that:

$$I' = (1+\alpha)\, I \qquad \qquad 2.4$$

Keeping the deflections constant and substituting equation (2.4) into equations (2.1) gives:

$$\begin{bmatrix} S'_{ij} \\[2ex] M'_{ij} \\[2ex] M'_{ji} \end{bmatrix} = (1+\alpha) \begin{bmatrix} \dfrac{12EI}{L^3} & -\dfrac{6EI}{L^2} & -\dfrac{6EI}{L^2} \\[2ex] -\dfrac{6EI}{L^2} & \dfrac{4EI}{L} & \dfrac{2EI}{L} \\[2ex] -\dfrac{6EI}{L^2} & \dfrac{2EI}{L} & \dfrac{4EI}{L} \end{bmatrix} \begin{bmatrix} v \\[2ex] \theta_i \\[2ex] \theta_j \end{bmatrix} \qquad 2.5$$

$$\underline{P}' \qquad\qquad\qquad \underline{K} \qquad\qquad \underline{Z}$$

Comparing equations (2.1) and (2.5) we note that:

$$\underline{P}' = (1+\alpha)\, \underline{P} \qquad \qquad 2.6$$

where $1+\alpha$ is a scaler.

The second moment of area of this member can be reduced, without affecting the forces and the deflections anywhere in the frame, provided that equal and opposite compensating loads $\underline{P} - \underline{P}'$ are applied to the joints i and j at the ends of the member. Now:

$$\underline{P} - \underline{P}' = \underline{P} - (1+\alpha)\,\underline{P} = -\alpha\underline{P} = -\alpha\,\{S_{ij}\ M_{ij}\ M_{ji}\} \qquad 2.7$$

and the shear force is in fact given by

$$S_{ij} = -\frac{M_{ij} + M_{ji}}{L} \qquad \qquad 2.8$$

Thus the compensation loads to be applied at i and j, in the
global coordinates are:

$$
\begin{bmatrix} S_{ix} \\ S_{iy} \\ M_i \\ S_{jx} \\ S_{jy} \\ M_j \end{bmatrix} = \begin{bmatrix} -mp & 0 & 0 \\ lp & 0 & 0 \\ 0 & 1 & 0 \\ mp & 0 & 0 \\ -lp & 0 & 0 \\ 0 & 0 & 1 \end{bmatrix} \begin{bmatrix} \alpha\, S_{ij} \\ \alpha\, M_{ij} \\ \alpha\, M_{ji} \end{bmatrix} \qquad 2.9
$$

where S_{ix} and S_{iy} are the component of S_{ij} in the x and y
directions, while mp and lp are the direction cosines of the
member. By resolution, the compensating load matrix is obtained
as:

$$\{S_{ix}\ S_{iy}\ M_i\ S_{jx}\ S_{jy}\ M_j\} = \{-\alpha mpS_{ij}\ \ \alpha lpS_{ij}\ \ \alpha M_{ij}\ \ \alpha mpS_{ij}\ \ -\alpha lpS_{ij}\ \ \alpha M_{ji}\}$$

$$2.10$$

These are shown in figure (2.2).

This load matrix will be used in chapter 3 to carry out the
rigorous nonlinear failure load analysis of reinforced concrete
frames.

2.c The unit load matrix:-

It was found[3] that an analysis of a rigidly jointed
plane frame under two unit loading cases applied at the joints i
and j is necessary to study the effect of the variation in the
second moment of area of a member joining i and j on the forces
and deflections in the structure. These unit load vectors can be
written as

$$\{S_{ix}\ S_{iy}\ M_i\ S_{jx}\ S_{jy}\ M_j\} = \{-\tfrac{1}{L}mp\ \ \tfrac{1}{L}lp\ \ 1\ \ \tfrac{1}{L}mp\ \ -\tfrac{1}{L}lp\ \ 0\} \qquad 2.11$$

and

y

p

$90 - \beta$

β

x

$\cos \beta = m_p$

$\cos(90 - \beta) = l_p$

a- SIGN CONVENTION

$-\alpha l_p S_{ij}$

$\alpha m_p S_{ij}$

p

αM_{ji}

$-\alpha M_{j'j}$

$S_{ji} = S_{ij}$

$-\alpha S_{ij} = \alpha \dfrac{M_{ij} + M_{ji}}{L}$

L_{ij}

αM

$-\alpha M_{ij}$

$-\alpha m_p S_{ij}$

$\alpha l_p S_{ij}$

b-COMPENSATING LOADS ON A MEMBER AND RELEVENT JOINTS
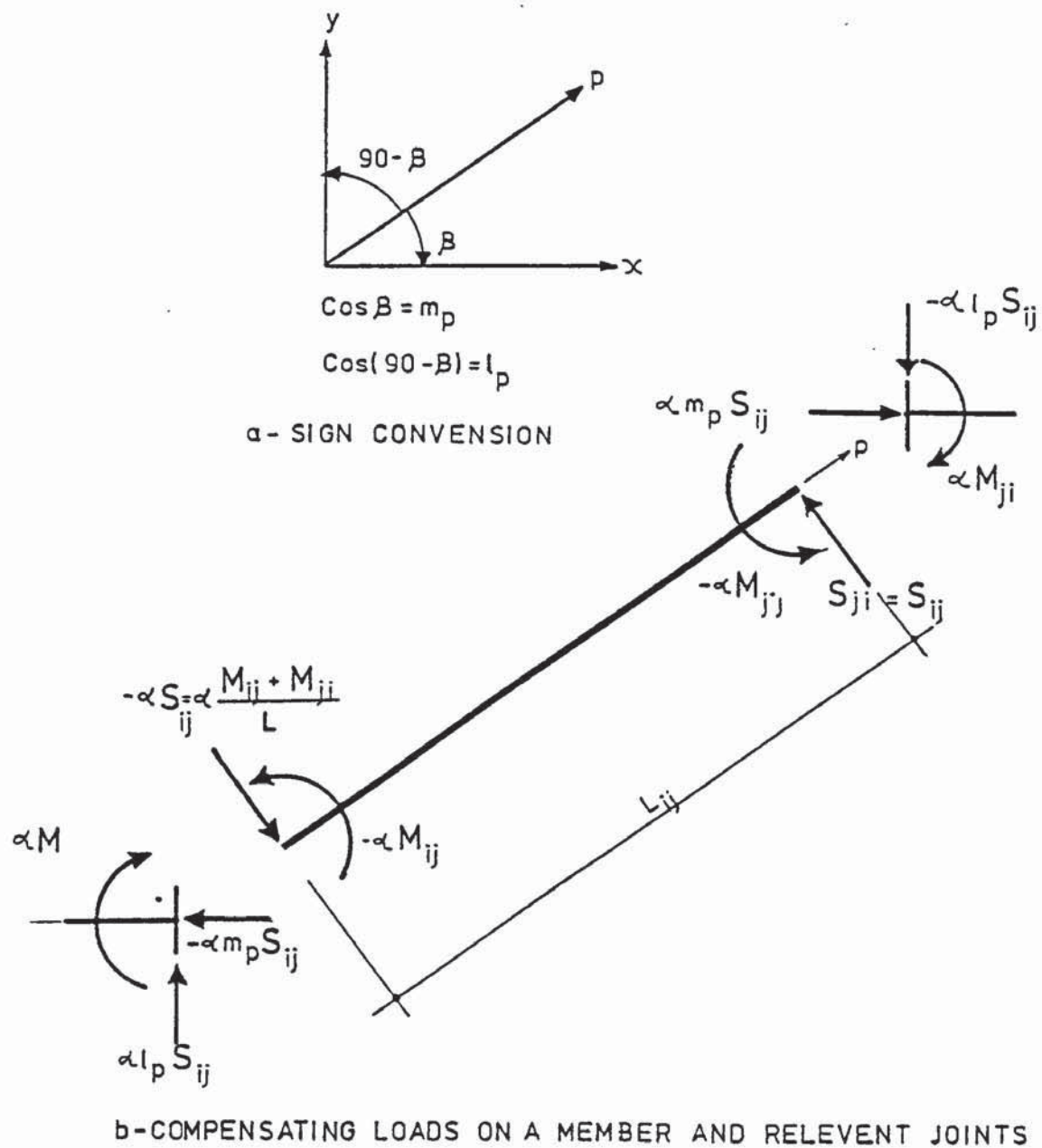
FIGURE 2.2: COMPENSATING LOADS IN GLOBAL COORDINATES

$$\{S_{ix}\ S_{iy}\ M_i\ S_{jx}\ S_{jy}\ M_j\} = \{-\tfrac{1}{L}\ mp\ \tfrac{1}{L}\ \ell p\ 0\ \tfrac{1}{L}\ mp\ -\tfrac{1}{L}\ \ell p\ 1\} \qquad 2.12$$

This is due to the fact that there are two variables directly related to the changing second moment of area. These are the bending moments M_{ij} and M_{ji}. When the member ij is in single curvature and its length is infinitally small, the end moments M_{ij} and M_{ji} are equal and opposite. In this case there is only one variable directly dependent upon I. The corresponding unit load matrix can therefore be obtained by subtracting equation (2.12) from equation (2.11) to give:

$$\{S_{ix}\ S_{iy}\ M_i\ S_{jx}\ S_{jy}\ M_j\} = \{\ 0\ \ 0\ \ 1\ \ 0\ \ 0\ \ -1\} \qquad 2.13$$

These unit loads are shown in figure (2.3). A single analysis of the frame under the unit load vector given by equation (2.13) is sufficient to study the effect of changing the second moment of area of ij on the rest of the structure.

To study the independent effects of varying several members requires an independent unit load vector to be applied on the frame. These vectors can be collected together and expressed in a matrix $\underline{C}$ which is called the unit load matrix of the frame. The contributions of two changing members ij and st to this matrix are given by:

$$
\underline{C} =
\begin{bmatrix}
\vdots & \vdots \\
0 & 0 \\
0 & 0 \\
1 & 0 \\
\vdots & \vdots \\
0 & 0 \\
0 & 0 \\
0 & 1 \\
\vdots & \vdots \\
0 & 0 \\
0 & 0 \\
-1 & 0 \\
\vdots & \vdots \\
0 & 0 \\
0 & 0 \\
0 & -1 \\
\vdots & \vdots
\end{bmatrix}
\begin{array}{l}
S_{ix} \\
S_{iy} \quad \text{At joint i} \\
M_i \\
\\
S_{sx} \\
S_{sy} \quad \text{At joint s} \\
M_s \\
\\
S_{jx} \\
S_{jy} \quad \text{At joint j} \\
M_j \\
\\
S_{tx} \\
S_{ty} \quad \text{At joint t} \\
M_t
\end{array}
\qquad 2.14
$$

a-FIRST END UNIT   b-SECON END UNIT   c-UNIT LOADING FOR

LOADING   LOADING   A MEMBER IN SINGLE

                                               CURVATURE
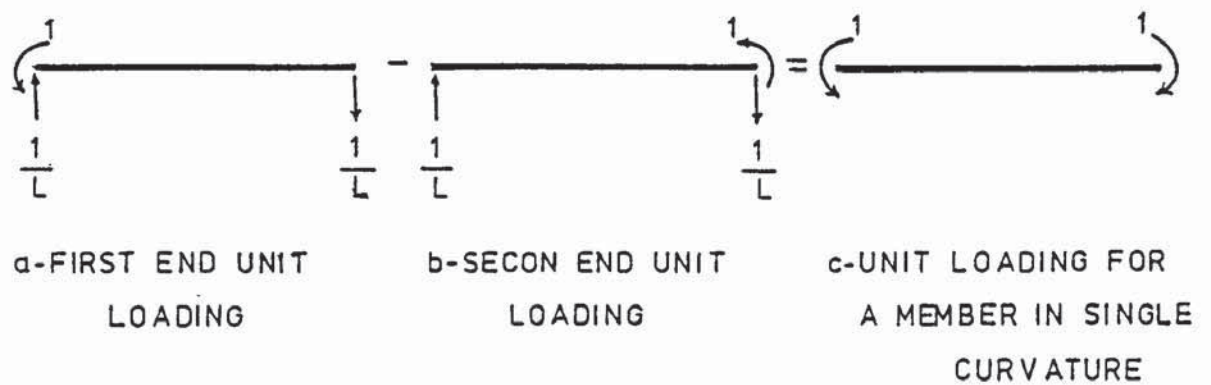
FIGURE 2.3: UNIT LOADINGS

In equation (2.14) i is the first end of ij while s is the first end of st. The first column of matrix $\underline{C}$ is constructed for member ij and the second for member st. Every column of $\underline{C}$ consists of zeroes except for a positive unit moment, at the joint connected to the first end, and a negative one at the second end of a changing member. When analysing a frame under the external loads $\underline{L}$ it is now possible to evaluate simultaneously the joint displacements and member forces due to $\underline{C}$ as well. This is particularly useful as it saves a great deal of computing time. For this reason the external load vector and the unit load matrix are compound to form a single vector$[\underline{L}\ \underline{C}]$which is used to solve $[\underline{L}\ \underline{C}] = \underline{K}\ \underline{X}$ once.

2.d Inserting a Hinge to a Frame:

A hinge in a frame can be represented by a member with zero flexural rigidity and infinitely small length.

This member can be used to study the effect of hinges on the member forces and deformations by means of the theorems of structural variation. To begin with the possible hinge locations are marked and infinitely small members are inserted into these locations. Then the compound load matrix $[\underline{L}\ \underline{C}]$ is constructed and the structure is analysed once.

If a hinge is required to be inserted into location k, the following steps are taken:

i   - Set the second moment of area of the member in that location to zero which makes:

$$\alpha = -\delta I/I = -1$$

ii - Calculate the variation factor from, see equation 1.10 in chapter 1,

$$r_{\alpha k} = \frac{-\alpha M_k}{1+\alpha \mu_k} \qquad\qquad 2.15$$

where M_k and μ_k are the bending moments on member k due to the external loads and unit loading at its ends respectively.

iii - For n members, calculate the new member forces by means of the first theorem of structural variation as:

$$M'_{v,q} = M_{v,q} + r_{\alpha k}\,\mu_{vq} \qquad v = 1,2; \; q = 1, n \text{ and } q \neq k$$

$$S'_q = S_q + r_{\alpha k}\,s_q \qquad\qquad q = 1,n$$

$$P'_q = P_q + r_{\alpha k}\,P_q \qquad\qquad q = 1,n \qquad\qquad 2.16$$

for $q = k$ and $v = 1$

$$M'_{1k} = (1+\alpha)\,M_{1k}/(1+\alpha\,\mu_{1k}) = 0$$

Where $M'_{1,q}$ and $M'_{2,q}$ are the new bending moments at the first and second ends of member q. S'_q is the new shear force and P'_q is the new axial force. $M_{2,q}$, S_q and P_q are those due to external loads while μ_{1q}, s_q and P_q are those due to unit moments at the ends of member k and n is the number of members.

iv - For m joints calculate the new deflections from the second theorem of structural variation as follows:

$$\psi_{vq} = X_{vq} + r_{\alpha k}\,X_{vq} \qquad v = 1,2,3; \; q = 1,m \qquad\qquad 2.17$$

where the values of suffix v 1, 2 and 3 refer to the deflections in x and y directions and rotation respectively, while q refers to the joint. The deflections $\psi_{3,q}$, $X_{3,q}$ and $X_{3,q}$ are the new rotation, rotation under external loads and rotation due to unit loading at the ends of member k, for joint q.

When some other hinges are required to be inserted, each of the unit load cases corresponding to those hinges are considered to be external loads in turn and the steps ii, iii and iv are carried out to modify the member forces and deflections. The

EXTERNAL LOADING   UNIT LOADING AT C-C'   UNIT LOADING AT D-D'
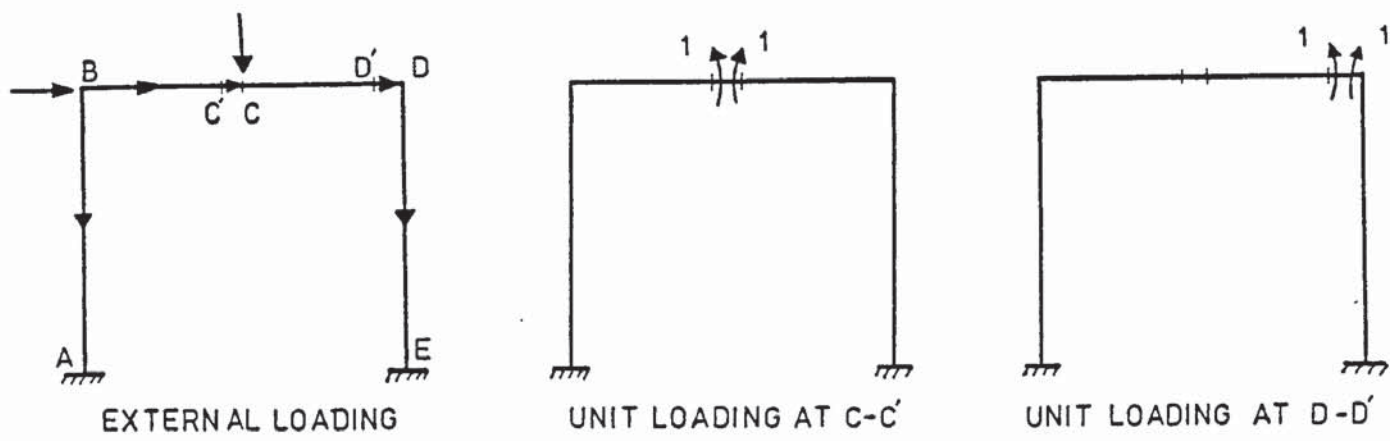
(a)
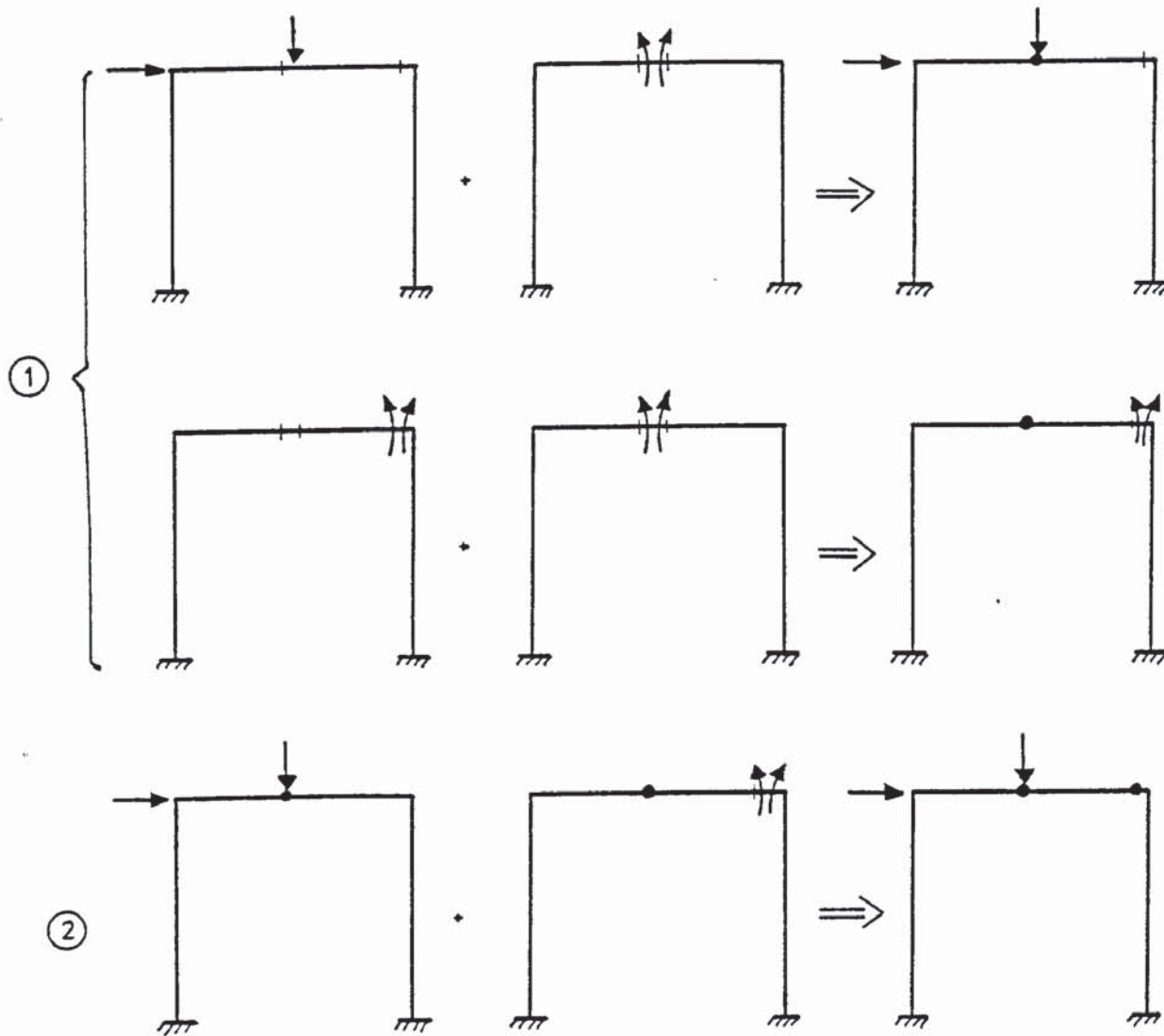
(b)

FIGURE 2.4: THE PROCEDURE FOR INSERTING
SUBSEQUENT HINGES

hinges are inserted one at a time.

For instance two hinges are inserted in to the locations CC' and DD' of the frame shown in figure 2.4. The structure is first analysed once under the external loads, unit loading at C-C' and unit loading at D-D'. Then the results of the unit loading at C-C' are used to calculate the member forces and deflections of the frame with a hinge at C-C' due to external loading and unit loading at D-D'. Finally the modified forces and deflections due to unit loading at D-D' are used to remodify the forces and deflections due to <ins>external loads and</ins> a hinge <ins>is</ins> inserted at D-D'.

The use of <ins>the theorems of</ins> structural variation in inserting a series of hinges into a frame by only using its initial linear elastic solution is useful for studying the elastic-plastic behaviour of that frame under increasing external loads. This will be studied in the next section.

2.e Elastic-Plastic Behaviour of Frames:

Consider a frame made out of a material which has an elastic-plastic stress-strain diagram as shown in figure (2.5). As the externally applied loads increase, the member forces and deflections increase proportionally until the bending moment somewhere in the frame first reaches the fully plastic hinge moment 'Mp' of the section. From then onwards this point acts as a hinge and the frames become more flexible. The deflections and the bending moments elsewhere in the structure now increase at a faster rate. The bending moment at the section, however, preserves its value 'Mp'. This state of affairs continues until a sufficient number of plastic hinges develop in the frame to form a mechanism and the frame fails. It should be pointed out, however, that the
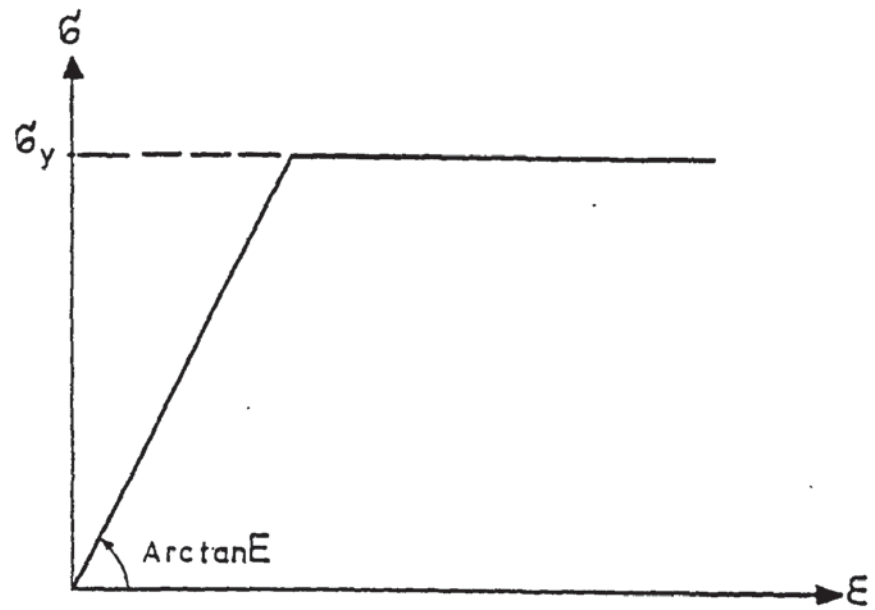
FIGURE 2.5: AN ELASTIC-PLASTIC STRESS-STRAIN
         DIAGRAM

presence of axial forces may decrease the value of Mp continuously. The frame may also fail by instability before a mechanism develops. A rigorous elastic-plastic analysis procedure dealing with these effects is given elsewhere[4]. However in the elastic-plastic analysis procedure by means of the theorems of structural variation given here, these effects of axial loads are ignored.

2.f. Piecewise Linear Elastic-Plastic Analysis:-

The following assumptions have been made in the development of the analysis.

1 - The loads are proportionally applied up to collapse. However the method given in chapter 4 may be used to deal with nonproportionally increasing loads.

2 - The structural material possesses elastic-perfectly plastic stress-strain and moment-curvature relationships. However this assumption is not always necessary. An approach considering nonlinear moment-curvature diagrams will be given in chapter 3.

3 - Plasticity occurs at discrete sections. In other words the shape factor of the sections are equal to 1.

4 - An increment of the bending moment at a section always causes an increment of curvature of the same sign.

5 - The effect of axial loads on the stability of frame is neglected.

The steps for the elastic-plastic analysis are as follows:

i   - All the possible hinge locations are marked, the compound load matrix [$\underline{L}$ $\underline{C}$] is constructed.

ii - The frame is analysed linear elastically once under [$\underline{L}$ $\underline{C}$] by any conventional method, such as matrix displacement method. The resulting member forces and joint deflections are found.

iii - For convenience the bending moments, axial forces and

deflections are stored in the matrices $\underline{M}$, $\underline{P}$ and $\underline{X}$ respectively as follows:-

a - Bending moment matrix $\underline{M}$:

$$\underline{M} = \begin{bmatrix} M_{11} & M_{21} & M_{12} & M_{22} & \cdots & M_{1n} & M_{2n} \\ \mu_{11}^1 & \mu_{21}^1 & \mu_{12}^1 & \mu_{22}^1 & \cdots & \mu_{1n}^1 & \mu_{2n}^1 \\ \vdots & & & & & & \\ \mu_{11}^f & \mu_{21}^f & \mu_{12}^f & \mu_{22}^f & \cdots & \mu_{1n}^f & \mu_{2n}^f \end{bmatrix} \qquad 2.18$$

The matrix $\underline{M}$ has $f + 1$ rows and $2n$ columns. Where f and n are the number of possible hinge locations and number of members respectively. The bending moments M_{12} and μ_{12}^f are the first end moments of member 2, due to the external loads and the unit loading at the ends of the member representing the hinge location at f.

b - Axial force matrix $\overline{P}$:

$$\overline{P} = \begin{bmatrix} P_1 & P_2 & \cdots & P_n \\ P_1^1 & P_2^1 & \cdots & P_n^1 \\ \vdots & & & \\ P_1^f & P_2^f & \cdots & P_n^f \end{bmatrix} \qquad 2.19$$

Where P_n and P_n^f are the axial forces in member n due to external loads and the fth unit loading.

c - Deflection matrix $\underline{X}$:

$$\underline{X} = \begin{bmatrix} x_1 & y_1 & \theta_1 & x_m & y_m & \theta_m \\ X_{11} & X_{21} & X_{31} & X_{1m} & X_{2m} & X_{3m} \\ X_{11}^1 & X_{21}^1 & X_{31}^1 & \cdot & \cdot & \cdot \\ \vdots & \vdots & \vdots & & & \\ X_{11}^f & X_{21}^f & X_{31}^f & X_{1m}^f & X_{2m}^f & X_{3m}^f \end{bmatrix} \qquad 2.20$$

where X_{31} and X_{31}^1 are the rotations of joint 1 due to the external loads and the first unit loading.

iv - The bending moments, axial forces and deflections due to external loads are collected to form the actual bending moment,

axial force and deflection matrices $\underline{MA}$, $\underline{PA}$ and $\underline{XA}$ respectively.
These matrices are as follows:

$$\underline{MA} = [M_{11}\ M_{21}\ \cdots\ M_{1n}\ M_{2n}] \qquad 2.21$$

$$\underline{PA} = [P_1\ P_2\ \cdots\ P_n] \qquad 2.22$$

$$\underline{XA} = [X_{11}\ X_{21}\ X_{31}\ \cdots\ X_{1m}\ X_{2m}\ X_{3m}] \qquad 2.23$$

v - Every possible hinge location is considered in turn and the
load factor λ_1^k at which a plastic hinge occurs at k is calculated
from

$$\lambda_1^k = \frac{M_p^k}{MA(1,k)} \qquad 2.24$$

Where M_p^k is the fully plastic moment of location k, MA(1,k) = -MA(2,k)
is the bending moment at the location k due to external working
loads.

The smallest of these predicted load factors is selected.
This is then the load factor λ_1 at which the first plastic hinge
develops in location k*. The current member forces and deflections
are obtained by scaler multiplying the matrices $\underline{MA}$, $\underline{PA}$, and $\underline{XA}$ by
λ_1. To preceed further, the member forces and deflections of the
frame with a hinge at k* under the external loads is necessary.
Conventionally a fresh analysis of the frame, i.e. a fresh solution
of $\underline{L} = \underline{KX}$, is required. However the use of the theorems of
structural variation saves all such analyses which are at the rate
of at least one per hinge.

vi - The bending moments, axial forces and deflections due to
unit loading at location k* are used to modify the forces and
deflections due to external loading and other unit loadings. This
is done using equations (2.15), (2.16), (2.17). From equation
(2.15) the variation factor for each loading case (for each row
of matrix $\underline{M}$) is calculated as

$$r_{\alpha k}^{k} = \frac{Mk^*}{1-\mu_k} = \frac{M(k,2u-1)}{1-M(\overset{*}{k}+1,2u-1)} \qquad k = 1, f+1 \qquad 2.25$$

where f is the number of possible hinge locations, k*+1 is the row
which corresponds to the unit loading case for location k*, u is
the hinge number at k*. The $\overset{*}{k}$+1st row of each of the matrices $\underline{M}$,
$\overline{\underline{P}}$ and $\underline{X}$ are multiplied by $r_{\alpha k^*}^{k}$ and added to their k^{th} rows.

Having done the above operation, the matrices $\underline{M}$, $\overline{\underline{P}}$ and $\underline{X}$ now
represent the bending moments, axial forces and deflections of
the structure with a hinge at k*.

vii - For a further increase $\Delta\lambda = \lambda - \lambda_1$ in the load parameter the
current member forces and deflections are calculated as

$$MA^{\lambda}(\ell) = MA^{\lambda_1}(\ell) + \Delta\lambda \times M(1,\ell) \qquad \ell = 1,2n \qquad (a)$$

$$PA^{\lambda}(\ell) = PA^{\lambda_1}(\ell) + \Delta\lambda \times P(1,\ell) \qquad \ell = 1,n \qquad (b) \qquad 2.26$$

$$XA^{\lambda}(\ell) = XA^{\lambda_1}(\ell) + \Delta\lambda \times P(1,\ell) \qquad \ell = 1,3m \qquad (c)$$

where $MA^{\lambda}(1)$ represents the first end moment of member 1 under λ
while $MA^{\lambda_1}(3)$ is the first end moment of member 3 under the load
factor λ_1. Again each hinge location is considered in turn. The
load factor at which a plastic hinge develops in that location is
calculated by equating the current bending moment to the fully
plastic moment of the section. Thus

$$\lambda_2 = \lambda_1 + \frac{Mp^k - MA(\ell)}{M(1,\ell)} \qquad 2.27$$

The lowest of these load factors is chosen as the load factor
which causes the next plastic hinge in the frame.

viii - The current member forces and deflections are calculated
from equations 2.26 by substituting $\Delta\lambda = \lambda_2-\lambda_1$ and $\lambda = \lambda_2$. If a
sufficient number of hinges have been developed to turn the
structure into a mechanism the process is stopped. Otherwise λ_2
is taken as λ_1 and the steps (v), (vi), and (vii) are repeated
until failure takes place.

2.g Effect of Changing Material Properties:

The changes in material properties can be expressed in terms of cross-sectional properties. This makes it possible to apply the theorems of structural variation to study the effect of changing material properties on the overall behaviour of frames. Ignoring the effect of shear stress on the deformations, the slope-deflection equations for a plane frame member can be written as follows

$$
\underbrace{\begin{bmatrix} P_{ij} \\ S_{ij} \\ M_{ij} \\ M_{ji} \end{bmatrix}}_{\underline{P}} = \underbrace{\begin{bmatrix} \dfrac{EA}{L} & 0 & 0 & 0 \\ 0 & \dfrac{12EI}{L^3} & -\dfrac{6EI}{L^2} & -\dfrac{6EI}{L^2} \\ 0 & -\dfrac{6EI}{L^2} & \dfrac{4EI}{L} & \dfrac{2EI}{L} \\ 0 & -\dfrac{6EI}{L^2} & \dfrac{2EI}{L} & \dfrac{4EI}{L} \end{bmatrix}}_{\underline{k}} \underbrace{\begin{bmatrix} u_{ij} \\ v_{ij} \\ \theta_{ij} \\ \theta_{ji} \end{bmatrix}}_{\underline{z}} \qquad 2.28
$$

If the modulus of elasticity E of the member is changed to $(1+\alpha)E$ by an amount $\delta E = -\alpha E$, the matrix $\underline{k}$ then becomes $(1+\alpha)\underline{k}$. This is in fact equivalent to simultaneous changes in the area and the second moment of area of the member by $\delta A = -\alpha A$ and $\delta I = -\alpha I$. Hence the problem is reduced to the member changing problem dealt by Saka[3].

2.h Examples:

A number of examples have been solved either manually or by using the computer program described in chapter 6. The results were compared with those obtained conventionally. It was found that they are exact.

2.h.1 Example 1 :-

The portal frame shown in figure (2.6.a) was first analysed manually by means of the elastic-plastic analysis procedure given in section (2.f). The results were compared with those obtained by Majid[4].

To begin with the possible hinge locations were marked as shown in figure (2.6.b) and an elastic analysis of the frame was carried out under the unit loading cases shown in figures (2.7.a, b,c,d) together with the given external loads shown in figure (2.6.a). The resulting bending moment matrix $\underline{M}$ was constructed as follows:

	$M_{C'-C}$	$M_{C-C'}$		$M_{D'-D}$	$M_{D-D'}$		
$\cdots$	$\cdots$	$\cdots$	$\cdots$	$\cdots$	$\cdots$	Due to external loads
$\cdots$	-8.45732624	8.47713093		6.87290761	-6.90366542	
$\cdots$	0.999331102	-0.999331109	$\cdots$	-0.000662169	0.000662156	Due to unit loading in figure (2.7.b)
$\cdots$	-0.000061746	0.000662584	$\cdots$	0.998909912	-0.99890906	Due to unit loading in figure (2.7.c)

$$\underline{M} = 5 \text{ rows}$$

$$2 \times 8 = 16 \text{ Columns}$$

λ

λ/4 →

B ———— C ———— D

EI   EI

508 mm

EI   EI

$M_p = 9,27$ kNmm

A   E

254 mm   254 mm

a- Frame and loading

253.492   0.508   253.492   0.508

0.508

507.492

507.492

0.508
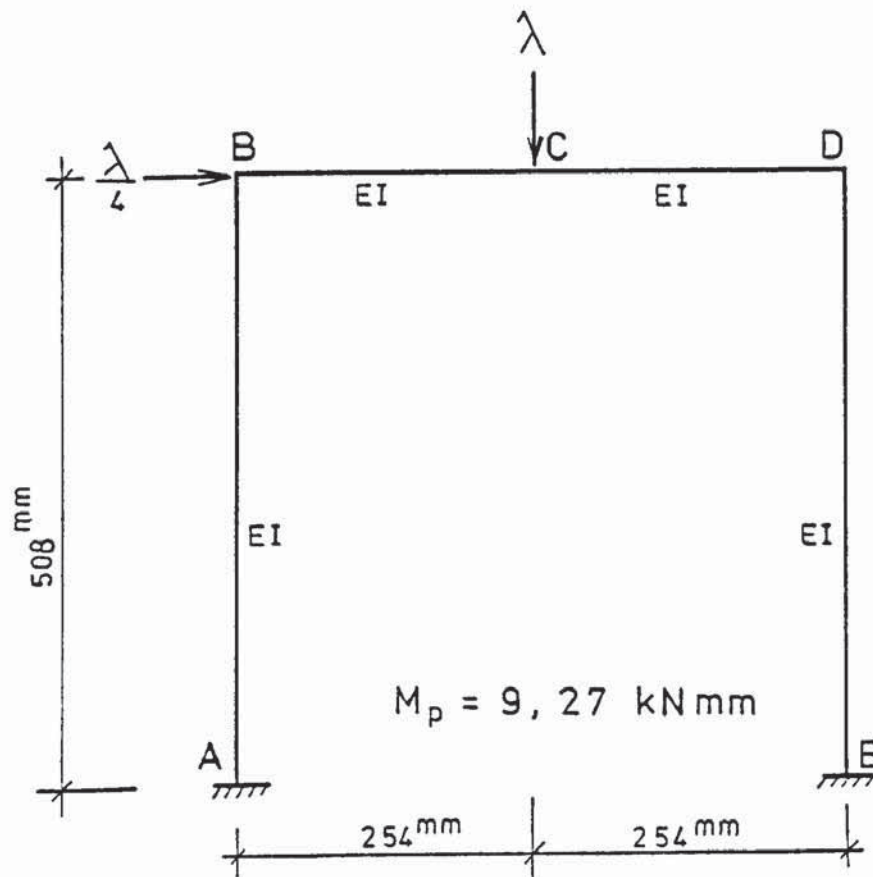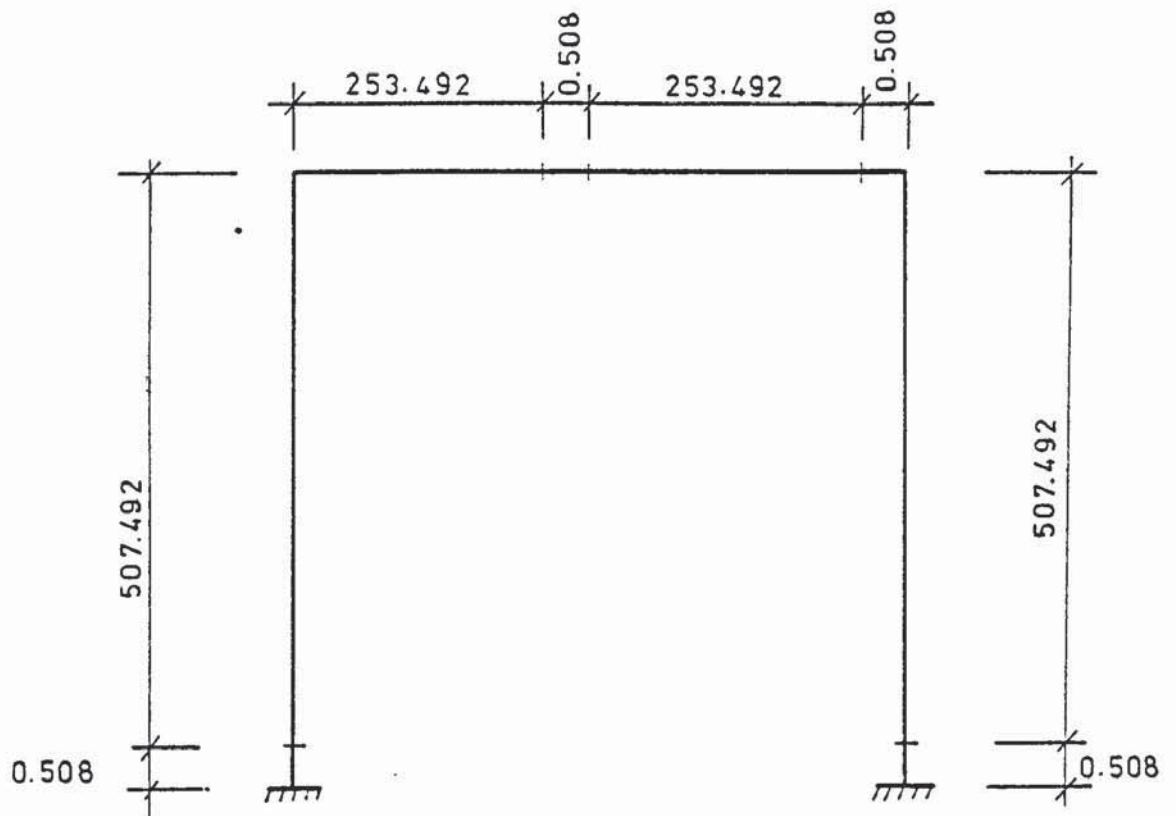
b- Members imposed into the expected hinge locations

FIGURE 2·6 : PORTAL FRAME AND LOADING
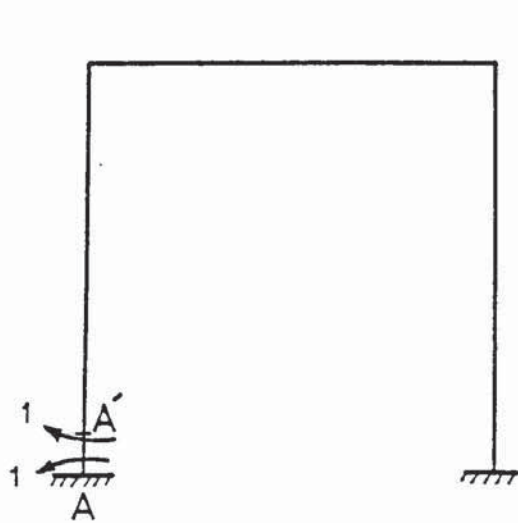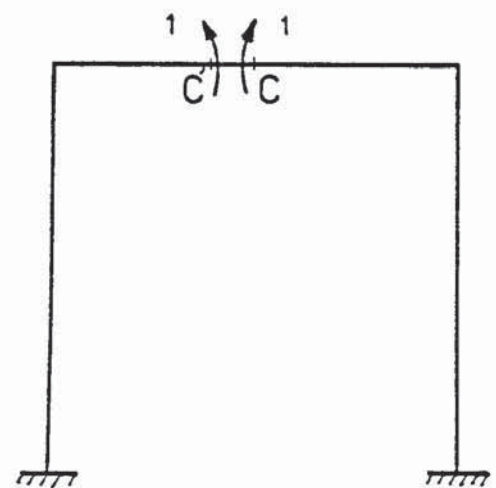
a- Unit loading at A-A'   b- Unit loading at C-C'
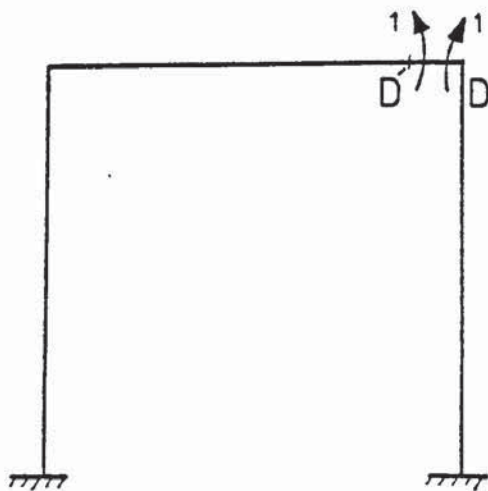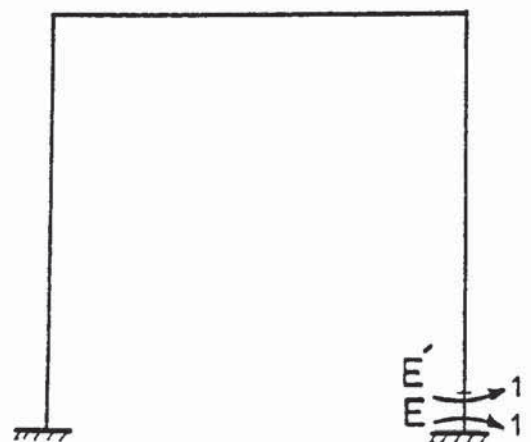
c- Unit loading at D-D'   d- Unit loading at E-E'

FIGURE 2.7: UNIT LOADINGS FOR THE PORTAL FRAME

The current bending moment matrix for $\lambda = 1$ is

$$MA^1 = [\cdots -8.4573 \quad 8.4771 \cdots 6.8729 \quad -6.9037 \cdots]$$

The small members A-A', C-C', D-D' and E-E' were considered in turn and a load factor at which a plastic hinge develops in each member was calculated from equation (2.24). The lowest load parameter is $\lambda_{C-C'} = 9.27/8.4771 = 1.0935, Mp = 9.27$. This causes the first plastic hinge in C-C'. The current bending moments at this load parameter were calculated as $\underline{MA}^{\lambda C-C'} = \lambda_{C-C'} \times \underline{MA}^1$. Thus

$$\underline{M}_A^{1.094} = [\cdots 9.2483 \quad 9.2700 \cdots 7.5157 \quad -7.5494 \cdots]$$

A hinge is now inserted at CC' as follows:

i - The vector of variation factors $\underline{r}_\alpha$ is constructed

$$\underline{r}_\alpha = \begin{bmatrix} -12673.7882 \\ \cdot \\ \cdot \\ \cdot \\ 0.99056 \end{bmatrix} \qquad \text{e.g. } r_\alpha(1) = -\frac{8.4771}{1-0.999331109} = -12673.7882$$

While calculating "r_α" the value of μ_k should always be positive, if not the unit loading pattern is multiplied by (-1). This can be done by multiplying the variation factor by -1 and taking the value of μ_k to be positive.

ii - The new bending moments can be calculated from equation (2.16) e.g. $M(1,12) = M_{DD'} = -6.9037-12673.7882\times0.000662156 = -15.2957$ and the new $\underline{M}$ matrix is constructed as

	$M_{C'C}$	$M_{CC'}$		$M_{D'D}$	$M_{DD'}$		
$\cdots$	0	0	$\cdots$	15.2648	-15.2957	$\cdots$	External loading
$\underline{M} =$							Unit loading for C-C' is cancelled
$\cdots$	0	0	$\cdots$	0.9995658	-0.999565	$\cdots$	Unit loading for D-D'

Hinge No	PRESENT THEORY		CONVENTIONAL	
	LOAD FACTOR	LOCATION	LOAD FACTOR	LOCATION
1	1.09	C-C'	1.09	C-C'
2	1.21	D-D'	1.20	D-D'
3	1.28	E-E'	1.28	E-E'
4	1.46	A-A'	1.46	A-A'

TABLE 2.1: COMPARISON OF THE ELASTIC-PLASTIC ANALYSIS RESULTS

FOR A PORTAL FRAME SHOWN IN FIGURE (2.6)

The process is repeated with A-A', D-D' and E-E' and a load factor
at which a plastic hinge develops in each location is calculated
from equation (2.27). The lowest of these load factors is chosen.
This was found to be for a hinge at D-D'.

This load factor is

$$\lambda_{D-D'} = 1.0935 + \frac{-9.27 - (-7.5494)}{-15.2957} = 1.206$$

where the value of actual moment at $\lambda = 1.0935$ is -7.5494.
The procedure was continued until a mechanism developed. The load
factors at each hinge formation are given in table (2.1) together
with those obtained using the conventional method.

2.h.2 Example 2 :

The irregular frame of figure (2.8) was originally designed
by Horne and Majid[5]. The cross-sectional properties and external
loading are shown in table (2.2) and in figure (2.8). The yield
stress was given as 16 tons/in^2 (0.247 kN/mm^2) while the modulus
of elasticity was 207.0 kN/mm^2. Altogether 21 hinges developed
when a mechanism condition was recorded. The load-deflection
diagram and the order of hinges obtained by present method are
shown in figure (2.9). The order of hinges obtained by Horne and
Majid[5] are also shown in boxes. Although there are some
discrepancies observed in the order of hinges, both analyses
predicted the same failure mechanisms and the same load factor at
collapse. The elastic-plastic failure load factor obtained by
Horne and Majid by taking the axial forces into account was 1.58
which is 9.2% below the failure load factor obtained by neglecting
these forces.

FIGURE 2.8: IRREGULAR FRAME AND LOADING
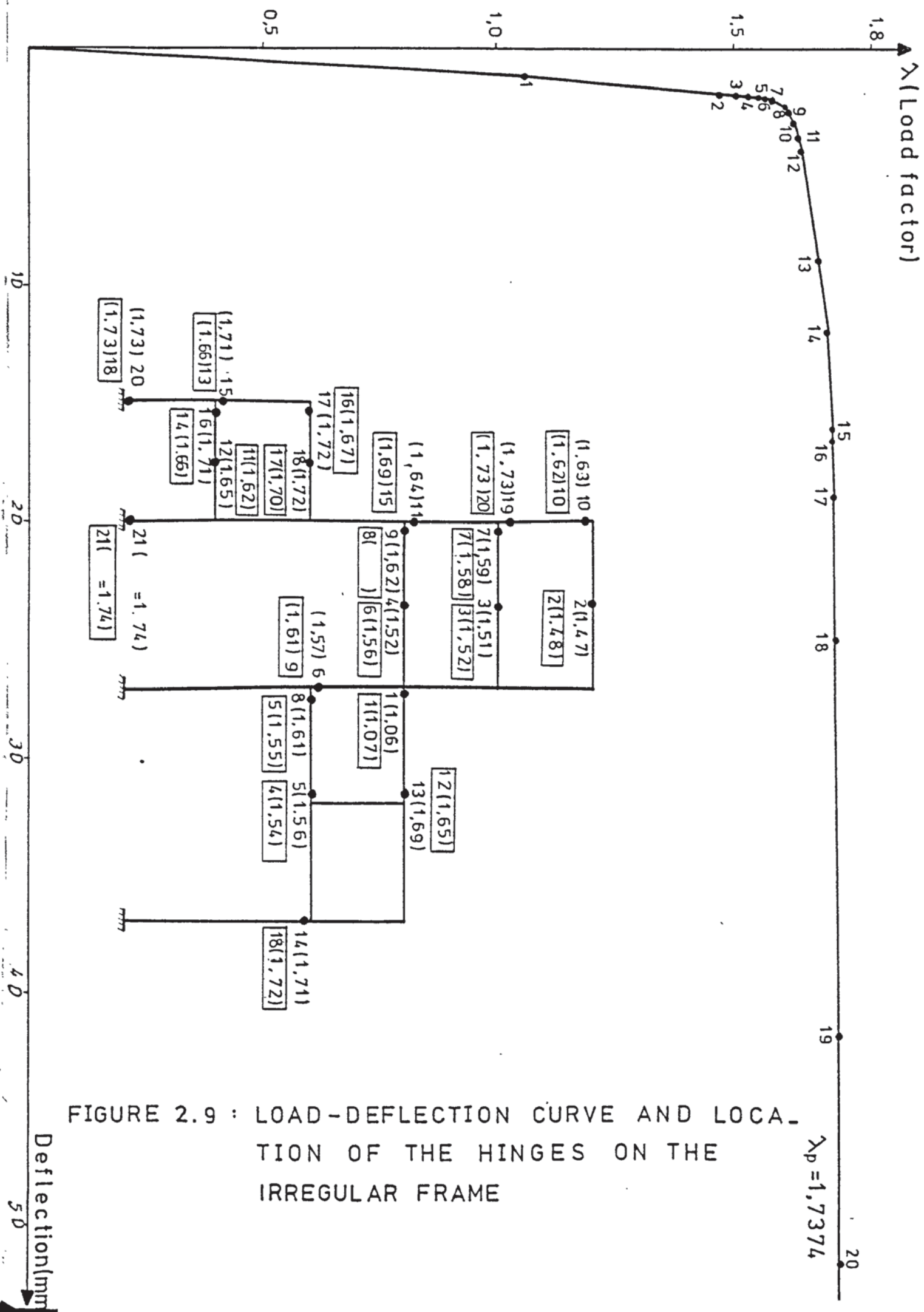
FIGURE 2.9 : LOAD-DEFLECTION CURVE AND LOCA-
TION OF THE HINGES ON THE
IRREGULAR FRAME

	MEMBER NO:	SECTIONS
BEAMS	2	10 x 5¾ x 21 UB
	5	8 x 5¼ x 17 "
	8,17	12 x 6½ x 27 "
	11	18 x 7½ x 55 "
	13	10 x 5¾ 25 "
	20	8 x 5¼ x 20 "
COLUMNS	1,4,14	6 x 6 x 20 UC
	3,6,7,16,18	8 x 8 x 31 "
	9,15	8 x 8 x 40 "
	10	12 x 12 x 65 "
	12	10 x 10 x 49 "
	19,21	6 x 6 x 25 "

TABLE 2.2   SECTIONS USED FOR THE IRREGULAR FRAME

2.h.3 Example 3:

To show the versatility of the theorems of structural variation, the braced portal no sway frame shown in figure 2.10 was considered. The dimensions, loading and cross-sectional properties are given in the figure. The topology of the frame was first changed by removing the members 1,2,9. Then the modulus of elasticity, the area, the second moment of area and the fully plastic moments of members AB and BC were doubled while those for member CD were halved. The derivative structure shown in figure 2.10-b was thus obtained. These operations were carried out by only using the initial analysis of the parent structure under the external loading and the unit load matrix. The forces and deflections of the parent structure due to unit load matrix given by equation (2.14) were also modified. Using these results the elastic-plastic analysis of the derivative structure was carried out. Altogether four hinges developed when a sway mechanism, shown in figure (2.10.b), developed at $\lambda = 1.571$. The load-deflection curve obtained from the analysis is given in figure 2.10.c. All these alterations as well as the elastic plastic analysis were the outcome of a single linear elastic analysis of the parent frame shown in figure 2.10.a. The rigid.plastic analysis of the final frame also gave $\lambda = 1.571$.

2.h.4 Example 4

The three storey, single bay braced no sway frame shown in figure (2.11.a) is subject to horizontal loads of 25 kN at joints H, F and 30 kN at joint D. The dimensions and cross-sectional properties are shown in the figure. The structure was initially analysed linearly. Members C-D, C-F, E-F, E-G, G-F, G-H were then

CROSS-SECTIONAL PROPERTIES

Section No	$A\,(m^2)$	$I\,(m^4)$	$M_p\,(kN{\times}m)$	$E\,(kN/mm^2)$
1	$11{,}01{\times}10^{-3}$	$83{,}74{\times}10^{-6}$	350,0	207,0
2	$10{,}44{\times}10^{-3}$	$320{,}58{\times}10^{-6}$	800,0	207,0
3	$36{,}6{\times}10^{-3}$	$878{,}43{\times}10^{-6}$	1200,0	2,07,0
1'	$22{,}02{\times}10^{-3}$	$167{,}48{\times}10^{-6}$	700,0	414,0
3'	$18{,}30{\times}10^{-3}$	$439{,}22{\times}10^{-6}$	400,0	103,5

λ (Load factor)

RIGID-PLASTIC $\lambda = 1{,}571$

$4\,(\dot{\lambda}=1{,}571)$
$3\,(\lambda=1{,}56)$
$2\,(\lambda=1{,}38)$
$1\,(\lambda=1{,}18)$

Sway at C(mm)

50   100   150   200

a – Parent structure

$200\lambda kN$

C
E_3
I_3
A_3
M_P3

B E_2, I_2, A_2, M_{P2}

E_1
I_1
A_1
M_P1

E

A

D

6,00 m   6,00 m

10,5 m

b – Derivative structure and hinge formation

$200\lambda kN$

C   1
$E_3/2$
$I_3/2$
$A_3/2$
$M_{P3}/2$

3   $2E_2$ etc.

B

$2E_1$
$2I_1$
$2A_1$
$2M_{P1}$

E

A   4

2D

c – Load-deflection curve of the derivative structure

FIGURE 2.10 · CHANGING TOPOLOGY AND ELASTIC–PLASTIC ANALYSIS RESULTS

λ(Load factor)

RIGID PLASTIC λ = 4,089

λ = 3,92

λ = 3,81

λ = 3,66

λ = 3,13

λ = 2,40

Section No	Area m²	I m⁴	Mp kN×m
1	0,00949	0,00023981	525,7
2	0,00683	0,00010119	295,2

$E = 207,0 \ kN/mm^2$

a- Parent structure

b-Derivative structure and order of hinges
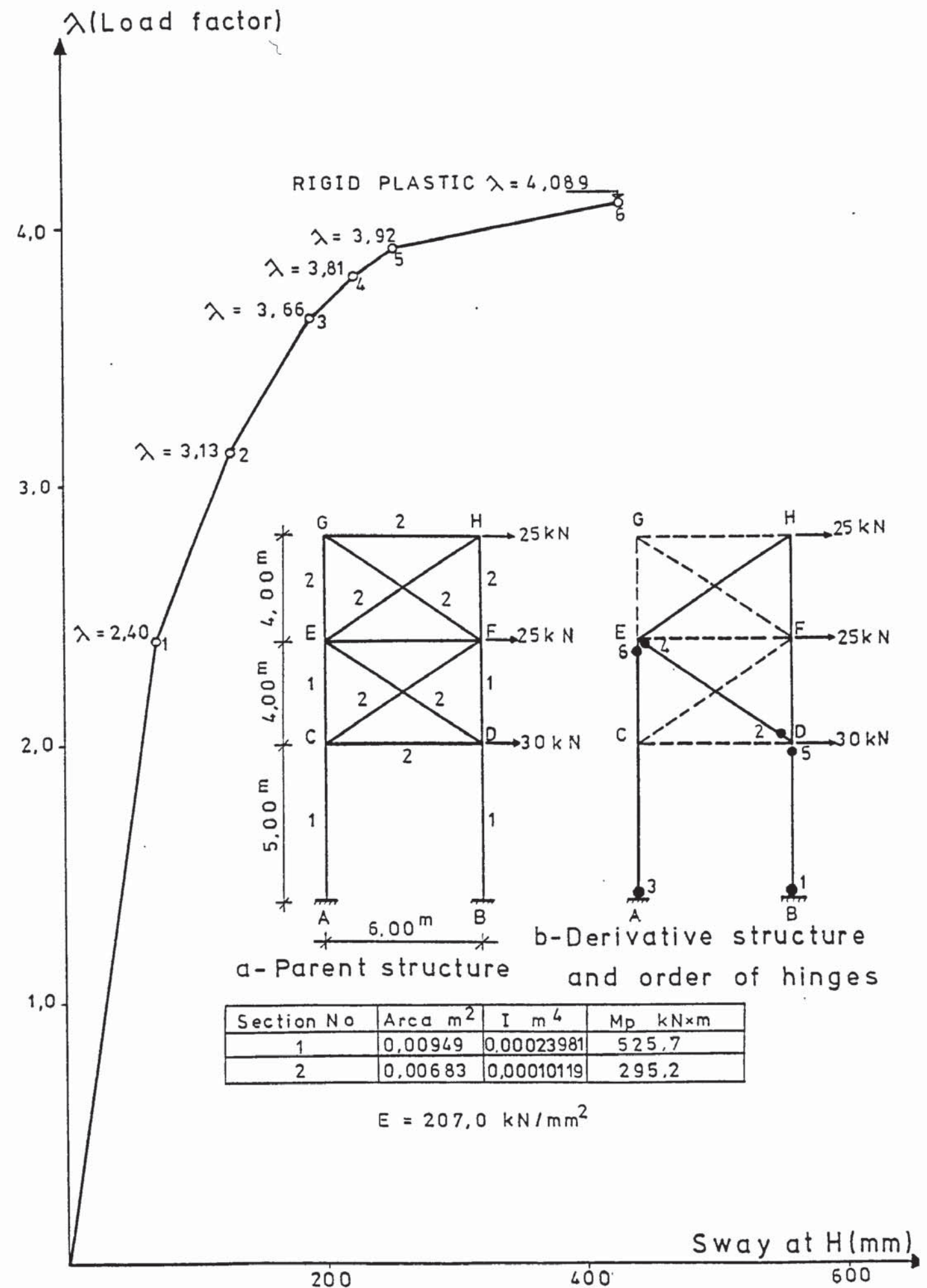
c-Load-deflection diagram of the derivative structure

Sway at H(mm)

FIGURE 2.11: A THREE STOREY AND SINGLE BAY STRUCTURE

removed and the derivative structure shown in figure 2.11.b was obtained. The solutions of this structure under external loads and the unit load matrix given by equation (2.14) were used to carry out the elastic-plastic analysis and the load deflection curve shown in figure (2.11.c) was obtained. The failure load factor was found to be equal to the rigid-plastic failure load factor of 4.083.

It is interesting to note that in this example six plastic hinges formed instead of four which are sufficient for a sway mechanism. Nonetheless, the load factor at failure had not reduced below that given by the rigid-plastic analysis with four hinges in columns AE and BD.

CHAPTER 3

NONLINEAR MOMENT CURVATURE ANALYSIS

3.a Introduction:-

Many methods have been suggested in the past (7,8,9,10,11,12)
for the nonlinear analysis of frames by using some form of
simplifications of the general nonlinear stress-strain curve shown
in figure (3.1.a). Most of these methods are either cumbersome or
costly for most practical purposes. The principal aim of this
chapter is to present methods of analysis which are simple in
concept, easier to use and fairly accurate.

Firstly, by directing the focus of attention to the nonlinear
material properties only, ignoring the stability effects, a
nonlinear method based on the theory of structural variation is
described. The procedure is also applied to the strain hardening
analysis of steel frames and the encountered problems are discussed.
Secondly reinforced concrete frames which are highly nonlinear
even in the elastic range, are dealt with. The application of
compensating loads (defined in chapter 2) to the failure load
analysis of concrete frames is then studied. Under the light of
this study, an incremental load factor method is given. This
method can also be used for the analysis of frames up to a given
load factor. The effect of axial loads are taken into account as
well as non-proportionally increasing external loads. Finally
some experimental structures are analysed by the proposed methods
to demonstrate their reliability.

3.b Nonlinear moment-curvature diagrams:-

Consider that the cross-section of a member is that shown in
figure (3.2). From strength of materials, the force equilibrium
equation along Z axis and the moment equilibrium equation about
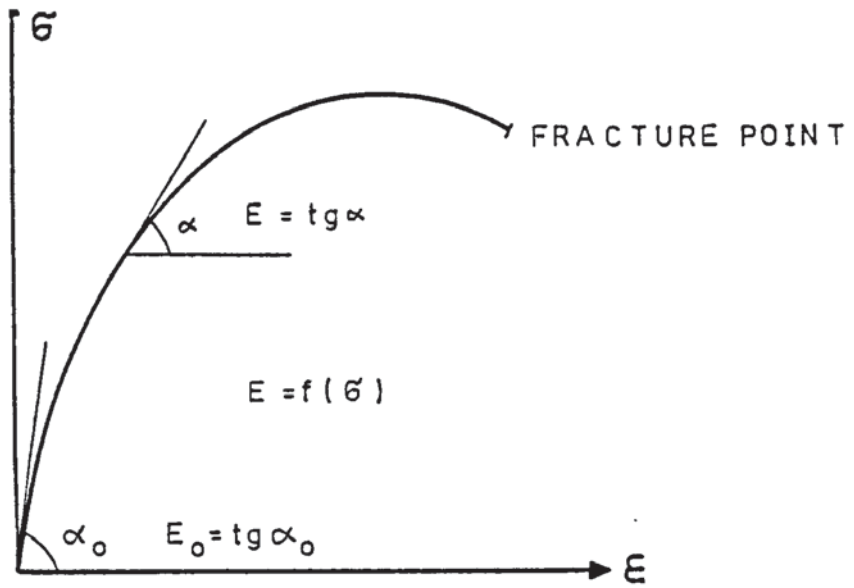
a-Nonlinear Stress-Strain Diagram
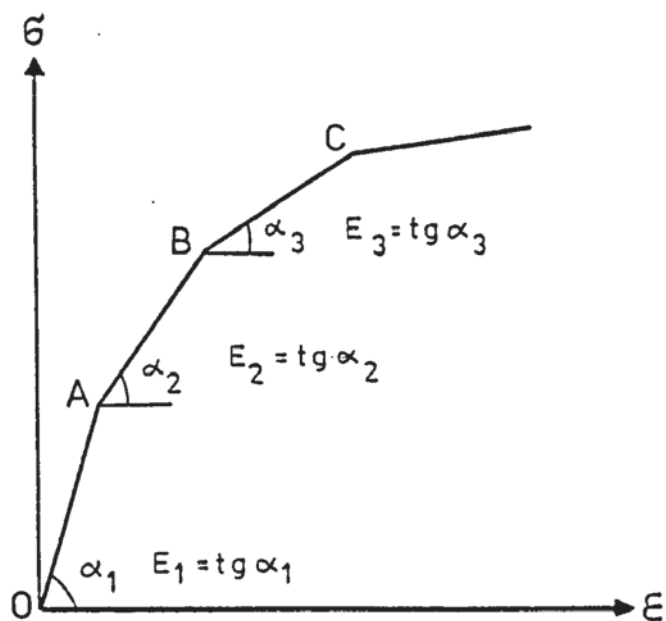
b-Piecewise Linear Stress-Strain Diagram
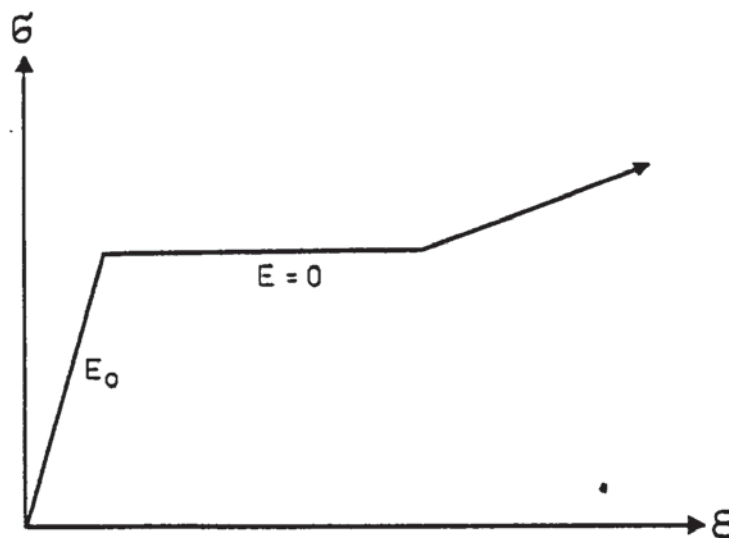
c-Elastic-Plastic Strain Hardening
Stress-Strain Diagram

FIGURE 3.1: VARIOUS STRESS-STRAIN DIAGRAMS
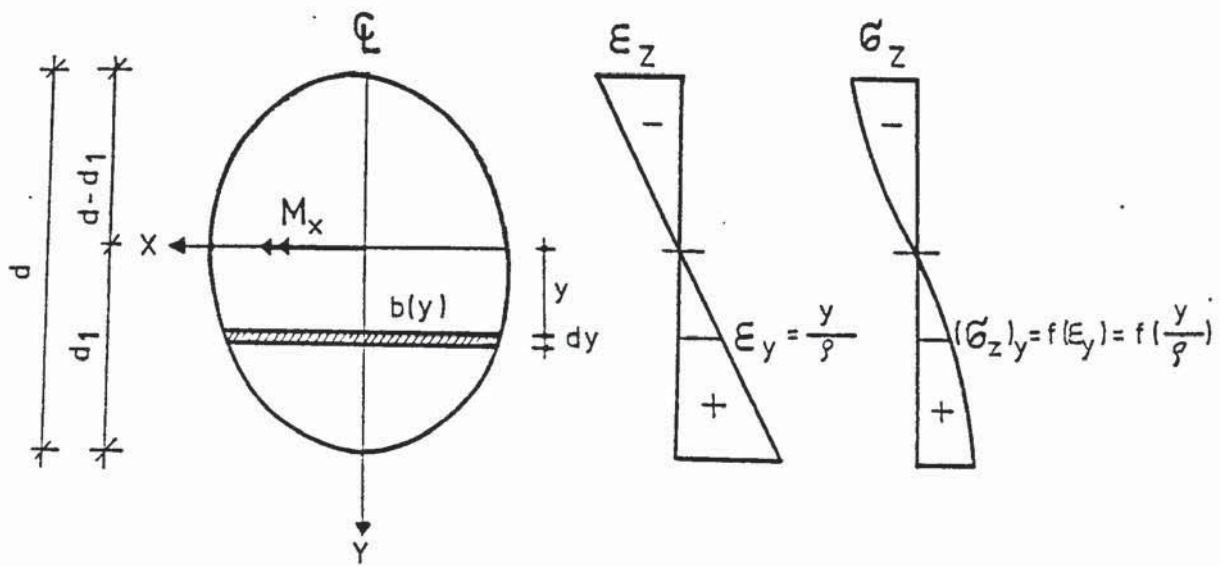
a- Cross Section   b-Strain Diagram   c- Stress Diagram
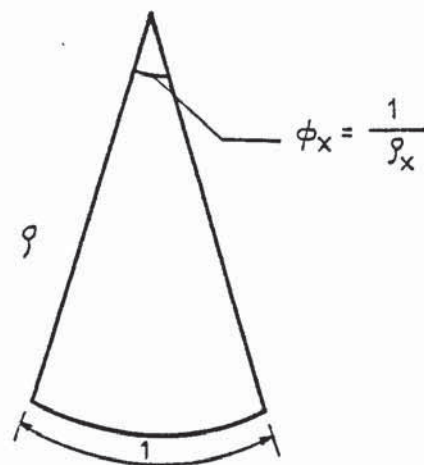
d- Curvature

FIGURE 3.2: A UNISYMMETRICAL CROSS-SECTION
SUBJECT TO BENDING

X axis are:

$$-(d-d_1)\int^{d_1}_{y} f(\tfrac{y}{\rho})\; b\,(y)\; dy = 0$$

$$-(d-d_1)\int^{d_2}_{y} f(\tfrac{y}{\rho})\; y\; b(y)dy = M \qquad\qquad 3.1$$

where d is the depth of the section, M is the bending moment while d_1 and $d-d_1$ are the distances of the compression and the tension faces from the neutral axis, respectively. ρ is the radius of curvature and $\tfrac{y}{\rho}$ represents the strain at a distance y from the neutral axis. $f(\tfrac{y}{\rho})$ is the stress-strain relationship of the material.

Once the unknowns d_1 and ρ are obtained from equations (3.1) for various values of M, the values of curvature $(\tfrac{1}{\rho})$ can be plotted against M to obtain the moment-curvature diagram of the section.

3.c Behaviour of Frames with Nonlinear Materials:-

In any frame, the bending moments vary along the members. This causes variations in the curvatures and thus in the flexural rigidity (EI) of the members. As the loads are increased, the overall stiffness of the frame as well as the individual stiffnesses of its members vary accordingly. Hence the conventional linear elastic method is incapable of predicting the actual behaviour of such a frame. In many cases, even the elastic-plastic methods are not suitable. In general, the constitutive equations i.e. the stress-strain and the moment-curvature relationship should be written in nonlinear form, then the equilibrium and the compatibility equations should be written accordingly. This is laborious and unsuitable for automatic programming.

Instead, the following technique is suggested here. The stress-strain and the moment-curvature diagrams are approximated by
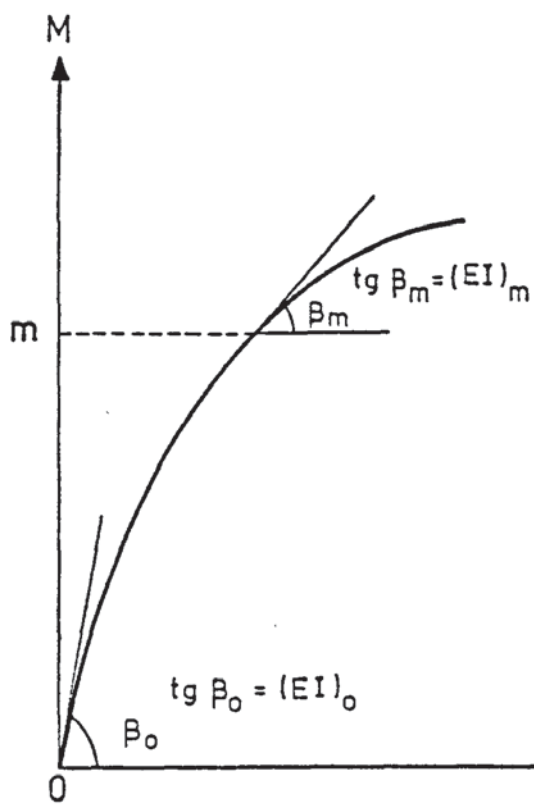
a- Nonlinear M-C Diagram
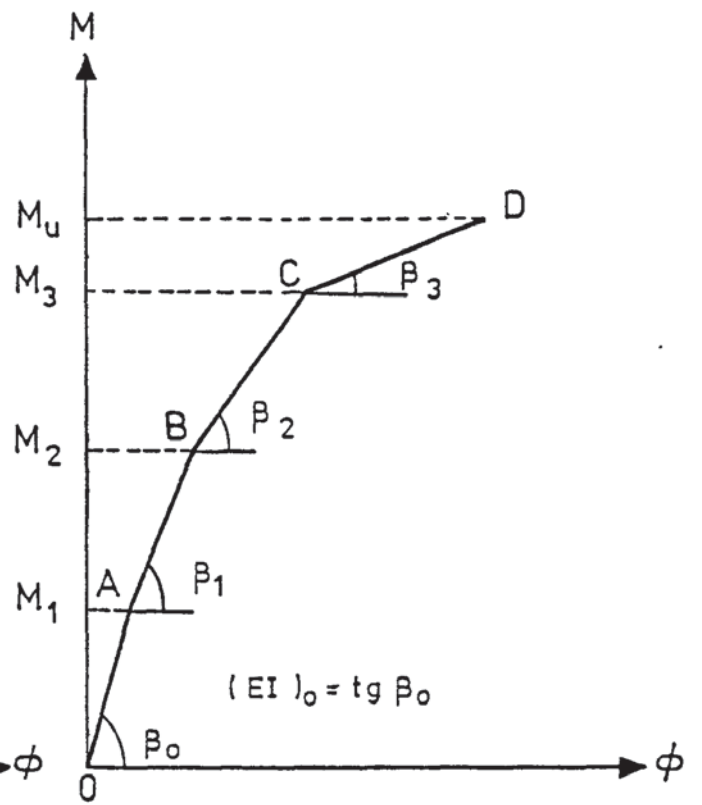
b- Piecewise Linear M-C Diagram
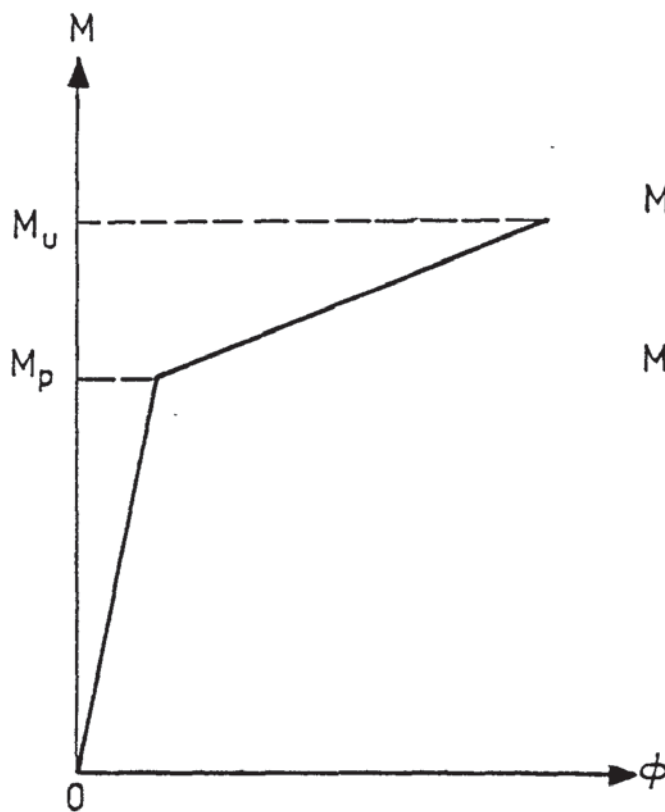
c- Elastic-Strain Hardening M-C Diagram (bilinear)
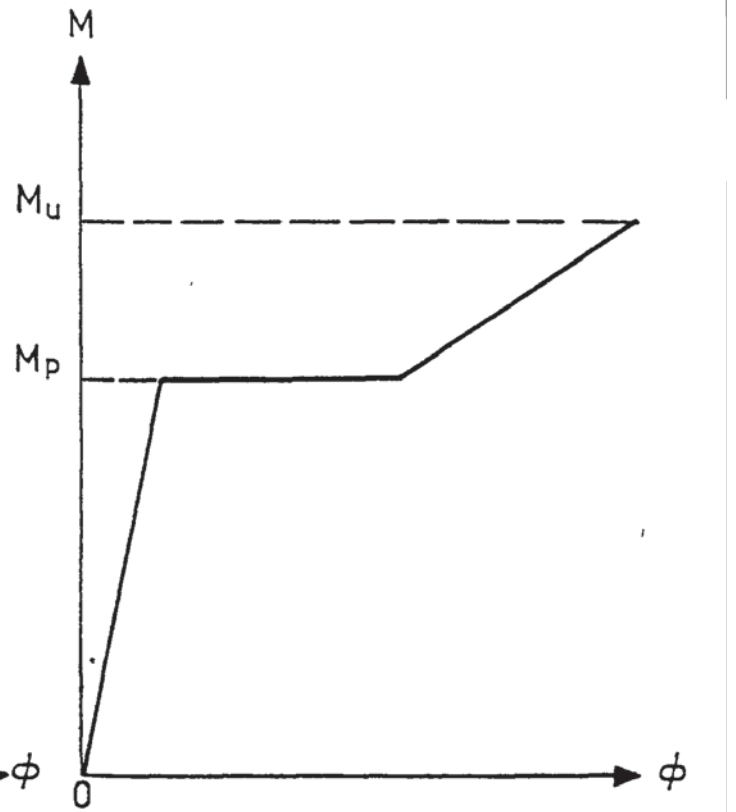
d- Elastic-Plastic Strain Hardening M-C Diagram (trilinear)

FIGURE 3.3: MOMENT-CURVATURE DIAGRAMS

straight lines. These are shown as OA, AB, etc. in figures (3.1.b) and (3.3.b). The points A, B, C, D etc are hereinafter called "critical points". The frame is analysed linear elastically once, with the initial values of EI for each member. The lowest load factor at which a critical point is reached on σ-ε and M-C diagrams of any member is then found iteratively. The flexural rigidity (EI) or the axial stiffness (EA) of that member is altered to the next value on the M-C or σ-ε diagram. The frame is reanalysed with new (EI) or (EA) value and further critical points are detected until a given load factor is reached or until failure occurs.

Using the theorems of structural variation a single initial linear-elastic analysis is sufficient to trace the behaviour of the frame up to failure. This is particularly true in the case of steel frames analysed taking the effect of strain hardening. In the case of reinforced concrete frames, however, it was found that ill conditioning develops once the EI values of several members are reduced. In the case there comes a stage when several members are about to reach their critical points. Once one of these members is selected for stiffness alteration, the frame becomes too weak to carry the applied loads. This results in a forecast of the next critical point somewhere in the frame but under reduced loading. Hence drifting takes place in the load deflection diagram. Further research is required to overcome this difficulty.

The effect of nonlinearity in the axial deformations is not as important as that of bending deformations. Hence this effect is ignored in the nonlinear analysis technique described in the following section.

3.d The Nonlinear Moment - Curvature Analysis:-

The steps for the method of analysis proposed here are as follows.

i - Construct the moment-curvature diagrams of the members and simplify them by a series of linear segments as shown in figure (3.3.b) and tabulate the critical moments and the regional flexural rigidity (EI) values.

ii - The compound load matrix[L C]is constructed in such a manner that for each member, matrix C contains a couple of unit loads as given by equations (2.11) and (2.12). On the other hand, L contains the externally applied loads.

iii - The structure is then analysed under the compound load matrix [L C] and the bending moments, the axial forces and the deflections are calculated in matrix form as M, $\bar{P}$ and X in the manner described in section (2.c). The dimensions of these matrices are (2n+1) x 2n for M, (2n+1) x n for $\bar{P}$ and (2n+1) x (3m+h) for X. Where n is the number of members, m is the number of joints and h is the number of real hinges that may be present in the frame.

iv - The equivalent moment for each member is calculated and the matrix M_E is constructed. It was mentioned earlier that because the bending moment along a member is not constant, its curvature varies from point to point and hence EI varies along the member. This is shown in figure (3.4). However in the linear elastic analysis, it is assumed that EI is constant along each prismatic member. To overcome this difficulty, an equivalent $\overline{EI}$ is described for each member. This corresponds to the constant bending moment along the member, covering an area, which is equivalent to the area under the actual bending moment diagram of the member. Since the external loads are applied to the joints only, the bending moment   -
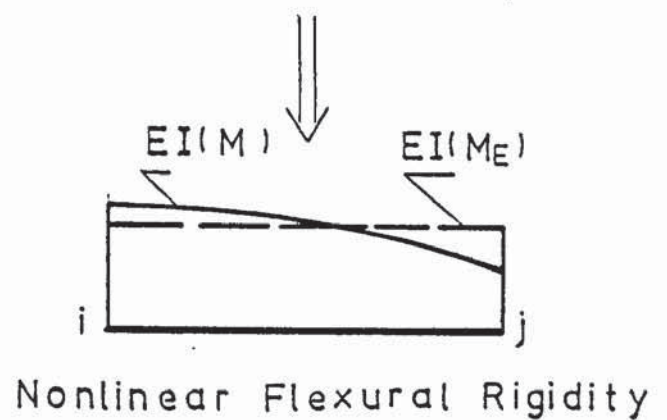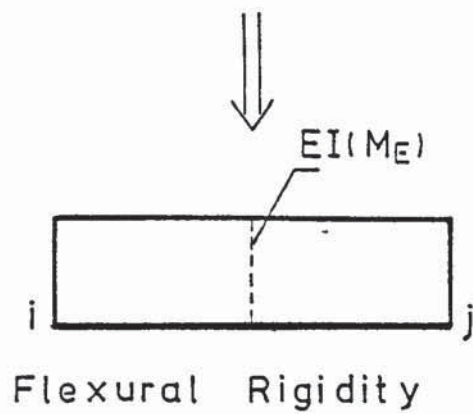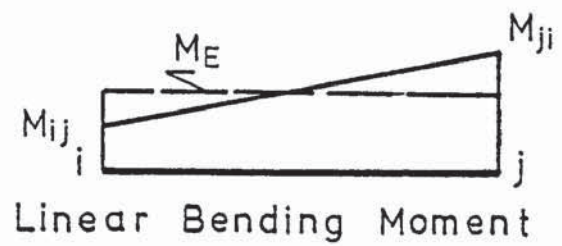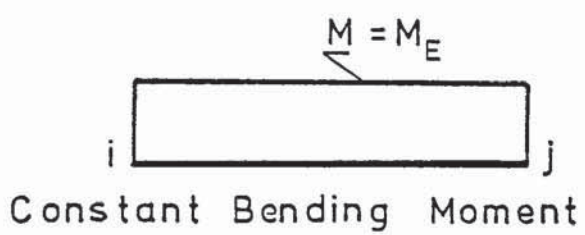
FIGURE 3·4: BENDING MOMENT AND FLEXURAL RIGIDITY
DIAGRAMS

varies linearly along a member. Hence the "equivalent bending moment" M_E for each member is the average of the end moments, i.e.

$$M_E = (\mid M_{ij} \mid + \mid M_{ji} \mid)/2 \qquad 3.2$$

where M_{ij} and M_{ji} are the bending moments at ends i and j of the member. It is necessary to mention that this is an approximation and assumes that the bending moment at end i due to a unit rotation at end j is equal to the bending moment at end j due to the unit rotation at end i. This can only be true when the (EI) diagram is symmetrical in the member.

(v) - The actual bending moment MA, axial force PA and deflection XA matrices are constructed in the same manner as explained in (2.f.iv).

(vi) - As the loads increase, the initial stiffness of a frame remains constant until the equivalent moment of one of the members reaches the first critical point on its moment-curvature diagram. The load factor λ which causes this is calculated for any member k as:

$$\lambda_k = \frac{DM(1,k)}{M_E(k)} \qquad 3.3$$

where DM (1,k) is the first critical moment. Considering all the members, let λ, be the lowest and let this correspond to member k*. The actual forces, equivalent moments and deflections due to this load factor are found by multiplying the matrices MA, PA, ME and XA by λ_1.

vii - The flexural rigidity of member k* is now altered to that given by the next portion of its M-C graph. Equation (2.15) is used to calculate the first end variation factor r_α^F for each load case in turn. Here M_k becomes M (1, 2k*-1) and μ_k becomes M(2k*,2k*-1). Equations (2.16) are then used for the first step modification of the member forces and deflections and the matrices

$\underline{M}$, $\overline{P}$ and $\underline{X}$ are altered to become $\overline{M}$, $\overline{P}'$ and $\overline{X}$.

For the second step modification, the variation factor r_α^s is calculated for each load case by using equation (2.15) with M_k becoming $\overline{M}(1,2k^*)$ and $\mu_k = \overline{M}(2k^*+1,2k^*)$. Using equations (2.16) again the new member forces and joint deflections $\underline{M}^n$, $\overline{P}^n$ and $\underline{X}^n$ are obtained. These are the axial forces, bending moments and joint deflections of the frame, with member k* having a new flexural rigidity. These will be used to iterate towards the next load factor, corresponding to a new critical point on the M-C diagram of one of the members.

viii - As the load factor is further increased, the actual forces and deflections are obtained by superposition. The equivalent moment for each member is obtained by combining equations (2.26.a) and (3.2) to give

$$M_E^\lambda(k) = M_E^{\lambda_1}(k) + (\lambda-\lambda_1) \frac{|M^n(1,2k-1)|+|M^n(1,2k)|}{2} \qquad 3.4$$

The next critical load factor for each member is calculated similarly. The load factor λ_k is calculated from:

$$\lambda_k = \lambda_1 + \frac{2[DM(q,k) - M_E^{\lambda_1}(k)]}{|M^n(1,2k-1)|+|M^n(1,2k)|} \qquad 3.5$$

where q refers to the order of the next critical point. This process is continued until the load factor applied to the frame reaches a specified value λ_G. For each iteration, equation (2.26) is used with $\Delta\lambda$ as the difference of two successive critical load factors. For a complete failure load analysis of a frame λ_G is set to a very large figure.

3.e Strain hardening analysis :-

The rigid plastic and elastic-plastic approximations are commonly used to represent the moment-curvature diagrams of steel

sections. However they both ignore the strength provided by strain hardening, and consequently the relevant theories underestimate the load-carrying capacity of steel structures in which the instability effects are small. The rigid plastic and elastic-plastic theories also assume that the plastic hinges occur at discrete sections while the rest of the structure remaining elastic. This assumption is not realistic since plasticity spreads away from a hinge as the material strain hardens.

A considerable amount of research has been carried out (7,8,11,12) in order to find a rational method of analysis which includes the effect of strain hardening. As an extension to Horne's[11] work, the method of analysis proposed by Davies[12] may be regarded as the most suitable. Davies considered strain hardening as well as instability prior to failure. However, he assumed the moment-curvature diagram to be bilinear as shown in figure (3.3.d). He also depended on Horne's strain hardening factor "k", which has to be determined experimentally. There was no limit imposed by Davies to restrict the plastic deformations in a section and total failure was defined by the complete loss of stiffness. In reality a section in a frame may itself fail after a finite amount of plastic deformation, and this may happen before a complete overall failure of the frame takes place.

The nonlinear moment-curvature analysis presented in section (3.d) can be easily utilised to carry out elastic-plastic analyses of frames with strain hardening effects. Although the moment-curvature diagrams can generally be constructed in the manner described in section (3.b), the tables and charts given by Hrennikoff[7] for universal beam sections can be used to reduce

the amount of work involved in this step. The moment-curvature diagrams are then represented by a series of straight lines. The spread of plasticity is catered for by inserting a series of small members in the vicinity of each expected hinge location. During the analysis, whenever plasticity is developed in one of these members, its flexural rigidity is reduced, thus enlarging the plastic region.

This treatment obviously increases the length of the analysis and consequently the computer time. To avoid this, these small members can be replaced by a single member whose length is a specified percentage of the length of the actual structural member. The validity of this assumption will be studied by reference to some examples, and suggestions will be made to try to indicate ways of reducing the loss of accuracy.

The plastic hinges develop and spread in discrete regions, the load factors being predicted for these regions only. The rest of the frame is disregarded in a manner similar to the elastic-plastic analysis given in chapter 2. This treatment is adopted to save computing time and also because a sufficient allowance is made for the spread of plasticity.

3.f Examples:-

To examine the analyses proposed so far in this chapter a number of examples were solved, the results of which are presented here.

3.f.1 The portal frame:-

Consider the portal frame shown in figure (3.5.a). All the members of the frame are of the same cross sectional properties with the moment-curvature relationship given by:

10 ton

8,0 ^{m}

4,0 ^{m} 4,0 ^{m}

a- Structure and Loading

M(tm)

16

12

8

4

$\phi\left(\frac{1}{m}\right)$

$\frac{20}{EI}$ $\frac{40}{EI}$ $\frac{60}{EI}$
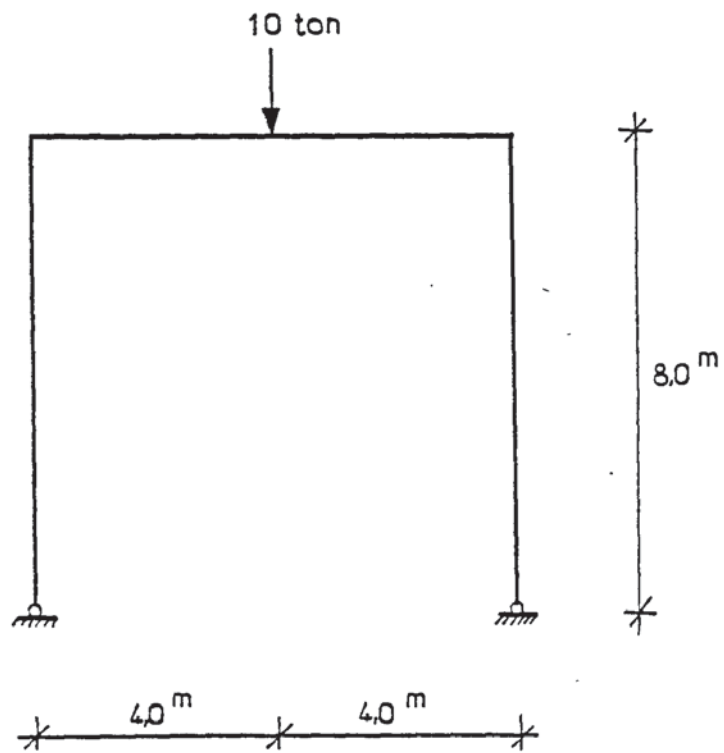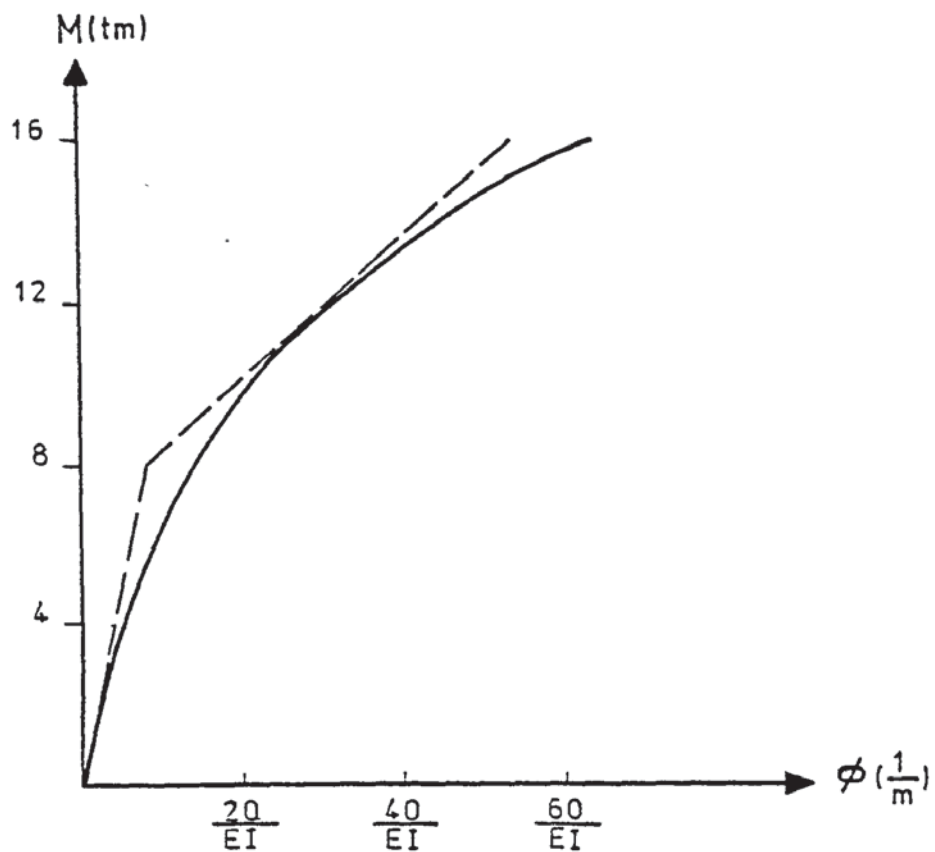
b- Moment- Curvature Diagram

FIGURE 3·5

	M_{BF} (Ton.m)	M_{FB} (Ton m)	max % diff.
Çakı.roğlu & Çetmeli	7.152	12.848	Assumed to be correct
Linear elastic analysis	6.00	14.00	16.1%
Bilinear M-C, no subdivision	7.110	12.890	0.6%
5 piece linear, no subdivision	7.176	12.824	0.33%
8 piece linear, members are halved	7.165	12.835	0.18%

(Rows 3–5 grouped under **PRESENT THEORY**)

TABLE 3.1   Comparison of results for the portal frame

$$\phi = \frac{16}{EI} [\frac{M}{16} + 3 (\frac{M}{16})^3]$$

This relationship was first approximated by two straight lines as shown in figure (3.6.b) and the frame was analysed manually. The members were treated without subdivision. The computer program described in the first part of chapter (6) was then utilised and the effects of finer piecewise linearisation of the M-C diagram and the subdivision of members were studied. The results are presented in table (3.1) and compared with those obtained by Cakiroglu & Cetmeli[10] who used a modified unit force method. It can be seen in table (3.1), that better results are obtained with finer subdivisions of the members and finer piecewise approximations of the moment-curvature diagram, while the roughest approximation is giving a maximum discrepancy of 0.6% in the bending moments.

3.f.2 Two Storey, Single Bay Portal frame:-

The frame ABCDEF shown in figure (3.6), was tested by Baker & Charlton[14] and was later analysed by Davies[12]. The beams and columns are 5"x3"x11 lb and 4"x3"x10 lb rolled steel joists respectively. Youngs modulus of elasticity E was taken as 211 kN/mm^2 (30000 kips/in^2), the yield stress σy was extracted from the work of Davies as 0.267 kN/mm^2 and the ultimate strain εu was assumed to be 0.065. The moment-curvature diagrams shown in figures (3.7) and (3.8) were obtained by using the method proposed by Hrennikoff[7].

Hrennikoff defined a parameter $\bar{m}$ which is independent upon the dimensions of the cross section but depends upon the stress-strain relationship for the material and a parameter $\bar{k}$ given as the ratio of the flange area A_f to half of the web area A_w. These were expressed in the form:

$$\bar{m} = {}_0\!\int^{\varepsilon_1} \sigma\varepsilon d\varepsilon + \bar{k}\,\sigma_1 \qquad\qquad 3.6$$
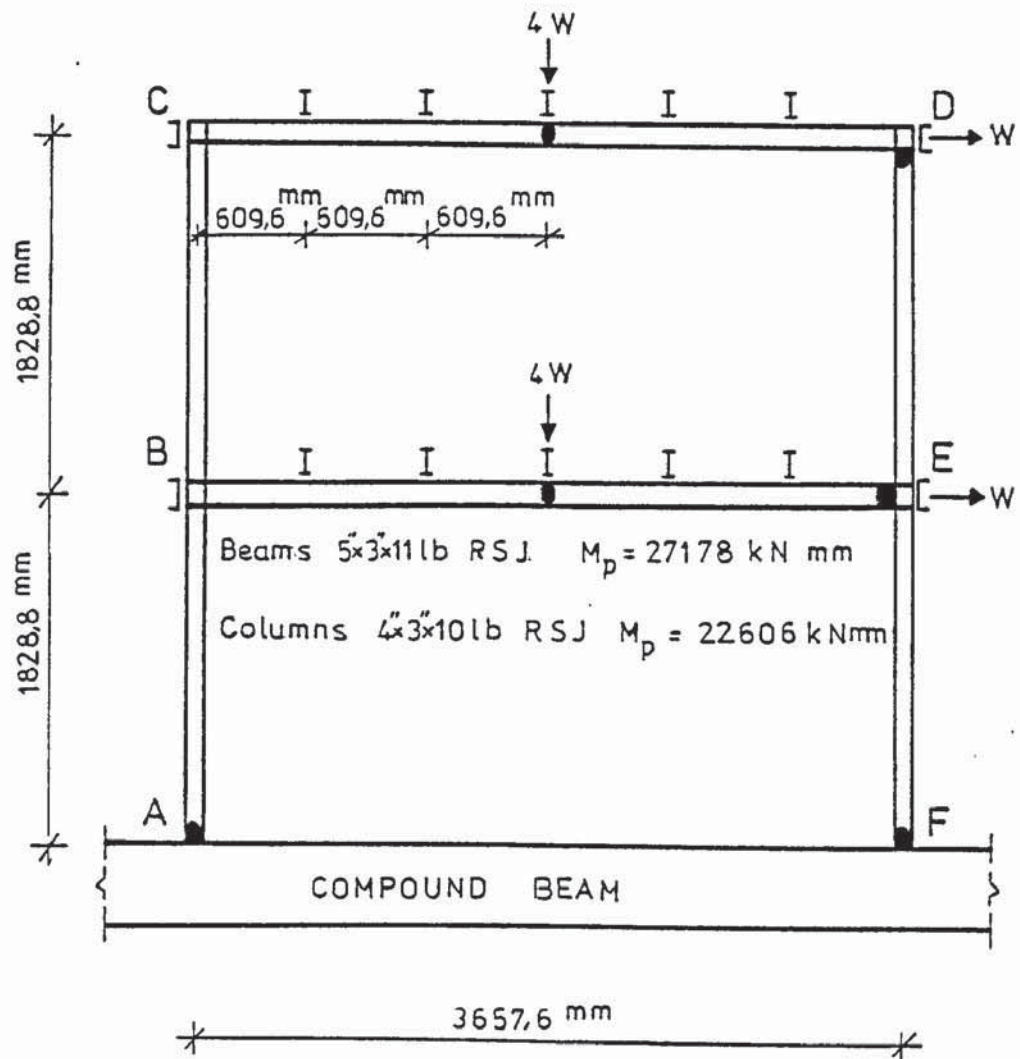
FIGURE 3.6: TWO STOREY PORTAL STRUCTURE AND LOADING

Within the figure:

4 W

C   I   I   I   I   I   D →W

1828,8 mm

mm   mm   mm
609,6 , 609,6 , 609,6

4 W

B   I   I   I   I   I   E →W

Beams 5×3×11 lb RSJ. M_p = 27178 kN mm

Columns 4×3×10 lb RSJ M_p = 22606 kN mm

1828,8 mm

A   F

COMPOUND BEAM

3657,6 mm

$\dfrac{2M}{A_wh}$ (kN / mm²)

CURVE OAB ⟶ BILINEAR
CURVE OABC ⟶ TRILINEAR

1,4

1,2

1,0

0,8 A   C
                                                          D
0,6   B

0,4

0,2

0,0
   O   0,01   0,02   0,03   0,04   0,05   0,06   0,07 $\dfrac{\phi \times h}{2}$
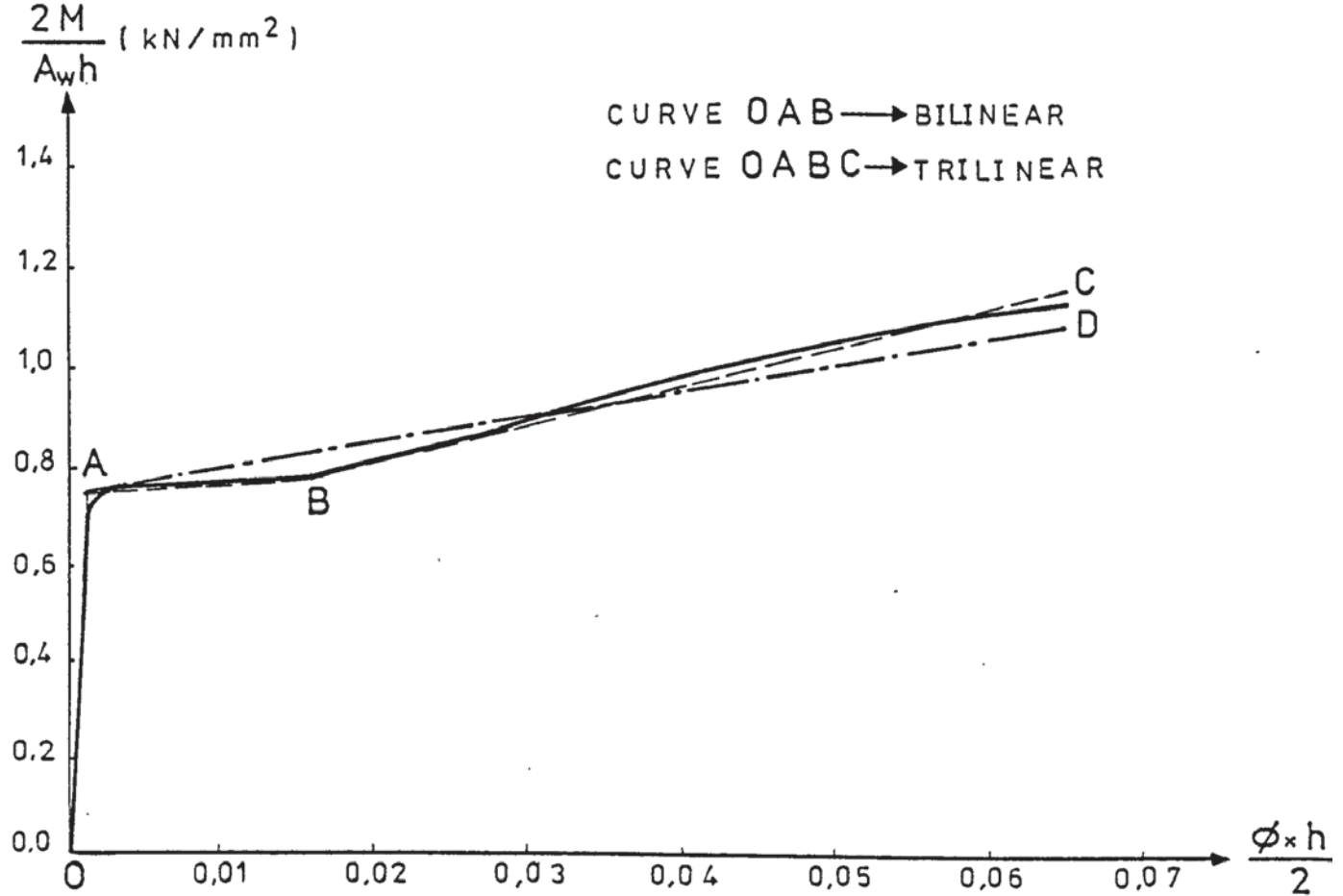
FIGURE 3.7: MOMENT-CURVATURE DIAGRAM FOR COLUMNS
MADE OF 4″× 3″×10 Lb. R.S.J.

$\dfrac{2M}{A_wh}$ (kN / mm²)

1,2   C
                                                          D
1,0

0,8 A

0,6   B

0,4

0,2

0,0
   O   0,01   0,02   0,03   0,04   0,05   0,06   0,07 $\dfrac{\phi \times h}{2}$
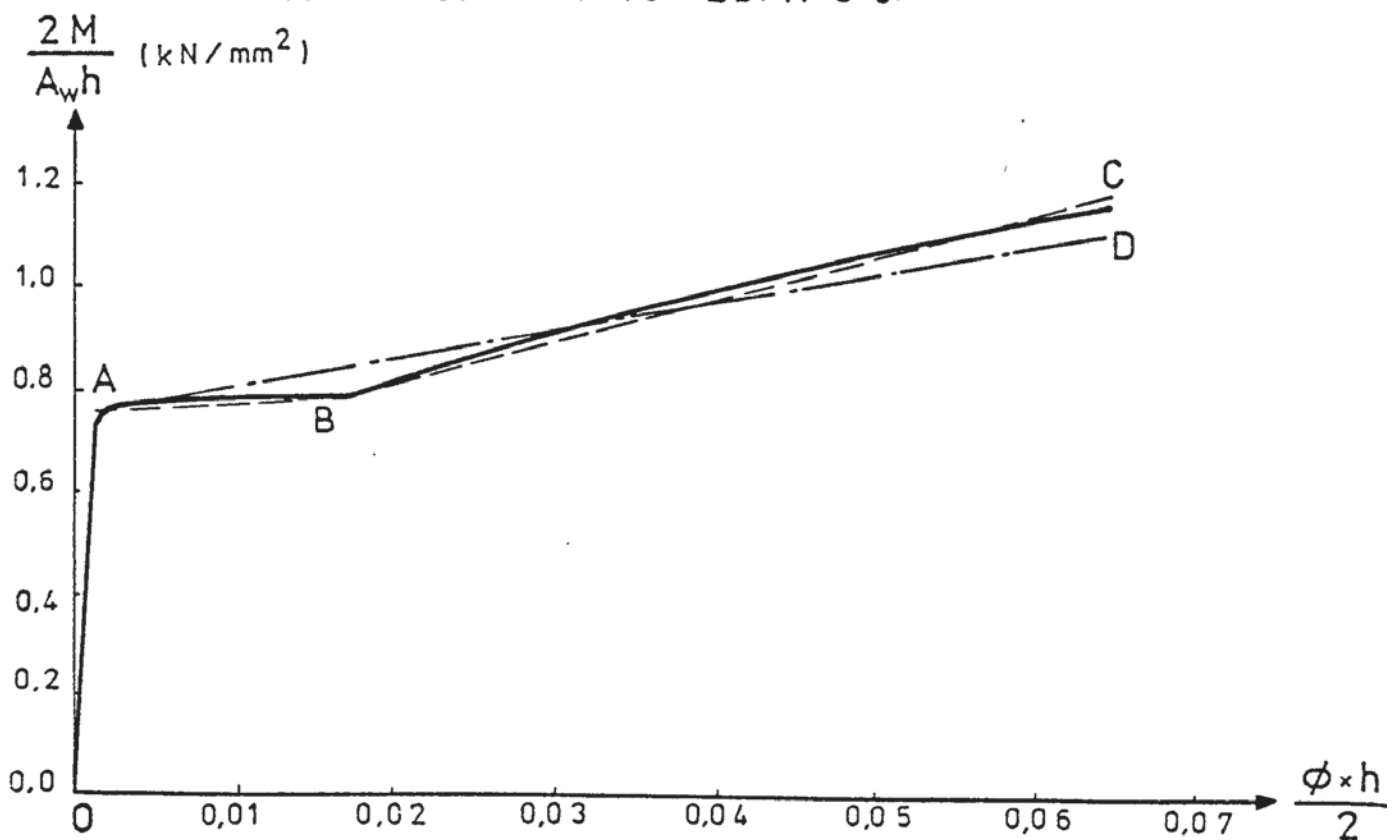
FIGURE 3.8: M-C DIAGRAM FOR BEAMS MADE OF
5″× 3″× 11 Lb. R.S.J.

where ε_1 is the strain in the outermost fibres and σ_1 is the corresponding stress. ε_1 is related to the curvature ϕ as

$$\phi = \frac{\varepsilon_1 \, d}{2} \qquad\qquad 3.7$$

where d is the depth of the section. Further, $\overline{m}$ was related to the applied bending moment M as

$$M = \frac{1}{2} \, \overline{m} \, Awd \qquad\qquad 3.8$$

Once the integral $\int_0^\varepsilon \sigma\varepsilon d\varepsilon$ has been calculated from the stress-strain diagram of the material for various values of ε_1, the corresponding values of $\overline{m}$ can be calculated from equation (3.6). The moment-curvature diagram of each section is then constructed point by point by using equations (3.7) and (3.8).

The structure was first analysed by the method proposed here using a trilinear approximation of the moment-curvature diagrams. Plasticity was allowed to spread through various small members inserted in the vicinity of each expected hinge location. The resulting load-deflection diagram is given in figure (3.9) together with the experimental diagram[14] and also that obtained by Davies. It can be seen from this figure that in spite of a purely theoretical approach, the load-deflection curve is in good agreement with the experimental curve and that obtained by Davies.

An investigation was also carried out to study the influence of varying the spread of plasticity on the load-deflection curve of the frame for various moment-curvature diagrams. Here the rate of spread of plasticity SPR is defined as:

$$SPR = \frac{\text{length of plastic region}}{\text{length of member}} \times 100$$

The frame was analysed for rates within the range 0.5% - 7%. The bilinear and the trilinear representations of the moment-

Total vertical load (kN)

Ultimate failure 137.6 kN

Davies

Proposed method

(Spread Plasticity is not restricted)

Experimental points
□
○

Vertical deflec--
tion at apex(mm)
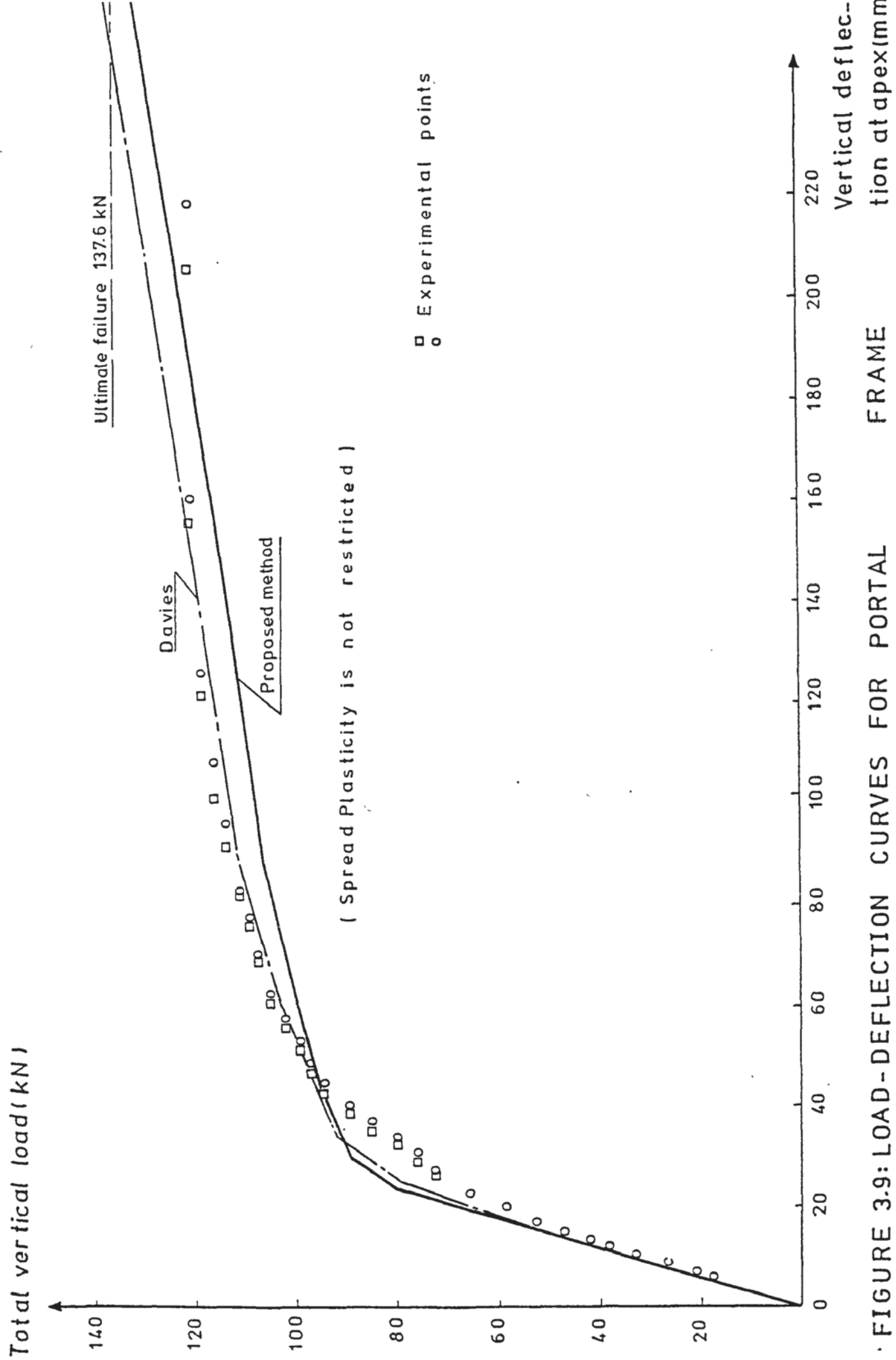
FIGURE 3.9: LOAD-DEFLECTION CURVES FOR PORTAL FRAME

curvature diagrams are shown in figures (3.7) and (3.8). In these OAD is the bilinear moment-curvature and OABC is trilinear. The analysis was stopped as soon as the fracture point C or D is reached in any section of the frame. This point is determined from the ultimate values of the bending moment and the curvature on a moment-curvature diagram which restricts the plastic deformation to a finite value, neglected in other analyses. This finite deformation makes it possible to reach the end of the moment-curvature diagram in one member before the formation of a mechanism in a frame.

In the present approach a mechanism is defined by the formation of fully yielded sections before fracture. In table (3.2) the loads that cause the formation of a mechanism and the ultimate load carrying capacity of the frame for non restricted and for various SPR values are compared with the experimental load of reference[14] and also with that obtained by Davies. Figure (3.10) compares the values of failure loads, obtained with different SPR, with the experimental result. This figure shows that for SPR > 1.5% the failure load is nearly constant. The figure also shows that changes in SPR does not affect the failure load considerably. Up to a value of 1.5% the ultimate failure load increases slightly and then becomes stable.

The portion of the graph for SPR < 1.5% can be disregarded because the value of the ultimate load is less than the load which is necessary to form a mechanism, and it is not expected since the value of the curvature at rupture is very much larger than the curvature when the section is fully yielded (see figure 3.7 for comparison).

Total vertical load(kN)

Ultimate failure (Trilinear)

Ultimate failure (Bilinear)

Experimental failure

Mechanism (Bilinear)

Mechanism (Trilinear)

4W

4W

4W

4W
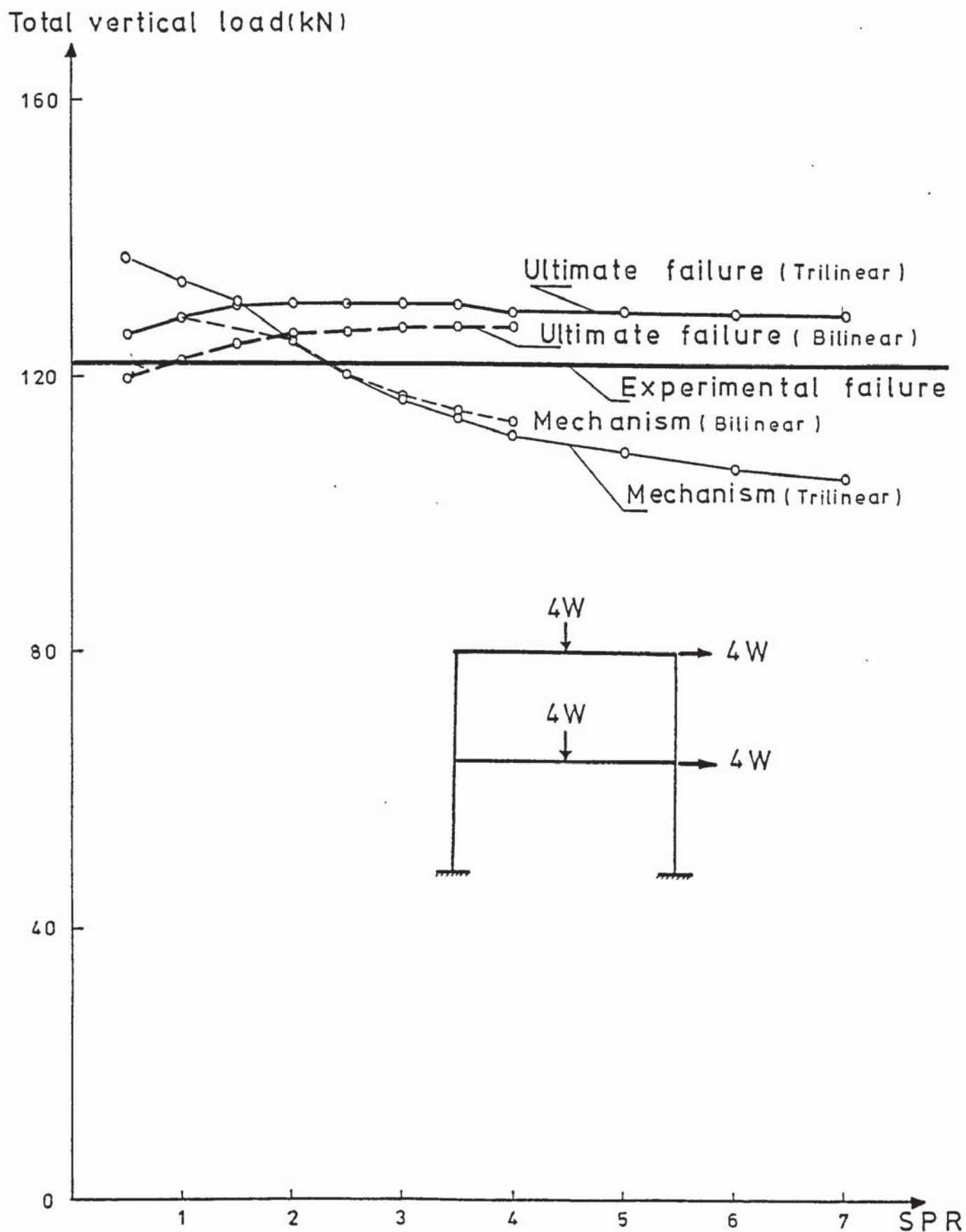
FIGURE 3.10: FAILURE LOADS VERSUS SPR

A maximum difference of 11% was obtained between the theoretical loads and the experimental failure load. This indicates that the present method yields acceptable results. It is obvious from table (3.2) and figure (3.10) that the mechanism load decreases for increasing values of SPR values. However it will be shown in the next example that this also becomes stable for very high values of SPR which may not often be encountered in practise. It may then be concluded that, when the strain hardening is considered, the mechanism load does not give a unique result for practically admissible values of SPR.

The load-deflection diagram obtained for SPR values of 2.5% and 4% for bilinear, and 3% and 4% for trilinear M-C approximations are plotted in figure (3.11) together with the experimental load-deflection diagram.

All the curves are in close agreement with the experimental load-deflection points. It is evident that as SPR is increased, the theoretical load-deflection curve flattens. This is particularly visible at the stages near failure. The curves obtained for the trilinear approximation of M-C diagrams are flatter than those obtained for the bilinear M-C diagrams. This is because the bilinear approximation overestimates the flexural rigidity within the range of the plastic flow. On the other hand the ultimate loads predicted from trilinear M-C approximation are slightly higher than those for the bilinear cases. This discrepancy may be due to the difference of the ultimate moment carrying capacities of the two cases.

As previously mentioned, the load-deflection curve given by Davies is also very close to the experimental results. However
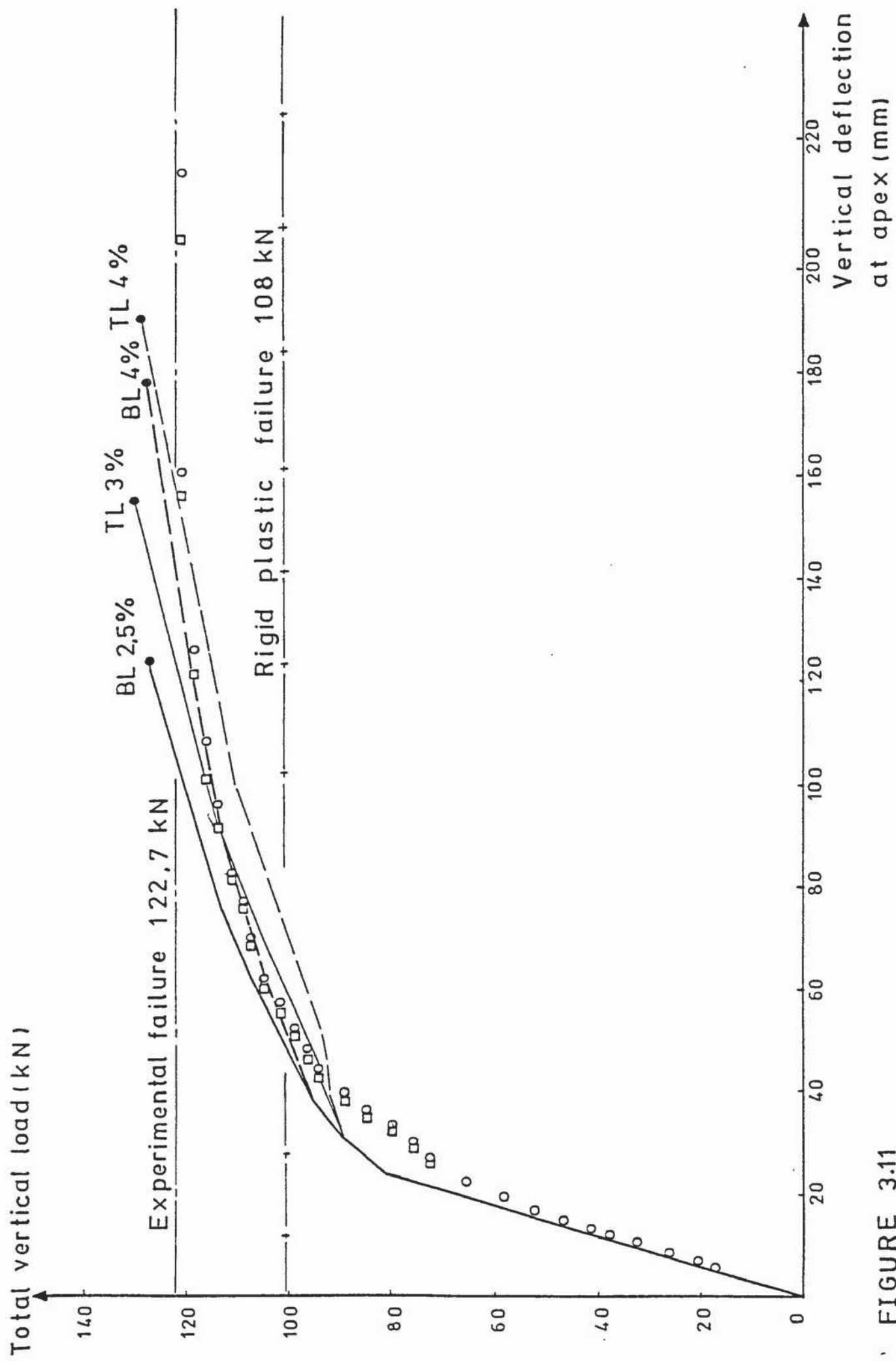
FIGURE 3.11

TYPE OF ANALYSIS	TOTAL VERTICAL LOAD (KN)			
	MECHANISM		ULTIMATE	
	LOAD (KN)	% DIFF.	LOAD (KN)	% DIFF.
EXPERIMENTAL	-	-	122.2	-
RIGID PLASTIC	100.8	-17.6	-	-
STABILITY BALANCE (HORNE)	100.5	-17.8	-	-
ELASTIC-PLASTIC	98.0	-19.9	-	-
ELASTIC-STRAIN HARDENING (DAVIES)	144.6	- 6.3	Continuing	
Bilinear, SPR* = 2.5% M-C	120.8	- 1.2	126.8	+ 3.7
Bilinear, SPR* = 3.0% M-C	117.6	- 3.8	127.2	+ 4.0
Bilinear, SPR* = 3.5% M-C	115.2	-- 5.8	127.4	+ 4.2
Bilinear, SPR* = 4% M-C	113.6	- 7.11	127.5	+ 4.3
Trilinear, SPR* 2.5% M-C	120.8	- 1.2	130.4	+ 6.62
Trilinear, SPR* 3.5% M-C	_114.0	- 6.8	130.2	+ 6.45
Trilinear, SPR* = 4.0% M-C	111.2	- 9.07	129.6	+ 6.00
Trilinear M-C, nonrestricted SPR*	106.8	-12.67	137.6	+11.00

The leftmost column of the last nine rows is labelled PRESENT THEORY.

*SPR: Spread of Plasticity Rate

TABLE 3.2 The Failure Loads of the Two Storey Portal Frame

this curve does not give sufficient information about the ultimate failure load because it does not define fracture by terminating the plastic deformation at some stage.

3.f.3 The Pitched Roof Portal Frame:-

As a further example, the frame shown in figure (3.12) is considered. This was originally described by Charlton[15] and later analysed by Davies[12]. Two similar frames were connected together by suitable purlins and sheeting rails. The plastic moment value of the 5"x3"x11 lb R.S.J. stanchions was 28.12 kN.m. The other physical properties are taken from the two storey portal frame analysed, discussed earlier. Again various analyses were carried out for bilinear and trilinear approximations of the M-C diagram for values of SPR between 0.5% and 20%. The results are compared with that obtained experimentally and are given in table (3.3). In figure (3.13) the ultimate and mechanism loads are plotted against the spread of plasticity rate (SPR). Again the ultimate failure load is not sensitive to SPR and its graph becomes stable after a value of SPR of about 2.5%. The mechanism load decreases for increasing values of SPR, but this curve also becomes stable, the mechanism load remaining nearly constant for values of SPR greater than 7%. For the values of SPR less than 2.5% no mechanism condition was obtained. This suggests that very small values of SPR yield erroneous results.

The maximum value of the ultimate failure load was obtained as 131.5 kN which is 22% higher than the experimental failure load of 107.5 kN. This difference may be due to the instability effects which are ignored in the present approach. The load-deflection diagrams obtained from various approximations, the experimental
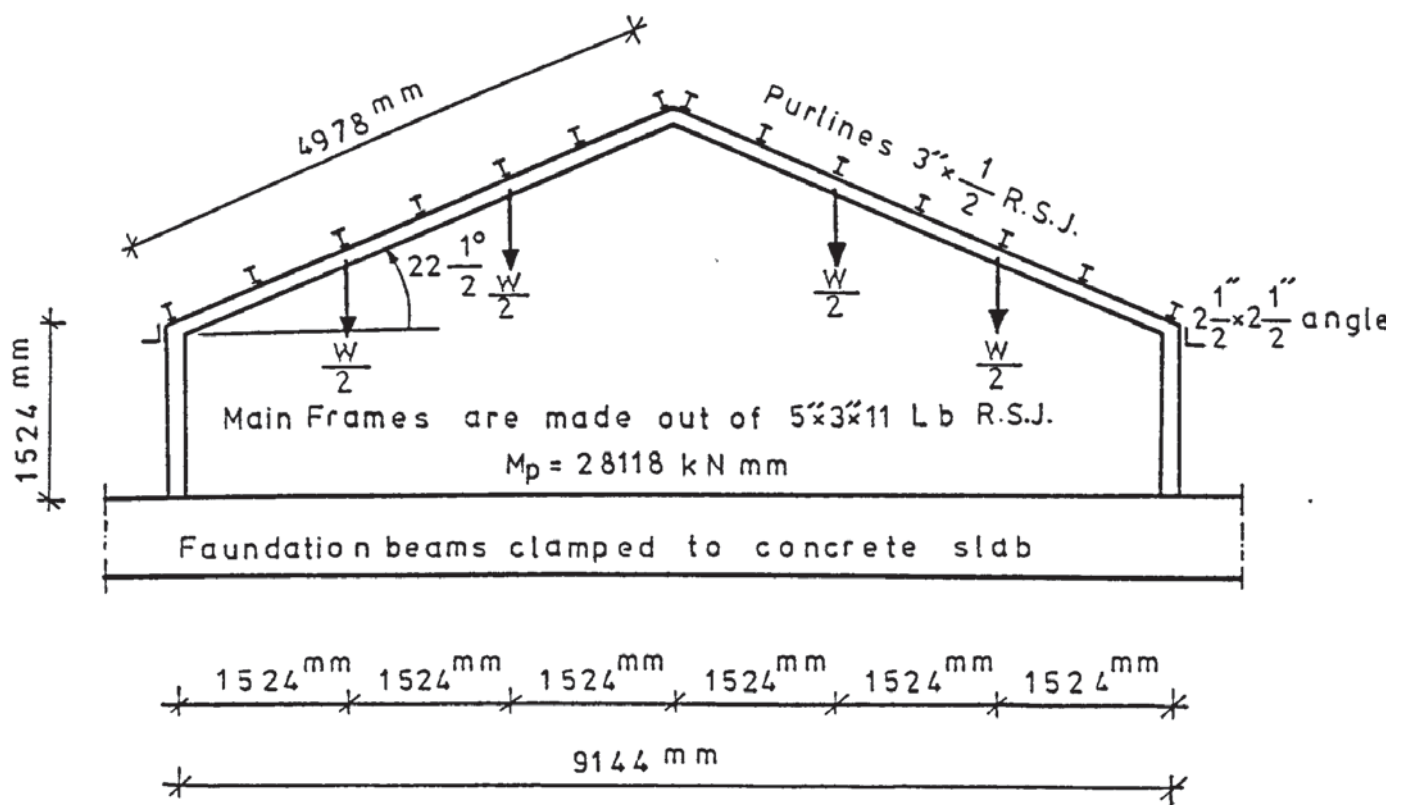
FIGURE 3.12: PITCHED ROOF STRUCTURE AND LOADING

| TYPE OF ANALYSIS | TOTAL VERTICAL LOAD (kN) | | | |
| | MECHANISM | | ULTIMATE | |
	LOAD	% DIFF.	LOAD	% DIFF.
EXPERIMENTAL			107.5	-
RIGID PLASTIC	95.0	-11.6%	-	-
STABILITY BALANCE (k=17.2)	92.8	-13.7%	-	-
ELASTIC-STRAIN HARDENING (DAVIES) k=6.2	104.0	- 3.3%	-	-
Bilinear, SPR = 3%	No Mechanism	-	119.5	+11.2%
Bilinear, SPR = 3.5%	116.5	+ 8.4%	121.4	+12.9%
Bilinear, SPR = 4%	114.0	+ 6.0%	121.6	+13.1%
Trilinear, SPR = 3%	119.5	+10.1%	124.0	+15.3%
Trilinear, SPR = 5%	106.0	+ 1.4%	126.8	+17.9%
Trilinear, SPR = 7%	101.0	- 6.0%	130.4	+21.5%
Trilinear, SPR = 10%	98.3	- 8.6%	130.5	+22.0%
Trilinear, SPR = 20%	96.0	-10.7%	128.6	+19.6%

The rows from "Bilinear, SPR = 3%" through "Trilinear, SPR = 20%" are grouped under the label **PRESENT THEORY**.

TABLE 3.3 Comparison of Various Results for the Pitched Roof Frame

Total vertical load (2W)

(Load parameter)

(7,5) 15 ——

ABINGTON'S TEST NO 10

(Pitched Roof Portal Frame)

She(Trilinear)

Experimental Failure

Mechanism (Trilinear)

Mechanism(Bilinear)

(5,0) 10 ——

She (Bilinear)

(2,5) 5 ——

0.5 W   0.5 W   0.5 W   0.5 W

0 ——

5 %   10%   15%   20%   SPR
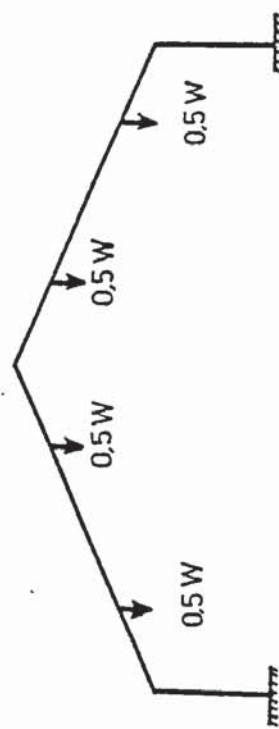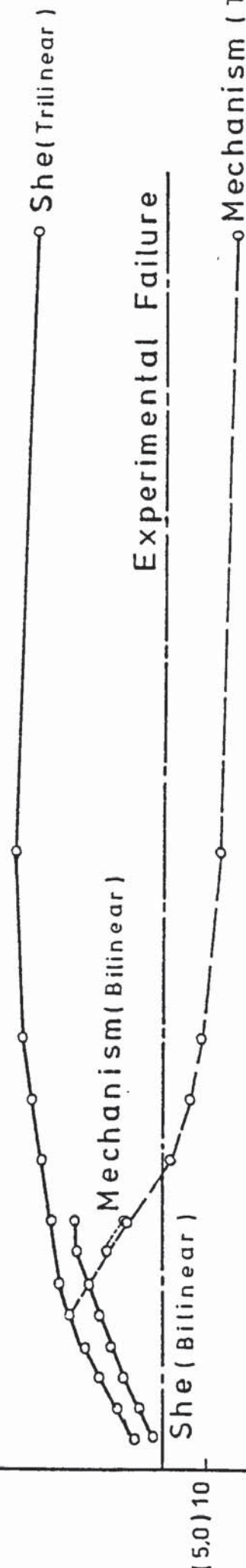
FIGURE 3.13: FAILURE LOADS VERSUS SPREAD OF PLASTICITY OVER LENGTH%

curve due to reference[14] and that obtained by Davies[12] are shown in figure (3.14). Again good agreement was achieved between the theoretical and the experimental curves. Those obtained from the trilinear M-C approximation are flatter than the curves for the bilinear M-C diagram while in both cases higher values of SPR result in making the load-deflection curves at stages near failure flatter.

Considering the last two examples, it may be proposed that any rate of spread of plasticity which is more than 3% may give fairly accurate estimation of the ultimate load carrying capacity. If on the other hand, more accurate results are required, then fine subdivisions around the expected hinge locations are necessary.

3.g. Conclusions:-

It is now clear that only one elastic analysis of a frame is necessary to predict its nonlinear behaviour caused by the nonlinearity in the material properties. Frames can be analysed in this manner under the given loading as well as up to and including failure. This is provided that there is no unloading in the plastic region. The proposed method can be applied to both elastic and plastic analyses.

In the strain hardening analysis, the rate of spread of plasticity does not influence the failure load and a rate of 3% - 10% may be adopted for practical purposes. Because the instability effect is ignored, the results obtained are slightly unconservative and, as it was mentioned in chapter 2, this requires further research on the structural variation theory to include this effect.

3.h.1 Moment-Curvature Diagrams of Reinforced Concrete Sections:-

A theoretical method for the construction of moment-curvature
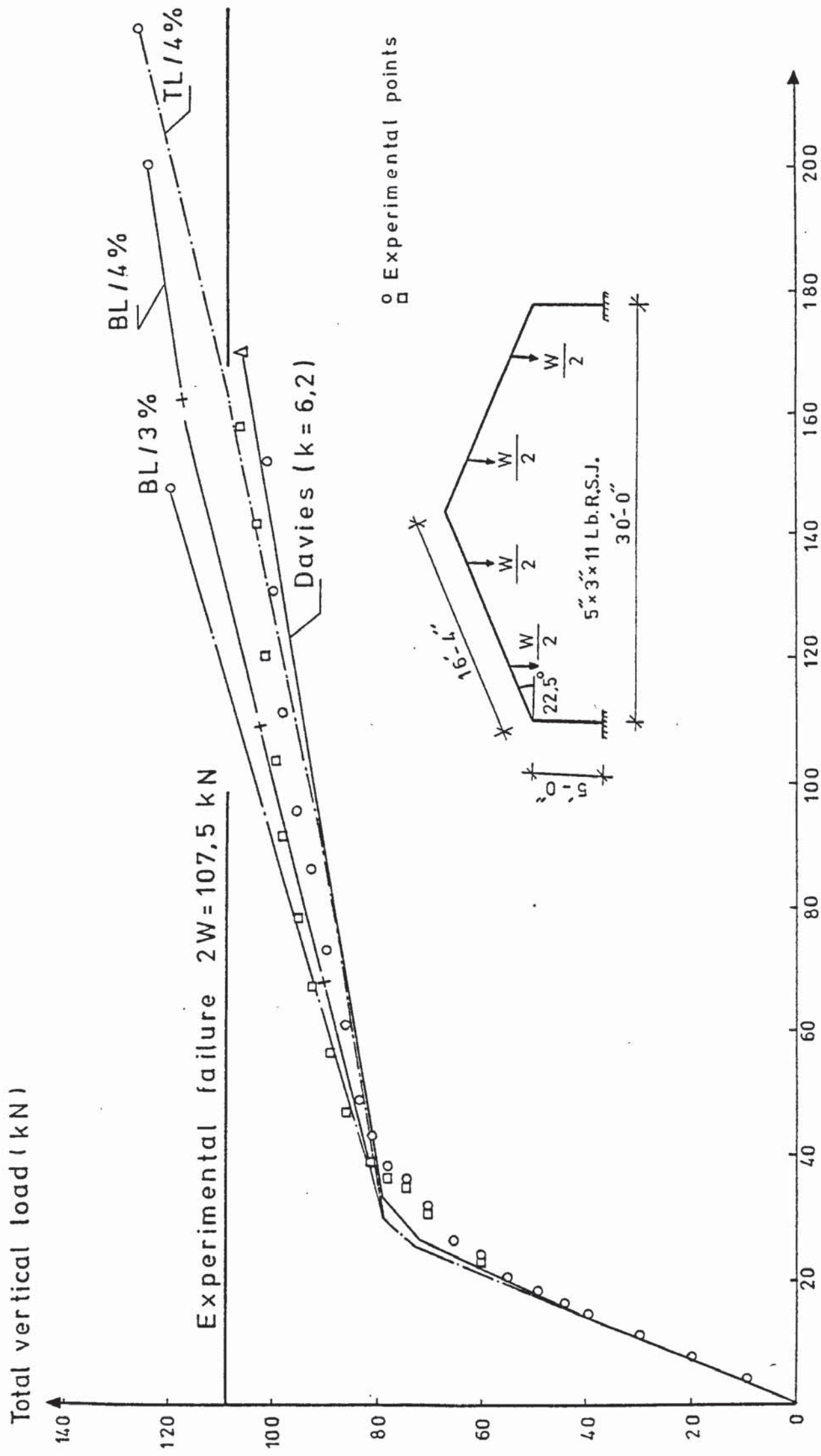
FIGURE 3.14: COMPARISON OF LOAD-DEFLECTION DIAGRAMS FOR PITCHED ROOF PORTAL FRAME

diagrams for homogenous sections was given in section (3.b). For
the case of reinforced concrete sections the problem is more
complicated because of their non-homogenous nature. This is
despite the fact that equations (3.1) may be still valid. For
this reason, the semi-empirical method given in reference (16) is
improved here to include a better estimate of the ultimate moment
of resistance of the section. The ultimate moment of resistance
for ordinary reinforced concrete members is calculated by using
the theory proposed by Hognestad et al[17]. Further, the ultimate
stage of deep, multilayered reinforced concrete panels is estimated
by means of interaction equations (5.e.20) or (5.e.23). These
consider the ratios of bending moment, the torsional moment and the
shear force acting on the panels and will be given in detail later
in chapter 5.

3.h.2 Actual M-C Relationships for Reinforced Concrete Sections :-

A typical moment-curvature diagram of an under-reinforced
section is shown in figure (3.15). Between points O and A the
relationship is reasonably linear. At A the extreme tensile
fibres begin to crack decreasing the flexural rigidity of the
section. The slope of the curve reduces after A and the
relationship is more or less linear up to B. This point
represents the stage at which the outermost tensile reinforcements
start yielding. For further increases in bending moment, the
flexural rigidity decreases drastically and the moment-curvature
diagram tends towards the horizontal. If the section is ordinary
reinforced concrete with two layers of reinforcement, the increase
in bending moment causes the neutral axis to rise and the tensile
reinforcements to strain harden. Ultimately the section may fail
due to crushing of the concrete in the compression zone.
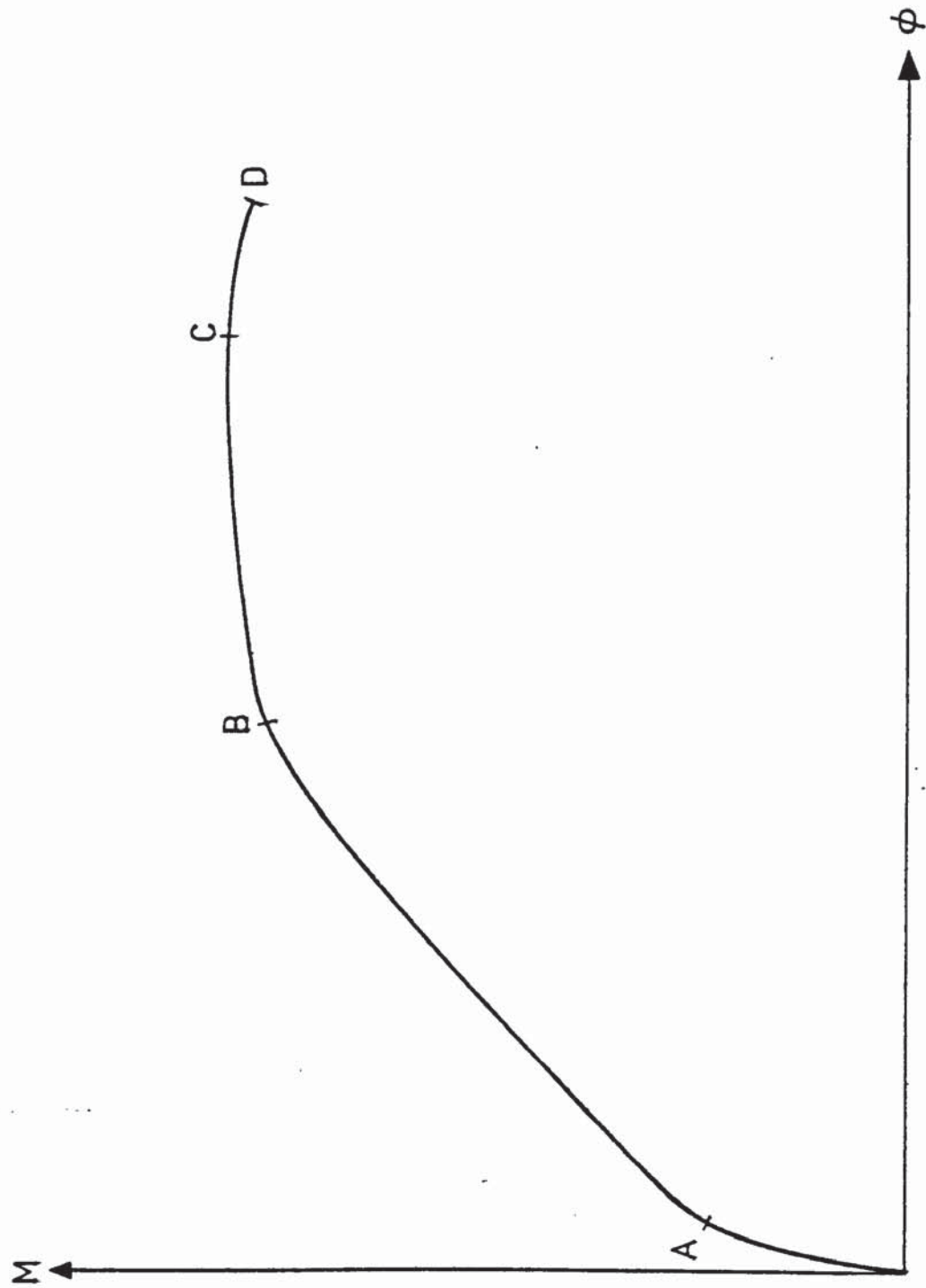
FIGURE 3.15: A TYPICAL M-C DIAGRAM FOR A REINFORCED CONCRETE SECTION

A multi-layered deep panel is different. When the outermost tensile reinforcement yields the inner ones are still elastic. Further increases in the bending moment increase the strain in the outer bars and also causes some inner bars to yield. The neutral axis also rises. Ultimately the section may fail due to excessive straining of the outermost tensile reinforcement.

The moment-curvature diagram shown in figure (3.15) may be simplified and replaced by three straight lines joining OA, AB and BC. Such a simplification is fairly reasonable for practical purposes.

3.h.3 Construction of Moment-Curvature Diagrams

for Reinforced Concrete Sections:-

A tri-linear moment curvature idealisation is shown in figure (3.16). To construct this the following parameters are required:

Mc, $\emptyset c$: These are the bending moment and the corresponding curvature at which the concrete first cracks in tension. Point A in figure (3.16).

$(EI)i$: The flexural rigidity of the section at the initial stage. This is the slope of OA in figure (3.16).

My, $\emptyset y$: The bending moment and curvature values at which the outermost tensile reinforcement yields (Point B in the figure).

$(EI)_c$: The flexural rigidity of the cracked section, i.e. the slope of A B D.

Mu, $\emptyset u$: The ultimate values of bending moment and curvature at point c.

$(EI)u$: The flexural rigidity after yielding takes place in the outermost tensile reinforcements. This is the slope of -
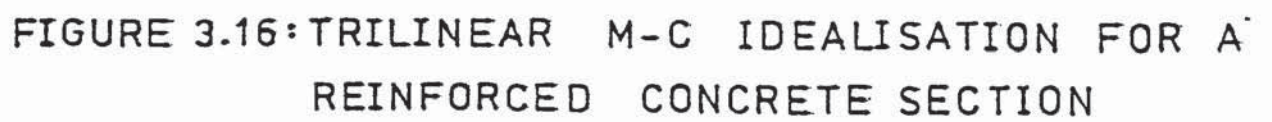
FIGURE 3.16: TRILINEAR M-C IDEALISATION FOR A REINFORCED CONCRETE SECTION

the straight line BC in the figure.

To construct this moment curvature diagram, the following assumptions are made:

1 - The concrete is elastic up to the yield point of the outermost tensile reinforcements for ordinary beams and up to failure for deep panels.

2 - Tensile cracks take place in the concrete when the tensile strength f_{ct} is reached.

3 - The initial flexural rigidity $(EI)_i$ remains unaltered until the section cracks.

4 - An empirical formula given by Monnier[18] can be used to evaluate (EI)c.

3.h.3.1 The uncracked state:

The initial flexural rigidity $(EI)_i$ is calculated by multiplying the modulus of elasticity of concrete Ec by the gross second moment of area of uncracked section I_G, thus:

$$(EI)_i = E_c \times I_G \qquad 3.7$$

The moment Mc at first crack is obtained from the product of the gross modulus of the uncracked section Ze and the tensile strength of the concrete, f_{ct}.

$$Mc = f_{ct} \times Ze \qquad 3.8$$

The curvature $\emptyset_c$ at A in figure (3.16) is calculated from:

$$\emptyset_c = Mc/(EI)_i \qquad 3.9$$

3.h.3.2 The cracked state:

In this state the behaviour of the section is rather complex due to the existence of uncracked zones between cracks in the structural members. For this reason the empirical formula suggested in reference (18) is used to determine the value of the

flexural rigidity $(EI)_c$. The formula relates the flexural rigidity of the cracked section to the values of the percentage tensile reinforcement r, the thickness˙and the effective depth d_1 of the section. This formula is in the ˛form:

$$(EI)_c = (-2.5r^2 + 13.9r - 1.1) \ t \ d_1^3 \times 10^3 \text{kg f.cm}^2 \qquad 3.10$$

The grade of the concrete, the diameter of the reinforcement bars and the presence of compressive reinforcement are considered to have little effect on the value of $(EI)_c$. The effective depth for an ordinary section is taken as the distance between the compression face and the tensile bars. For multi-layered deep panels, this depth may be taken as the distance between the compression face and the resultant of the forces sustained by the tensile reinforcements. For practical purposes an approximate value of d_1 may be taken as 0.75d. In fact this value was used to construct the M-C diagrams for the shear walls and slabs of the structures analysed here and reasonable agreements were obtained between the theoretical and the experimental load - deflection curves.

The bending moment My, causing yield in the outermost tensile reinforcement can be calculated from equations (5.b.15) and (5.c.10) of chapter 5, by substituting the yield strain of the steel for the ultimate strain and setting the number of layers, in the plastic zone, equal to one. The curvature at this stage can be obtained from the triangles OAA' and ABA'', figure (3.16), as follows

$$\emptyset y = \emptyset c + (My - Mc)/(EI)c \qquad 3.11$$

3.h.3.3 The ultimate state:-

For deep beams, the failure criteria given later in chapter 5 by equations (5.e.20) or (5.e.23) can be used to predict the value of the bending moment Mu at failure. On the other hand ordinary

sections generally fail due to excessive straining of the outermost fibres of the concrete in the compression zone. Let us consider the section shown in figure (3.17.a). The stress-strain diagram of the bars is a nonlinear curve such as that shown in figure (5.16). To calculate the ultimate moment carrying capacity of the section, equations of compatibility and longitudinal equilibrium are used together with the moment equilibrium equation about the $\bar{x}$ axis passing through the compression centre. The basic assumptions involving this approach are as follows:

1 - Plane sections remain plane.

2 - The tensile strength of the concrete is negligible.

3 - The compressive stress distribution at failure is represented by two parameters. These parameters are the average stress c/tx and the distance of the compression centre from the extreme compressive fibre. Hognestad[17] proposed the following equations to define these parameters.

$$\beta_1 = 0.5 - \frac{fcu}{700} \qquad\qquad 3.12$$

$$\beta_2 = \frac{27 + 0.27\ fcu}{28.3 + fcu} \qquad\qquad 3.13$$

$$\varepsilon_{cu} = 0.004 - \frac{fcu}{57000} \qquad\qquad 3.14$$

Where fcu is the cube strength of concrete (N/mm^2), εcu is the ultimate strain of concrete. The factors β_1 and β_2 define the location of the compressive centre and the average stress coefficient respectively.

The longitudinal equilibrium is established by equating the compressive force carried by the concrete, to the tensile force carried by the reinforcement. Thus:

$$C = T$$

or

$C = \beta_2 \cdot f_{cu} \cdot t \cdot X$

$\beta_1 x$

x

d

$T = A_{st} f_m$

$\mathcal{E}_{cu}$ A'

A

O

B

$\mathcal{E}_s$

B'

x

COMPRESSION ZONE

TENSION ZONE

$\bar{x}$

$\bar{y}$

C

A_{st}

a- Cross Section

b- Strain at Failure
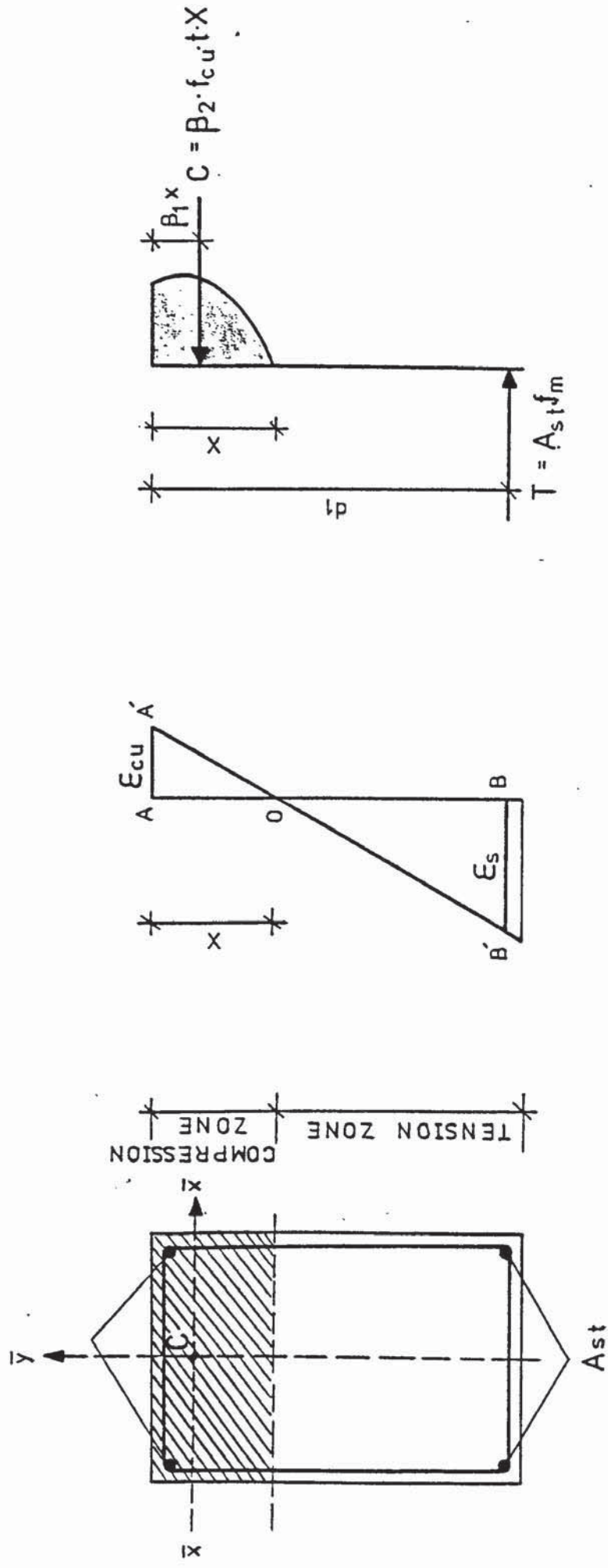
c- Forces at Failure

FIGURE 3.17: A REINFORCED CONCRETE SECTION AT FAILURE

$$\beta_2 \text{ fcu t X} = \text{As} \times \text{fm} \qquad \qquad 3.15$$

where As is the area and fm is the stress of the tensile
reinforcement. From equation (3.15) the depth of the neutral axis
is obtained as

$$X = \frac{\text{As fm}}{\beta_2 \text{ fcu t}} \qquad \qquad 3.16$$

The similar triangles OAA' and OBB' of the strain diagram in
figure (3.17.b) give the strain compatibility equation as

$$\frac{\varepsilon cu}{X} = \frac{\varepsilon s}{d_1 - X} \qquad \qquad 3.17$$

and it follows that

$$\varepsilon s = \varepsilon cu \frac{d_1 - X}{X} \qquad \qquad 3.18$$

Using equations (3.16), (3.18) and the stress-strain diagram
of the reinforcement, the depth of the neutral axis is obtained
iteratively as follows:

i -   Assume X = Xo

ii -   Calculate ε_s from equation (3.18) and obtain fm from the
        stress-strain diagram of the reinforcement by using ε_s.

iii -   Calculate the new value of X_n from equation (3.16).

iv -   Compare the new and the old values of X. If the difference
        is less than a specified tolerance, stop the iteration.
        Otherwise repeat from step ii with Xo = Xn until the
        tolerance test is satisfied.

Having calculated the depth of the neutral axis, the ultimate
moment is obtained from the moment equilibrium equation about
$\bar{x} - \bar{x}$ axis, through the compression centre, as follows

$$Mu = Asfm \ (d_1 - \beta_1 X) \qquad \qquad 3.19$$

The ultimate curvature $\emptyset u$ can be obtained from the strain diagram
shown in figure (3.17.b) as

$$\emptyset u = (\epsilon_{cu} + \epsilon_s)/d_1 \qquad\qquad 3.20$$

Finally, the flexural rigidity between B and C is obtained from the triangle. BB"C shown in figure (3.16) as follows.

$$(EI)_u = (Mu - My)/(\emptyset u - \emptyset y) \qquad\qquad 3.21$$

The value of $(EI)_u$ given by equation (3.21) is the slope of the chord BC in figure (3.16). In reality, the actual curve between these points is nonlinear and is shown as the chain line between B and C. Alternatively the curve OABDC in figure (3.16) can be used to represent the moment curvature diagram. This is particularly convenient, because there is no need to calculate the yield moment My. Having calculated Mu, the curvature $\overline{\emptyset}u$ is obtained from triangles OAA' and ADA''' as

$$\overline{\emptyset}u = \emptyset c + (Mu - Mc)/(EI)_c \qquad\qquad 3.22$$

The region between D and C is perfectly plastic and point C is the fracture point which limits the rotation of the section.

The effect of axial loads on the moment-curvature diagrams has been studied by Cranston[19] and a numerical technique has been proposed. This effect is however neglected in the analysis proposed in this chapter.

3.i The Use of Compensating Loads in the
    Failure Analysis of Reinforced Concrete Frames :-

The flexural rigidity of a reinforced concrete member is a function of its forces. i.e. its bending moments, shear force and axial force. The effect of the shear force may be ignored when the depth to length ratio of the member is comparatively small. As the load acting on a frame is increased, the flexural rigidities of its members decrease. In section 3.h , it was suggested that the flexural rigidity of a section can be idealized

to change at discrete values of the applied bending moment. As
soon as the first change occurs in a structure it becomes more
flexible, requiring a fresh analysis to predict its subsequent
behaviour. This analysis however, should give the same forces
and deflections in the frame after the change occurs but before
increasing the external loads. Suppose a change occurs in member
ij at a load factor λ_k. The flexural rigidity EI_{ij} of the member
reduces to $(1+\alpha)EI_{ij}$. A fresh analysis of the new structure,
without compensation, results in an erroneous set of joint
deflections and member forces. To rectify this, compensation
loads given by equation (2.10), are applied at joints i and j.
This is on top of the actual loads at the load factor λ_k.

As the load factor is further increased, member ij acts with
the new flexural rigidity $(1+\alpha)EI_{ij}$.

To clarify the above treatment, consider the example of the
portal shown in figure (3.18) which has a constant EI throughout.
Ignoring the effect of axial deformations, the bending moment and
the shear force diagrams for $\lambda = 2$ are shown in figures (3.19 a
and b). Let the flexural rigidity of member BC be reduced to
0.2EI, so that the change in EI is $\delta EI = -0.2EI + EI = +0.8EI$ and
hence $\alpha = -0.8$. To maintain the forces and deflections of the
structure, the forces acting on member BC are multiplied by the
variation ratio $\alpha = -0.8$ and applied at joints B and C together
with the external loads. The original forces in member BC and
the compensating loads of the member are shown in figure (3.19.c)
and (3.19.d) respectively.

As the new structure is analysed under the combined action
of external and compensating loads, see figure (3.20), the bending
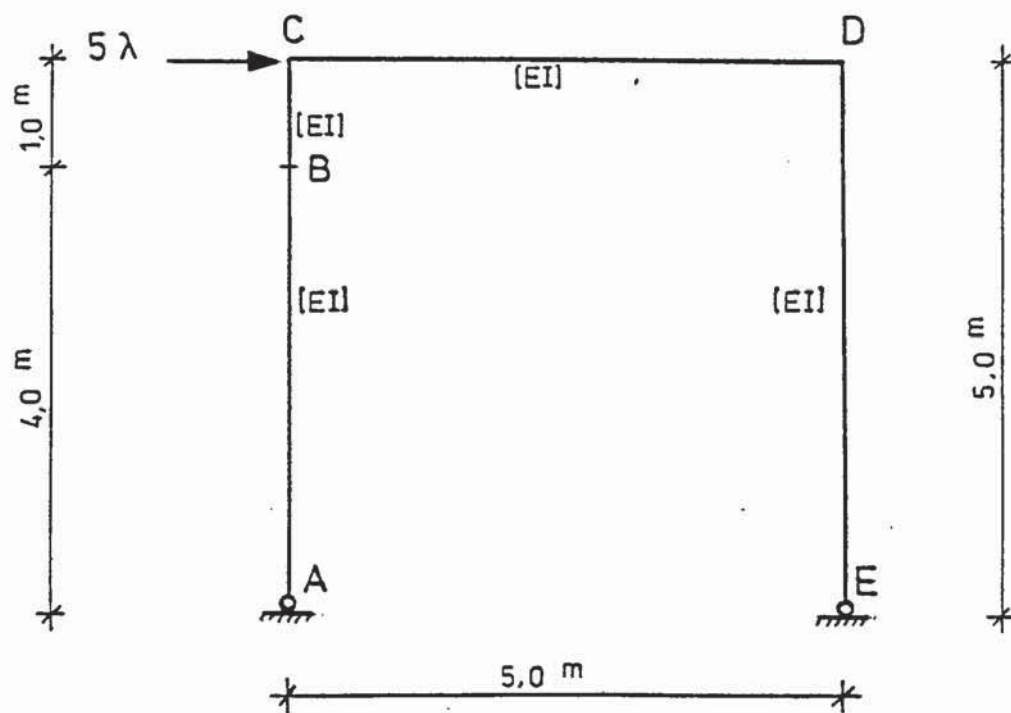
FIGURE 3.18: PORTAL FRAME AND LOADING
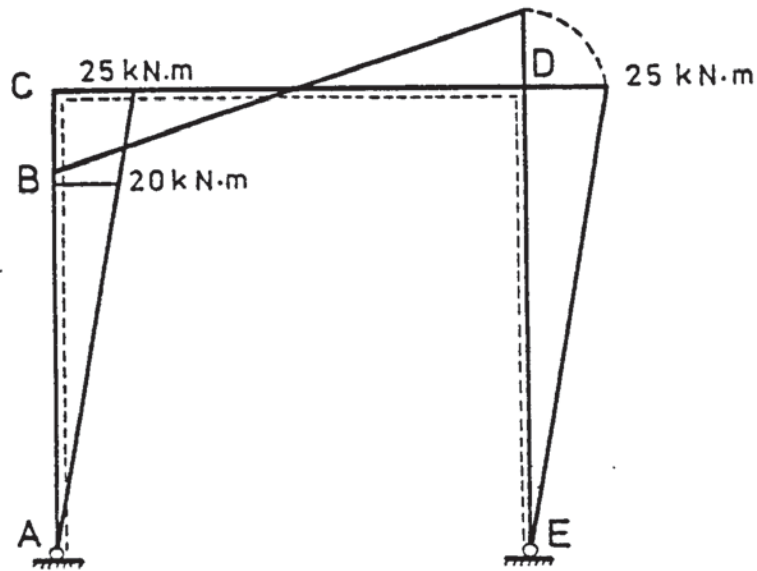
a- Bending Moment Diagram

b- Shear Force Diagram

c- Bending Moments and
Shear Forces on member B-C

d- Compensating Loads for
member B-C

FIGURE 3.19

b – Compensanting loads for mem_ ber A B alone
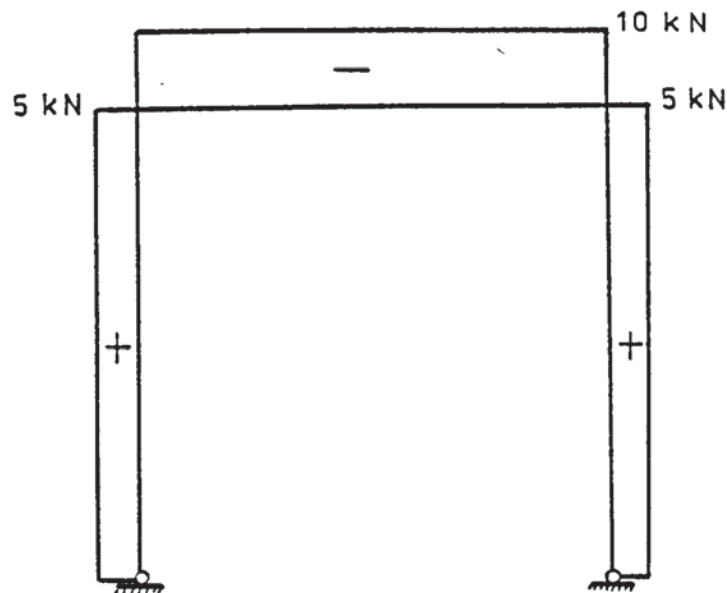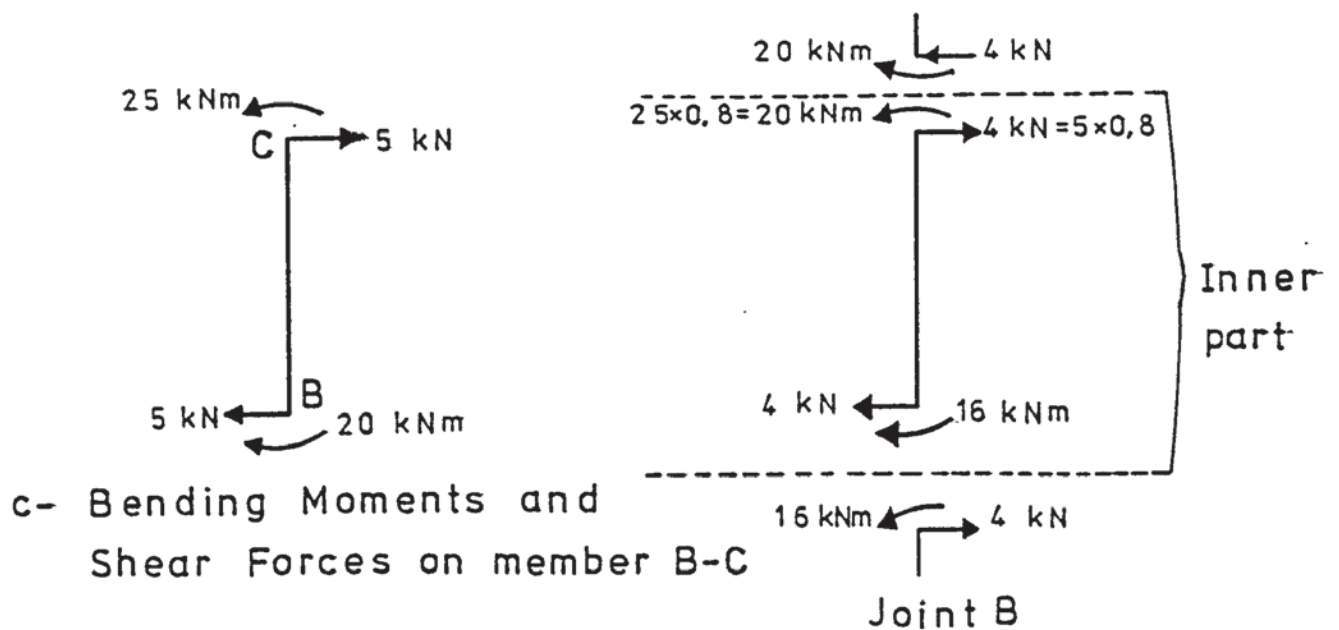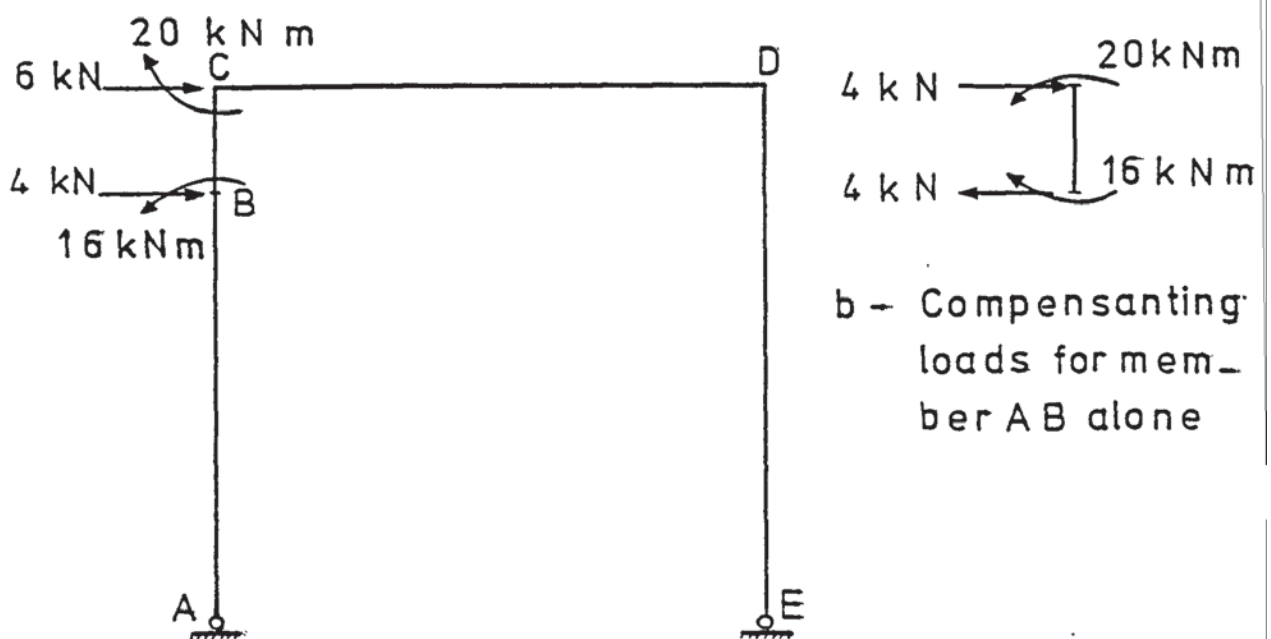
a – External loading + compensating loads on frame

FIGURE 3.20
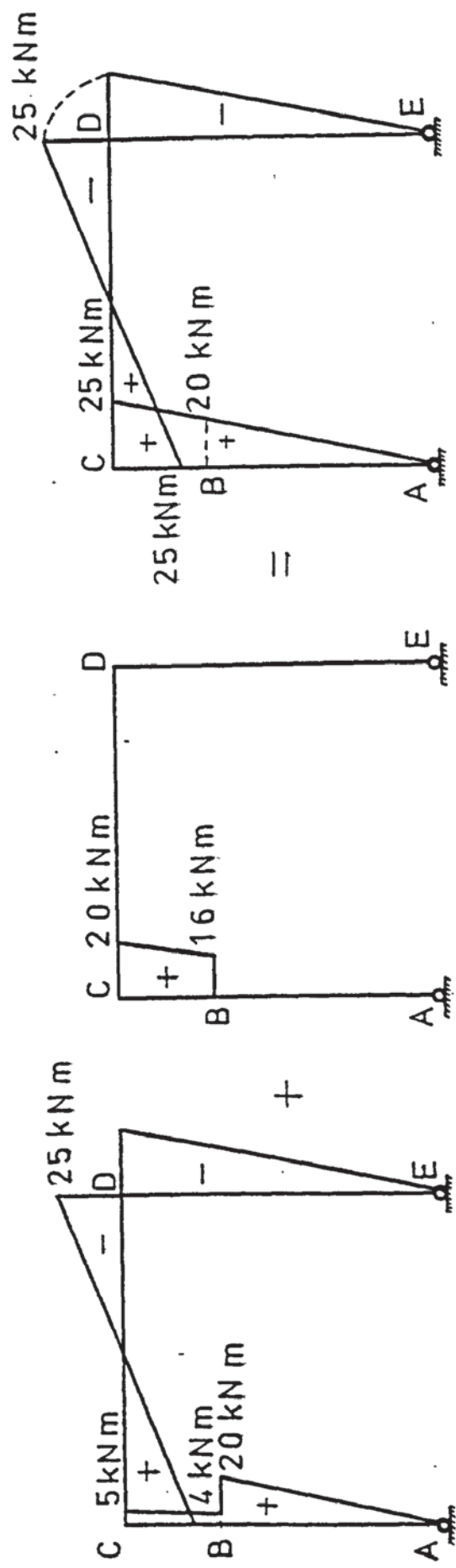
a- Bending moment diag-
ram due to external
loads and comensation
loading

b- Bending moment of
member BC alone due
to loads shown in figu-
re 3.6 b

c- Final bending moment diagram

FIGURE 3.21

10 kN

10 kN

5 kN

5 KN

−

+

+

=

4 kN

−

+

10 kN

10 kN

1 kN

5 KN

5 KN

−

+

+
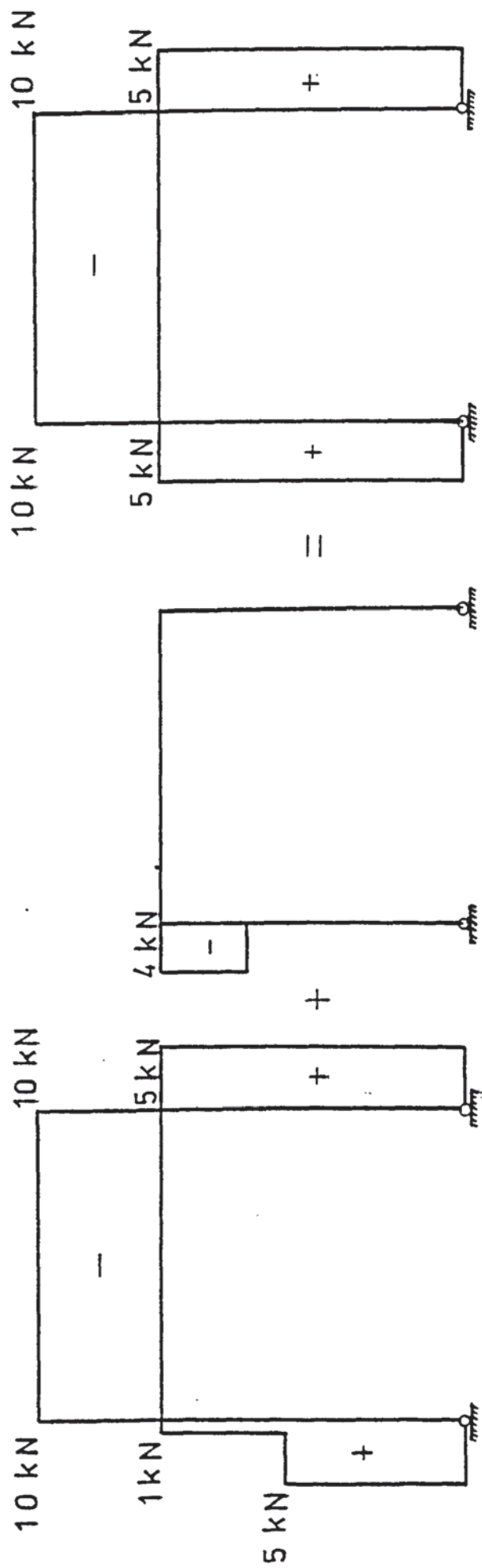
a- Shear force diagram
due to external loads
and compensation loading

b- Shear force diagram
member BC alone due
to loads shown in fi-
gure 3.6 b

c- Resultant shear force diagram

FIGURE 3.22

moment and the shear force diagrams shown in figures (3.21.a) and (3.22.a) are obtained. These diagrams are similar to those obtained for the initial structure except for member BC itself. The bending moment and the shear-force diagrams due to compensating loads acting on BC alone and shown in figures (3.21.b) and (3.22.b) are now added to those in figures (3.21.a) and (3.22.b) to give the diagrams shown in figures (3.21.c) and (3.22.c). These are now identical to the initial ones shown in figures (3.19.a and b)

3.j Assumptions involved in the failure load

analysis of reinforced concrete frames:

1 - The flexural rigidity of a section is a function of the bending moments acting on it.

2 - The moment-curvature diagram is assumed to be a series of straight lines.

3 - Generally the bending moment in a member varies along its length. Therefore its curvature and its flexural rigidity also vary. It is here assumed that the flexural rigidity along a short member is constant. In the case of a long member, the error involved in this assumption is reduced by diving it into smaller sub-members. Secondly, an effective bending moment may be calculated to give a moment area equal to that present on the member. The flexural rigidity corresponding to this effective bending moment may be considered as the constant flexural rigidity of the member. This assumption is discussed in detail in section 3.d.

4 - The small deflection theory is valid.

Adopting these assumptions the nonlinear analysis of a reinforced concrete frame up to and including failure can be carried out in the manner described in the following section.

3.k The Failure Load Analysis of Reinforced Concrete Frames:-

The basic principle of this method is to trace the load-deflection history of a frame by moving from one critical point on the moment-curvature diagram to another until the load factor reaches a specific value or until failure takes place. This principle was used by Majid and Anderson[20] in carrying out the rigorous elastic-plastic analysis for steel frames. However the "plastic hinge concept" advocated for steel frames is replaced here with the critical point concept for the case of reinforced concrete frames. A critical point is defined as the intersection of two successive linear portions on the moment-curvature diagram. Once a critical point is reached in a member of the frame, its flexural rigidity is set to that given by the next linear portion of the M-C diagram. The lowest load factor at which the next critical region is reached in any member is extrapolated and applied to the frame and by an iterative process, the exact value of this load factor is calculated.

The steps involved in such an analysis are:

1 - Initially the frame is assumed to be elastic; its overall stiffness matrix is constructed by using the initial flexural rigidities of its members. At this stage it is assumed that the axial forces in the members are zero.

2 - The joint equilibrium equations $\underline{L} = \underline{KX}$ are solved with a given load factor λ_1 to obtain the joint deflection vector $\underline{X}$. The member forces are then obtained from $\underline{P} = \underline{k} \underline{A} \underline{X}$. Using the bending moments at the ends of each member, a corresponding effective moment is calculated in the manner given in section 3.d.

3 - By a linear extrapolation the load factor at which the

effective moment of each member, reaches its next critical point is calculated. The lowest of these, λ^*, is the load factor at which it is expected that the next critical point is reached in any member of the frame. This is then applied to the frame as the new load factor. In the case of a frame subject to non proportional loading, the method given in chapter 4 is used to calculate the external loads for λ^*.

4 - The axial loads in the members under λ^* are also extrapolated using those already calculated in step 2. This new set of axial loads are employed to calculate the stability functions which are used in constructing a new stiffness matrix for the frame.

5 - The revised set of equations $\underline{L} = \underline{K}\,\underline{X}$ are now solved with the current load factor λ^*. The resulting joint displacements are then used to calculate the new axial forces and bending moments which are used to calculate a fresh set of effective moments.

6 - The·process is now repeated from step 3. The stage will be reached when after j iterations λ_j^*, calculated at the end of a cycle, is within a specified tolerance of the value expected at the start of that cycle. This indicates that a critical point is definitely reached in one of the members, say k, of the frame.

7 - As soon as the effective moment in member k reaches a critical value, its flexural rigidity EI_k is set to the slope of the next transition region on its M-C diagram.

Using the new and old values of EI_k, the variation ratio α_k is calculated from:

$$\alpha_k = -\frac{(EI_k)new - (EI_k)old}{(EI_k)old} \qquad 3.23$$

The corresponding compensation loads are calculated from equation (2.10).

8 - To initiate the search for the next critical point, the load factor is increased by a small amount and the corresponding external loads are calculated. The new compensating loads are added to the external loads while the old ones are subtracted. For one cycle the axial loads are kept constant at their values and the search for the next critical point is initiated from step 3. Every time a critical point is reached, the determinant of the overall stiffness matrix with the new flexural rigidity for member k is calculated. The analysis is terminated when this determinant becomes negative, indicating that the frame has collapsed.

3.l. Examples :-

3.l.1. Portal Frame: To verify the method given in section (3.k) a portal frame tested by Deeble[16] was analysed for various approximations of the moment-curvature diagram. The results are compared with the experimental load-deflection curve and also with that obtained from the actual M-C diagram, using the method given in section (3.d). The frame is shown in figure (3.23), and has a height and a span of 1200mm. The columns are pinned at the base. The beams and the columns are made out of 100mm x 125mm rectangular section. The members of the frame are subdivided in the manner shown in the figure. This is to reduce the error due to assumption 3 given in section (3.j).

The experimental moment-curvature diagram, obtained by Deeble for a beam of the same property as the frame is represented by curve "a" in figure (3.24). Curve "b" in the figure represents a trilinear approximation which covers the same area as curve a. Curves c, d and e represent various bilinear approximations as
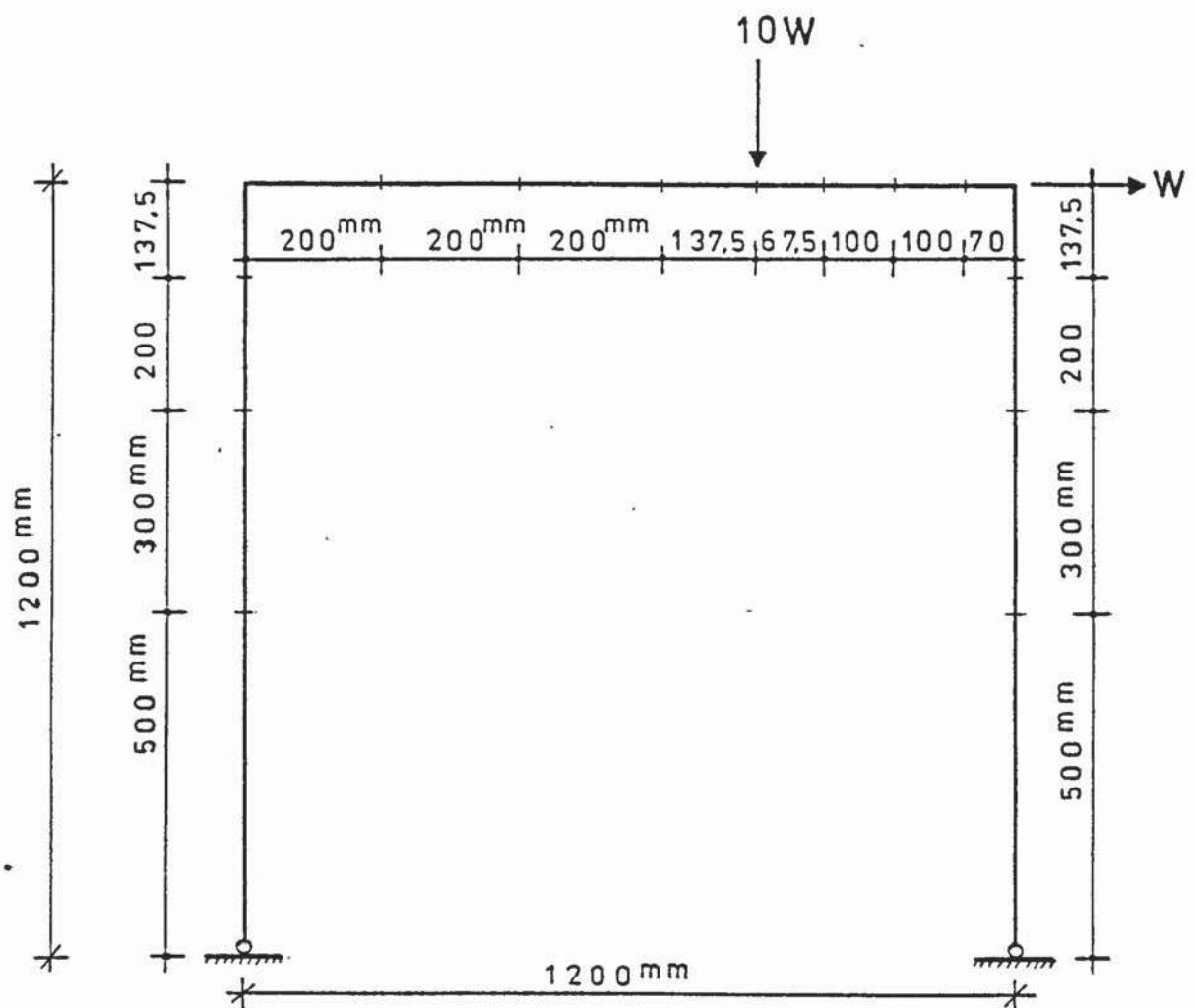
FIGURE 3.23: THE PORTAL FRAME, LOADING AND
SUBDIVISION
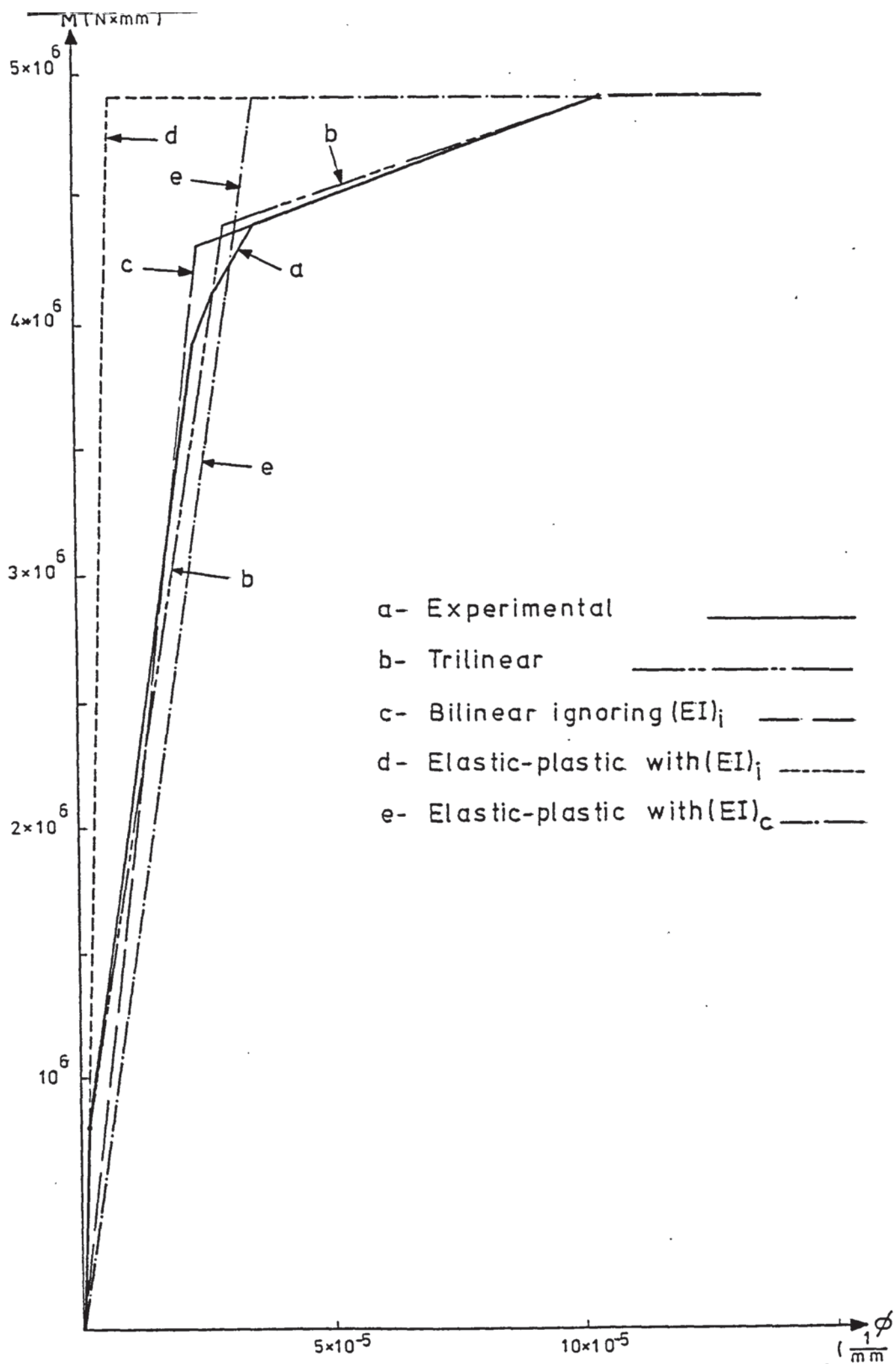
FIGURE 3.24: EXPERIMENTAL M-C DIAGRAM AND VARIOUS
APPROXIMATIONS FOR THE PORTAL FRAME
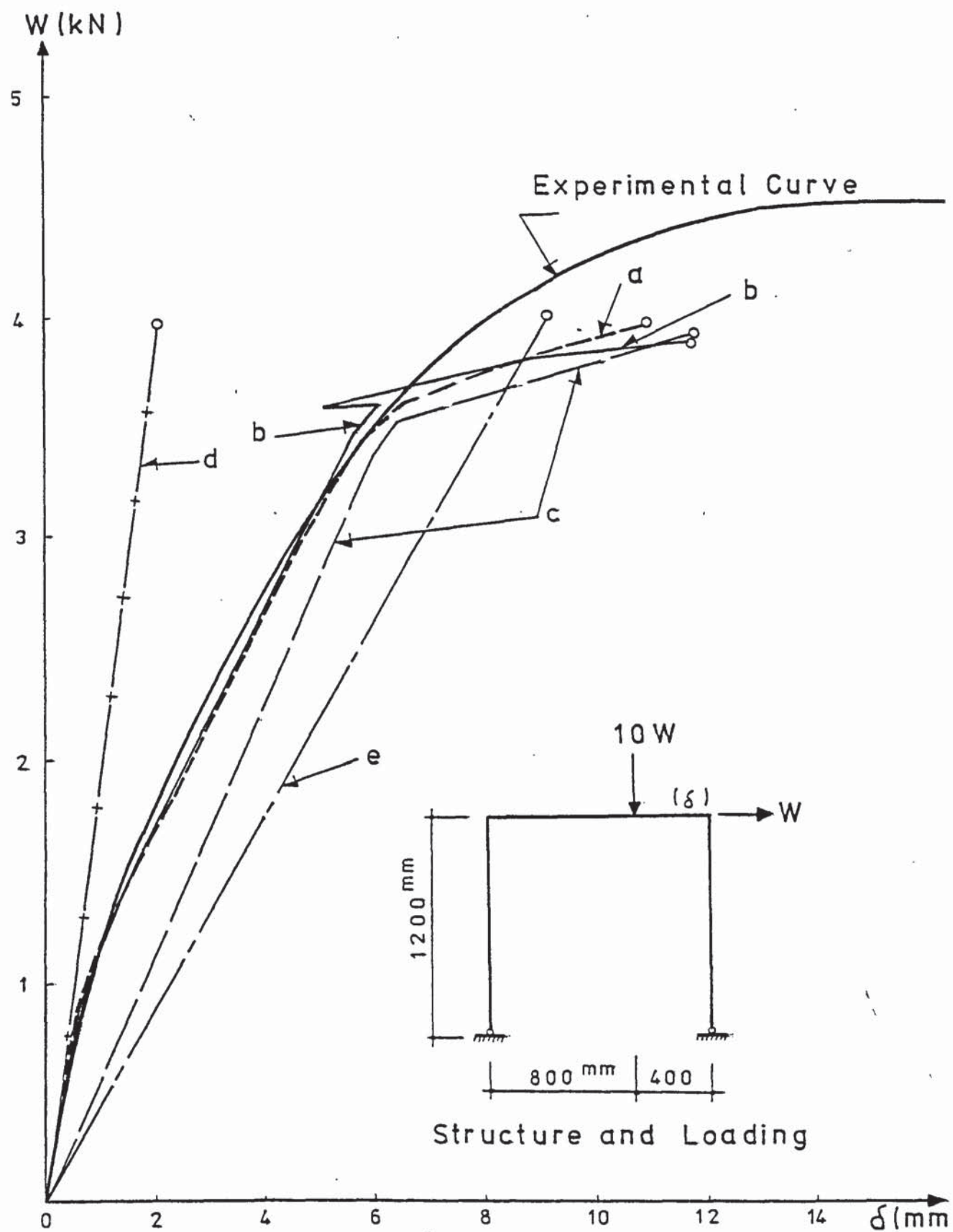
FIGURE 3.25: EXPERIMENTAL AND THEORETICAL
LOAD-DEFLECTION CURVES

indicated in the figure. The results of the analyses are summarised in table (3.4) and the load-deflection diagrams are represented in figure (3.25). The curves in figure (3.25) are indexed with the same letter as for the M-C curves in figure (3.24) to represent the particular M-C curve used for each analysis. The analysis using the trilinear M-C curve "b" gives a failure load of W = 3.89 kN being 14% lower than the experimental failure load of W = 4.52 kN. The nonlinear M-C analysis of section (3.d) using the experimental M-C curve, predict a failure load of 3.98 kN. This is indicated as curve "a" in figure (3.25). The analyses using other approximate M-C curves give almost similar values for the failure load. All of the failure loads are lower than the experimental value.

The load-deflection curves "a" and "b" of figure (3.25), obtained from the method of section (3.d) for the experimental M-C diagram and from the method given in section (3.k) for the trilinear M-C curve, are almost matching to the experimental one up to a load of 3.6 kN. This in fact shows that both of the methods may be sufficiently accurate to deal with the nonlinearity due to material properties. It may also be concluded that the trilinear representation of M-C diagrams of reinforced sections given in section (3.h) is sufficiently accurate and simple for practical use.

On the other hand, the bilinear M-C curve "c" of figure (3.24) which ignores the effect of initial flexural rigidity, over estimates the deflections although the ultimate deflection obtained by using this curve is nearly to those obtained for the M-C curves "a" and "b" of the figure. The elastic-plastic M-C curve "d" for

which the initial flexural rigidity is held up to the ultimate point under estimates the deflections while the M-C curve "e" gives the highest deflections up to a load of 3.8 kN.

It was observed that the frame is very sensitive to slight changes in the M-C diagram. As the failure stage is approached, the flexural rigidity of the members reduce and the frame becomes very sensitive to even smaller changes in the load factor. At a load of 3.6 kN the load-deflection curve "b" of figure (3.25) moves backward and then forward again, this indicates how a small alteration in the stiffness of one member at this stage can effect the behaviour of the frame considerably. At this load, more than one critical point is reached within the given tolerance. The critical point which gives the lowest load is thus selected while the others being left to be selected at a later stage which follows immediately and at the same load factor. This kind of "drift" is experienced even more in the analysis of the portal described in the next section.

3.l.2 Two Storey, Single Bay Portal Frame:-

As a second example on reinforced concrete plane frames, the two storey, single bay frame shown in figure (3.27.a) was analysed. It is one of the two storey frames tested by Deeble[16]. The dimensions of this frame are shown in the figure. The ground floor columns are simply supported at the base. All the members have the same cross section with 175mm depth and 100mm width.

The corresponding moment-curvature diagram is given in figure (3.26). This diagram was obtained experimentally be Deeble in the same manner as in the case of the portal frame of the foregoing section. To reduce the computing time involved in the
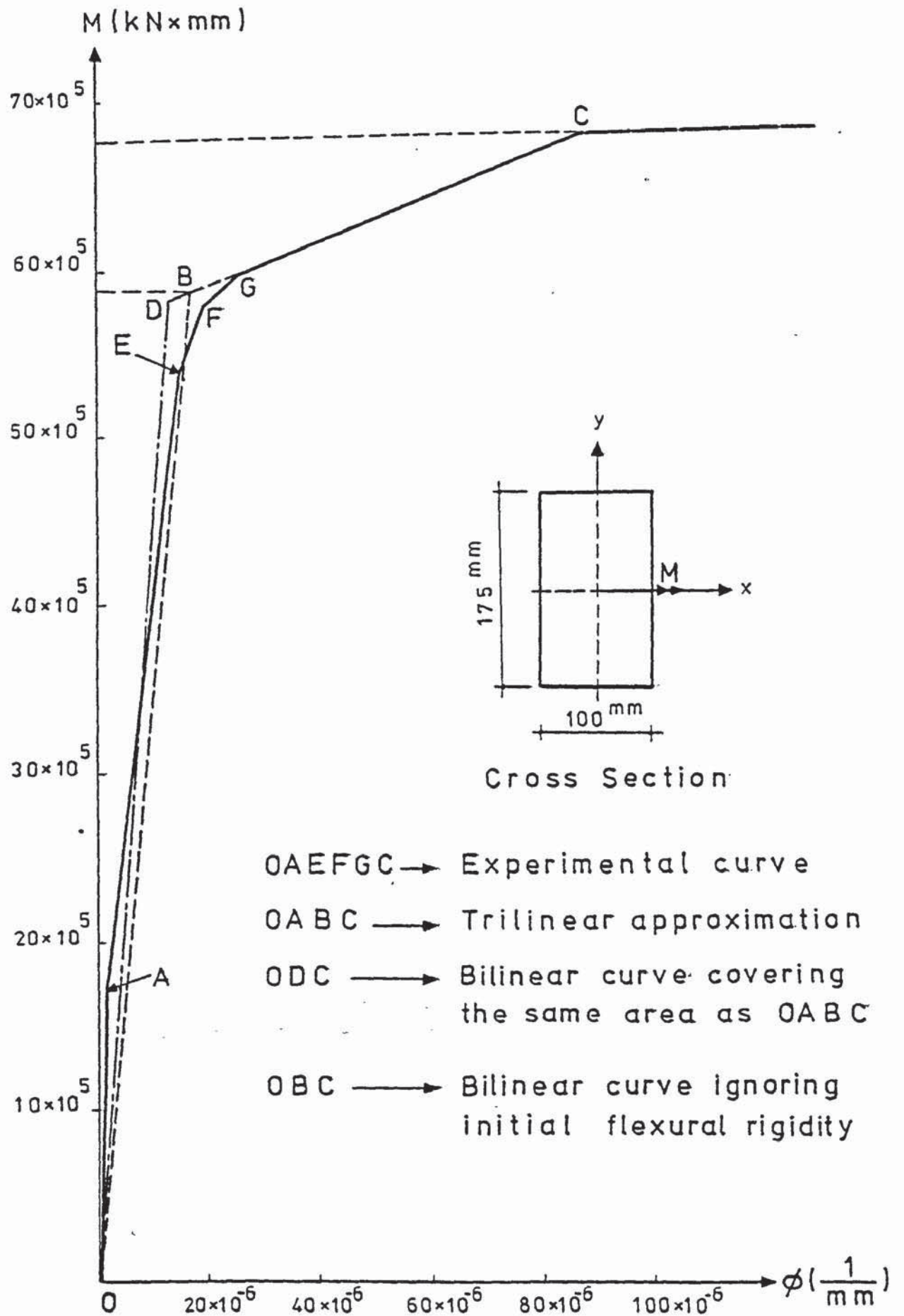
FIGURE 3.26: MOMENT CURVETURE DIAGRAM FOR THE CROSS
SECTION USED IN THE ANALYSIS OF THE TWO
STOREY FRAME

OAEFGC → Experimental curve

OABC → Trilinear approximation

ODC → Bilinear curve covering
the same area as OABC

OBC → Bilinear curve ignoring
initial flexural rigidity

W (KN)

7,5

7

6

5

4

3

2

1

EXPERIMENTAL
FAILURE W=7,47kN

ULTIMATE PREDICTED LOAD WITH NONLINEAR M-C ANALYSIS

ULTIMATE PREDICTED LOAD WITH INCREMEN.
TAL LOAD FACTOR METHOD
W = 6,566 kN

W=7,204 kN

W = 5,16 kN
Vertical deflecitios become
excessive(eventual failure)

STRUCTURAL VARIATION ANALYSIS

INCREMENTAL LOAD FACTOR METHOD

2 4 6 8 10 12 14 16 18 20 22 24 δ (mm)

10 W

W

δ

512,5 mm
512,5 mm

1070 mm

862,5 mm

1025 mm

a- Structure and Loading

FIGURE 3.27: THEORETICAL AND·EXPERIMENTAL LOAD-DEFLECTION CURVES FOR
TWO STOREY FRAME
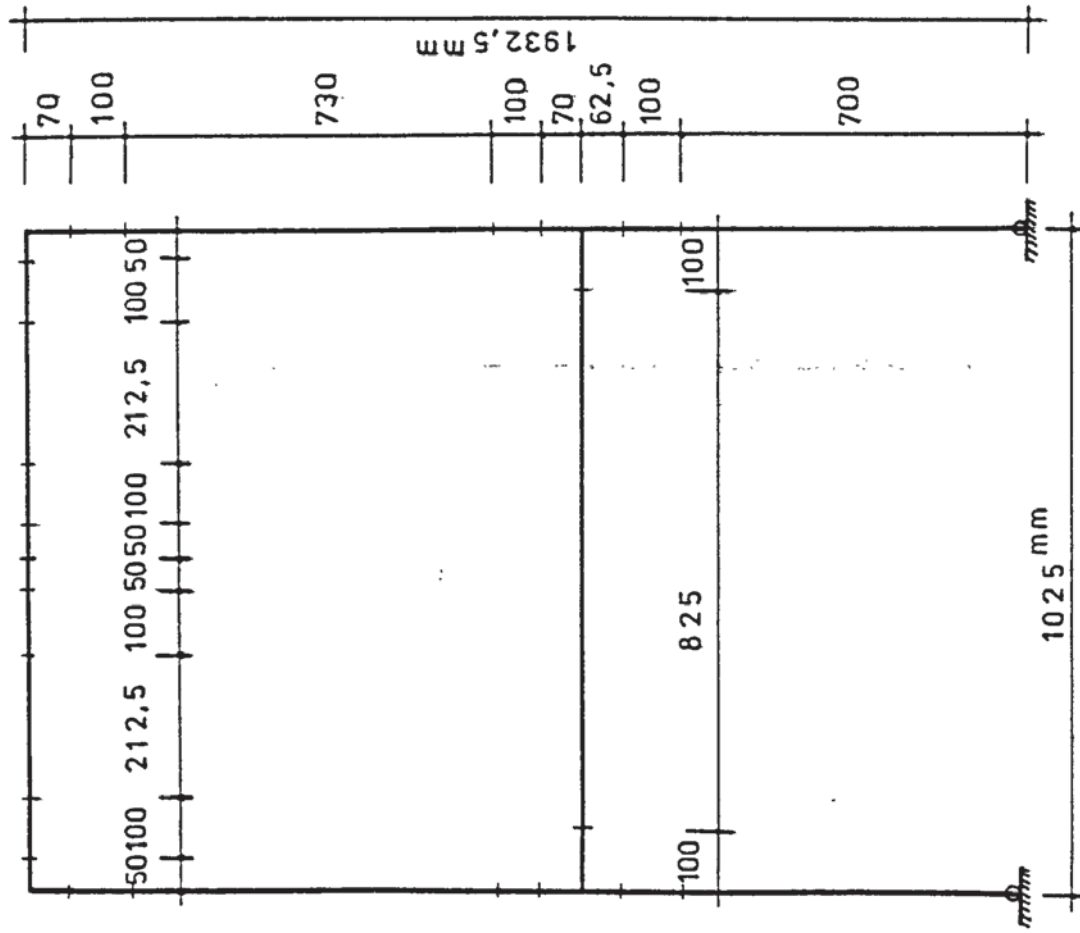
b - Second subdivision for the top storey beam (Subdivision of the rest of the structure is similar to case a)

75 100 162,5 100 7575100 162,5 100 75

c - Third subdivision for the top storey beam (The rest of the subdivision is similar to case a)

80 95 162,5 95 8080 95 162,5 95 80

a - Subdivision 1

1932,5 mm

70 100 730 100 70 62,5 100 700

50100 212,5 100 5050100 212,5 100 50

50 100 212,5

100

825

100

1025 mm

FIGURE 3.28 : SUBDIVISION OF THE MEMBERS FOR TWO STOREY PORTAL FRAME

analysis, this diagram is slightly modified and expressed by three successive straight lines connecting the points O, A, B and C in the figure. To improve the accuracy, the members were subdivided as shown in figure (3.28.a). The theoretical load deflection curves obtained by the incremental load factor method given in section (3.k) and the nonlinear M-C analysis of section (3.d) are given in figure (3.27) together with the experimental curve.

The curve obtained by the incremental load factor method gives a better estimate of the deflections than the nonlinear M-C analysis. It is reasonably smooth up to a load of 5.5 kN. After that some drifting is noticed. The analytical failure load was noticed to be 6.566 kN, which is 12.1% lower than the experimental failure load of 7.47 kN.

The curve obtained by nonlinear M-C analysis is steeper than the other curves up to a load of 5.00 kN. A sudden drift was then experienced and the vertical deflections became excessive at w = 5.16 kN. For further increases in the loads, the horizontal deflections also increased drastically until an overflow was registered by the computer at w = 7.204 kN. In spite of drifting encountered in the load-deflection diagrams, both theories give conservative results compared to the experimental, which makes them safe to be used. The difference between the theoretical and the experimental failure loads may also be due to experimental errors e.g. supports not being perfect knife edges.

To investigate the cause of drifting in the load-deflection curve, the frame was also analysed for bilinear M-C curves OBC and ODC of figure (3.26). The analysis for curve ODC was repeated for the subdivisions shown in figures (3.28.b) and (3.28.c).
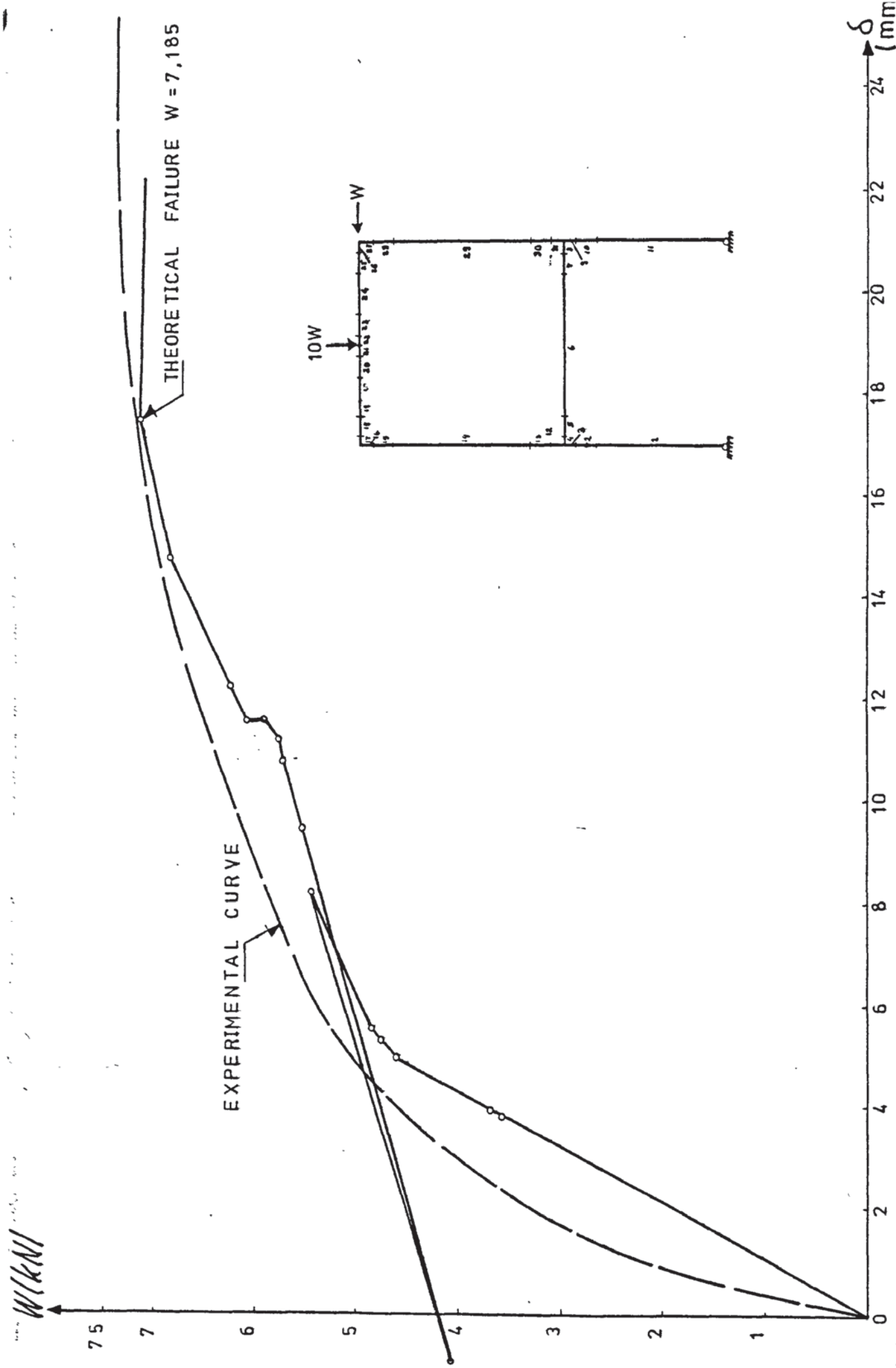
FIGURE 3.29: EXPERIMENTAL AND THEORETICAL LOAD-DEFLECTION CURVES FOR TWO STOREY PORTAL FRAME [Bilinear M-C curve OBC of fig.(3.26) and subdivision of fig. (3.28 b) were employed]
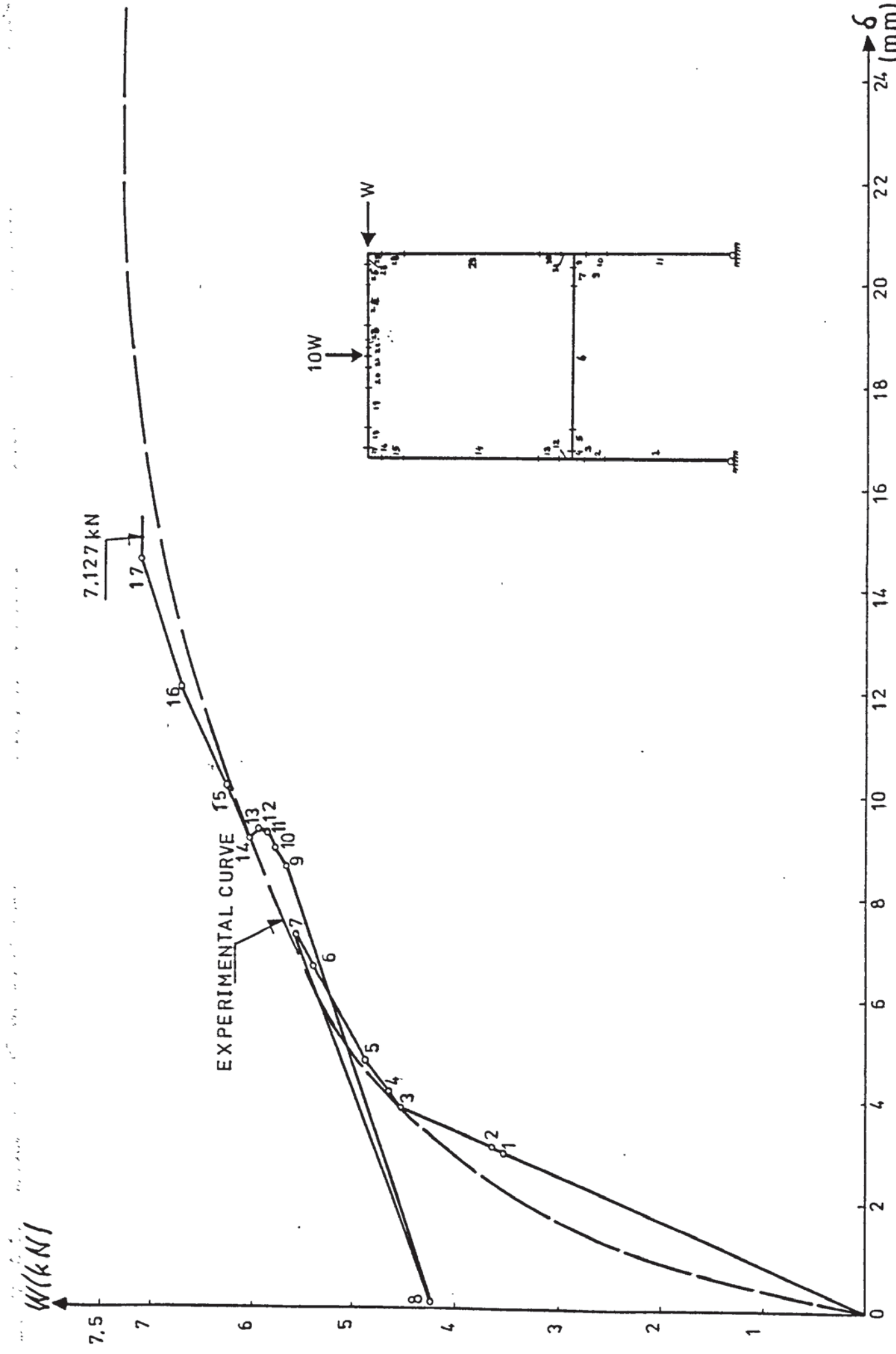
FIGURE 3.30: EXPERIMENTAL AND THEORETICAL LOAD DEFLECTION CURVES OF TWO STOREY FRAME [Theoretical curve was obtained for bilinear M-C curve ODC of figure (3.26) and subdivision in figure (3.28a)]

Drifting was also observed in the analyses employing the M-C diagrams OBC and ODC of figure (3.26) for the subdivision given in figure (3.28.a). However it was not as significant as that occurred in the analysis employing the trilinear M-C diagram OABC of figure (3.26). The load-deflection curves obtained from these analyses are shown in figures (3.29) and (3.30).

The load-deflection curves obtained from the analyses employing the M-C curve ODC of figure (3.26) and the subdivisions given in figures (3.28.b) and (3.28.c) are presented in figures (3.31) and (3.32) respectively. In figure (3.31) the load-deflection curve is reasonably smooth throughout, but a slight drifting can still be observed. However, no drops in the load factor was experienced.

. The load-deflection curve was further improved in the last analysis. It can be seen in the corresponding figure (figure 3.32), that the drifting has almost vanished, and the theoretical load deflection curve almost matches that obtained experimentally after a load of 4.60 kN. The deflections, however, were overestimated at the earlier stages of loading. This is due to the fact that the M-C diagram employed ignores the initial flexural rigidity.

These results may indicate that the drifting at a stage is mainly caused by picking only one of the many critical points which are about to be reached almost at the same time. As soon as all of these points have been taken account of, the load deflection curve becomes smooth again. Because the incremental load factor approach involves a repeated solution of joint equilibrium equations, the prediction of each critical point on the load-deflection curve is not affected by any other point on it.
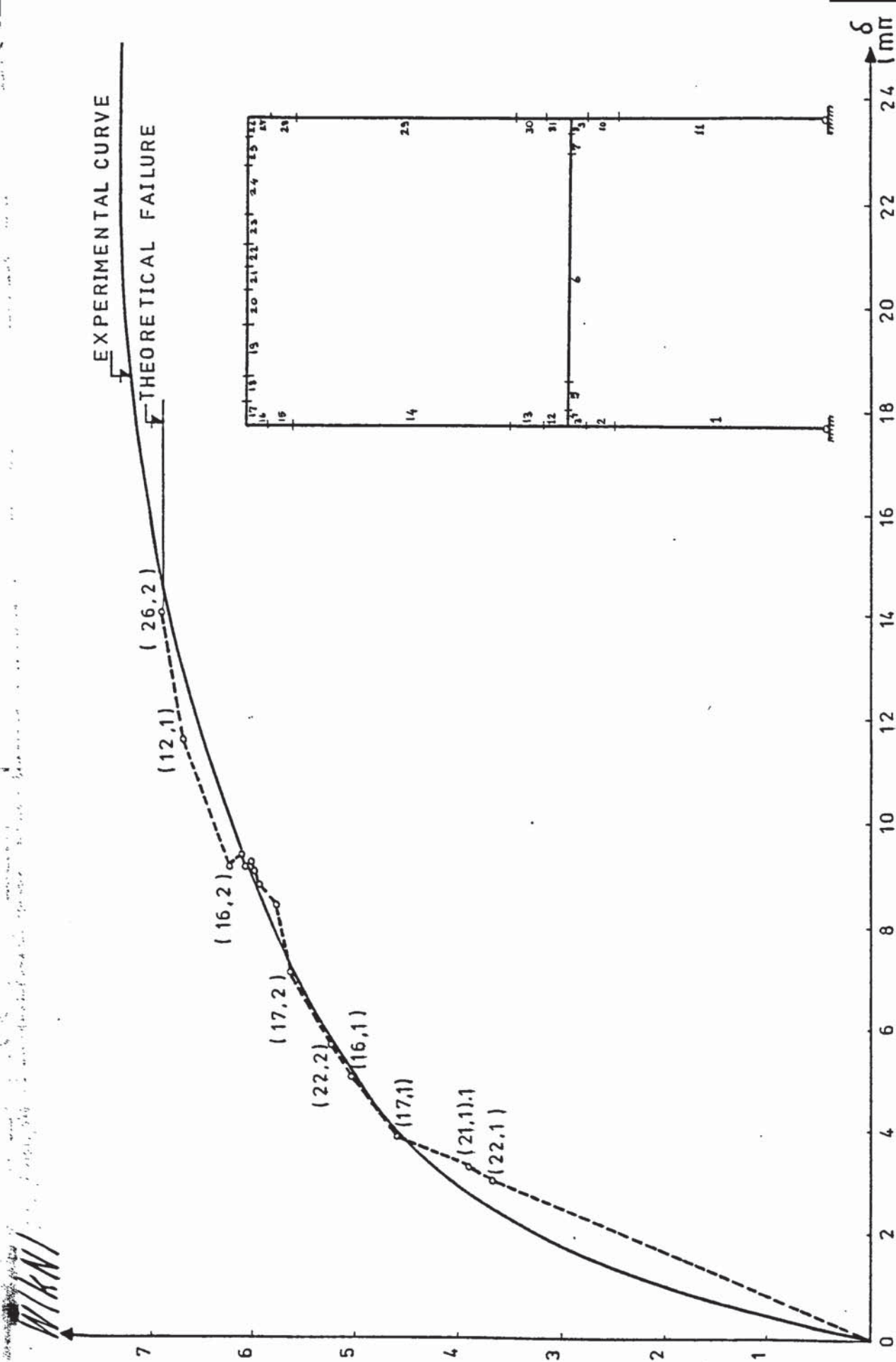
FIGURE 3.31: EXPERIMENTAL AND THEORETICAL LOAD DEFLECTION CURVES FOR THE TWO STOREY PORTAL FRAME [The theoretical curve was obtained for M-C diagram ODC of fig.(3.26) and subdivision of fig.(3.28b)]
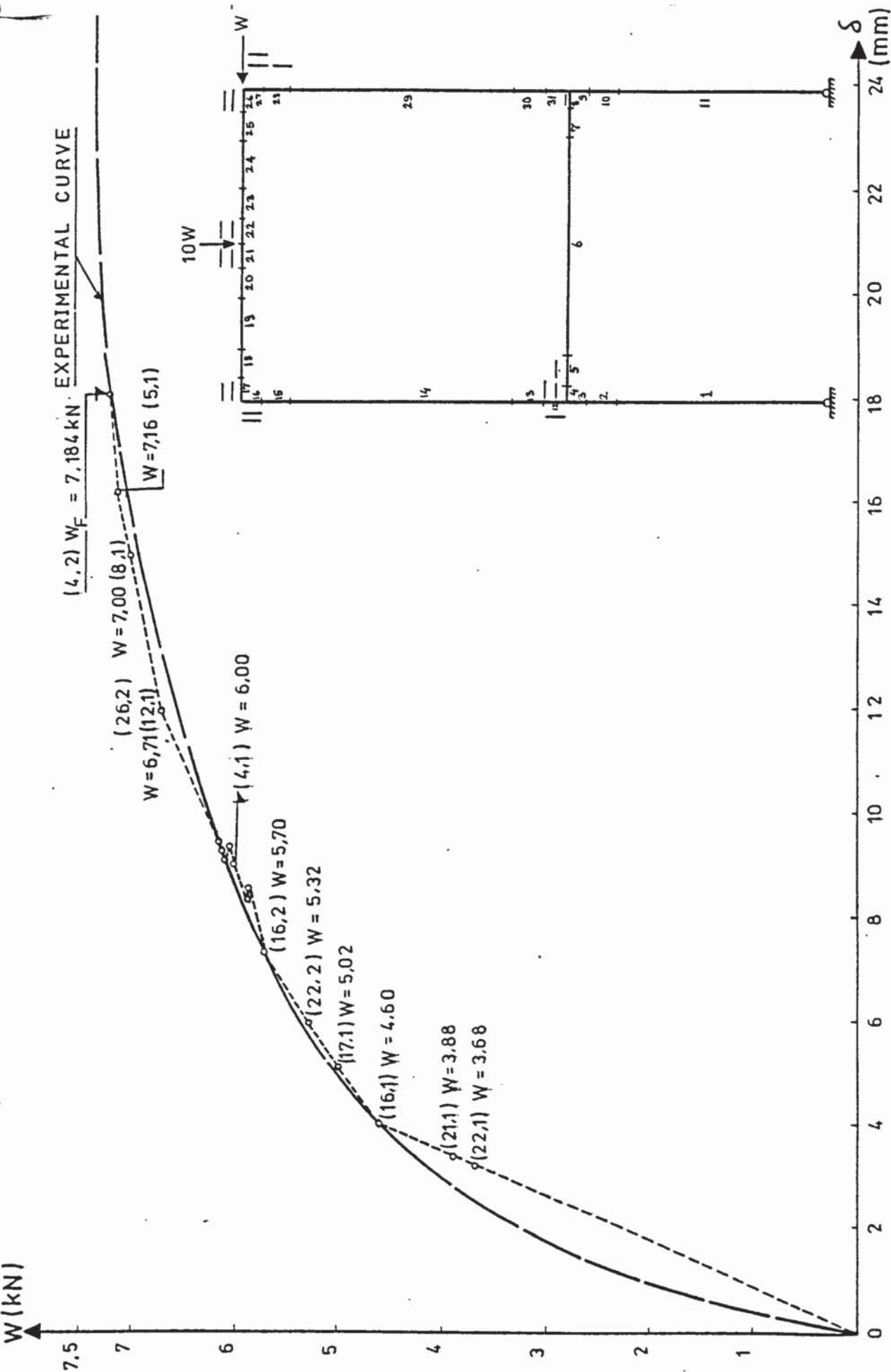
FIGURE 3.32: EXPERIMENTAL AND THEORETICAL LOAD DEFLECTION CURVES FOR THE TWO STOREY PORTAL FRAME [The theoretical curve was obtained for the M-C diagram ODC of figure (3.26) and subdivision of figure (3.28 c)]

Therefore a drifting may be experienced in a region until the program automatically corrects itself, and the rest of the load-deflection curve remains unaffected.

It is also shown that a suitable subdivision of the members may eliminate the drifting.

Finally, it may also be concluded that simpler M-C diagrams, covering the same area as the original one may estimate the deflections reasonably well at stages close to failure.

3.1.3 Six Storey, Single Bay Reinforced Concrete Frame:-

For a further justification of the incremental load factor method given in section (3.k.), the practical type frame shown in figure (3.33) is considered. This was originally described by Corradi et al[22] and analysed under the working loads also given in the figure. The finite element method was used in conjunction with the method of imposed rotations[23]. The effect of axial forces were taken into account both on the stability and on the M-C relationships of the columns.

In the present analysis, the axialca. loads were calculated approximately from a basic isostatic frame obtained by releasing the redundant forces. Moment-curvature relationships of columns corresponding to these axial forces were obtained by interpolation of the M-C diagrams in figure (3.34.a), given in reference (22). Some difficulties were encountered in choosing the appropriate M-C relationship for the inner parts of the beams, from those of figure (3.34.b), given by Corradi. Two different M-C diagrams were given for the inner and outer cross sections, viz. the curves A and B in the figure. They were both derived for the case when the compression zone is at the bottom face of the beam. However
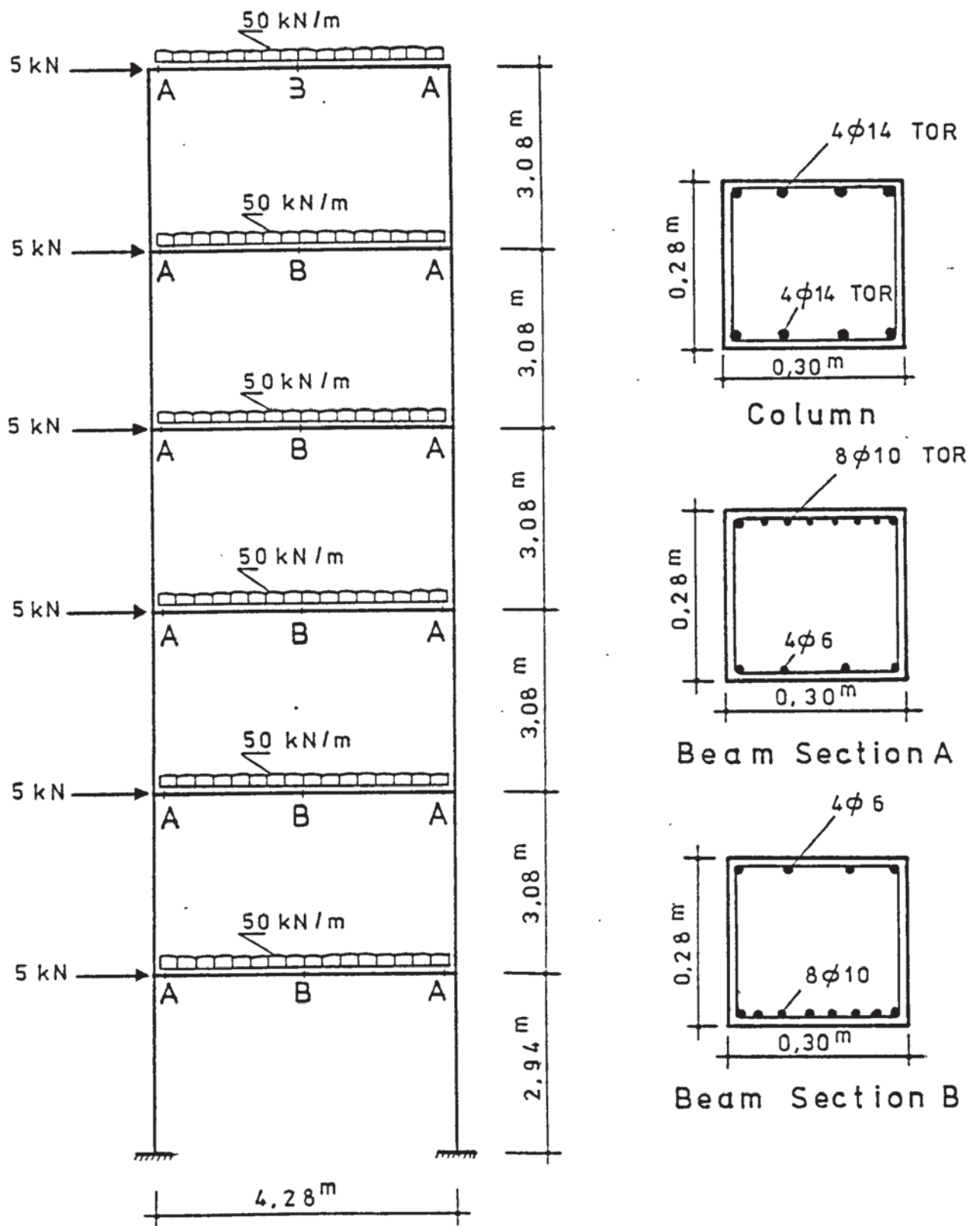
FIGURE 3.33: SIX STOREY FRAME AND LOADING
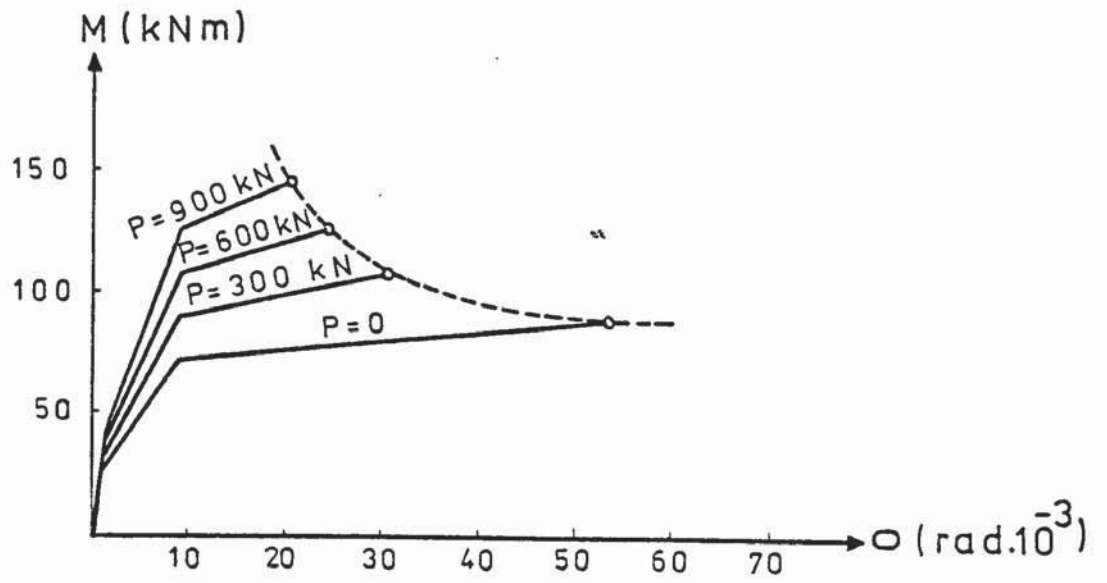
a- M—C Diagrams for columns
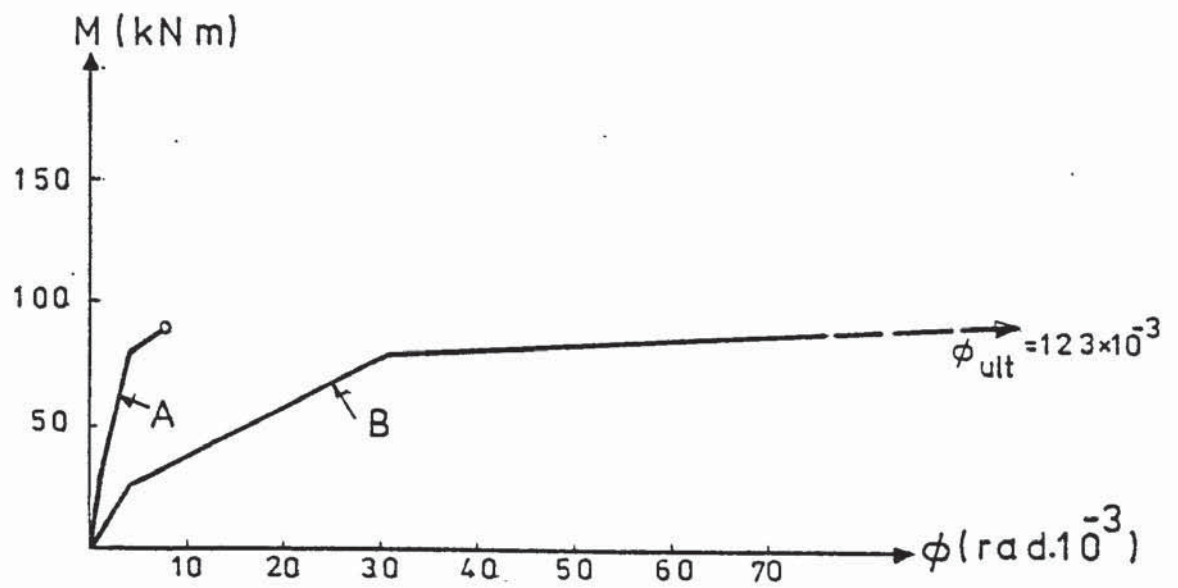
b- M—C Diagrams for beams

FIGURE 3.34: MOMENT CURVATURE DIAGRAMS

100 kN.m

Moment Scale

67.4
45.1
35.1

C

D

80.8
54.0
46.1

D

B

C

B

B

3.08 m

3.08 m

D

3.08 m

3.08 m

9.5 kN.m

13.9 kN·m

C

D

3.08 m

34.8 kN·m

B

2.94 m

4,028 m

A

C

B

D

1 2 3 4 5 6 c
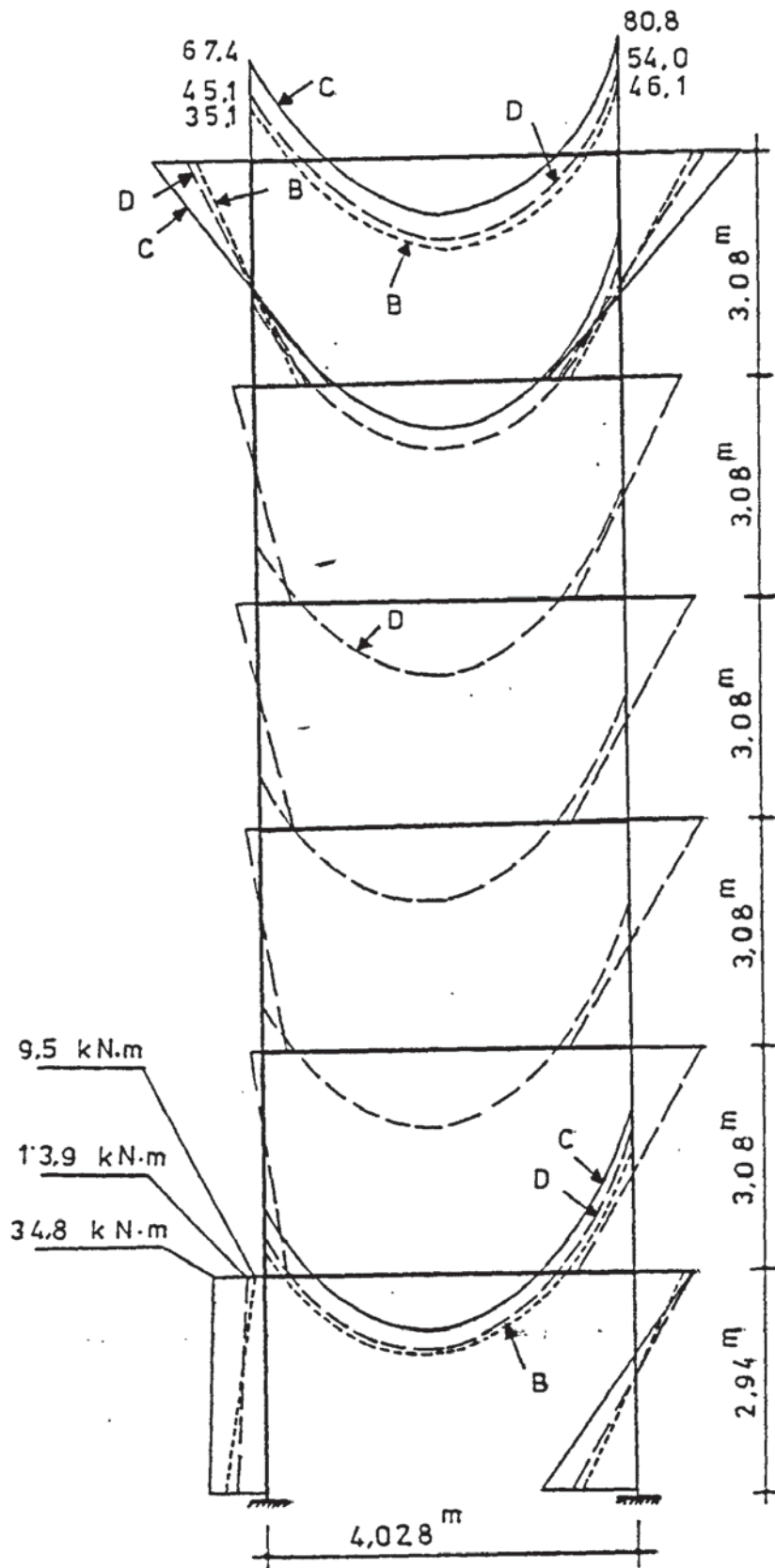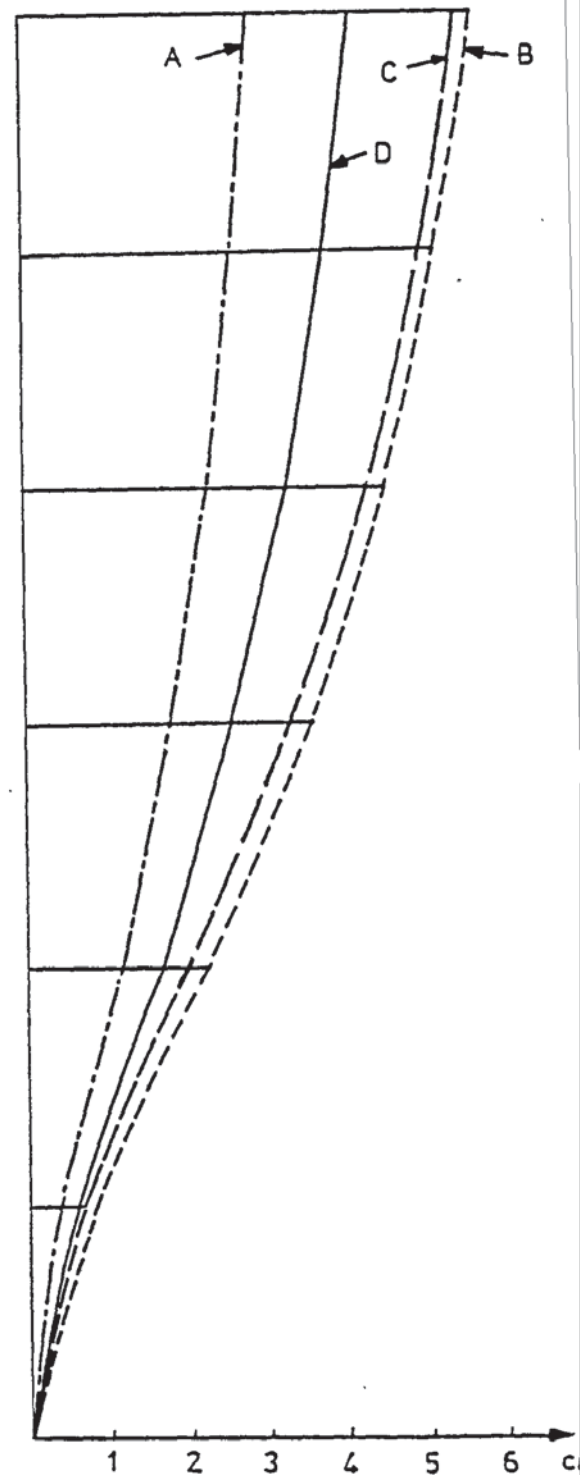
b–Horizontal deflection

a–Moment diagram

FIGURE 3.35: COMPARISON OF THE BENDING MOMENT AND
LATERAL DEFLECTION DIAGRAMS FOR SIX-
STOREY R.C. FRAME

it may be seen from figure (3.33) that sagging moments may act in the spans of the beams, under the given loading. Thus the compression zone takes place at the top of the inner cross sections. This implies that the M-C diagram adopted for the outer parts would also be used for the inner parts.

Two analyses were carried out by the author. The first analysis uses the M-C diagrams as implied by Corradi. The resulting bending moment and deflection diagrams are shown as curves C in figures (3.35.a) and (3.35.b) respectively. In the same figures curves B represent the moments and deflections obtained by Corradi. The deflection diagram obtained from the linear elastic analyses is given by curve A in figure (3.35.b). The deflection curves B and C of figure (3.35.b) are in a very close agreement, although the corresponding bending moments were found to be considerably different.

In the second analysis the M-C curve A, of figure (3.34.b), was employed both for the inner and outer parts of the beams. The resulting bending moment and deflection diagrams are given by curves D in figures (3.35.a) and (3.35.b). The maximum deflection obtained in this case was about 23% less than that obtained by Corradi, while the bending moments obtained in both analyses are in a reasonably good agreement.

CHAPTER 4

FAILURE LOAD ANALYSIS OF COMPLETE BUILDING STRUCTURES

4.a. Introduction:

The aim of this chapter is to present a method for the failure analysis of multistorey buildings consisting of a grillage system of parallel floor slabs and shear walls, together with an arbitrary arrangement of parallel skeletal sway frames as shown in Figure (4.1). The material of the frame and grillage may be the same or different. For instance, the entire structure may be made out of reinforced concrete. On the other hand, the frames may be manufactured out of steel while the slabs and the shear walls may be made out of reinforced concrete. In the case of structures prepared for laboratory tests, the shear walls and slabs may also be manufactured out of perspex.

The method traces the behaviour of these structures up to and including the stage of failure. As the external loads acting on a structure are increased progressively a number of qualitative "critical changes" take place in the structure. These are:

i - A plastic hinge may develop in one or more of the steel frames. Contrary to the expectation of plane frame analysts, these hinges do not develop all at once[70] nor do they develop in one, say the weakest, of the frames. In the case of reinforced concrete frames such hinges do not take place. Instead the moment curvature relationships of the cross sections change in some parts of these frames.

ii - One or more of the shear walls or slabs may crack while the overall structure remains capable of carrying further loads.

iii - In the case of laboratory structures, one or more of the slabs or shear walls may buckle.
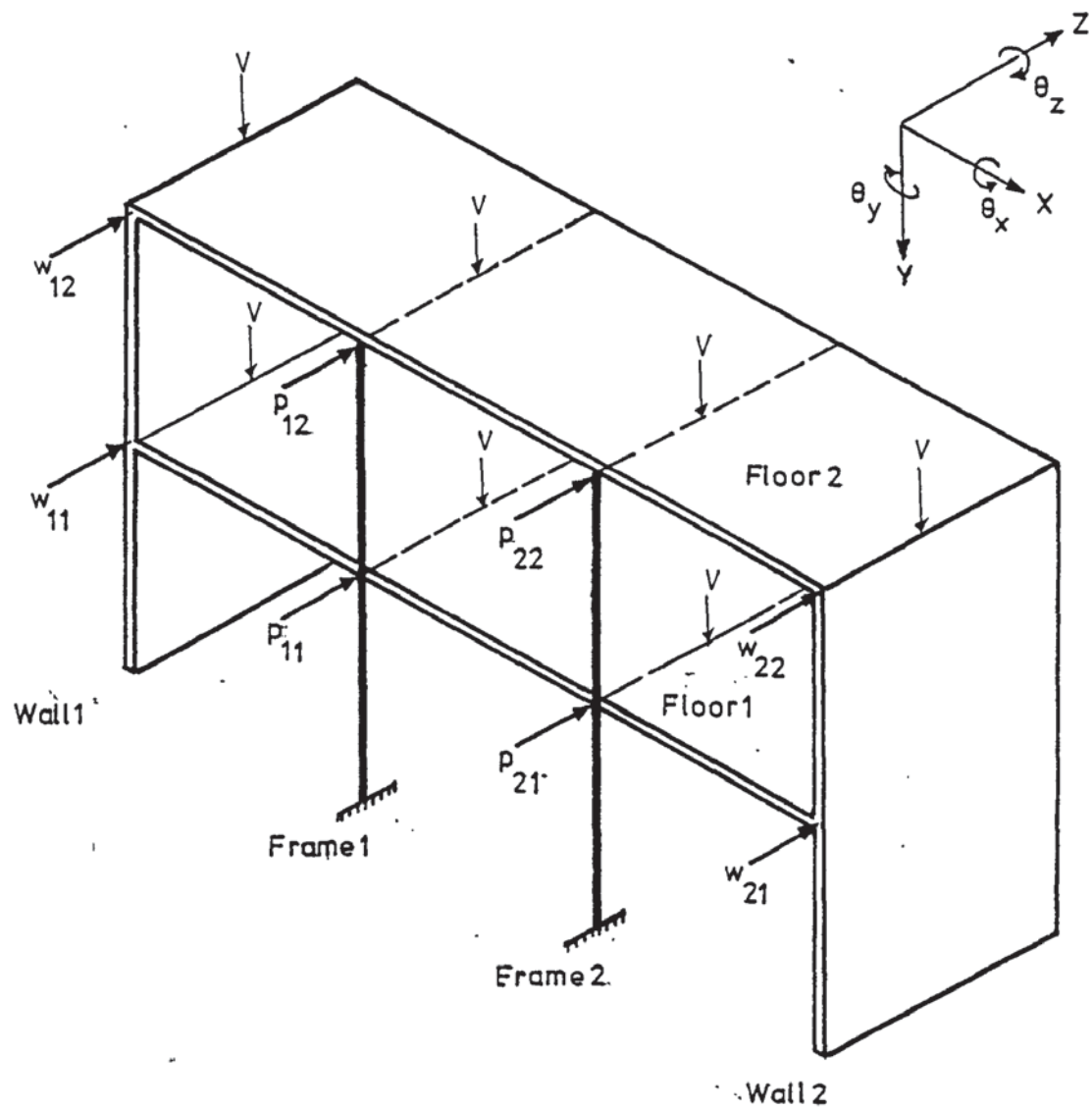
FIGURE 4.1: A COMPLETE STRUCTURE, LOADING AND
SIGN CONVENSION

The overall failure of the structure takes place not as a result of one of the above mentioned "critical" changes but due to the combination of these factors.

4.b. Separation of Wind Loads:

Plastic theoreticians[70] have assumed that the loads acting on a frame may be considered to increase proportionally. The exact opposite of this assumption is true. In reality, even if a complete structure is loaded proportionally, the part of that load transmitted to any of its frames does not follow this pattern. Thus the whole concept of plastic analysis of frames is invalid. Furthermore, before any analysis can proceed it becomes necessary to calculate, at each of loading, the portion of the external loads transmitted to each part of the structure. To do this, the method proposed in references (31) and (66) are also adopted here. This considers the complete structure as if it consists of two distinct components. These are the bare frames and the grillage system of slabs and shear walls. The applied vertical loads $\underline{V}$ shown in Figure (4.1) are those carried by the frames and may be increased proportionally. The wind load vector $\underline{P}$ acting at the junctions of the frames and the slabs is divided into a vector $\underline{f}$ transmitted to the frames and another vector $\underline{g}$ transmitted to the grillage system of slabs and shear walls. Thus

$$\underline{P} = \underline{f} + \underline{g} \qquad\qquad 4.1$$

It will be shown later that while $\underline{P}$ may be increasing proportionally, in the same manner as $\underline{v}$ vectors $\underline{f}$ and $\underline{g}$ do not follow $\underline{P}$. Indeed, while $\underline{P}$ is increasing some elements of $\underline{f}$ or g may even reverse their directions. Vectors $\underline{f}$ and $\underline{g}$ are calculated making use of the compatibility conditions at the junctions of the frames and floors.

Thus the horizontal deflection of the grillage and bare frames at the junctions must be equal[31,66], giving:

$$\underline{f} = (\underline{G} + \underline{F})^{-1} (\underline{G} \, \underline{P} + \underline{a}) \qquad\qquad 4.2$$

where $\underline{a}$ is the vector of horizontal deflections of the junctions when loads $\underline{w}$, shown in figure (4.1), are applied to the shear walls. The symmetrical matrix $\underline{G}$ is the influence coefficient matrix of the grillage and defines the horizontal displacement at each junction of the grillage due to unit loads at the various junctions of the floors and frames. Similarly the symmetrical matrix $\underline{F}$ is the influence coefficient matrix for the frames and has the same order as G.

4.c. Assumptions:

i - While the frames may be different from one another, they are assumed to remain parallel to each other and deflect in the zy plane. Each joint of the frame has three degrees of freedom in z, y and θ_x directions. The cooordinate axes are shown in figure (4.1).

ii - The grillage consists of shear walls and slabs that are either rectangular or can be divided into rectangles by lines drawn parallel to the coordinate axes. The stiffness of each panel is obtained from the slope deflection equations for a deep beam in which the shear stress distribution is parabolic[71]. Each joint in the grillage is assumed to have freedom in z, θ_x and θ_y directions.

4.d. Progress Towards Failure:

The major steps for the full analysis of a complete structure up to collapse are as follows:

1 - To begin with the structure is elastic. Matrix displacement method is used to calculate the influence coefficients of each

frame and also of the grillage system in the same manner as in references (31) and (66). Equations (4.2) are then used to calculate the force vectors $\underline{f}$ acting on each frame. Equations (4.1) then give the force vector $\underline{g}$ acting on the grillage. If the external loads are now multiplied by a load factor λ, the total vertical load at a joint in the frame will become λV where V is the working vertical load at the joint.

On the other hand the external working wind load P_{ij} at junction ij is divided between the frame i and the slab to which it is connected at floor level j, thus:

$$P_{ij} = f_{ij} + g_{ij} \qquad\qquad 4.3$$

Thus when the load factor is λ the junction ij of the frame is subject to a horizontal load λf_{ij} while the grillage is subjected to a horizontal load λg_{ij} at the same junction.

2 - Each frame is now analysed elasto-plastically to obtain the load factor λ at which a plastic hinge develops. The procedure for this is similar to that given in references 20 or 31.

As the loads $\underline{f}$ acting on each frame are different from frame to frame, the load factor for the formation of a hinge is also different from one frame to another. The lowest load factor λ_{FL} of these is selected as being the one that causes a plastic hinge to form anywhere in the structure.

3 - On the other hand the grillage is analysed elastically under factored loads $\lambda_G \underline{g}$ acting at the junctions and $\lambda_G \underline{w}$ acting on the shear walls. This is to calculate the load factors λ_{GC} at which one of the panels cracks and λ_{GB} at which one of them buckles.

4 - The next critical stage in the structure is obtained by calculating the "critical load factor" λcr. This is the lowest

of λ_{FL}, λ_{GB} or λ_{GC}. Thus a critical load factor is defined as at which a change takes place either in one of the frames or in one of the panels. At the kth critical stage this load factor is λcr_k.

5 - If $\lambda cr = \lambda_{FL}$ a hinge is inserted in the frame for which λ_{FL} was selected. This hinge alters the frame basically and makes it more flexible and incapable of sustaining its share of the transmitted loads. Part of these have therefore to be transferred to the slabs and transmitted to the other frames and the shear walls.

If on the other hand, $\lambda_{cr} = \lambda_{GC}$ or $\lambda_{cr} = \lambda_{GB}$, the stiffness of the panel that has cracked or buckled is reduced drastically to the extent that the panel may now be disregarded. In the computer program written for this purpose, it is assumed that, from now on, the modulus of elasticity E and the shear modulus G of this panel are reduced to ψE and ψG, where ψ is a small preselected factor such as 0.01.

6 - Once λ_{cr} is decided for the whole structure, the member forces and deflections in the grillage and each frame are calculated for this load factor.

7 - The influence coefficient matrix of a frame is changing continuously. This is not merely because the axial loads in its members are changing but also because a frame with hinges is more flexible than without or with fewer number of hinges. Similarly the influence coefficient matrix of the grillage also changes when one or more of its panels crack or buckle. At each critical load factor therefore, once the property of a frame or a panel alters, the new influence coefficient matrices $\underline{F}_n$ or $\underline{G}_n$ are recalculated.

Each time a new matrix $\underline{F}_n$ or a new matrix $\underline{G}_n$ is prepared, the inverse matrix transformation (4.2) is carried out to calculate the new forces $\underline{f}_n$ transmitted to the frames. Equations (4.2) are

now in the form:

$$\underline{f}_n = (\underline{G}_n + \underline{F}_n)^{-1} (\underline{G}_n \underline{P} + \underline{a}_n) \qquad 4.4$$

The new influence coefficient matrix $\underline{G}_n$ is reconstructed only when the stiffness of a panel is altered while $\underline{F}_n$ is reconstructed after every new plastic hinge. Notice that as soon as the flexibility of the grillage changes, the deflections $\underline{a}$ due to loads acting on the shear wall change to $\underline{a}_n$.

8 - Once a critical load factor λ_{cr} is calculated the search is continued for the next one and the process is terminated when the sway deflection of the structure increases considerably and further analysis cannot be carried out due to an overall loss of stiffness.

4.e. Non-Proportional Loading:

It was shown above that the separate flexibilities of the frames and the grillage are changing continuously. These changes cause the amount of external wind loads transmitted to any frame to vary non-proportionally. This is in spite of the fact that the external loads on the structure itself may be increasing proportionally. Consider that k-1 critical stages have been attained by a structure at load factors λ_{cr_2}, λ_{cr_2}, $\cdots$, $\lambda_{cr(k-1)}$ and that the next, i.e. k^{th}, critical stage is to take place at the unknown load factor λ_{crk}. If the working vertical load acting at a joint m in a frame is V_m then the element of the load vector corresponding to this load is $\lambda_{crk} V_m$. Thus the vertical loads acting on the structure and on each frame increase proportionally. Similarly, the horizontal wind load acting on the shear walls also increases proportionally and at stage k the load vector acting on these walls is $\lambda_{crk} \underline{w}$.

Every time equations (4.4) are solved the forces $\underline{f}_n$ transmitted to a frame are calculated. Consider that the horizontal forces transmitted to junction ij of a frame are $f_1, f_2, \cdots, f_{k-1}, f_k$. The total load acting on the frame at this junction is therefore given by

$$\ell_{ijk} = \lambda_{cr_1} f_1 + (\lambda_{cr_2} - \lambda_{cr_1}) f_2 + \cdots + (\lambda_{crk} - \lambda_{cr(k-1)}) f_k$$

i.e. $\ell_{ijk} = -(f_2-f_1)\lambda_{cr_1} + (f_2-f_3)\lambda_{cr_2} + \cdots$

$$+ (f_{k-1} - f_k)\lambda_{cr(k-1)} + f_k \lambda_{crk} \qquad 4.5$$

All the terms in equation (4.5) are known except the last in which f_k is known but λ_{crk} has to be found iteratively. To do this λ_{crk} is replaced by a specified value $\delta\lambda$ and the load ℓ^*_{ijk} acting at ij on the frame is calculated from equation (4.5). The usual iteration method is then used to calculate λ_{crk} (see reference 31). A similar procedure is used to calculate the critical load at which one of the panels of the grillage cracks or buckles.

Because the loading is non-proportional, the possibility of plastic hinges becoming inactive increases. This is yet another reason why a simple plastic approach becomes unacceptable[70]. In the present work the method used to deal with inactive hinges is that given by Davies[30].

4.f. Lateral Buckling of Slabs:

Thick reinforced concrete slabs are often used for the floors and shear walls of practical structures. These are unlikely to buckle before they crack or before the frames collapse. However to make the proposed method general some, approximate method should be included to cover the case of slab buckling. This becomes particularly useful in laboratory test cases in which the slabs

are manufactured out of thin perspex sheets.

The method presented here is for the elastic lateral buckling of a deep rectangular panel subject to unequal end moments about its major axis. The panel is elastically restrained at its ends about its minor axis. This method is developed by combining those given by Horne[73] and by Trahair[75].

The slab shown in figure (4.2) has x-x as its major axis and Y-Y as its minor axis. It has a span L, a depth d and thickness t. At both ends the slab is simply supported about its minor Y-Y axis and subjected to unequal end moments M_{yz} and M'_{yz} as shown in the figure. Horne dealt with the case of an I beam which was simply supported at both ends and subject to unequal end moments. However by neglecting the flanges of such a beam, the slab shown in figure (4.2) is obtained.

The slab shown in figure (4.3) has the same dimensions as that shown in figure (4.2). This slab is elastically restrained at its ends about its Y-Y axis and subjected to equal and opposite end moments M_{yz} and $-M_{yz}$ as shown. This is the case dealt with by Trahair.

In dealing with the lateral buckling of slabs, the following assumptions are made.

1 - Because the cross-section of the slab is very narrow rectangle, the warping rigidity of the slab is neglected.

2 - Warping is not prevented at the ends of the slab.

3 - The stiffness EI_{xx} is very high compared to EI_{yy} and GJ of the section. Here E is the modulus of elasticity, I_{xx} and I_{yy} are the second moment of area about the major and minor axes respectively and GJ is the torsional stiffness of the section.
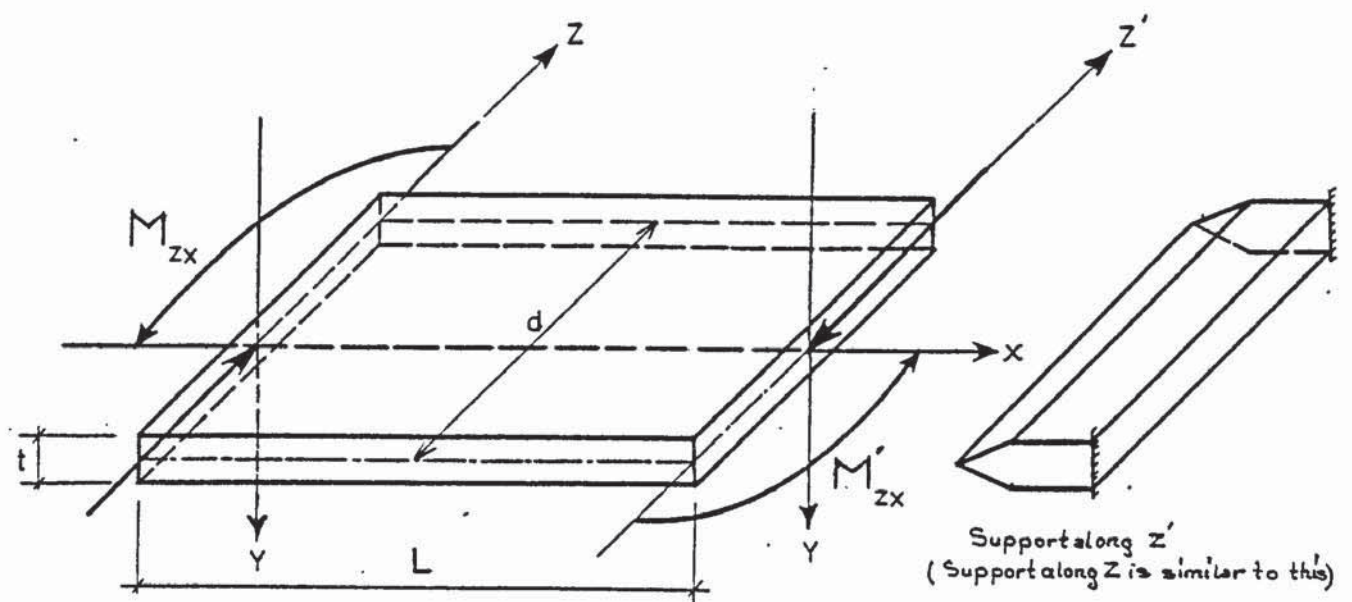
FIGURE 4.2 : PANEL WITH NO LATERAL END RESTRAINTS
AND SUBJECT TO UNEQUAL END MOMENTS
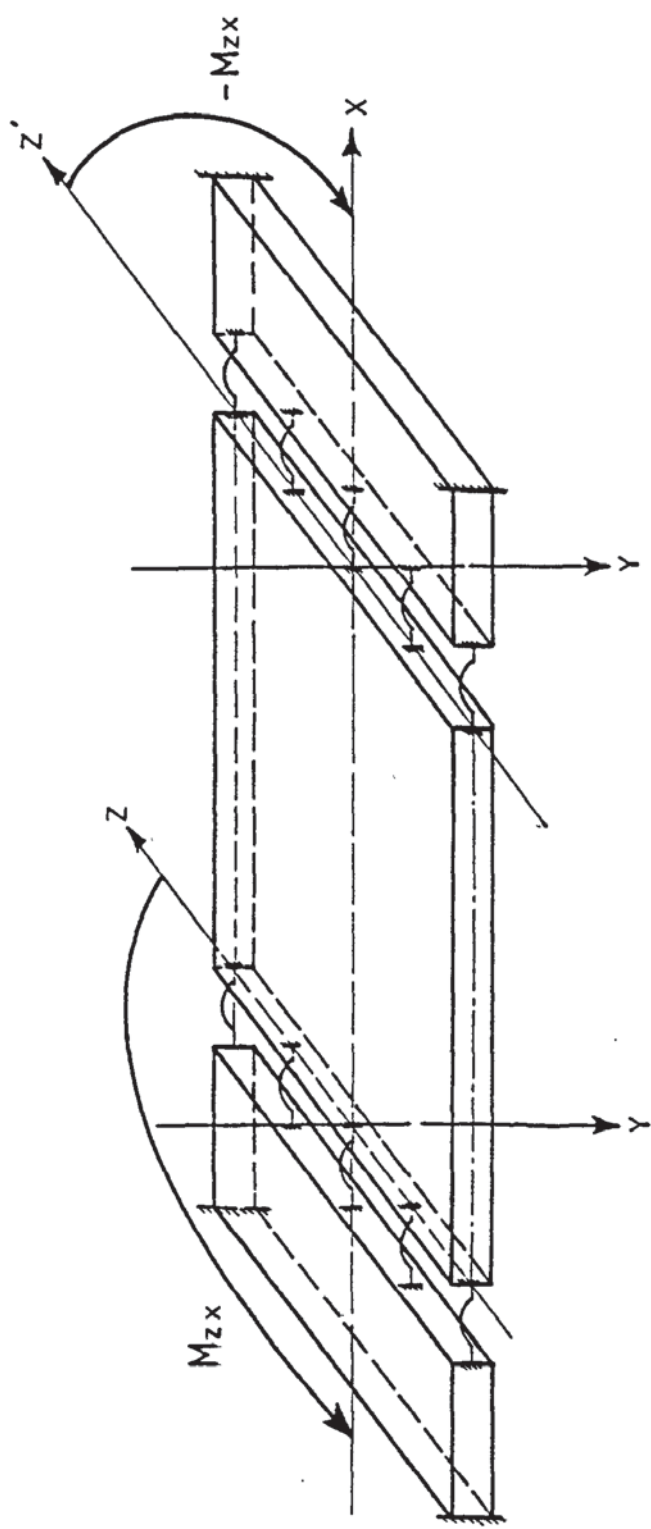
FIGURE 4.3: PANEL WITH END RESTRAINS AND SUBJECT TO EQUAL AND OPPOSITE END MOMENTS

4 - The stiffness EI_{xx} is not affected by the end moments until the lateral instability takes place.

5 - The end supports provide sufficient restraints against torsion and any torsion developed has no effect on the lateral buckling.

A number of other simplifying assumptions are also made and are given later in the text.

Horne expressed the elastic critical moment M_{yzcr} in the form:

$$M^2_{yzcr} = (F + F'\delta) M^2_{Eyz} \qquad 4.6$$

where δ defines the warping rigidity factor of the section which is assumed to be zero here as the section is a narrow rectangle. Thus equation (4.6) becomes:

$$M^2_{yzcr} = F M^2_{Eyz} \qquad 4.7$$

The factor F is a parameter which depends on the ratio $\zeta = M'_{yz}/M_{yz}$ and its values were tabulated by Horne and reproduced here graphically in figure (4.4).The range of ζ between +1 and -1 covers all the possible cases. In equations (4.6) and (4.7) M_{Eyz} is the elastic critical moment for the case when the end moments are equal and opposite. This critical moment is given by[89]:

$$M_{Eyz} = \pi \sqrt{EI_{yy}GJ}/L \qquad 4.8$$

Substituting for M_{Eyz} from equation (4.8) into equation (4.7) we obtain:

$$M_{yzcr} = \pi \sqrt{F} \cdot \sqrt{EI_{yy}GJ}/L \qquad 4.9$$

On the other hand, for the case of equal and opposite moments, figure (4.3), Trahair expressed the magnitude of the elastic critical moment as:

$$| M_{yzcr} | = \delta \sqrt{EI_{yy}GJ}/L \qquad 4.10$$

where δ is a function of the rotational restraining stiffness of
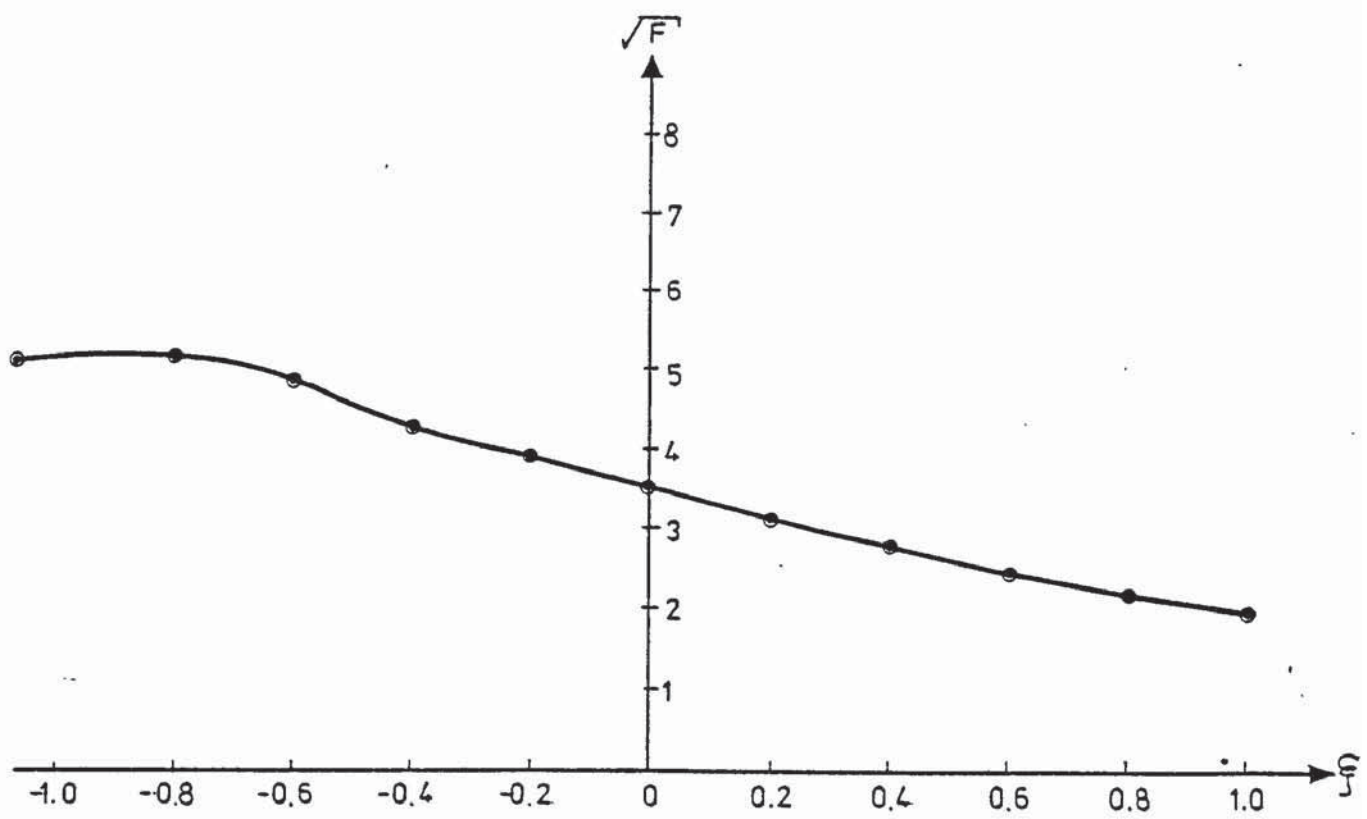
FIGURE 4.4: VARIATION OF $\sqrt{F}$ VERSUS ξ

the supports and was tabulated in terms of the restraint rate ϕ', which itself is given as:

$$\phi' = k\theta_{yz}/(k\,\theta_{yz} + 2\,EI/L) \qquad\qquad 4.11$$

where $k\,\theta_{yz}$ is the rotational stiffness of the supports. The manner in which this is calculated is given later.

For the general case of a beam restrained at the ends elastically while subjected to unequal end moments, equations (4.9) and (4.10) are combined to give

$$M_{yzcr} = \delta\,\sqrt{F}\,\sqrt{EI_{yy}\,GJ}/L \qquad\qquad 4.12$$

In fact when the ends have no restraint the value of δ is equal to π while when $\delta = 6.34$ the end restraint is infinite.

It is interesting to note that on the one hand when the slab is subjected to equal and opposite moments, Horne's approach reduces to that given by equation (4.12) with $\delta = \pi$. On the other hand for the case when $F = 1$, i.e. when the slab is subject to equal and opposite moments equation (4.12) reduces to equation (4.10), derived by Trahair.

The rotational stiffness of the supports at one end of the slab uv, figure (4.5), is calculated as the sum of 3 EI/L of the other slabs meeting at that end. Thus at u the slab is connected to three other slabs, these are numbered 1, 2 and 3, and the rotational restraining stiffness of end u is:

$$k\,\theta_{yu} = \frac{3\,EI_{y1}}{L_1} + \frac{3\,EI_{y2}}{L_2} + \frac{3\,EI_{y3}}{L_3} \qquad\qquad 4.13$$

while at v, the restraining stiffness is:

$$k\,\theta_{yv} = \frac{3\,EI_{y4}}{L_4} + \frac{3\,EI_{y5}}{L_5} \qquad\qquad 4.14$$

Equations (4.13) and (4.14) make the safe assumption that members 1 to 5 are themselves pinned at their far ends as shown
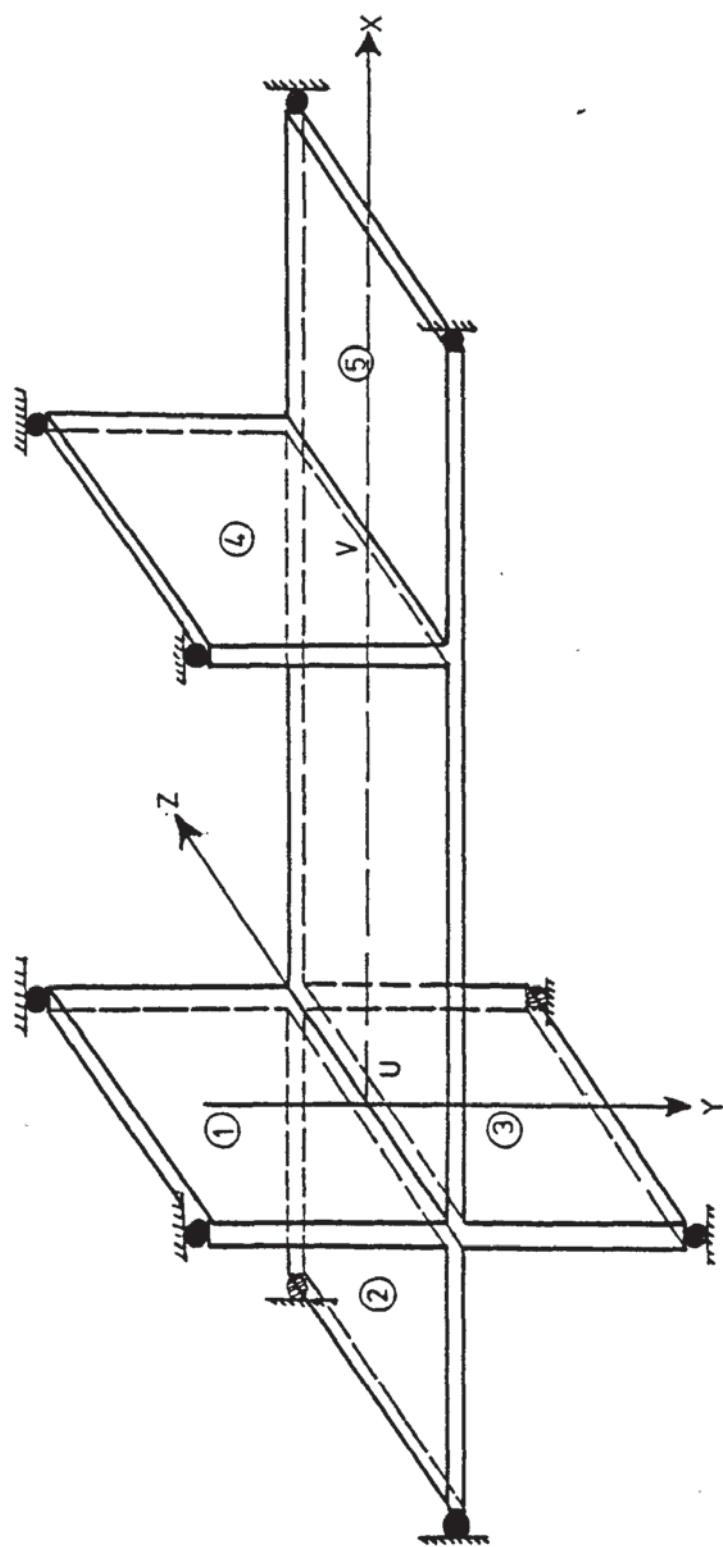
FIGURE 4.5: A GRILLAGE MEMBER CONNECTED TO THE JOINTS i AND j; THE ASSUMPTION
OF SIMPLY SUPPORTED JOINNING MEMBERS AT FAR ENDS

in figure (4.5). In the computer program written for this purpose it was further assumed that the lower of the two values of $k\theta$ given by equations (4.13) and (4.14) is the rotational stiffness at both ends. The restraining effect of any frame supporting a slab was neglected and it was assumed that a frame simply supports the slab. These assumptions are all safe.

Again, when preparing the computer program, values of $\sqrt{F}$ and δ were represented by polinomials of the form:

$$\sqrt{F} = 1.765 - 1.015\ \zeta + 0.2446\ \zeta^2 - 0.08219\ \zeta^3 - 0.01952\ \zeta^4$$
$$+ 0.3182\ \zeta^5 - 0.2117\ \zeta^6 \qquad 4.15$$

$$\delta = 3.14 + 1.542\ \phi - 3.127\ \phi^2 + 21.681\ \phi^3 - 53.97\ \phi^4$$
$$+ 69.65\ \phi^5 - 41.912\ \phi^6 + 9.337\ \phi^7 \qquad 4.16$$

Finally GJ for a thin rectangular plate was taken as.:

$$GJ = (1 - 0.6302\ t/d)\ d\ t^3 G/3 \qquad 4.17$$

as given by Patel et al[79].

During the process of predicting the load factor at which one of the panels buckles, both M_{yz} and M'_{yz}, and therefore ζ, are unknown. Thus the exact value of ζ can not be calculated. To overcome this difficulty, it was assumed that between one critical stage and the next the ratio $\zeta = M'_{yz}/M_{yz}$ has not altered significantly from its value calculated at the beginning of the current stage. This assumption is reasonable for two reasons: Firstly, because the interval between one critical stage and the next is small, especially as failure is approached. This means that even if the increments $\delta\ M_{yz}$ and $\delta\ M'_{yz}$ are large, the updated total values of M_{yz} and M'_{yz} are much larger than their current increments and thus the value of ζ is not significantly in error. Secondly figure (4.4) shows that the value of $\sqrt{F}$ is not very sensitive to changes in ζ

and thus a small error in ζ does not alter the value of M_{yzcr} of equation (4.12).

4.g. Cracks of Homogeneous Brittle Slabs:

If the slabs of a structure are made out of homogeneous brittle material, then they may crack due to the combined effect of bending, torsion and shearing. The cross section of a typical slab is shown in figure (4.6.b) which has a depth d and thickness t. This is subject to an in-plane bending moment M_b about the x axis, a shearing force S_y parallel to the Y axis and a torque M_t about the z axis of the slab. In figure (4.6.a) the points that may crack first are marked as A and A' at the top and the bottom of the section and also points B and B' on the x axis. Figures (4.6.c) and (4.6.d) and (4.6.e) show the stress distribution due to the bending, shear and torsion respectively.

At A and A' the maximum bending stresses $\pm \sigma_b$ are $\pm M_b/Z_b$ where $Z_b = td^2/6$ is the section modulus. The shear stresses τ_{tA} and $\tau_{tA'}$ due to torsion are $\pm M_t/Z_t$, where Z_t is the elastic modulus in torsion and can be expressed[80] as:

$$Z_t = \eta \, dt^2 \qquad\qquad 4.18$$

The factor η is a function of d/t and can be calculated using the theory of elasticity. For values d/t > 2, as is the case here, this is expressed as:

$$\eta = 1/(2.1952 + 2.703 \, t/d) \qquad\qquad 4.19$$

This gives a maximum error of about 4%.

The principal stresses at A and A' due to the combined effect of bending and torsion are thus:

$$\sigma_{max}, \; \sigma_{min}, \; = \pm \frac{M_b}{2Z_b} \pm \sqrt{(\frac{M_b}{2Z_b})^2 + (\frac{M_t}{Z_t})^2} \qquad\qquad 4.20$$
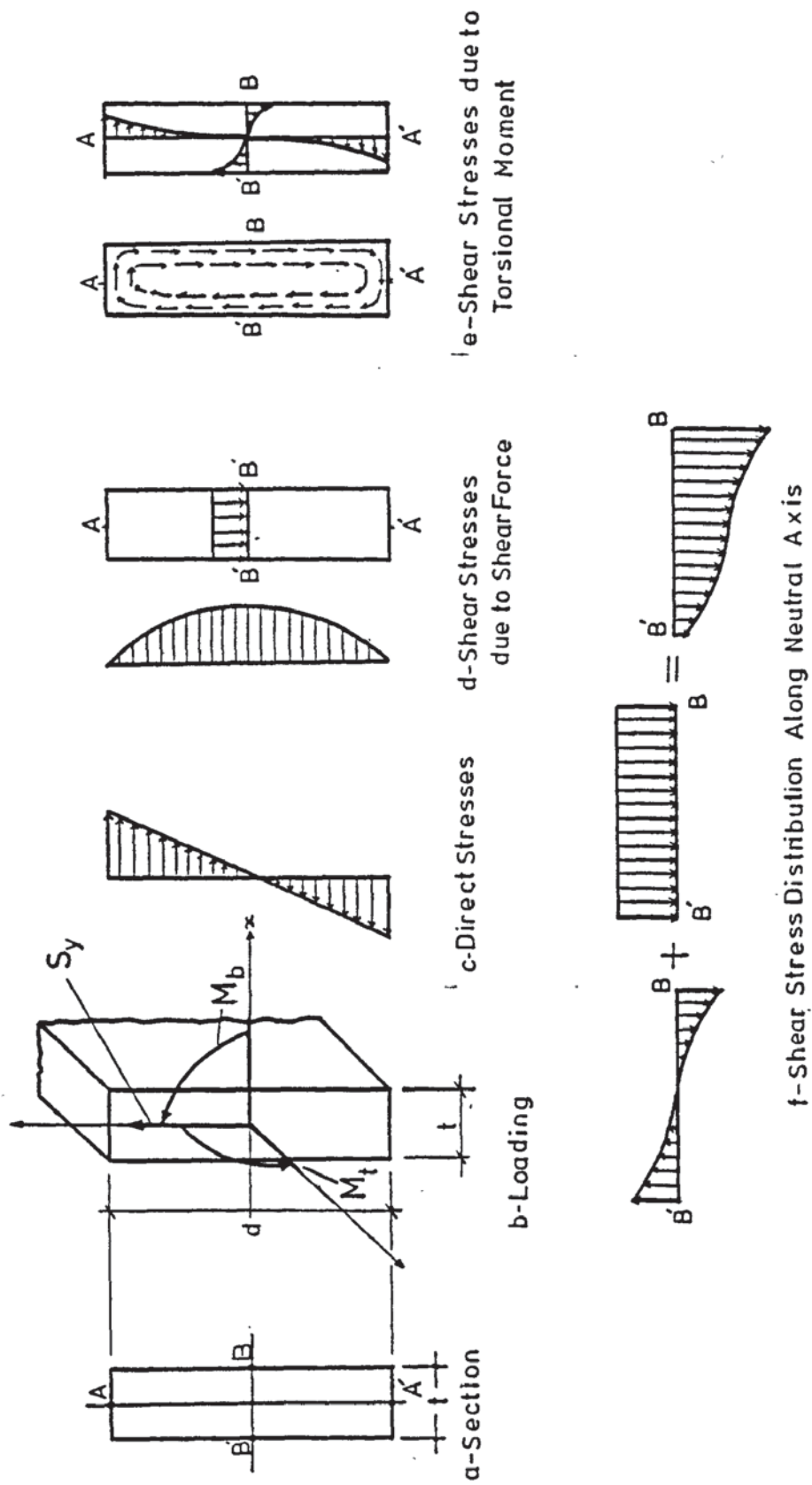
FIGURE 4.6: STRESSES ON A CROSS-SECTION

A crack develops at either A or A' when the maximum shear stress $\tau_{max} = \frac{1}{2} \sigma_y$ where σ_y is the yield stress of the material. Thus using equation (4.20) a crack develops when

$$\sigma_y = 2 \tau_{max} = \sigma_{max} - \sigma_{min} = 2\sqrt{(\frac{M_b}{2Z_b})^2 + (\frac{M_t}{Z_t})^2} \qquad 4.21$$

defining

$$\alpha = 2 Z_b/Z_t = d/3 t \, \eta$$

and $\qquad\qquad\qquad\qquad\qquad\qquad\qquad\qquad\qquad\qquad\qquad$ 4.22

$$M_F = Z_b (\sigma_{max} - \sigma_{min}) = \sqrt{M_b^2 + \alpha M_t^2} ,$$

the section cracks at A or A' when

$$M_F = \sigma_y t d^2/6 \qquad 4.23$$

Alternatively, this section may crack at B or B' due to the combined effect of direct shear and torsion. The maximum direct shear stress at B and B' is $1.5 \, S_y/t \, d$. The shear stresses τ_{tB} and $\tau_{tB'}$ due to torsion may be expressed[80] as:

$$\tau_{tB}, \tau_{tB'} = \pm M_t/\eta' d t^2 \qquad 4.24$$

where η' is also dependent on d/t and can be approximated as:

$$\eta' = 1/(3 + 1.8 \, t/d) \qquad 4.25$$

which is accurate to within 2%.

The resultant maximum shear stress τ_R at B or B' due to the combined effects of shear and torsion is thus given by:

$$\tau_R = \frac{3}{2dt} (Sy + \frac{2 M_t}{3 t \, \eta'}) \qquad 4.26$$

and when this is equal to $\frac{1}{2} \sigma_y$ a crack develops at B or B'.

Because the material of the section is brittle it is assumed that once a crack develops, it spreads right across the section. It is also considered that only one crack can develop at either end of the panel. This is either at A, A' or B, B'.

The load factor at which a crack develops at one end of the

panel is calculated by linear extrapolation. This is selected as the lowest of the load factors that causes a crack at one of the above four points. However during the whole process of loading the structure up to failure, more than one panel can suffer a crack. The failure load analysis is therefore not terminated with the first crack.

Often, as was the case in the experiments, carried by Önen,[32] the shear walls may be bolted to the foundations. To cater for these, it is simply assumed that stress concentration round the holes reduces the yield stress σ_y to σ_y' given by

$$\sigma_y' = Z_b' \, \sigma_y / Z_b \qquad\qquad 4.27$$

where Z_b' is the net section modulus.

4.h. Analysis of Two Storey Structures:

As applications seven two storey structures were analysed by the proposed method. These structures were actually tested by Önen earlier in 1973 and were found to fail at load factors totally different from those suggested by Önen. The differences were mainly due to the fact that Önen, while separating the wind loads into those transmitted to the frames and those to the grillage, overlooked the behaviour of the latter and concentrated on the frames.

A typical structure tested is shown in figure (4.7) while the dimensions of the structures as well as the results obtained are given in table (4.1). For experimental purposes, Önen manufactured the grillages out of perspex with variable dimensions and thicknesses. The frames were all made out of 12.7 mm square black mild steel with the span of their beams being 20 mm more than the width of the slabs. The fully plastic hinge moment M_p of
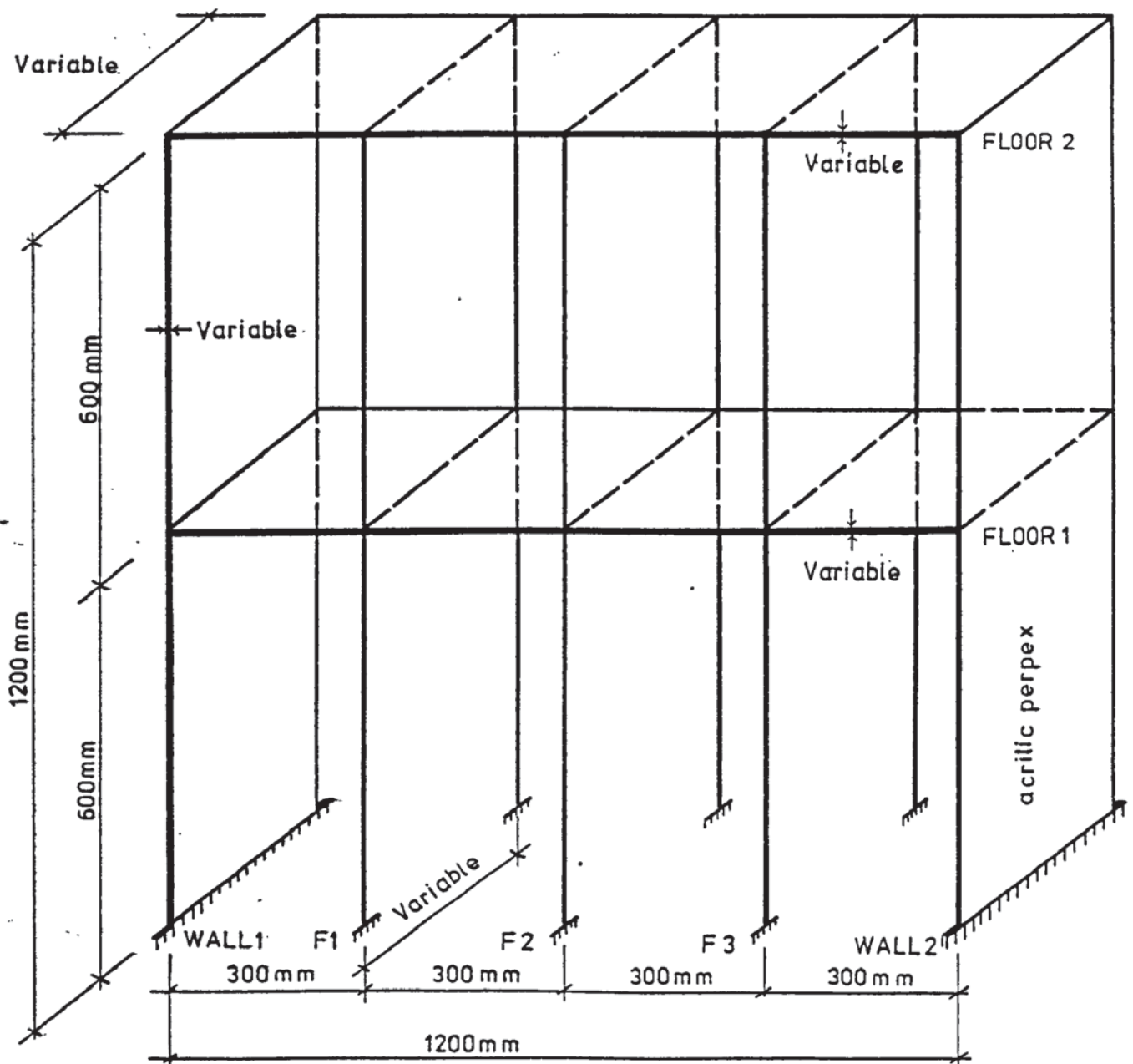
FIGURE 4.7: CONFIGURATION OF ONEN'S TWO STOREY
STRUCTURES

Structure No.	Thickness of walls (mm)	Thickness of Slabs		Width of Frames	Width of walls and slabs (mm)	M_p value for steel frames (kN mm)	Failure loads (kN)				% difference between present method & exp.
		1st Floor	2nd Floor				Bare Frame	"Onen"	Present Method	Experiment by Onen	
1	15.875	7.94	7.94	200	180	122.556	0.544	2.414	1.566	1.578	- 0.76%
2	"	"	"	250	230	"	"	2.432	1.954	1.874	+ 4.4 %
3	"	"	"	300	280	"	"	6,956	2.278	2.826	-20.2 %
4	"	12.70	"	250	230	123.33	0.548	6.604	2.586	1.952	+24.5 %
5	"	15.88	"	"	"	"	"	6.624	2.702	2.088	+22.7 %
6	20.0	12.7	7.94	"	230	124.051	0.550	5.092	3.276	2.746	+16.2 %
7	"	15.875	12.7	"	"	131.524	0.584	5.586	3.392	3.334	+ 1.7 %

TABLE 4.1   PROPERTIES AND FAILURE LOADS OF "ÖNEN'S TWO STOREY STRUCTURES

the steel bars are given in table (4.1) and the value of the modulus of elasticity was obtained by Önen for the batch as 202.2 kN/mm². The material properties of the perspex were supplied by the manufacturers.

Figure (4.8) shows the load-deflection graphs obtained by four different methods for structure 1. Curve 1 is that obtained by the present method. Curve 2 was obtained experimentally while curve 3 was obtained by Önen. Finally curve 4 shows the results obtained by the elasto-plastic analysis[32] of one of the bare frames.

The present method predicted that the first floor slabs spanning frames F1 and F2 would buckle first at a load factor of 0.96. In fact Önen reported that experimentally at a load factor 0.98 these slabs first buckled and then fractured. The point at which this took place is marked as GB1 on the theoretical curve 1 and GB, GC on the experimental curve 2.

As the analysis continued 13 plastic hinges were developed in the frames. Throughout the procedure, the symmetry of the structure was unaffected. None of the frames failed either due to the formation of a mechanism nor as a result of instability. In fact the structure finally collapsed with the buckling of the slabs spanning frame 1 to 3 at the second floor. Notice in figure (4.8) that contrary to the expectation of the plastic theory, the hinges did not all develop in the middle frame. Once the first two did develop in this frame, it became flexible, giving rise to a redistribution of the wind loads away from this frame to the outer ones. Thus the next four hinges took place in the outer frames.

Figure (4.9) shows the fraction of the wind load transmitted to the separate frames during the loading process at the first
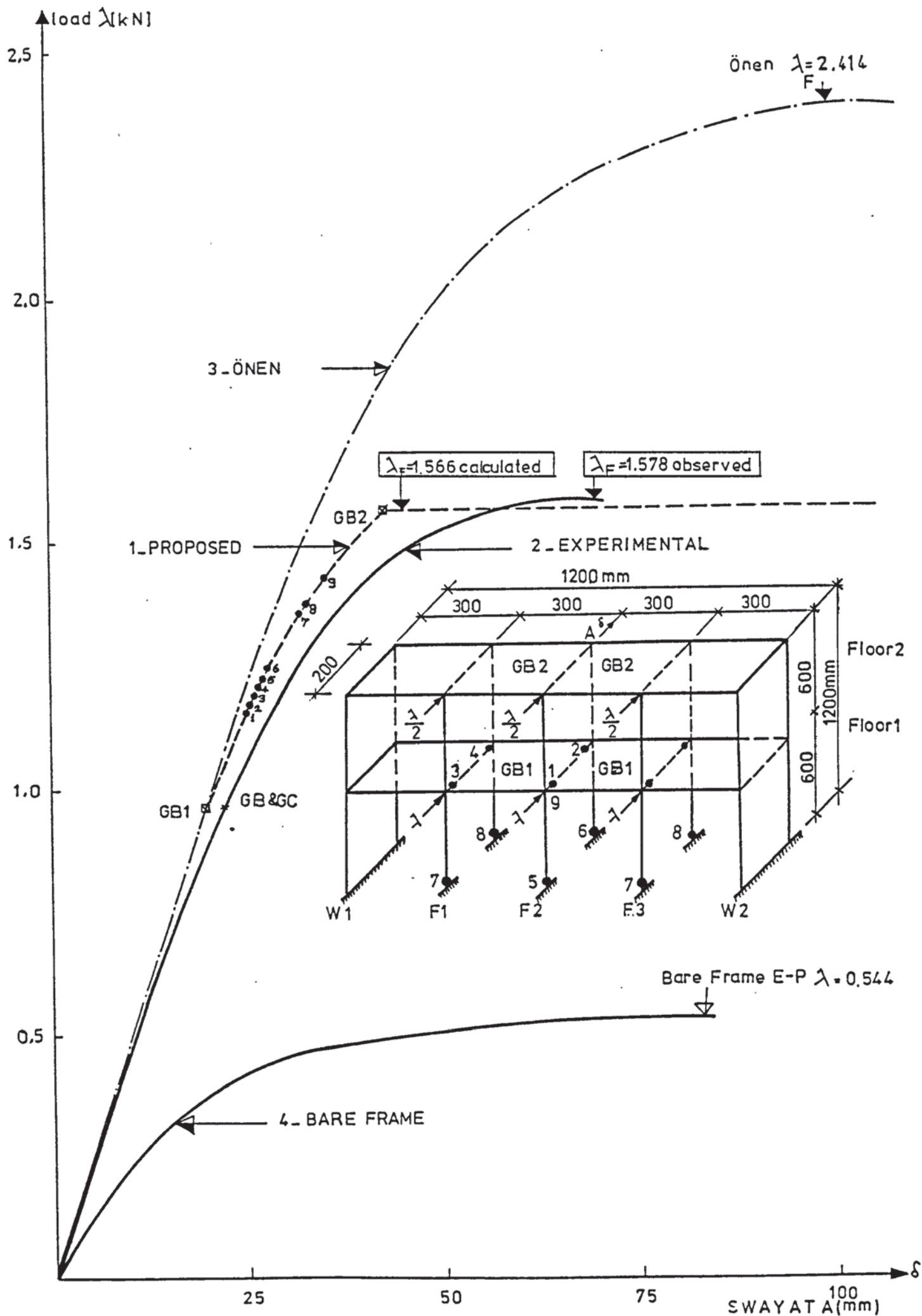
FIGURE 4.8: LOAD DEFLECTION GRAPHS FOR ONEN'S FIRST
TWO STOREY STRUCTURE

FRACTION OF UNIT LOAD

For the first floor
level of frame 2

For the first floor
level of frame 1

$\lambda = 1.566$
F

LOAD FACTOR

λ
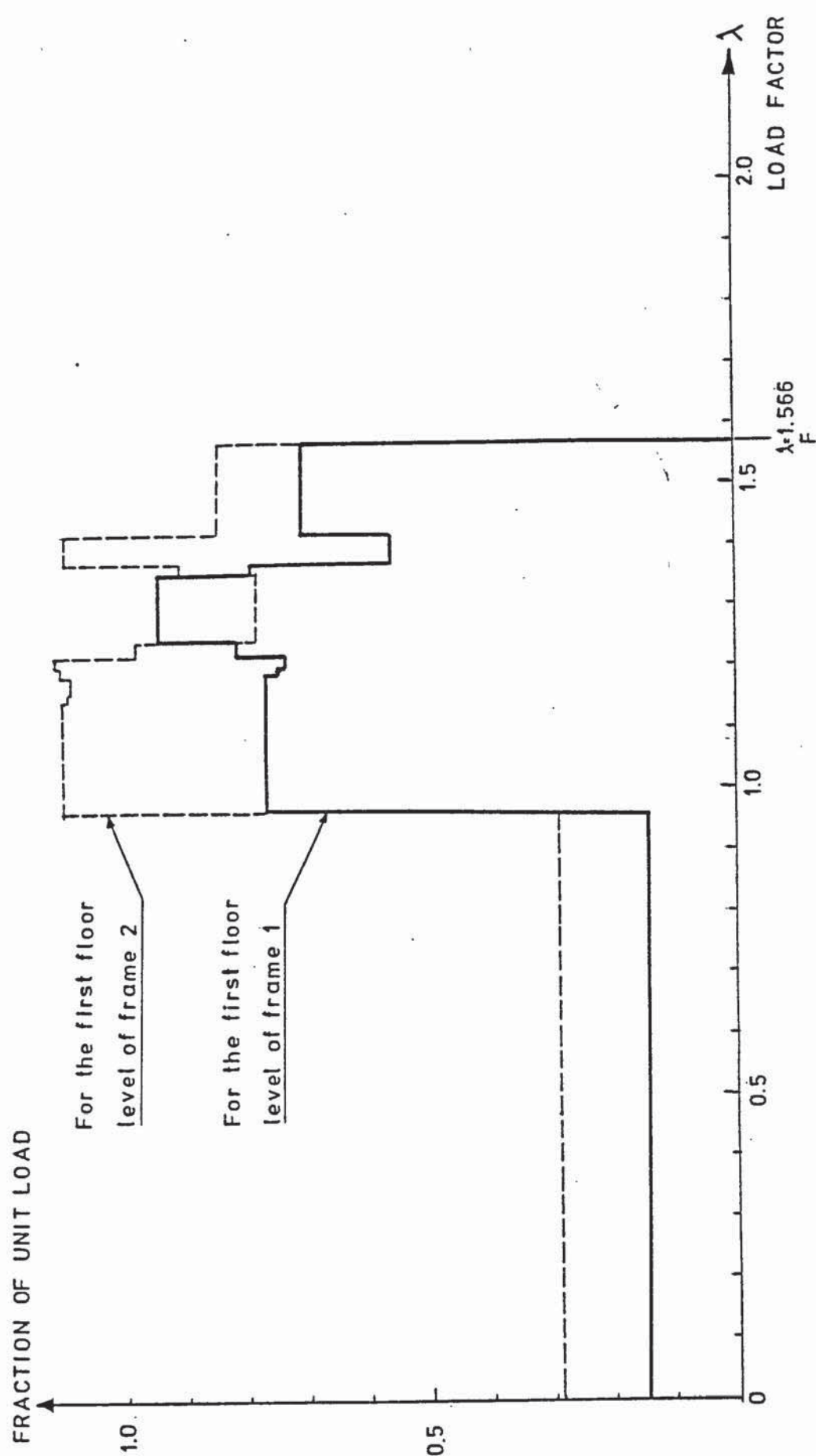
FIGURE 4.9: VARIATION OF THE FRACTION OF A UNIT LOAD TRANSMITTED TO
FRAMES 1 AND 2 OF ÖNENS FIRST TWO STOREY STRUCTURE
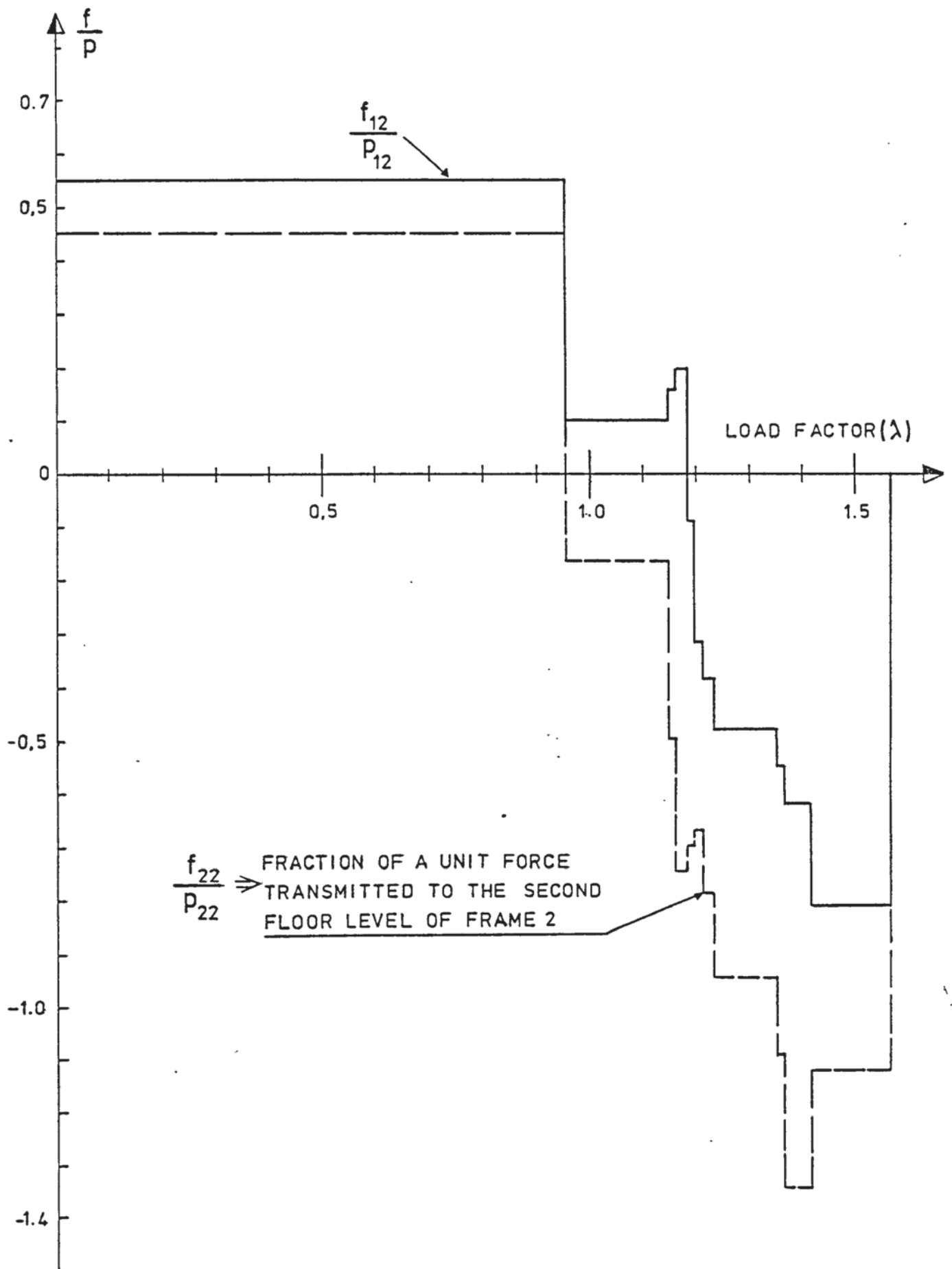
FIGURE 4.10: VARIATION OF LOADS TRANSMITTED TO
THE SECOND FLOOR LEVELS OF THE FRAMES
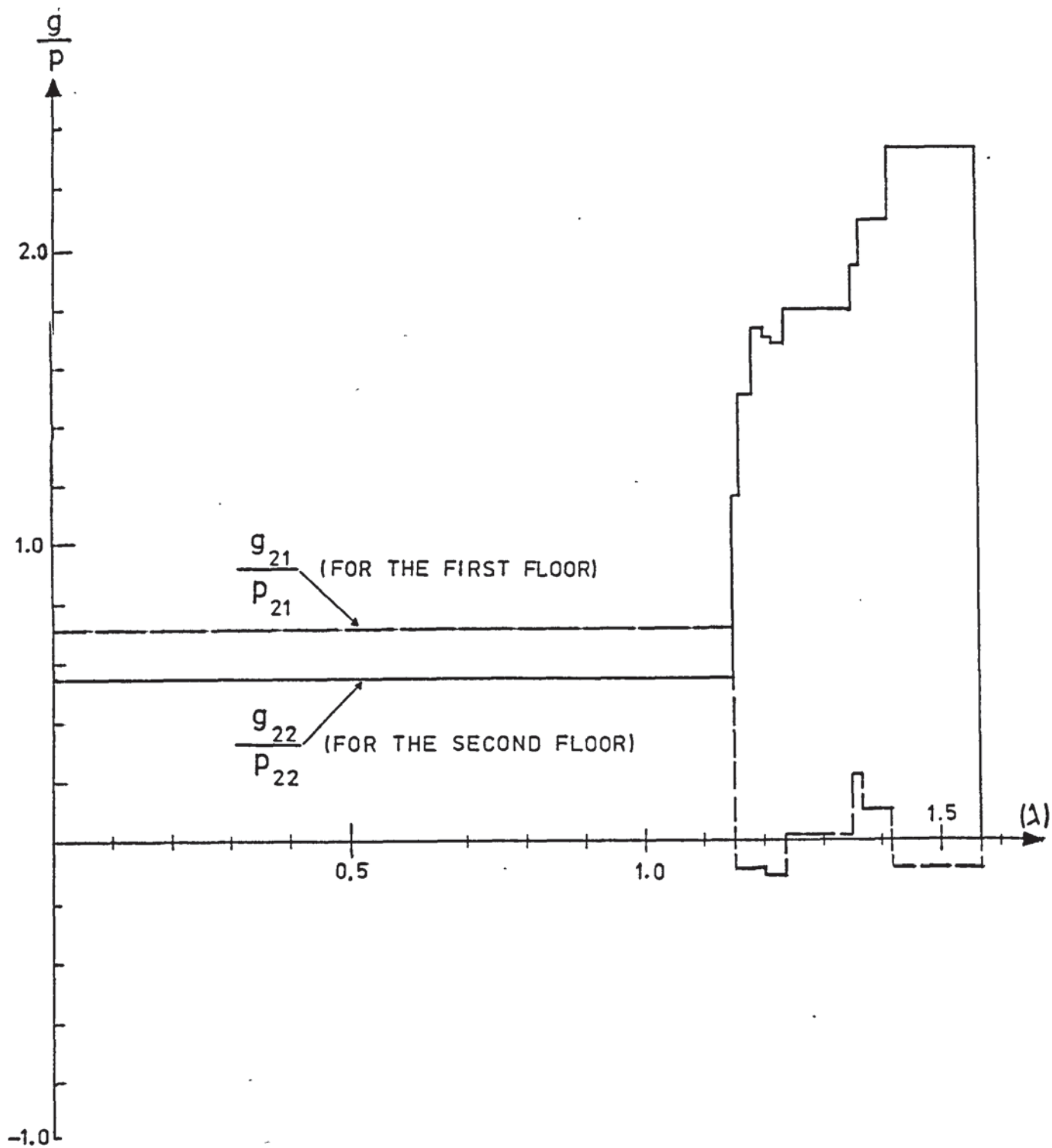
FIGURE 4·11: VARIATION OF LOADS TRANSMITTED
TO THE GRILLAGE

floor level while figure (4.10) shows the loading of the frames at the second floor level. Finally figure (4.11) shows the grillage loads during the whole process. These figures clearly indicate that while the external loads increased proportionally, neither the frames nor the grillage were exposed to proportional loading.

In figure (4.8) curve 4 shows that an accurate elastic-plastic analysis of one of the bare frames has no resemblance whatsoever to the actual behaviour of the structure. Such an analysis, which is in itself more accurate than that given by the plastic theory, puts the collapse load of the structure at less than a third of its actual value. This glaring discrepancy has been hitherto disguised by comparing the theoretical results of plane frame analyses, not with the actual behaviour of structures but with experiments carried out on plane frames.

CHAPTER 5

FAILURE OF REINFORCED CONCRETE PANELS

5.a. Introduction:

A reinforced concrete panel may be either a slab or a shear wall forming a unit of a grillage system. A slab panel extends from one frame to another or to a shear wall. Such a panel fails under the combined action of shear and bending while the effect of torsion is sufficiently small that it can be neglected. On the other hand, a shear wall panel joining two floors may fail under the combined effect of shear, bending and torsion.

Research on failure of reinforced concrete, due to the interaction of bending shear and torsion, has been hitherto limited to simple beams. A sound approach to this problem was made by Elfren, Karlsson and Losberg[88] who assumed that the height of the concrete compression zone is so small that the centre of this zone is located at the level of the horizontal stirrups at the top of the beam. It was further assumed that the neutral axis is also located at this level. Thus it was assumed that the contribution of the compression force C, sustained by the concrete, to the equilibrium equation can be virtually neglected.

Unlike a beam, a reinforced concrete panel has a large number of layers of reinforcement. At failure a deep section of the panel, with several layers of bars can be in compression, with the neutral axis extending to a level well within the panel. Furthermore, instead of stirrups, the reinforcement may be in the form of one or two parallel meshes which may or may not be connected to each other as shown in figure (5.1). For these reasons the methods

a-Single reinfor-
cement in the
middle

b-Double reinfor-
cement

c Double reinforcement
with closed stirrups
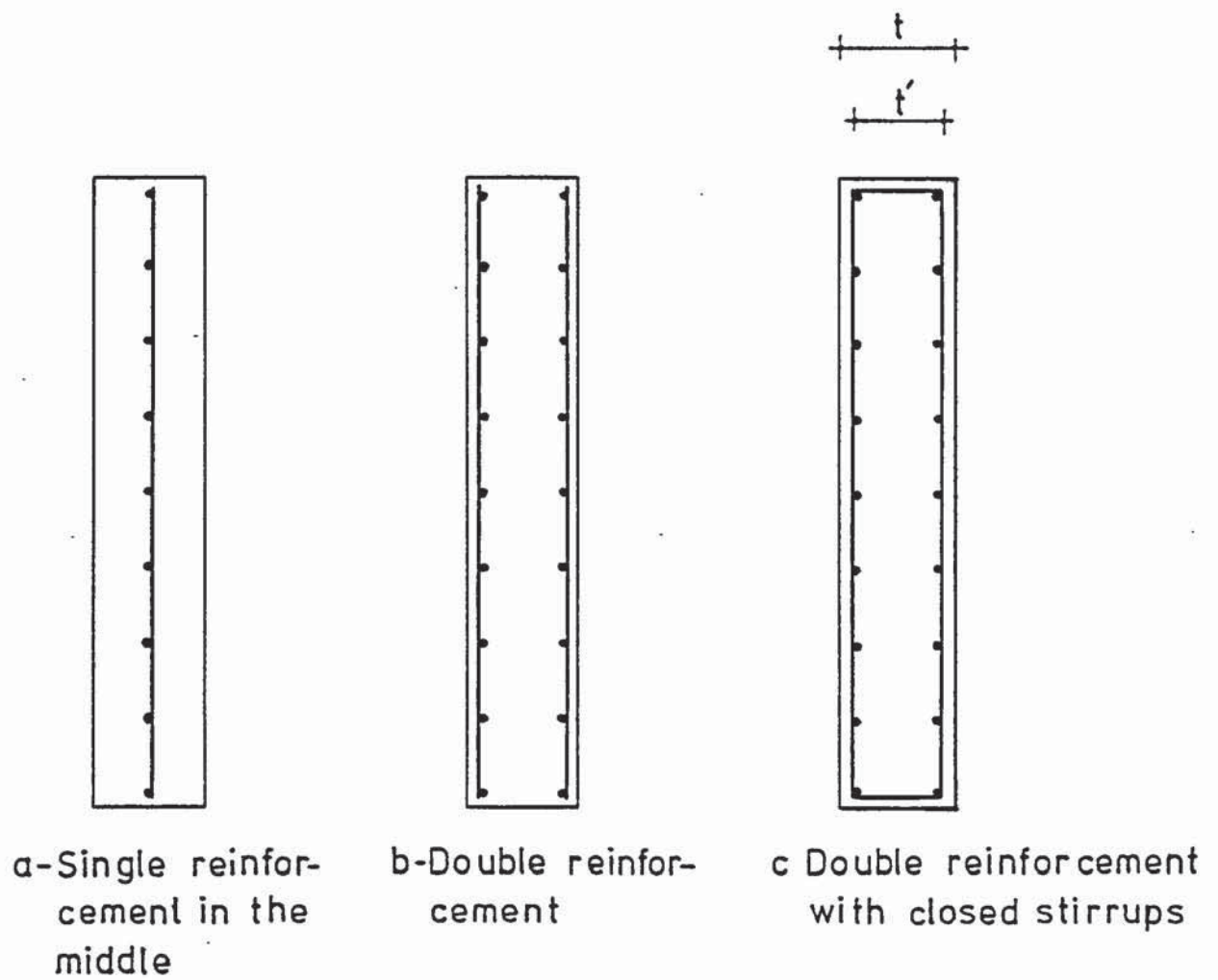
FIGURE 5.1

proposed for the failure analysis of R.C. beams cannot be applied to panels. In the latter case it is first necessary to determine the depth of the neutral axis, the centre of the concrete compression zone and the magnitude of the compressive force in concrete. These are some of the tasks to be solved in this chapter. The procedure proposed by Elfren et al[88] is then generalised to cover the case of failure of deep beams due to the various interactive effects.

5.b. Location of Neutral Axis:

In calculating the depth of the neutral axis for a panel it is assumed that:

1 - The reinforcement is spaced equally throughout the depth of the panel.

2 - The position of the neutral axis is unaffected by the existence of either torsion or shear. This is valid since both shear and torsion do not give rise to direct tensile or compressive stresses in the section. However, it will be shown that torsion and shear alter the width of the compression zone and thus when they are present, this width must be calculated before proceeding with the calculation of the neutral axis.

3 - At failure, excessive strains take place in the outermost fibres but the strain distribution is linear across the depth of the section.

4 - The section is under-reinforced and failure takes place in the steel bars first. The concrete in the compression zone, on the other hand, remains either elastic or partially plastic. In practice, most slabs and shear walls are under-reinforced and thus this assumption covers the practical cases.

5 - The stress-strain relationship for the steel reinforcement is elastic - perfectly plastic. This assumption can be relaxed or removed to cover any other stress-strain relationship obtained experimentally.

In figure (5.2a) the cross section of a deep shear wall panel is shown with depth d and thickness t. The spacing of the horizontal layers of reinforcements is a and altogether there are $\bar{m}$ such layers. It is evident that the distance between the outermost bars is $(\bar{m} - 1)a$. The section is divided into three distinct zones. The top zone, with a depth x, is in compression and the depth of the neutral axis is therefore equal to x. The bars in the middle, cracked zone are elastic and those in the bottom zone have developed plasticity of some degree or another. Altogether there are i layers of bars in the plastic zone.

The difficulty of calculating the depth of the neutral axis, for a beam with many layers of reinforcement, becomes evident when it is realised that not only is this depth unknown but the number i of the layers in the plastic zone is also unknown. This difficulty is resolved by expressing x in terms of i and then finding the latter iteratively.

The strain diagram for the section is shown in figure (5.2.b) in which ε_c is the strain at the compression face, ε_y is the strain in the bars at first yield and ε_u is the ultimate strain for steel. The corresponding stress diagram of the section is shown in figure (5.2.c) where it is evident that the bars in the bottom zone are subject to a constant yield stress f_y. Again in this diagram, the horizontal force carried by the concrete is marked C while the algebraic sum of the forces in all the reinforcement
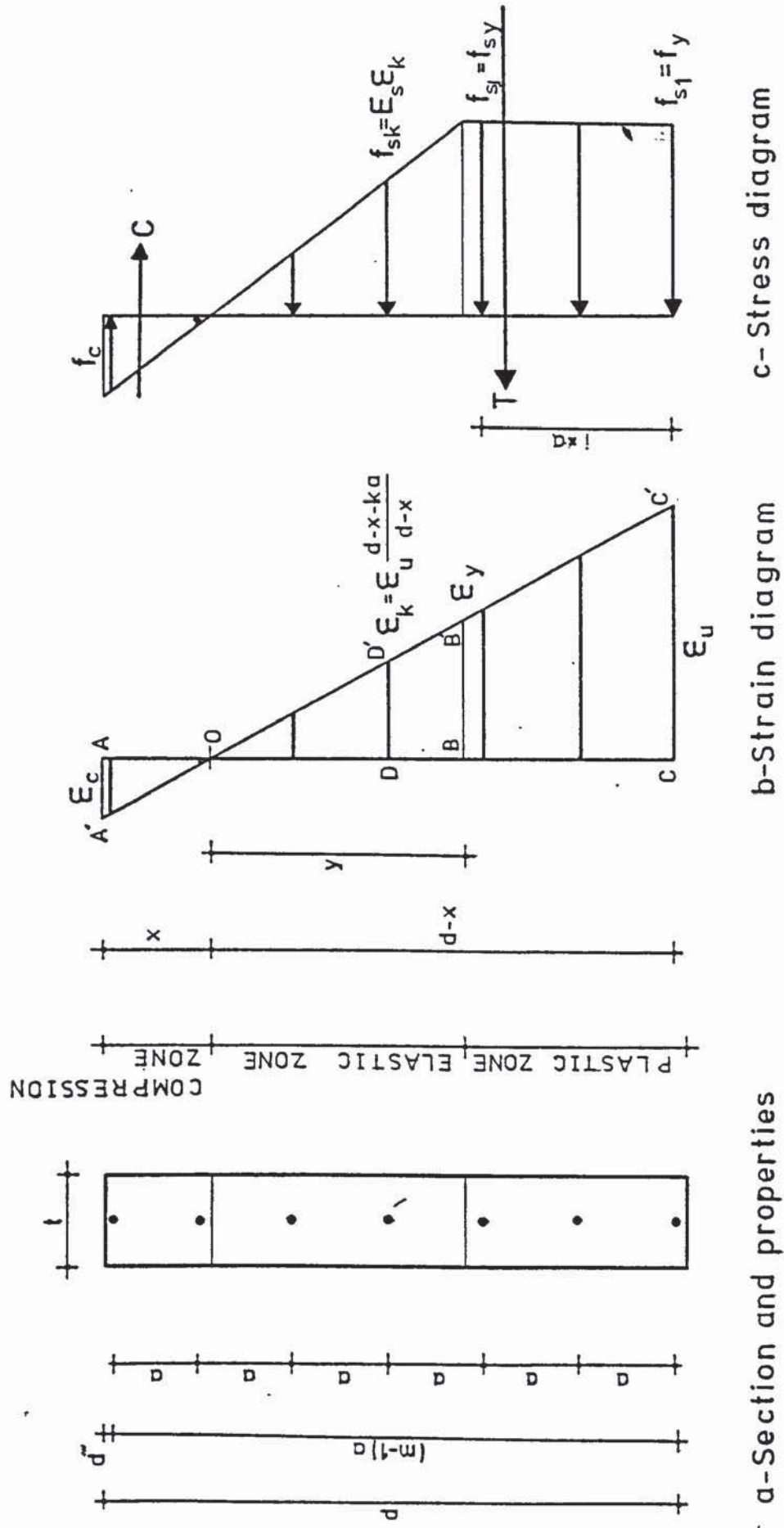
FIGURE 5.2:A' SECTION UNDER PURE BENDING

c-Stress diagram

b-Strain diagram

a-Section and properties

add up to T. For horizontal equilibrium therefore:

$$C = T \qquad\qquad 5.b.1$$

The elastic compressive force C in the concrete is the product of the area of the compression zone and the average stress acting on it, thus:

$$C = 0.5 \, f_c \, t \, x \qquad\qquad 5.b.2$$

where f_c is the maximum compressive stress developed at the top face.

The total force T in the steel bars is the algebraic sum of the forces in all the layers, i.e.

$$T = F_1 + F_2 + \cdots + F_{\overline{m}} = \sum_{j=1}^{\overline{m}} F_j \qquad\qquad 5.b.3$$

Some of the steel layers are in fact in the compression zone and T must be calculated with the correct sign of each force as will be shown later.

With the plastic zone covering i layers, there are altogether i-1 whole spaces in the yielded region. The force in each layer here is the ultimate force F_u that can be carried by a steel layer. Needless to say that, because the material is considered to be elastic-perfectly plastic, $F_y = F_u$ where F_y is the yield force. The total force carried by the yielded layers is T_u given by:

$$T_u = \sum_{j=1}^{i} F_{uj} = \sum_{j=1}^{i} f_{uj} \, A_s \qquad\qquad 5.b.4$$

where A_s is the area of the steel in a layer and f_u is the ultimate stress.

In the elastic zone, layer no $k + 1$, which is k spaces above the bottom bars, has strain ε_k. This is calculated from the similar triangles OCC' and ODD', shown in figure (5.2.b), as:

$$\varepsilon_k = \varepsilon_u = [(d - x) - ka]/(d - x) \qquad\qquad 5.b.5$$

The force in this layer is $F_k = A_s E_s \varepsilon_k$ where E_s is the modulus of elasticity of steel. Using equation (5.b.5) and remembering that $F_u = A_s E_s \varepsilon_u$, the total force in the elastic layers is T_E, given by:

$$T_E = \sum_{k=i}^{\overline{m}-1} F_{uk} \frac{(d-x) - ka}{d - x} \qquad 5.b.6$$

Notice that in compression layers $ka > d - x$ and DD', in figure (5.2.b), will be above the neutral axis. However the correct negative sign of a compressive force in a layer is automatically catered for by equation (5.b.6) because $(d - k) - ka$ becomes negative. In this manner T_E gives the net force in the elastic layers. The total tensile force in the bars is $T = T_u + T_E$ which is calculated from equations (5.b.4) and (5.b.6), i.e.

$$T = \sum_{j=1}^{i} F_{uj} + \sum_{k=i}^{\overline{m}-1} F_{uk} \frac{(d-x) - ka}{d - x} \qquad 5.b.7$$

Notice that j is a counter of layers while k is counting the spaces above the bottom layer.

The limits of the second summation in equation (5.b.7) can be altered so that counting starts from the first space above the bottom bars, equation (5.b.7) then becomes:

$$T = \sum_{j=1}^{i} F_{uj} + \sum_{k=1}^{\overline{m}-1} F_{uk} \frac{(d-x) - ka}{d - x} - \sum_{k=1}^{i-1} F_{uk} \frac{(d-x) - ka}{d - x} \qquad 5.b.8$$

which can be simplified to read:

$$T = i\, F_u + \frac{F_u}{d-x} \left[(m-i)(d-x) - a \left(\sum_{k=1}^{m-1} k - \sum_{k=1}^{i-1} k \right) \right] \qquad 5.b.9$$

where $F_u = F_{uj} = F_{uk}$ is the ultimate force in any layer.

Since

$$\sum_{k=1}^{m-1} k = \frac{m\,(m-1)}{2}$$

and

$$\sum_{k=1}^{i-1} k = \frac{i\,(i-1)}{2} \qquad 5.b.10$$

equation (5.b.8) can be simplified to:

$$T = \frac{F_u}{d-x}\{m\ (d-x) - \frac{a}{2}[m\ (m-1) - i\ (i-1)]\} \qquad \text{5.b.11}$$

The distance y between the neutral axis and the bottom of the elastic zone is calculated from the similar triangles OBB' and OAA' in the strain diagram of figure (5.2.b). Thus the compatibility equation is:

$$\frac{\varepsilon_c}{x} = \frac{\varepsilon_y}{y} \qquad \text{5.b.12}$$

Furthermore, the similar triangles OBB' and OCC' give

$$\frac{\varepsilon_u}{d-x} = \frac{\varepsilon_y}{y}$$

That is:

$$y = \frac{(d-x)\ \varepsilon_y}{\varepsilon_u} \qquad \text{5.b.13}$$

Now $\varepsilon_c = f_c/E_c$, with E_c being the modulus of elasticity of concrete and $\varepsilon_y = f_y/E_s = f_u/E_s$, equations (5.b.12) and (5.b.13) give

$$\frac{f_c}{f_u} = \frac{x}{\alpha_e\ \eta\ (d-x)} \qquad \text{5.b.14}$$

where $\alpha_e = E_s/E_c$ is the modular ratio and $\eta = \varepsilon_y/\varepsilon_u$ is the ratio of strains in the steel at first yield and at failure.

Equating the total force C in the concrete to the total steel force T, making use of equations (5.b.2), (5.b.7) and (5.b.14), we obtain the positive value of the depth x of the compression zone as:

$$x = \zeta\ (\sqrt{1 + \frac{\{2d - a\ [(m-1) - i\ (i-1)/m]\}}{\zeta}} - 1) \qquad \text{5.b.15}$$

where

$$\zeta = A_s\ \alpha_e\ \eta\ m/t \qquad \text{5.b.16}$$

5.b.1 Iteration for the Depth of the Neutral Axis:

Equation (5.b.15) calculates the depth of the compression zone. This is provided that the unknown number of layers i in

the plastic zone is first calculated. This can be performed
iteratively as follows:

(1) Assume $i_0 = i$ to start with

(2) Calculate x from equation (5.b.15)

(3) Using equation (5.b.13) calculate y, figure 5.2.b.

(4) Count the number of layers i_n within the depth $d-(x+y)$ of
the plastic zone.

(5) Check if $i_0 = i_n$. If it is, the iteration is stopped and
the value of x calculated in step (2) is correct.

(6) If $i_0 \neq i_n$, set i_0 to the current value of i_n and repeat
from step (2) until two consecutive values of i are equal.

In equations (5.b.15) and (5.b.16) it is noticed that the
position of the neutral axis depends on the thickness t of the
panel. This is true only for the case of pure bending where t is
equal to the thickness of the compressive zone. When the section
is subject to bending shear and torsion it is necessary to
calculate the thickness of the compressive zone before calculating
the compression area. This thickness will be shown to be different
from the thickness of the panel. For this reason determination of
the position of neutral axis for such cases will be given after
we have presented the failure analysis of such sections.

5.c. Interaction between Bending and Torsion in Deep Panels:

5.c.1 Introduction:

The difference between a beam and a deep beam is that the
latter is subject to a high shear force which cannot be neglected.
Failure analysis of panels subject to bending and torsion, without
shear, is therefore hypothetical. Nevertheless, this case is
presented first because it is easier and expressions obtained here

FIGURE 5.3.b: DEEP BEAM LOADED WITH BEN-
DING AND TORSION AND FAILURE
SURFACE
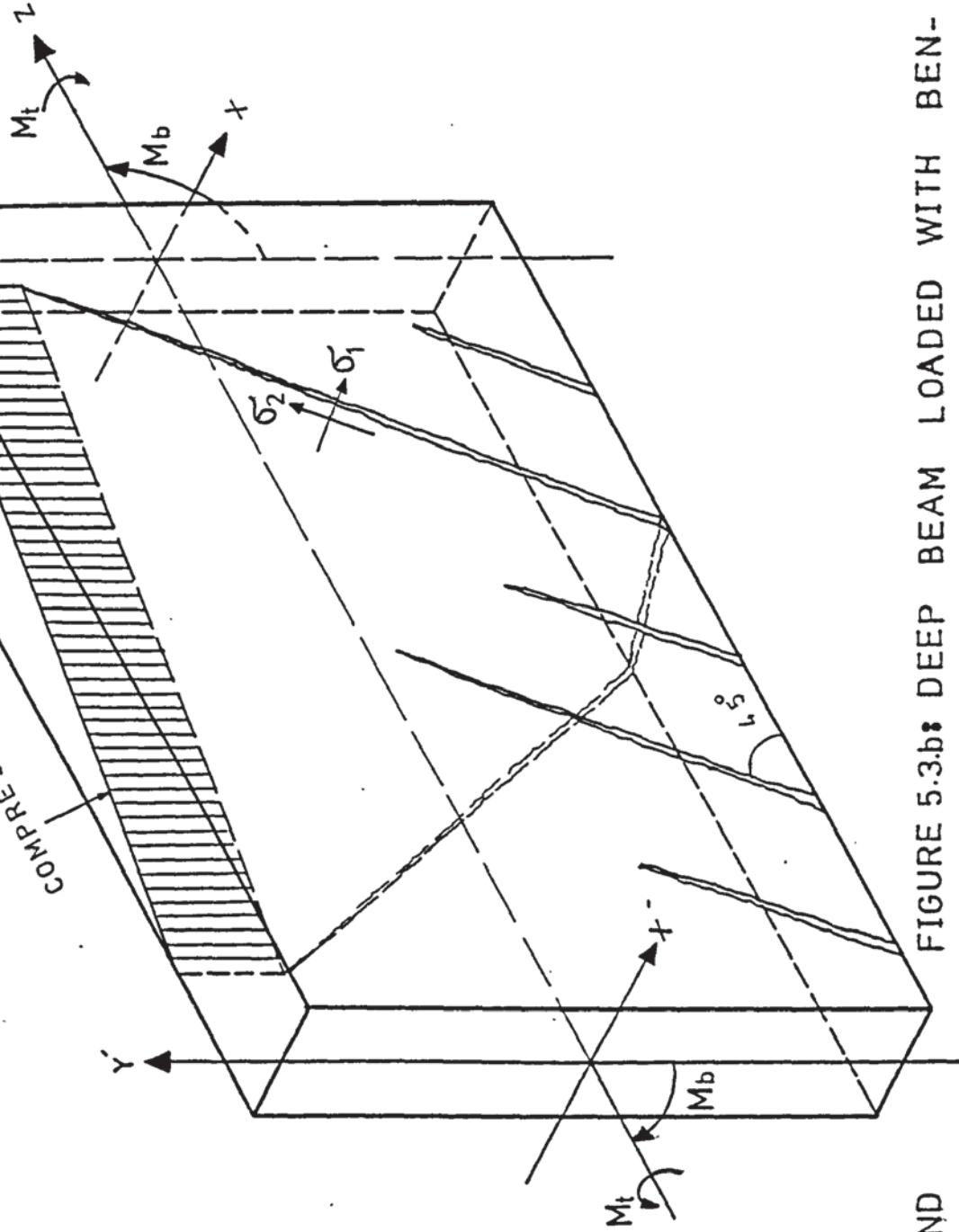
FIGURE 5.3.a: CROSS SECTION AND
DIMENSIONAL PROPERTIES

are later modified or used directly to deal with the actual case of failure due to shear bending and torsion.

The reinforced concrete panel shown in figure 5.3 has a depth d and thickness t. The area of the longitudinal reinforcements at each layer is A_s. The stirrups, shown looped in the figure, have height d' and width t'. Each stirrup has an area A_w and they are spaced s apart. The compression zone is shown shaded in the figure and the distance between the neutral axis and the outermost layer of tension bars is d''.

This panel is subject to a torque M_t about z axis and an inplane bending moment M_b about x axis. As these moments are increased, inclined cracks begin to develop at angles which can be assumed to be 45°. Eventually failure takes place with a skew failure surface ACBDE as shown in figure(5.4.a).

At failure it is assumed that:

(1) - The vertical stirrups have all yielded and are behaving plastically.

(2) - The strain varies linearly along the depth of the section.

(3) - The strain in the outermost tensile reinforcements has reached its ultimate value. Nevertheless, it is considered that some of the inner reinforcements are still elastic.

5.c.2. Moments of Resistance of the Longitudinal Bars:

At failure, the moment of resistance of the reinforcements about x axis is the net result of that sustained by the longitudinal bars and that of the vertical stirrups. Considering the longitudinal bars first, the stress and the strain diagrams are shown in figure (5.5). Considering the tensile zone; the contribution of the longitudinal bars in layer j, to the ultimate moment sustained, is the product of the force F_j in these bars and the distance of the
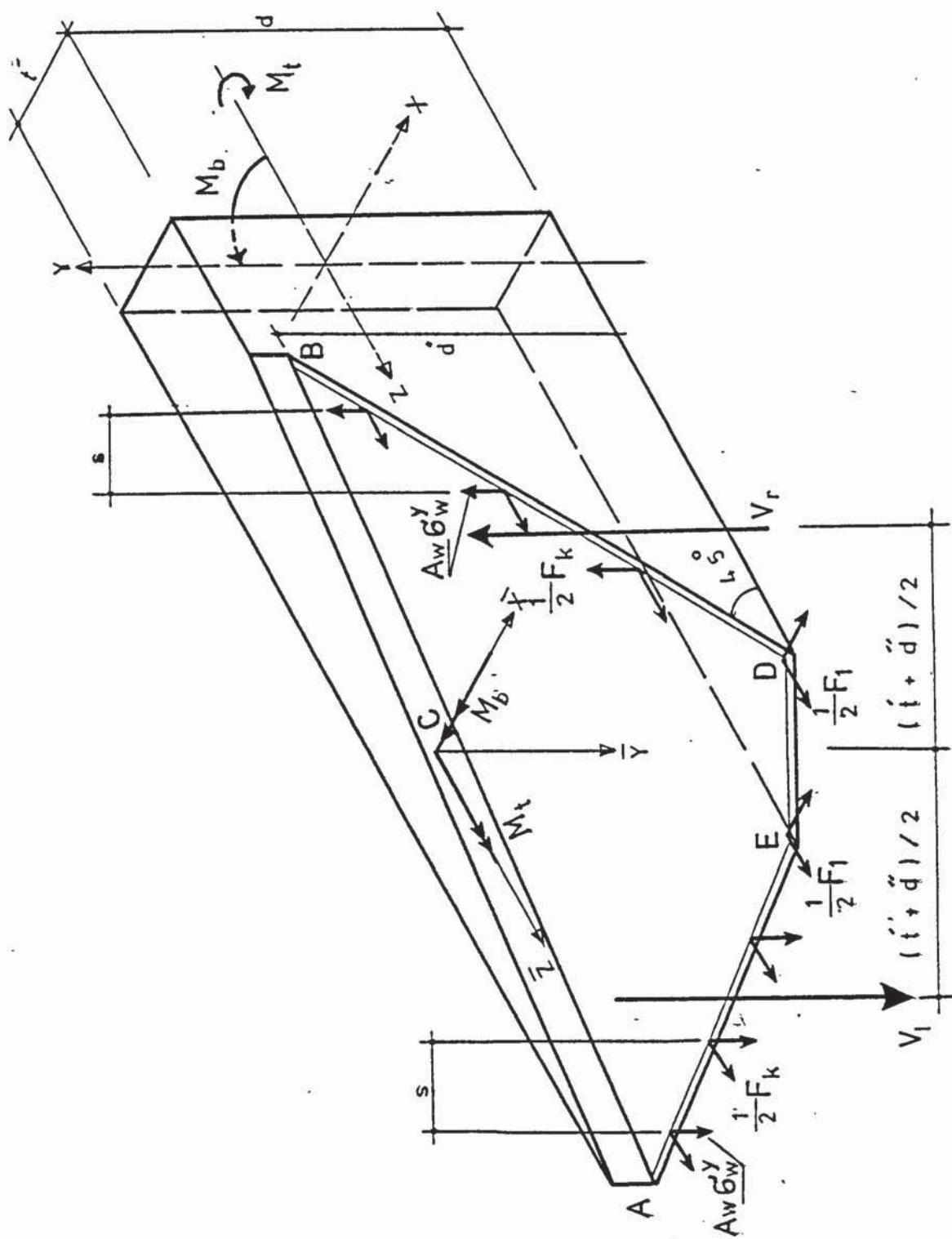
FIGURE 5.4 a: BASIC SIMPLIFIED FAILURE MODE (Isometric view)
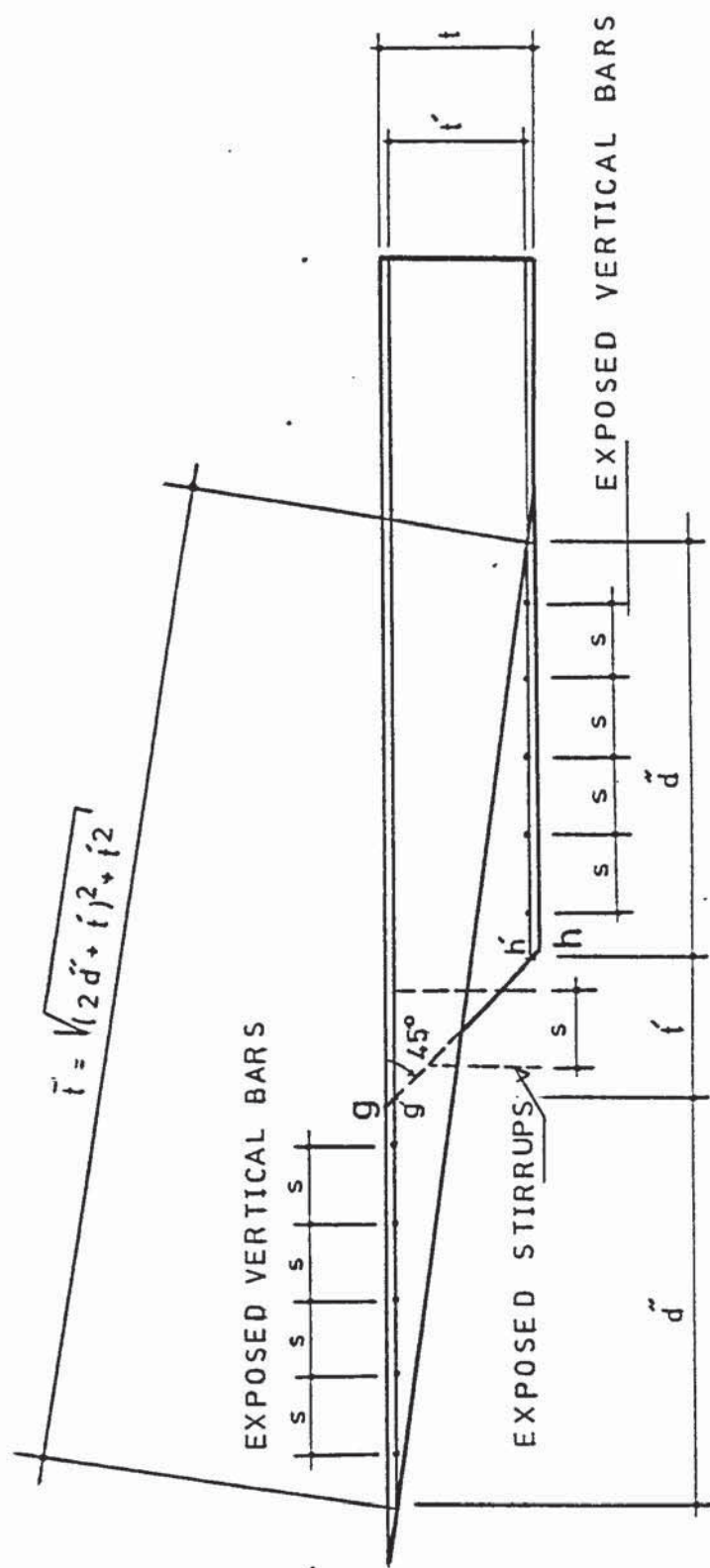
FIGURE 5.4.b: TOP VIEW OF BASIC SIMPLIFIED FAILURE MECHANISM

layer from the compression centre. For a total of m layers in
this zone, the ultimate moment sustained by the longitudinal bars
alone, is therefore given by:

$$M_{ult} = \sum_{j=1}^{m} F_j [\overline{d} - a(j-1)] \qquad 5.c.1$$

where $\overline{d}$ is the distance between the compression centre and the
outermost layer in tension.

The force F_j carried by the bars in layer j can be calculated
from the strain diagram of the section and the stress-strain
diagram of the reinforcement. Triangles OAA' and OBB' in figure
(5.5.a) are similar and the strain ε_j at layer j can be obtained
from:

$$\frac{\varepsilon_j}{d'' - a(j-1)} = \frac{\varepsilon_u}{d''} \qquad 5.c.2$$

where ε_u is the ultimate strain of the reinforcement. The cover,
which is here considered to be the distance between the top
surface of the panel and the centre of the top stirrups, is d'''
and d' is defined as:

$$d' = d - d''' \qquad 5.c.3$$

The depth of the tensile zone d'' can be expressed as a factor γ
of d', i.e.

$$\gamma = d''/d' = (d-x)/d' \qquad 5.c.4$$

Equation (5.c.2) then gives ε_j as:

$$\varepsilon_j = \varepsilon_u [\gamma d' - a(j-1)]/\gamma d' \qquad 5.c.5$$

In the special case when the stress-strain relationship of the
reinforcements is considered to be elastic-perfectly plastic, the
force F_j is calculated either from:

$$i- \qquad F_j = E_s \varepsilon_j A_s \qquad 5.c.6a$$

because layer j is elastic and $\varepsilon_j < \varepsilon_y$, or from:

$$ii- \qquad F_j = A_s f_y \qquad 5.c.6b$$

ε_c

$\frac{1}{3}(d'+d''-\breve{d}) = X'$

x

O

Layer m

$\varepsilon_j = \varepsilon_u \dfrac{\gamma d' - a(j-1)}{\gamma d'}$

F_j Layer j

A' A

$(j-1)a$

a

F_2 Layer 2

B' B

F_1 Layer 1

d'''

d

$\bar{d}$

$_c d''$

a-Strain diagram   b-Stress diagram
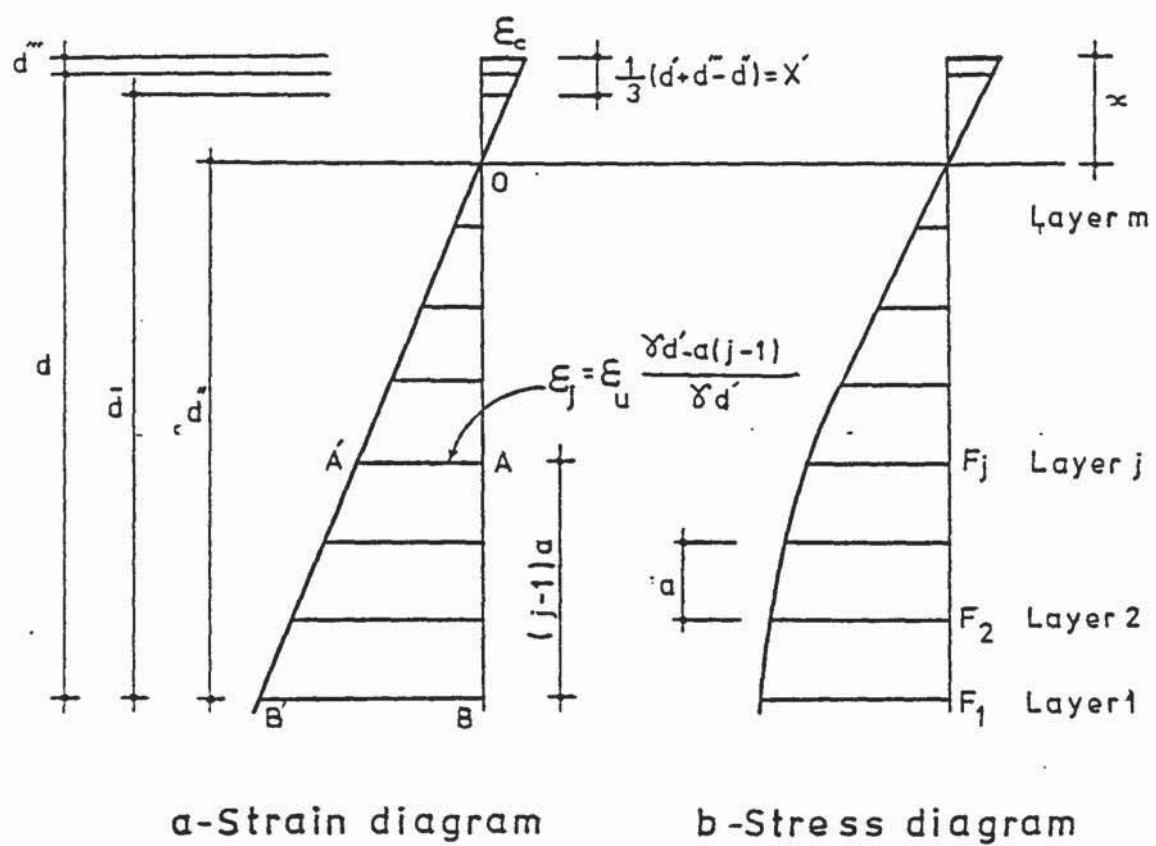
FIGURE 5.5

because the bars in layer j have yielded and $\varepsilon_j > \varepsilon_y$. Here $f_y = f_u$ is the yield (or ultimate) stress in steel.

In the general case, when the stress-strain relationship of the bars is totally nonlinear, the stress f_j corresponding to a particular strain ε_j must be taken from the stress-strain diagram. In this case, the force F_j is taken as:

$$F_j = A_s f_j \qquad\qquad 5.c.6c$$

The distance $\overline{d}$ between layer 1 and the compression centre can also be calculated from the strain diagram of figure 5.4.a. The depth of the compression zone is noticed to be $d' + d''' - d''$ and since the concrete in this zone is considered to be elastic, the depth of the compression centre X' is obtained from:

$$X' = \frac{1}{3}(d' + d''' - d'') \qquad\qquad 5.c.7$$

Defining β as:

$$\beta = 2\, d'''/d', \qquad\qquad 5.c.8$$

$\overline{d}$ becomes:

$$\overline{d} = d'\,(2 + \beta + \gamma)/3 \qquad\qquad 5.c.9$$

Notice that $\gamma = d''/d'$, see equation 5.c.4, is the ratio of the depth of the tensile region to the distance between the outermost reinforcements. Substituting for $\overline{d}$ in equation (5.c.1), we obtain the ultimate moment sustained by the longitudinal bars as:

$$M_{ult} = \sum_{j=1}^{m} F_j \left[\frac{2+\beta+\gamma}{3}d' - a\,(j-1)\right] \qquad\qquad 5.c.10$$

5.c.3. The Interaction Equations:

The interaction equation between bending and torsion can now be deduced by taking moments about two horizontal axes through the compression centre C, of the skew failure surface shown in figure 5.4a. These are axes $\overline{x}$ and $\overline{z}$. With cracks inclined at 45°, the crack depth is d'' and the projection of the cracks on to the

x-z plane is also d". This is shown in figure 5.4.b for each side of the panel. This figure also shows the actual crack on the bottom surface as gh. At failure the bottom stirrup legs within gh will be exposed and visible. These are marked in figure 5.4.b. Now because gh is at 45° to the X axis of the panel and t' is the distance between the longitudinal reinforcements, see figure 5.4.b, it is obvious that the stirrups will be exposed between g'h' measured along z axis of the panel. This distance g'h' is also equal to t'.

At failure the number of exposed vertical stirrup legs are thus d"/s on either side of the panel with a total of 2d"/s of such bars. The number of horizontal stirrup legs, on the other hand, is t'/s. With yield stress in the stirrup taken as σ_{wy}, the force in each leg is $A_w \sigma_{wy}$.

Two moment equations can now be written. These are:
i - Moments about $\bar{z}$ axis: This axis passes through the compression centre C. The lever arm of each vertical stirrup leg is t'/2 while a horizontal stirrup leg has a level arm of $\bar{d}$, see figure 5.5.a. The resultant (total) vertical force carried by all the exposed legs on each side is thus $A_w \sigma_{wy} d"/s$. The moment of this force about $\bar{z}$ axis is $(t'/2) \times A_w \sigma_{wy} d"/s$. The total resultant force carried by all the exposed horizontal stirrup legs is $A_w \sigma_{wy} t'/s$ and the moment of this force about $\bar{z}$ axis is $\bar{d} A_w \sigma_{wy} t'/s$. Thus the torque M_t is given by:

$$M_t = \frac{t'}{s} A_w \sigma_{wy} \bar{d} + 2 \left(\frac{d"}{s} A_w \sigma_{wy} t'/2\right) \qquad 5.c.11$$

Using equations (5.c.4) and (5.c.9) equation (5.c.11) becomes:

$$M_t = A_w \sigma_{wy} t' d' (2 + \beta + 4 \gamma)/3s \qquad 5.c.12$$

If the stirrups are merely unlooped vertical bars of a mesh, the contributions of the horizontal legs vanish and equation (5.c.12) reduces to:

$$M_t = A_w \, \sigma_{wy} \, t' \, d' \, \gamma/s \qquad\qquad 5.c.13$$

ii - Moments about $\bar{x}$ axis: The horizontal stirrups have no moment about this axis. The resultant force of all the vertical stirrup legs exposed on each side of the panel is $A_w \, \sigma_{wy} \, d''/s$. These are at distance $(t' + d'')/2$ from $\bar{x}$ axis, this distance being measured along the compression surface AB, see figure 5.4.a.

The moment produced by the exposed vertical stirrup legs is thus

$$M_{\bar{x}} = 2 \left(A_w \, \sigma_{wy} \, \frac{d''}{s} \cdot \frac{t' + d''}{2} \right) \qquad\qquad 5.c.14$$

This moment acts in a direction opposite to M_{ult} calculated in equation (5.c.10). Thus the resultant bending moment M_b about $\bar{x}$ axis is, from equations (5.c.10) and (5.c.14), making use of equation (5.c.4) to eliminate d'', is given by:

$$M_b = \sum_{j=1}^{m} F_j \left[\frac{2+\beta+\gamma}{3} d' - a \, (j-1) \right] - A_w \, \sigma_{wy} \, \gamma \, d' \, (t' + \gamma \, d')/s$$
$$5.c.15$$

The interaction equation between M_t and M_b can now be obtained by substituting $A_w \, \sigma_{wy} \, d'/s = 3 \, M_t \, (2 + \beta + 4 \, \gamma)t'$ from equation (5.c.12) into (5.c.15). We thus obtain:

$$M_b = \sum_{j=1}^{m} F_j \left[\frac{2+\beta+\gamma}{3} d' - a \, (j-1) \right] - \frac{3(t'+\gamma d')}{(2+\beta+\gamma)t'} M_t \qquad 5.c.16$$

which show that the bending moment of resistance of the section reduces with the presence of a torque.

5.d. The Neutral Axis under Combined Bending and Torsion:

The failure surface for this case is shown in figure (5.4.a). The breadth of the compression zone AB is shown in figure 5.4.b

as t. Since the cracks are at 45°, the value of $\bar{t}$ can be calculated from this figure as:

$$\bar{t} = \sqrt{(2d''+t')^2+t'^2}$$

and with $d'' = \gamma d'$

$$t = \sqrt{(2\gamma d'+t')^2+t'^2} \qquad\qquad 5.d.1$$

where t' is the horizontal distance between the reinforcements at either side of the panel.

Proceeding as in section 5.b leads to the value of x given by equation (5.b.15), provided that, in equation (5.b.16), $\bar{t}$ replaces t. However $\bar{t}$ is dependent on γ and a further iteration process becomes necessary. This is carried out as follows:

1 - Assume some value of γ, such as $\gamma=\gamma_0$

2 - Calculate $\bar{t}$ from equation (5.d.1)

3 - With $t = \bar{t}$ calculate x from equation (5.b.15)

4 - Calculate a new value of $\gamma = \gamma_n$ from equation (5.c.4)

5 - If γ_n and γ_0 are within a specified tolerance, the iteration process is complete.

6 - If not, replace γ_0 with the current value of γ_n and repeat the iteration from step 2. The value of γ_n thus obtained will be exact and it will be an upper bound to that obtained for pure bending.

5.e. Interaction of Bending, Shear and Torsion:

5.e.1 General:

Three expressions are required to be developed for developing the interaction equation. These are the moments of resistance due to bending and torsion and the shearing resistance of the reinforcements. The shear stress due to a torque M_t spirals around the deep beam while the vertical shear force S_y causes

shear stress in the Y direction. The separate shear stresses, developed by M_t and S_y, on one of the sides of the panel have the same sign and help each other. Those on the opposite side have different signs and oppose each other. The shear stress distribution due to S_y is parabolic and vanish at the top and the bottom surfaces of the beam. For this reason the only shear stresses acting at these surfaces are those due to torsion. The shear stress distribution at various points in a section are shown in figure 5.6.

When the panel is subject to a bending moment M_b, a torque M_t and a shear force S_y the skew failure surface ACBDE, shown in figure 5.7 may develop. Because the sides AE and DB are subject to different shear stresses, their inclination to the horizontal will also be different. The inclination of these sides are α_L and α_r respectively. The angle between the bottom crack DE and the z axis is α_b. These angles are also shown in the figure.

5.e.2 Resisting Moments of the Section at Failure:

The procedure for calculating the resisting moments of the reinforcements, about two axes through the compression centre, is similar to that presented in section 5.c and can be summarised as follows:

1 - The length of the cracks AE, ED and DB are calculated

2 - The number of bars exposed along each of these lines are counted or calculated.

3 - The force in each bar is calculated from the product of the area of each bar and the stress in it.

4 - The resultant of the forces in the bars along AE, ED and DB are found.
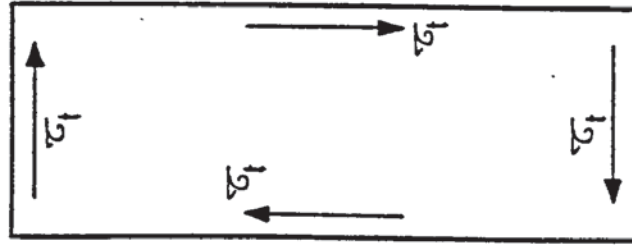
a Shear stresses
   due to torque
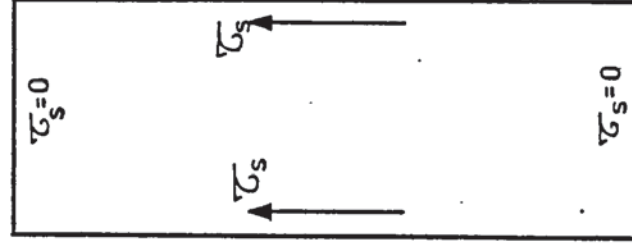
b Shear stresses
   due to shear force
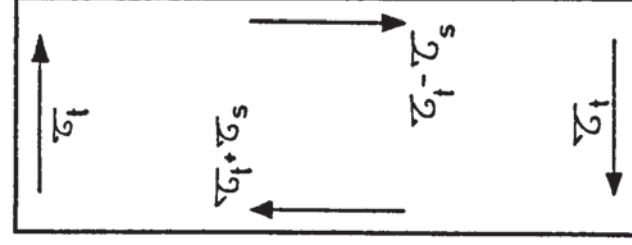
c Combined shear
   stresses

FIGURE 5.6: SHEAR STRESSES IN A SECTION DUE TO TORSION AND SHEAR FORCE

FIGURE 5.7: SKEW FAILURE SURFACE DUE TO BENDING, SHEAR AND TORSION

5 - The lever arms of these forces from the centre of compression are calculated.

6 - Finally the moments of the resultants are obtained from the product of each resultant and its lever arm. The two moments of resistance are now obtained.

1 - Moment of resistance about $\bar{z}$ axis:-

This axis is parallel to the z axis of the panel but passes through the compression centre C. The length AE' is d"Cot α_L, DB' is d"Cot α_r while ED' = t' Cot α_b where t' is the distance between the reinforcements on either side of the panel as shown in figure 5.8a. Thus the number of exposed stirrup legs along AE, ED and DB are d" Cot α_L/s, t'Cot α_b/s and d"Cot α_r/s respectively. The force in each leg is $A_w \sigma_{wy}$ and thus the three resultant forces are $A_w \sigma_{wy}$ d" Cot α_L/s, $A_w \sigma_{wy}$ t' Cot α_b/s and $A_w \sigma_{wy}$ d" Cot α_r/s.

The lever arm of the vertical resultant forces about $\bar{z}$ axis is t'/2 while that of the bottom stirrup legs is $\bar{d}$. The moment of resistance M_t about $\bar{z}$ thus becomes:

$$M_t = \frac{A_w \sigma_{wy} \; d'' \; Cot \; \alpha_L . t'}{2s} + \frac{A_w \sigma_{wy} \; t' \; Cot \; \alpha_b . \bar{d}}{s}$$

$$+ \frac{A_w \sigma_{wy} \; d'' \; Cot \; \alpha_r . t'}{2s} \qquad\qquad 5.e.1$$

Using equations (5.c.4) and (5.c.9) for γ and $\bar{d}$; M_t becomes:

$$M_t = A_w \sigma_{wy} \left[\frac{2+\beta+\gamma}{3} . \frac{Cot \; \alpha_b}{s} . t' . d' + \frac{\gamma \; t' \; d'}{2s}(Cot \; \alpha_L + Cot \; \alpha_r)\right]$$

$$\qquad\qquad 5.e.2$$

2 - Moment of resistance about $\bar{x}$ axis:

The bottom horizontal stirrup legs are parallel to $\bar{x}$ axis and have no moment about this axis. The resultant of the forces in the legs along AE and DB respectively are:

a TOP VIEW

b SIDE VIEW

FIGURE 5·8:

FAILURE MECHANISM FOR COMBINED BENDING

TORSION AND SHEAR

$$V_L = A_w \, \sigma_{wy} \, \frac{d'' \text{Cot } \alpha_L}{s} \qquad\qquad 5.e.3$$

and

$$V_R = A_w \, \sigma_{wy} \, \frac{d'' \text{Cot } \alpha_R}{s} \qquad\qquad 5.e.4$$

These resultants are shown in figure 5.8.b. This figure also shows the projection of the compression zone AB along the z axis. Here the distance AB is given by:

AB = d'' Cot α_L + d'' Cot α_r + t' Cot α_b and BC = AC = 0.5AB.

Point B' in this figure is vertically below B and the distance FB' is d'' Cot α_r. The resultant force V_R acts midway between F and B'. Thus its lever arm L_r from the axis $\overline{x}$, passing through c is

$$L_R = \quad BC - 0.5 \text{ FB'}$$

$$= \quad (d'' \text{ Cot } \alpha_L + t' \text{ Cot } \alpha_b)/2 \qquad\qquad 5.4.5$$

Similarly the lever arm L_L for the force V_L is:

$$L_L = (d'' \text{ Cot } \alpha_F + t' \text{ Cot } \alpha_b)/2 \qquad\qquad 5.e.6$$

In figures 5.7 and 8, point R is located midway between D and E at the bottom of the panel. Due to the external loads, the bending moment at this point is $M_{bR} = M_b$ and the shear force at R is S_y. The shear force at R and C are equal because there is no external force acting on the beam between these points. However, S_y at R has a moment $S_y \, a_1$, about $\overline{x}$, where a_1 is the distance along z axis between R and C as shown in figure 5.8.b. Thus the external moment applied at C is

$$\overline{M} = M_{bR} + S_y \, a_1 \qquad\qquad 5.e.7$$

This moment is balanced by three resisting moments these are:

(a) The moment M_{ult}, given by equation 5.c.10, and sustained by the longitudinal bars,

(b) The moment M_L sustained by the vertical stirrup legs along AE and given by:

$$M_L = V_L \, L_L = -A_w \, \sigma_{wy} \, \frac{d'' \, \text{Cot} \, \alpha_L}{s} \, (d'' \, \text{Cot} \, \alpha_r + t' \, \text{Cot} \, \alpha_b)/2 \qquad 5.e.8$$

(c) The moment M_R sustained by the stirrup legs along BD and given by:

$$M_R = V_R \, L_R = -A_w \, \sigma_{wy} \, \frac{d'' \text{Cot} \alpha_r}{s} \, (d'' \text{Cot} \alpha_L + t' \text{Cot} \alpha_b)/2 \qquad 5.e.9$$

The directions of both M_L and M_R are opposite to that of M_{ult} and therefore they are given negative signs. The moments in (a), (b) and (c) add up to $\overline{M}$, thus

$$M_{bR} + S_y \, a_1 = \sum_{j=1}^{m} F_j \, [\frac{(2+\beta+\gamma)d'}{3} - \alpha \, (j-1)]$$

$$- A_w \, \sigma_{wy} \, \frac{d'' \text{Cot} \alpha_L}{s} \, (t' \text{Cot} \alpha_b + d'' \text{Cot} \alpha_r)/2$$

$$- A_w \, \sigma_{wy} \, \frac{d'' \text{cot} \alpha_R}{s} \, (t' \text{Cot} \alpha_b + d'' \text{Cot} \alpha_L)/2 \qquad 5.e.10$$

5.e.3 The Shear Resistance of the Failure Surface:

Assuming that the concrete in the compression zone and the longitudinal bars do not carry any shear force - An assumption which is on the safe side. The shearing force acting vertically is the algebraic sum of the forces carried by the vertical stirrup legs, thus

$$S_y = V_L - V_R$$

$$= \frac{d'' \text{Cot} \alpha_L}{s} \, A_w \, \sigma_{wy} - \frac{d'' \text{Cot} \alpha_r}{s} \, A_w \, \sigma_{wy},$$

which gives:

$$S_y = A_w \, \sigma_{wy} \, d'' (\text{Cot} \alpha_L - \text{Cot} \alpha_r)/s \qquad 5.e.11$$

5.e.4 Inclinations of the Compressive Struts:

The values of the angles of inclination α_L, α_r and α_b and the lever arm a_1, used in the above equations, are calculated in the manner proposed in reference (88). This was done by considering the equilibrium along a horizontal cut fg shown in figure 5.9. It was assumed that near failure the torque and the
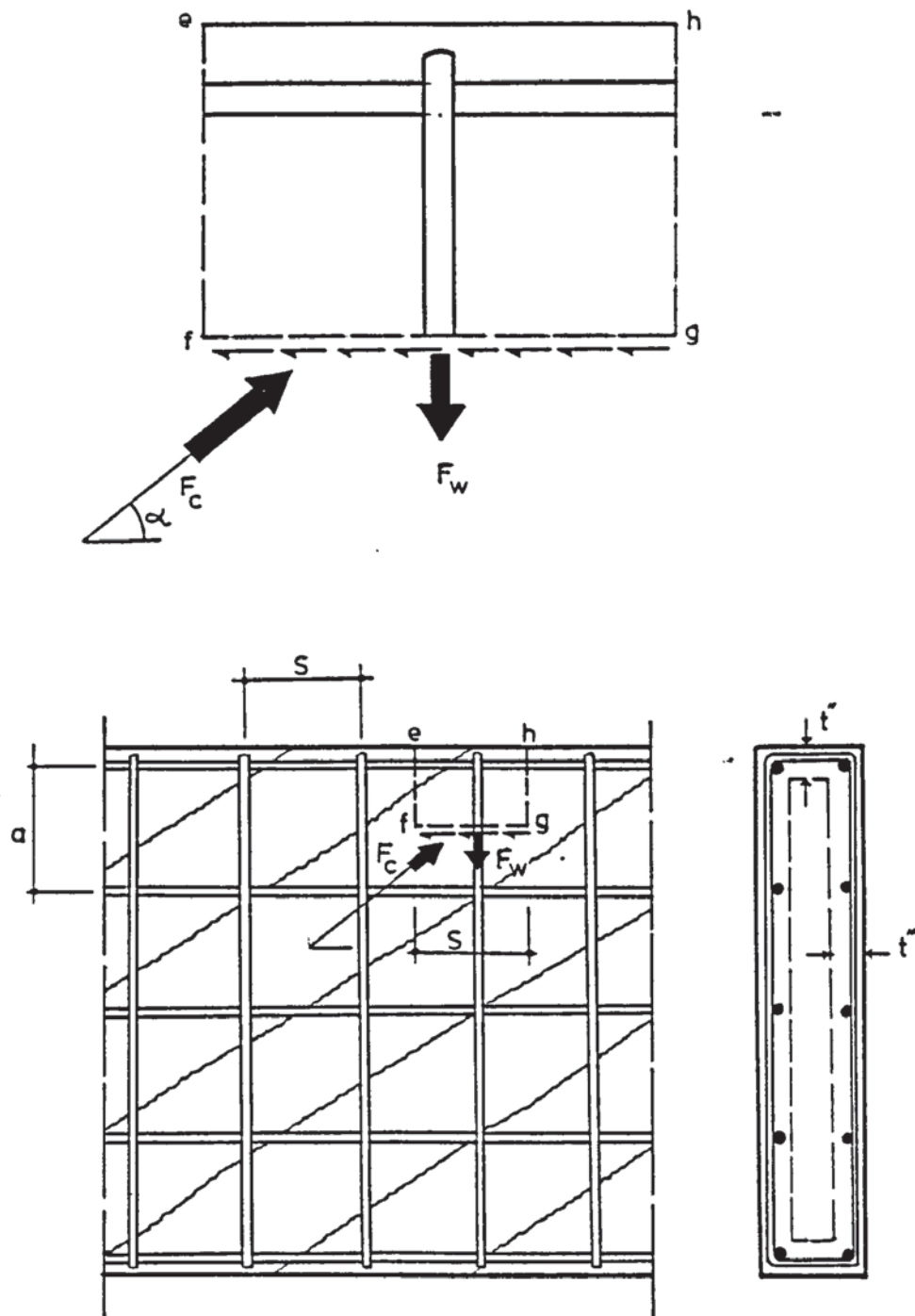
FIGURE 5.9: FORCES ALONG HORIZONTAL CUT IN
BEAM SIDE

vertical shear are mostly resisted by the outer portions of the cross section which has a thickness t". Vertical and horizontal equilibrium of forces acting on fg, while assuming that at failure the force F_W in a stirrup is the same in all the sides, made Cot α in figure 5.9 proportional to the shear stress τ. With α_{Mt} as the inclination of the concrete compressive struts when the torque M_t is acting alone and α_{sy} be the same angle for pure shear, it was found that:

$$\text{Cot } \alpha_L = \text{Cot } \alpha_{Mt} + \text{Cot } \alpha_{sy}$$

$$\text{Cot } \alpha_r = \text{Cot } \alpha_{Mt} - \text{Cot } \alpha_{sy} \qquad \text{5.e.12}$$

$$\text{Cot } \alpha_b = \text{Cot } \alpha_{Mt}$$

The distance a_1 can be calculated from figure 5.8a and equations (5.e.12) as:

$$a_1 = d'' \cot \alpha_{sy} \qquad \text{5.e.13}$$

5.e.5 The General Interaction Equation:

Now that expressions for the resisting force and moments have been derived, it is easy to formulate the general interaction equation. First of all equations (5.e.2), (5.e.11) and (5.e.12) give

$$\text{Cot } \alpha_{Mt} = \frac{3 M_t s}{t'd'A_w\sigma_{wy}(2+\beta+4\gamma)} \qquad \text{5.e.14}$$

$$\text{Cot } \alpha_{sy} = s\, S_y / (2\gamma d'A_w\sigma_{wy}) \qquad \text{5.e.15}$$

These expressions are then substituted in equation (5.e.10), while eliminating a_1, Cot α_b etc. to obtain:

$$M_b = \sum_{j=1}^{m} F_j \left[\frac{2+\beta+\gamma}{3} d' - a(j-1)\right] - A_w\sigma_{wy} \frac{\gamma d'}{s}\left[(t'+\gamma d') \frac{9 M_t^2 s^2}{A_w\sigma_{wy}^2 (t'd')^2(2+\beta+4\gamma)^2}\right.$$

$$\left. - \gamma d' \frac{s^2 S_y^2}{(2\gamma d')^2 (A_w\sigma_{wy})^2} - \gamma d' \frac{s S_y^2}{2\gamma d'A_w\sigma_{wy}}\right] \qquad \text{5.e.16}$$

The first term in this expression is the ultimate moment M_{ult} given by equation (5.c.10) and sustained by the longitudinal bars. Thus using M_{ult} in equation (5.e.16) gives:

$$\frac{M_b}{M_{ult}} + \frac{9 M_t^2}{[(2+\beta+4\gamma)t'd']^2} \cdot \frac{(t'+\gamma d')\gamma d'}{M_{ult}} \cdot \frac{s}{A_w \sigma_{wy}}$$

$$+ \frac{S_y^2}{(2\gamma d')^2} \cdot \frac{(\gamma d')^2}{M_{ult}} \cdot \frac{s}{A_w \sigma_{wy}} = 1 \qquad \text{5.e.17}$$

This is the general interaction equation between bending torsion and shear. From this the ultimate carrying capacities M_{ult}, for pure bending, M_{tult}, for pure torque and S_{yult}, for pure shear are extracted as:

(a) With $M_b = S_y = 0$:

$$M_{tult} = \frac{2+\beta+4\gamma}{3} t'd' \frac{\sigma_{wy} A_{wy}}{S} \sqrt{\frac{M_{ult}}{(t'+\gamma d')\gamma d'} \cdot \frac{s}{A_w \sigma_{wy}}} \qquad \text{5.e.18}$$

(b) With $M_b = M_t = 0$:

$$S_{yult} = \frac{\gamma d' A_w \sigma_{wy}}{s} \sqrt{\frac{M_{ult}}{(\gamma d')^2} \cdot \frac{s}{A_w \sigma_{wy}}} \qquad \text{5.e.19}$$

(c) With $S_y = M_t = 0$, M_{ult} is given by equation (5.c.10). The interaction equation (5.c.17) can then be simplified to become:

$$\frac{M_b}{M_{ult}} + \left(\frac{M_t}{M_{tult}}\right)^2 + \left(\frac{S_y}{S_{yult}}\right)^2 = 1 \qquad \text{5.e.20}$$

5.e.6 Special Cases:

As a special case, when the stirrups are not looped, the term contributed by the horizontal stirrup legs to equation (5.e.2) vanishes, giving:

$$M_t = 0.5 A_w \sigma_{wy} \gamma t'd' (\text{Cot } \alpha_L + \text{Cot } \alpha_r)/s \qquad \text{5.e.21}$$

This reduces the ultimate torque of equation (5.e.18) to:

$$M_{tult} = \gamma d't' \frac{A_w \sigma_{wy}}{s} \sqrt{\frac{M_{ult}}{(t'+\gamma d')\gamma d'} \cdot \frac{s}{A_w \sigma_{wy}}} \qquad \text{5.e.22}$$

Furthermore, if the reinforcement is put in the middle of the section, figure 5.1.a, then t' reduces to zero. With it the
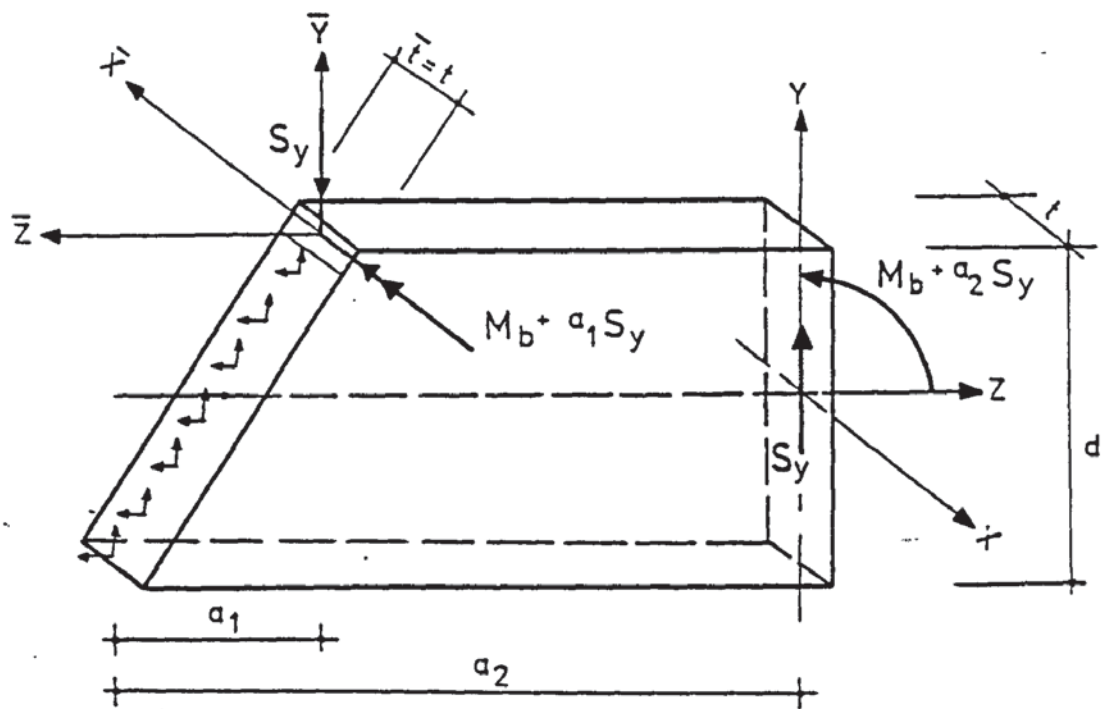
FIGURE 5·10: FAILURE SURFACE UNDER COMBINED
BENDING AND SHEAR
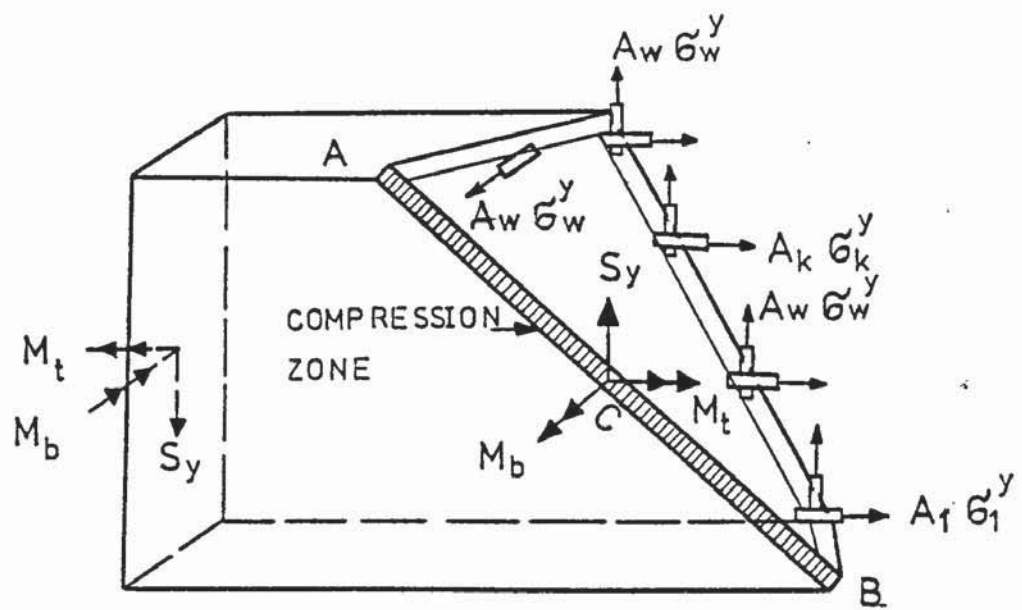
FIGURE 5.11: SIDE MODE OF COMBINED FAILURE
MECHANISM

ultimate torsional capacity of the section vanishes. Any small torque sustained by the longitudinal bars or by the concrete is neglected anyway.

Another special case is when the torsion in the panel is small and can be neglected. Equation (5.e.20) then reduces to:

$$\frac{M_b}{M_{ult}} + (\frac{S_y}{S_{yult}})^2 = 1 \qquad\qquad (5.e.20a)$$

The failure surface in this case is an inclined plane shown in figure (5.10).

Finally, when the torque and the shear force dominate and the bending moment is neglected, the failure surface changes to that shown in figure 5.11. Here the compression zone on one side of the panel. A procedure similar to that of reference[84], for this case, gives the interaction equation as:

$$(\frac{M_t}{M_{tult}^s})^2 + (\frac{S_y}{S_{yult}^s})^2 + \frac{M_t}{M_{tult}^s}\frac{S_y}{S_{yult}^s} \cdot \frac{2d'}{\sqrt{d'(t'+d')}} = 1 \qquad 5.e.23$$

where

$$M_{tult}^s = 2t'd' \frac{A_w \sigma_{wy}}{s} \sqrt{\frac{\sum_{j=1}^{\overline{m}} A_j \sigma_{yj}}{(d'+t')} \cdot \frac{s}{A_w\sigma_{wy}}} \qquad 5.e.24$$

and

$$S_{yult}^s = 2d' \frac{A_w \sigma_{wy}}{s} \sqrt{\sum_{j=1}^{\overline{m}} \frac{A_j \sigma_{yj}}{d'} \cdot \frac{s}{A_w\sigma_{wy}}} \qquad 5.e.25$$

Here M_{tult}^s and S_{yult}^s are the ultimate torque and ultimate shear carrying capacities when the compression zone is located in a side of the panel.

5.e.7. The Neutral Axis for Combined Bending and Shear:

The failure surface for this case is shown in figure 5.10. The shear force has no contribution to the horizontal equilibrium. Because there is no torsion $\overline{t} = t$ which is the thickness of the panel and equations (5.b.15) and (5.b.16) remain valid as they are.

5.e.8. The Neutral Axis for Combined Bending Torsion and Shear:

The length $\overline{t}$ = AB of the compression zone is that shown in figure 5.7 which is:

$$\overline{t} = \sqrt{\gamma d' (Cot\alpha_L + Cot\alpha_r) + t' Cot\alpha_b]^2 + t^2} \qquad 5.e.26$$

Using equations (5.e.12), $\overline{t}$ becomes:

$$\overline{t} = \sqrt{[2\gamma d' + t']^2 Cot^2\alpha_{Mt} + t^2} \qquad 5.e.27$$

As M_t decreases Cot α_{Mt} tends to zero and $\overline{t}$ reduces to t. On the other hand when the shear force is zero, Cot α_{Mt} = 1.

These values of $\overline{t}$ should be used to calculate the depth of the neutral axis from equation (5.b.15) and (5.b.16).

5.f. Experimental Investigation of the Depth of the Neutral Axis:-

The variation of the location of the neutral axis was investigated experimentally on test structures 11 and 12. Some critical sections of the slabs and the shear walls were equipped with longitudinal strain gauges, five on each side as shown in figure (5.12). Every time the loads were increased, the gauge readings were taken by an online computer. The measured strains were then plotted and the zero strain points, at each side of the critical section, connected to obtain the neutral axis at each loading level. The section along which the eventual failure occurred, gave the full information about the neutral axis.

As an example, the variation of the neutral axis at the critical section in structure 11, during the loading process, is shown in figure (5.13). It can be seen from this figure that as the loads are increased, the neutral axis tends to rise and to be parallel to the top and bottom faces of the beam. At the stage just before the failure (figure 5.13.g) the neutral axis reached its top level and became parallel to the top face of the panel.

FIGURE 5.12: POSITION OF STRAIN GAUGES
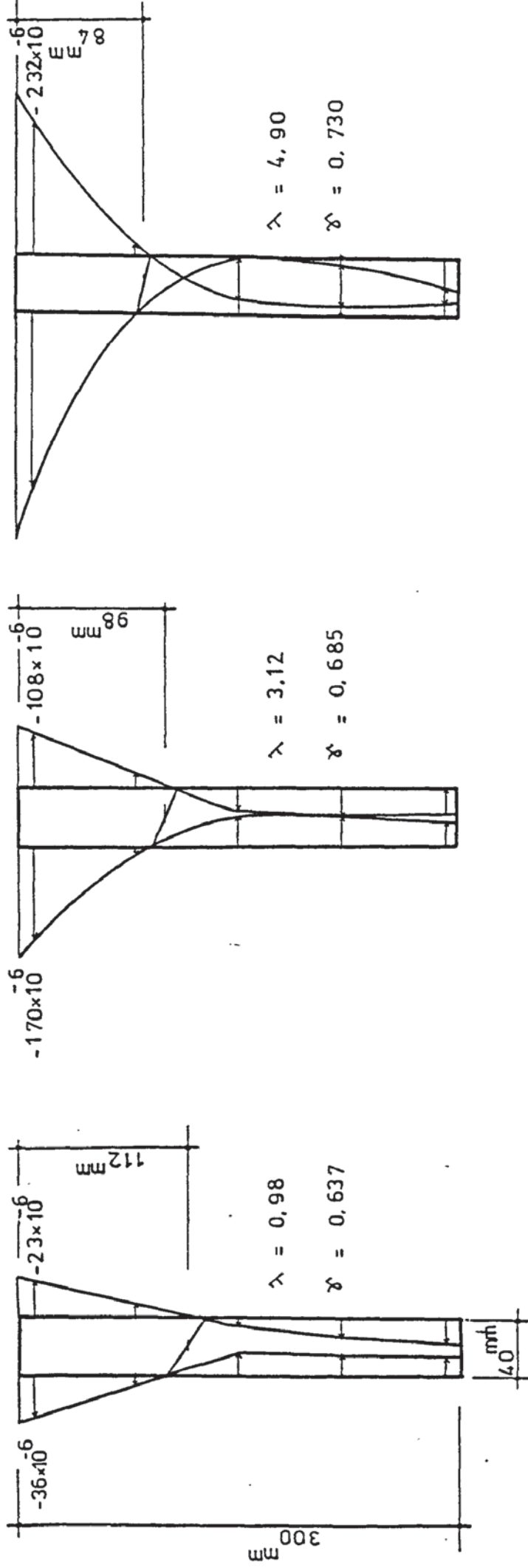
FIGURE 5.13.a

FIGURE 5.13.b

FIGURE 5.13.c

FIGURE 5.13 — STRAIN DIAGRAMS AND THE POSITIONS OF NEUTRAL AXIS
THROUGHOUT THE LOADING OF TEST STRUCTURE 11   (continued)

-683×10^{-6}

$\gamma = 6,67$

$\delta = 0,866$

77 mm

FIGURE 5.13·f

-652×10^{-6}

$\gamma = 6,39$

$\delta = 0,861$

76 mm

FIGURE 5.13·e

-303×10^{-6}

-397×10^{-6}

$\gamma = 5,93$

$\delta = 0,752$

81 mm
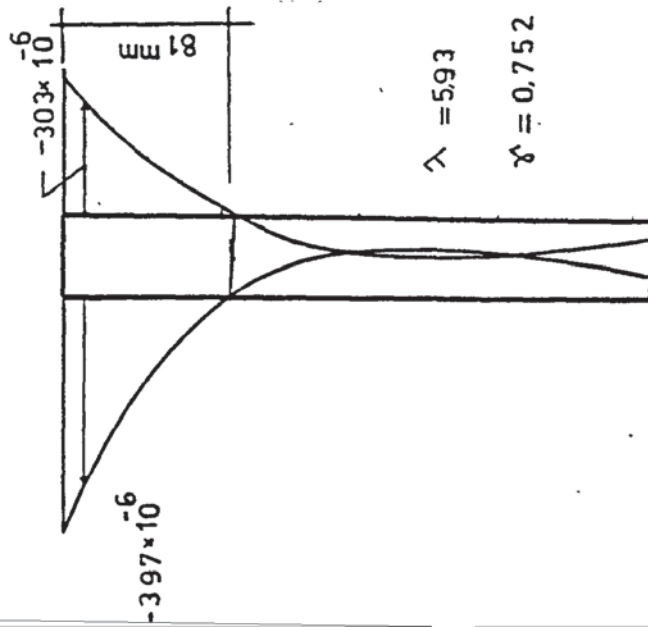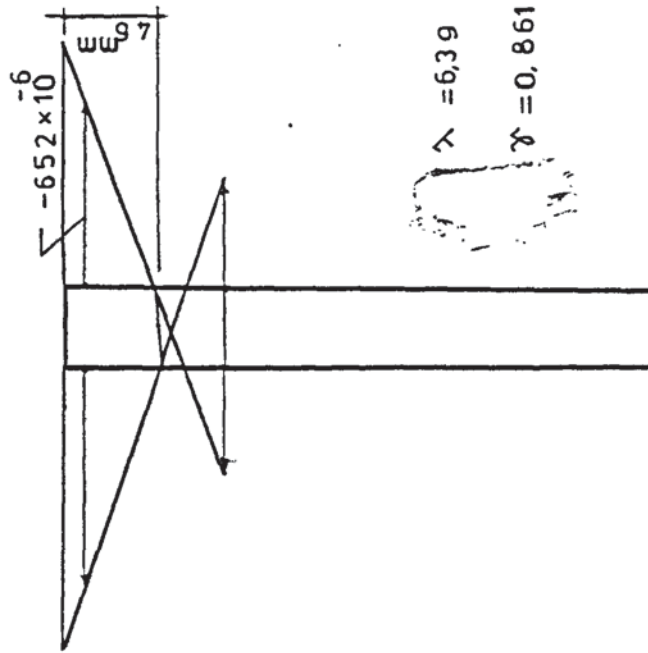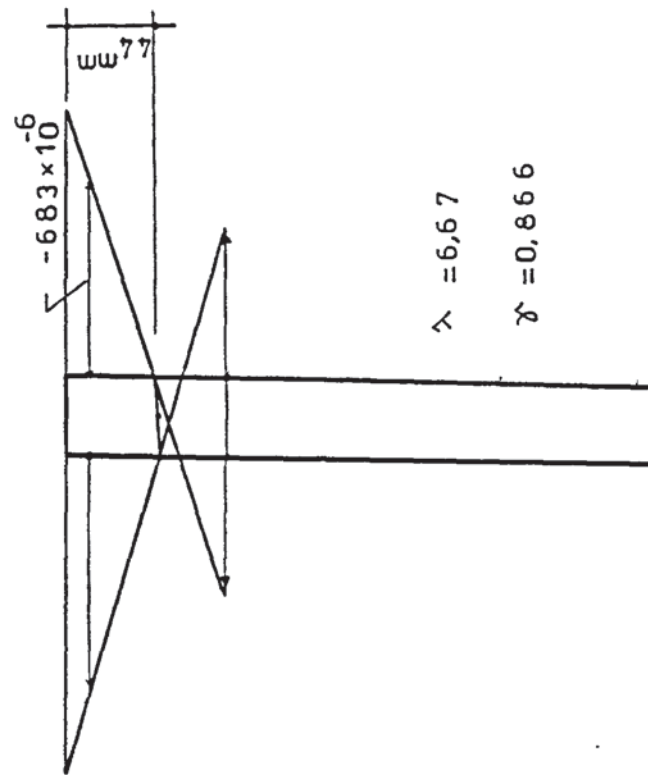
FIGURE 5.13·d

FIGURE 5.13 (continued)

-743×10^{-6}

-659×10^{-6}

40 mm

$\lambda = 7.09$

$\gamma = 0.876$
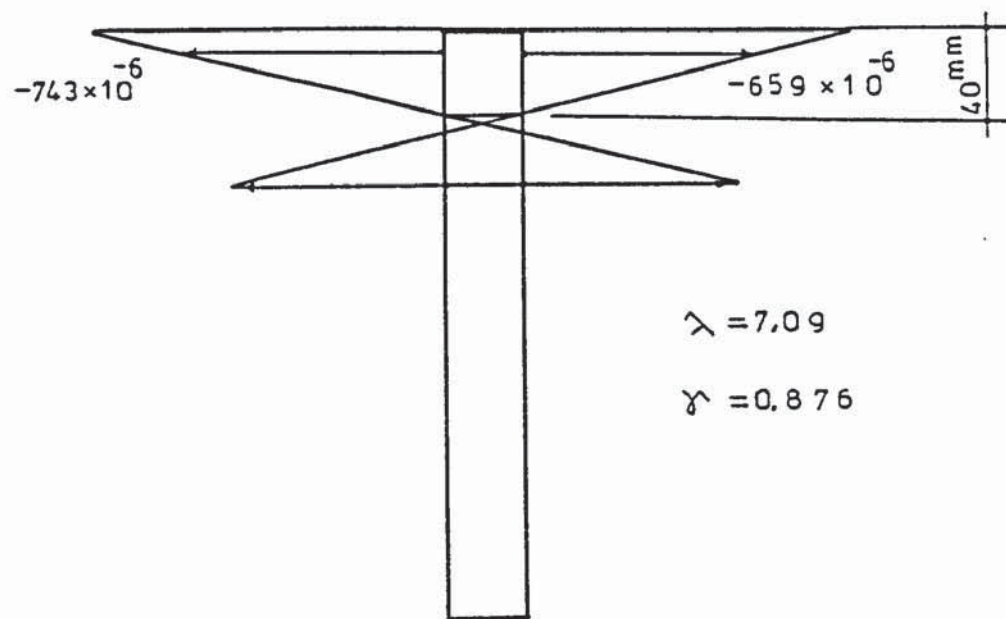
FIGURE 5.13.g — Strain diagram and position of
neutral axis just before the
failure
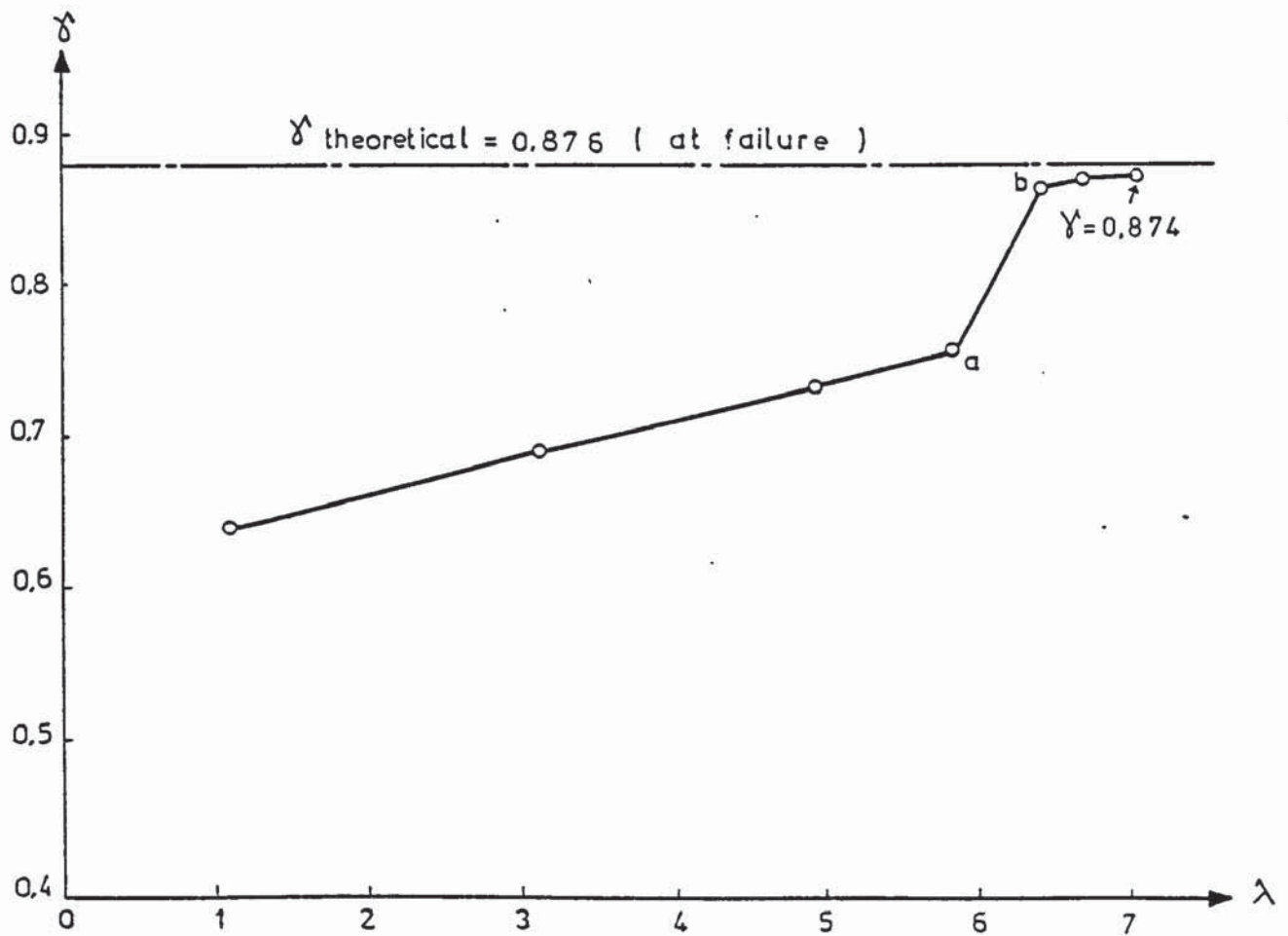
FIGURE 5.14: VARIATION OF γ VERSUS λ FOR
TEST STRUCTURE 11

This in fact proves that the assumption of the compression zone with uniform thickness in the assumed failure mode is true. In figure (5.14) the value of γ is plotted against the load parameter, λ, of structure 11. For the values of λ up to 5.8 (point a) the neutral axis, and thus γ, rised almost linearly. Between the points a and b, γ increased abruptly. The reason for this may be due to major cracks elsewhere in the structure which caused more loads to be transferred to the section. Further increases in the load factor caused slight rises of γ and finally the section failed when $\gamma = 0.874$. The theoretical value of γ at the ultimate stage was also calculated, from equations (5.b.15) and (5.c.4), to be 0.876 which is 0.23% higher than that obtained experimentally. In structure 12 the theoretical value of γ was calculated to be 0.865, being 4.05% above the experimental value of 0.829. These figures show that the proposed method of calculating the depth of the neutral axis, and therefore the value of γ, may be based on realistic considerations.

Furthermore, the effect of the value of γ on the failure loads of complete structures was studied. The test structure 7 of table (7.2) in chapter 7 was analysed for different values of γ and the failure loads were plotted in figure (5.15). This graph shows that the failure load is very much dependent on the value of γ. It is noticed that as γ increases from 0.5 to 0.95 the load factor at failure increases from 2.2 to 3.13. This means that neglecting the depth of the compression zone, as was done in reference (88), introduces a large error in failure load calculation.
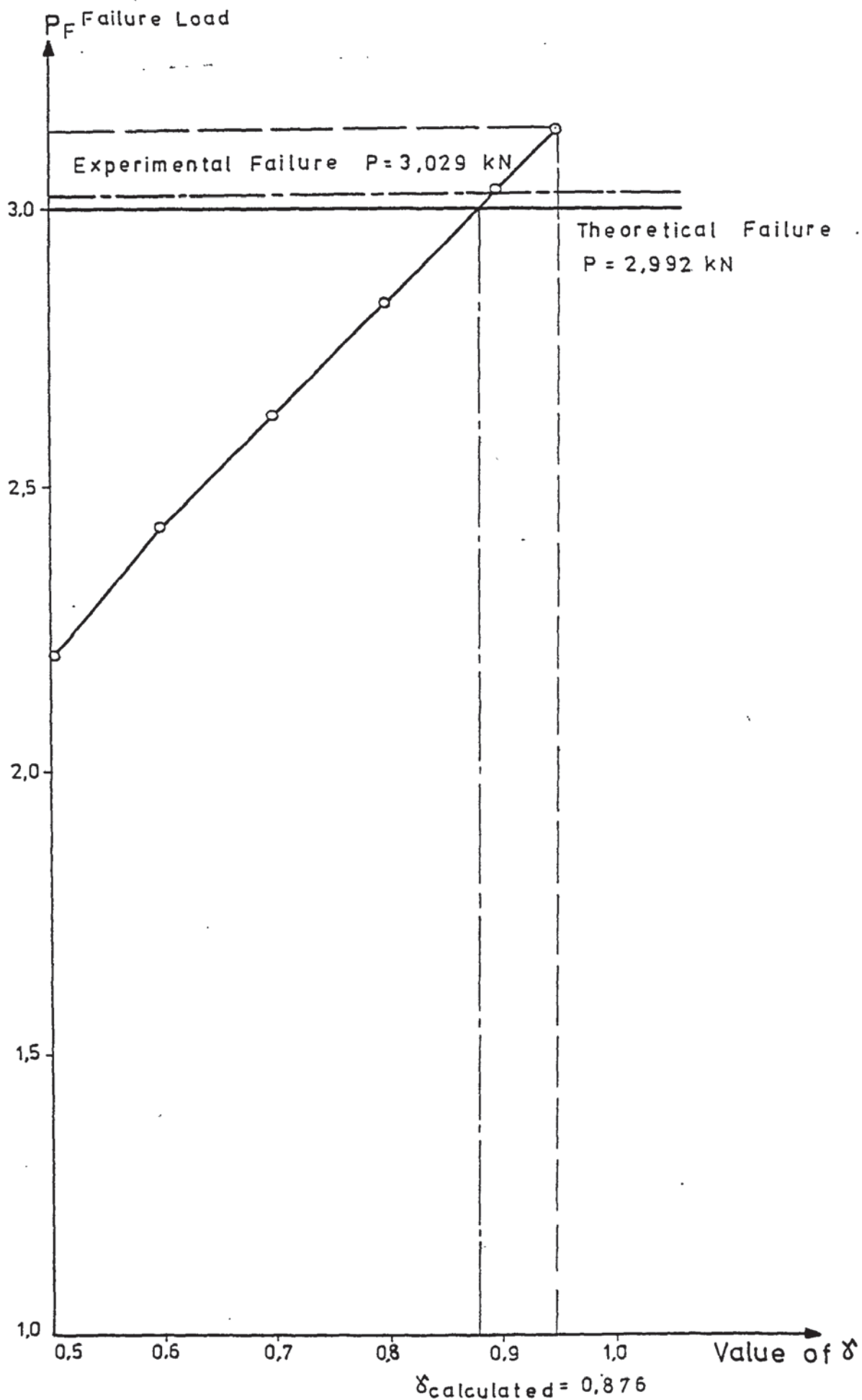
FIGURE 5.15: EFFECT OF γ ON FAILURE LOAD OF TEST STRUCTURE 7 (Bilinear M-C is assumed for the grillage)

5.g. A Failure Analysis of the Grillage System:

An iterative method is used to single out the panel of a grillage that fails first and the load factor at which it fails. Consider that the load factor of the applied loads acting on a structure is increased by an increment $\Delta\lambda_i$. The resulting bending moment, torque and shear force in a panel after this increment are given by:

$$M_{bi} = M_{bi-1} + \Delta\lambda_i \, \overline{M}_{bi}$$

$$M_{ti} = M_{ti-1} + \Delta\lambda_i \, \overline{M}_{ti} \qquad\qquad 5.g.1$$

$$S_{yi} = S_{yi-1} + \Delta\lambda_i \, \overline{S}_{yi}$$

The existing element forces are M_{bi-1}, M_{ti-1} and S_{yi-1} and $\overline{M}_{bi}$, $\overline{M}_{ti}$ and $\overline{S}_{yi}$ are those caused when $\Delta\lambda_i = 1$.

Equation 5.e.20 is then written as:

$$\frac{M_{bi-1}+\Delta\lambda_i\overline{M}_{bi}}{M_{ult}} + \left(\frac{M_{ti-1}+\Delta\lambda_i\overline{M}_{ti}}{M_{tult}}\right)^2 + \left(\frac{S_{yi-1}+\Delta\lambda_i\overline{S}_{yi}}{S_{yult}}\right)^2 = 1 \qquad 5.g.2$$

This equation can be written in a quadratic form in $\Delta\lambda_i$ as:

$$A\Delta\lambda_i^2 + B\Delta\lambda_i + C = o \qquad\qquad 5.g.3$$

and its positive root:

$$\Delta\lambda_i = \frac{-B + \sqrt{B^2-4AC}}{2A} \qquad\qquad 5.g.4$$

gives the value of $\Delta\lambda_i$ at which the panel fails. During the analysis of the complete structure and after each critical stage, each panel of the grillage is tested and its $\Delta\lambda_i$ value is calculated. The lowest of these, $\Delta\lambda_i^*$, decides which panel is going to fail next. The load factor $\lambda_{i-1} + \Delta\lambda_i^* = \lambda_i^*$ causes this failure. If this load factor is also the one that brings about the next critical stage of the structure then it is concluded that the panel in question has failed and its stiffness is reduced to some nominal value.

It should be pointed out that, if the bending moment is small and dominated by the torque and the shear force, then equation 5.e.20 is replaced by equation 5.e.23.

5.h Application to the Failure Load Analysis of Complete Structures:

The method given in chapter 4 for the failure load analysis of complete structures is also valid for the case when the structure consists merely of reinforced concrete slabs or frames. Under the light of the studies given in the second part of chapter 3 and in this chapter, the following modifications are necessary to take the full non-linear moment-curvature properties and the interaction of bending, torsion and shear within the grillage panels into account.

The proposed modifications in the analysis with respect to the steps given in chapter 4, section (4.d) are stated below:

i - In step 2: Each reinforced concrete frame is analysed by means of the method given in chapter 3, section k, to obtain the load factor λ' at which a critical point is first reached on the M-C diagram of any member of the frame.

ii - In step 3: The grillage is analysed under factored loads $\lambda_G \underline{g}$ acting at the junctions and $\lambda_G \underline{w}$ acting on the shear walls. This is to calculate the load factor λ_G at which a critical point is reached on the M-C diagram of one of the panels.

iii - In step 5: If $\lambda_{cr} = \lambda_F$ a new flexural rigidity is adopted for the member of a frame for which λ_F was selected. This flexural rigidity is the slope of the next transition region of the M-C diagram of that member.

If on the other hand $\lambda_{cr} = \lambda_G$ the stiffness of the panel for which λ_G is calculated, is altered in the following cases:

a - If the cracking point A, fig. 3.16 is reached on the M-C diagram, the flexural rigidity of the cracked section $(EI)_c$ is selected as its flexural rigidity EI_{new}. The torsional rigidity GJ is also altered by the same variation ratio, thus $GJ_{new} = (1+\alpha) GJ$

In reality the change in the value of GJ may be different from that of EI but it is assumed that α is the same and thus the construction of a "Torque rotation" diagram is avoided.

In the case when a relatively high torsional moment is acting on the panel, the cracking moment M_c, figure 3.16, depends on the interaction of bending and torsion. Equation (3.8) over estimates this moment. The effect of torque can be taken into account by means of equation (4.2 1). The elastic section modulus Z_b in bending is calculated from the gross uncracked section, while the elastic section modulus Z_t in torsion is calculated from equation (4.18).

Although the initial flexural rigidity $(EI)i$ and the cracked flexural rigidity $(EI)_c$ are predetermined, the critical moments M_c and M_u are decided by means of equations (4.21) and (5.e.20) or (5.e.23) respectively.

b - If the ultimate moment defined by equations (5.e.20) or (5.e.23) is reached, then the stiffness of the whole panel is reduced drastically as in the case of homogeneous panel.

5.i Examples:

5.i.1 Failure Load Analysis of Single Storey

Structures with no Intermediate Frames:

To demonstrate the method of analysis and to verify the validity of the interaction equation (5.e.20) the first series of reinforced concrete structures tested by the author were analysed manually. Details of these are given in table (7.1). In table (5.1) the theoretical and the experimental results are compared.

STRUCT. NO.	EXPERIMENTAL FAILURE LOAD (kN)	THEORETICAL FAILURE LOAD (kN)	% DIFFERENCE	γ THEORETICAL
1	1.577	1.889	+16.51 %	0,912
2	1.727	1.894	+8.81 %	0,910
3	5.963	5.850	-1.88 %	0,861
4	6.362	5.869	-7.00 %	0,874

TABLE 5.1: COMPARISON OF THEORETICAL
AND EXPERIMENTAL FAILURE
LOADS FOR SINGLE STOREY
STRUCTURES WITHOUT FRAMES
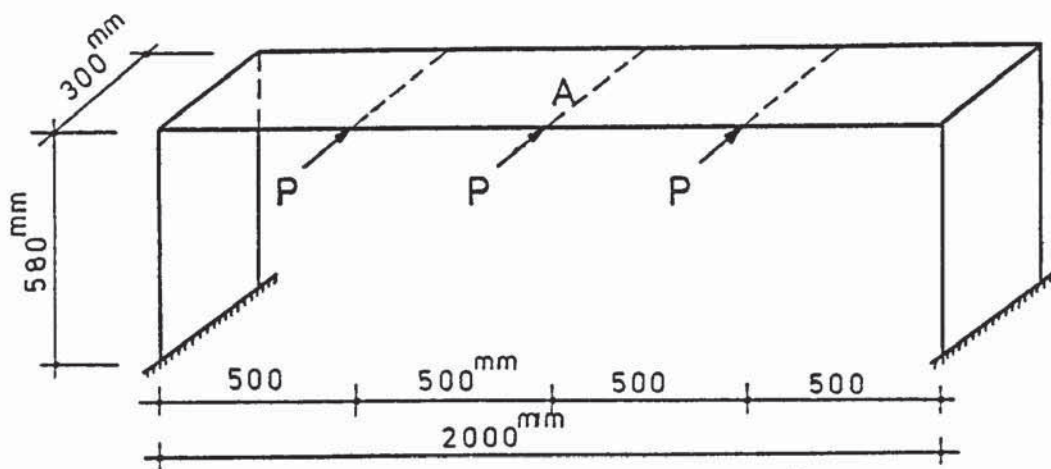
a-Structure and Loading
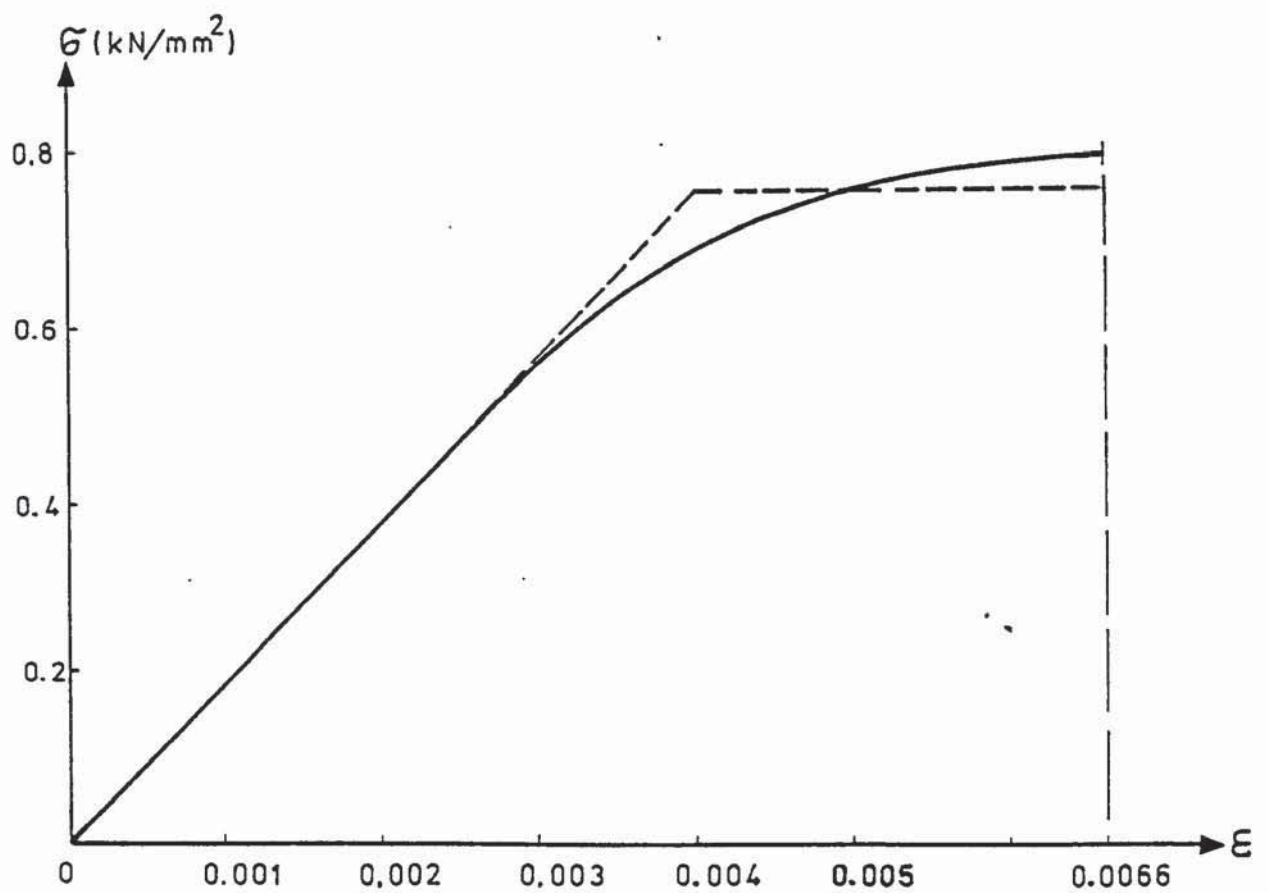
b Stress Strain Diagram of reinforcement

FIGURE 5.16: TEST STRUCTURE 3

A maximum relative discrepancy of 16.51% is recorded. As an example the analysis of structure (3) will be given here. The overall dimensions of this are shown in figure (5.16.a). The reinforcements were placed in the middle of the cross section as shown in figure (5.17.a). The modulus of elasticity and ultimate strength of the concrete are 19.60 kN/mm^2 and 0.02 kN/mm^2 respectively. The modulus of elasticity, the yield strain and the ultimate strain of the reinforcement are 209.0 kN/mm^2, 0.00365 and 0.00660. The stress-strain diagram of the reinforcement steel, obtained experimentally, is shown in figure (5.16.b). The cross sectional properties of the shear walls and floor slab are similar. From figure (5.17.a) the number of layers $\overline{m}$ = 12, the depth of the section d = 289.7 mm and the cover''' = 10.3 mm. Using modular ratio α_e = E_s/E_c = 10.66 and the ratio of strains in the steel at first yield and at failure $\eta = \varepsilon_{sy}/\varepsilon_{su}$ = 0.553, equation (5.b.16) gives ζ = 9.76. To begin with assuming that there are 5 layers in the plastic zone thus i = 5; equation (5.b.15) gives the depth of the neutral axis as x = 48.76mm, equation (5.c.4) now gives the value of γ as 0.861. Knowing x and ε_{su} the strain diagram shown in figure (5.17.b) is constructed. It can be seen that the number of layers in the plastic zone are in fact 5 thus the values of x and γ are correct. Using this strain diagram and the stress-strain diagram shown in figure (5.16.b) the force diagram in figure (5.17.c) was constructed. The lever arm of the force in each layer is also marked in the figure. Hence, using equation (5.c.10) the ultimate moment of the section is obtained at M_{ult} = 5900.09 kNmm, with γ = 0.861, d = 289.7, s = 25.4, $A_w\sigma_{wy}$ = 4.4 kN, equation (5.e.19) gives the ultimate shear force S_{yult} = 31.97 kN.
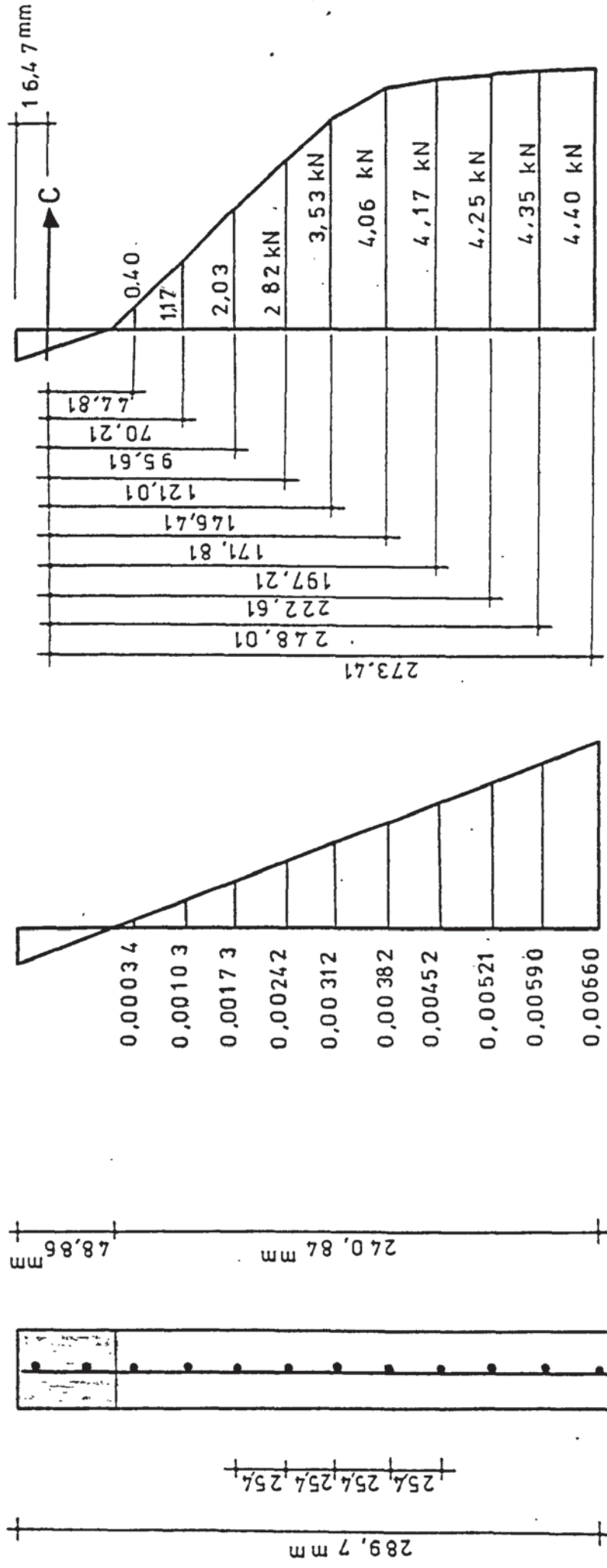
a - Cross Section

b - Strain Diagram

c - Forced Diagram and distances to the compression centre

FIGURE 5.17

500   500^{mm} 500   500

580 mm

1000P kN×mm

750P   750P

A

870P kn×mm   870P

a- Inplane Bending Moment Diagram

1.5P kN

0.5P kN

1.5P kN   0.5P kN

1.5P kN

1.5P kN
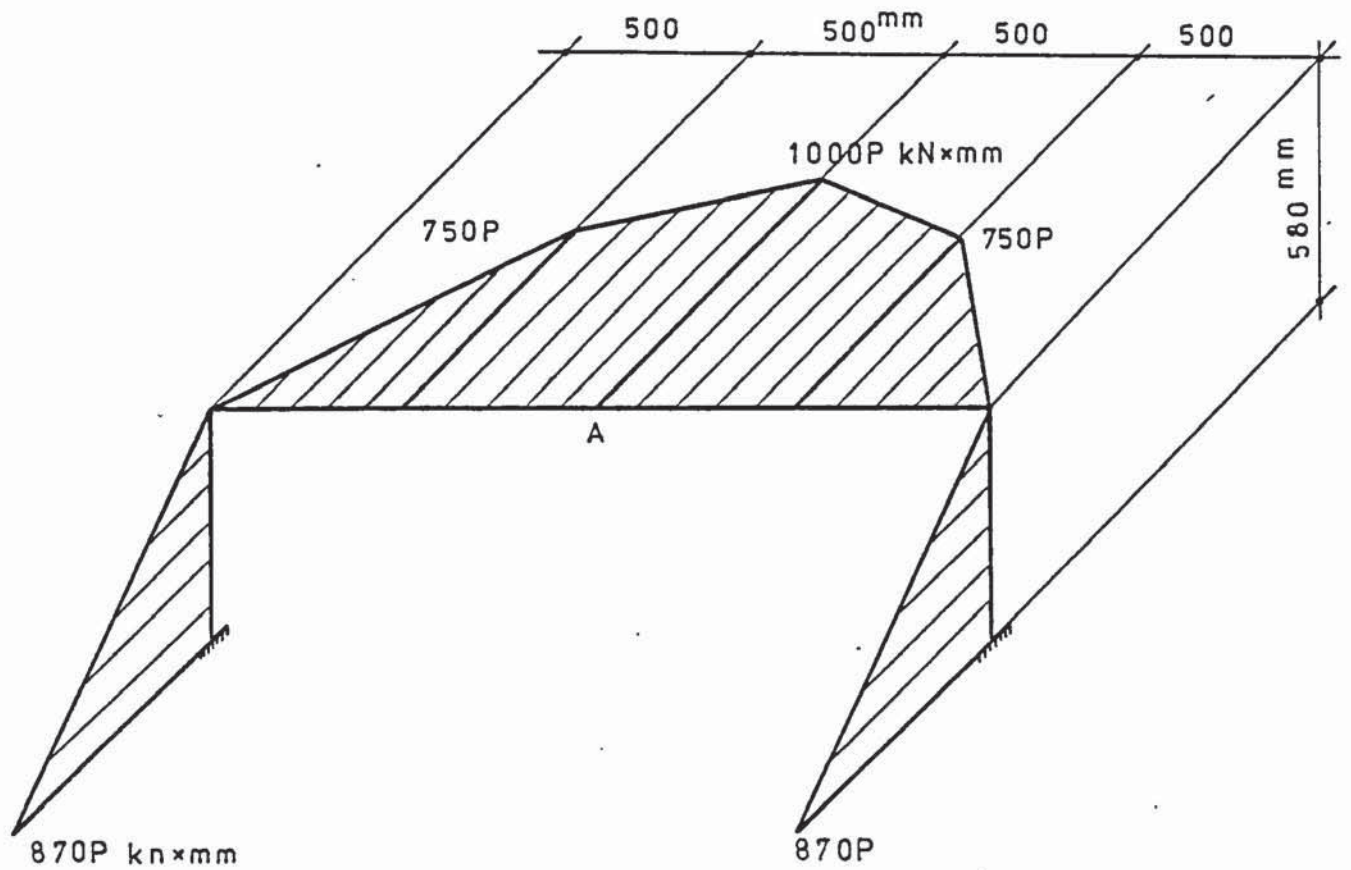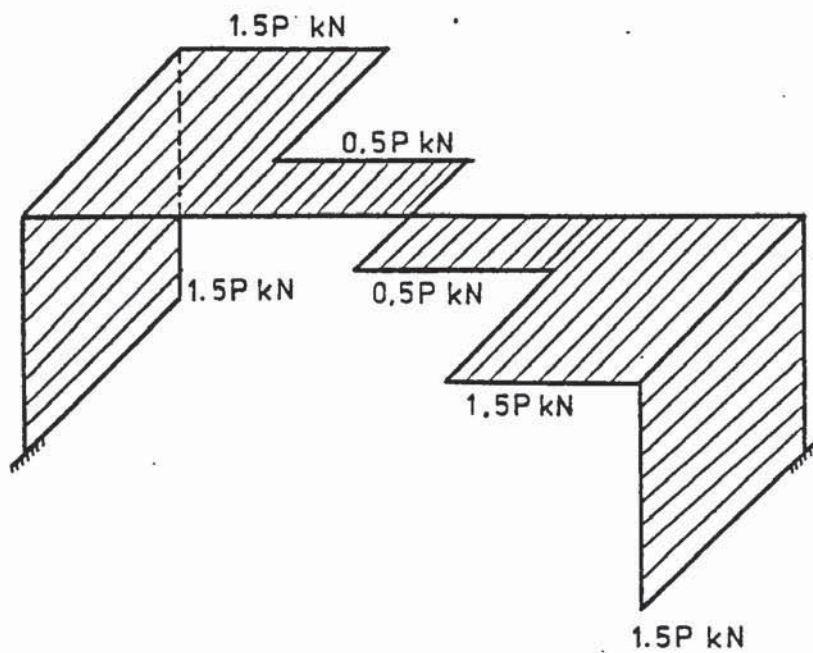
b-Shear Force Diagram

FIGURE 5.18: BENDING MOMENT AND SHEAR

FORCE DIAGRAMS FOR STRUCTURE 3
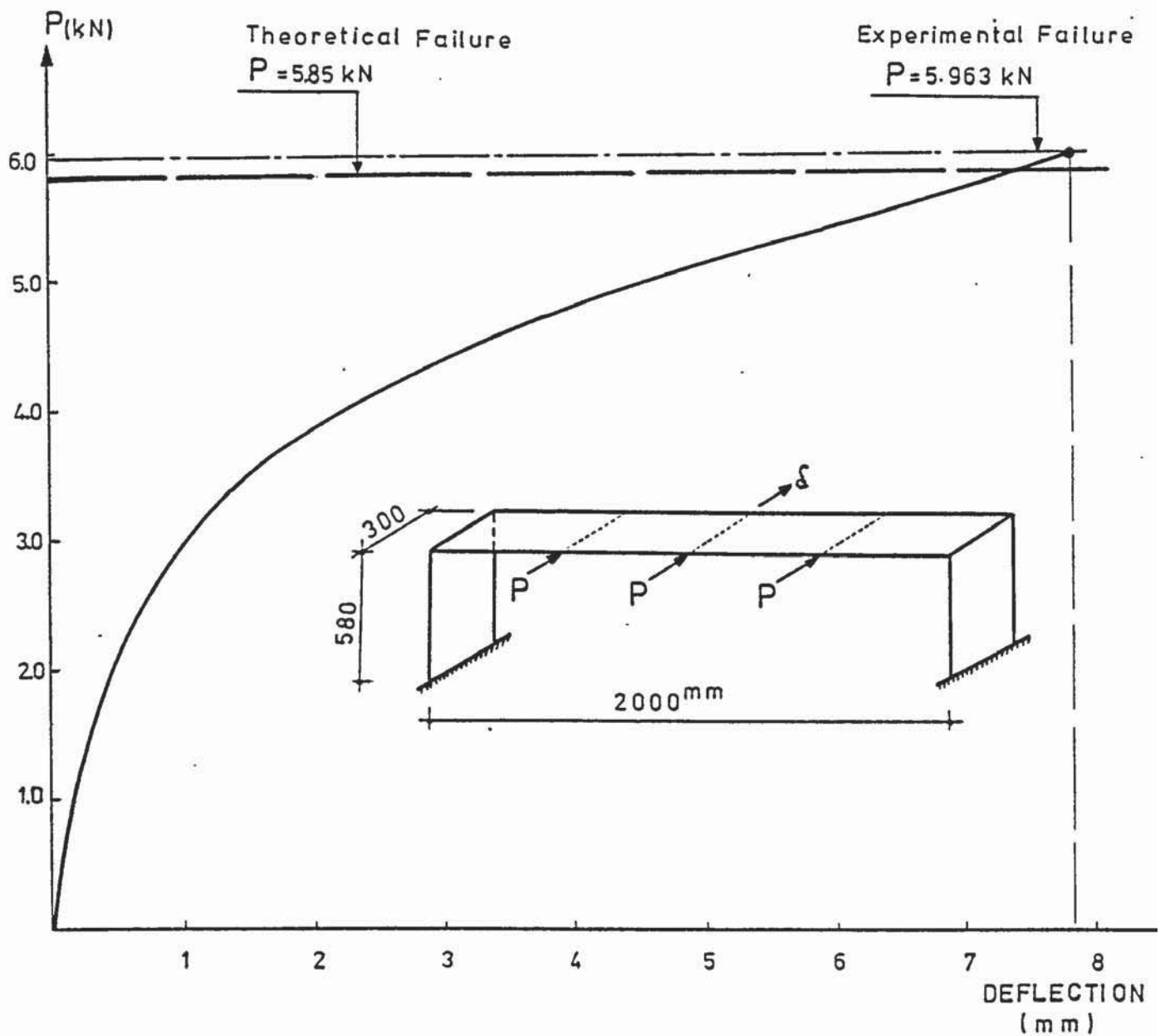
FIGURE 5.19: LOAD DEFLECTION DIAGRAM FOR A
ONE STOREY STRUCTURE WITHOUT
INTERMEDIATE FRAMES

Ignoring the torsional stiffnesses of the panels at the
ultimate stage, the bending moment and shear force diagrams of
the structure were constructed as shown in figure (5.18), where
it is noticed that A is the most critical section. Here the
bending moment M_b = 1000 P kN mm and shear force S_y = 0.5 P kN are
acting together. In fact the experimental failure also took place
at A. Again, ignoring the effect of torsion, equation (5.e.20)
gives the failure criterion as:

$$\frac{10000 \ P}{5900.09} + (\frac{0.5 \ P}{31.97})^2 = 1$$

and the value of failure load P is obtained as 5850 kN which is
only 1.88% lower than the experimental failure load 5.963 kN.
The experimental load-deflection curve and the theoretical failure
load are shown in figure (5.19).

V

CHAPTER 6

6.a. A COMPUTER PROGRAM FOR THE ELASTIC-PLASTIC AND

NONLINEAR M-C ANALYSIS OF FRAMES

6.a.1 Introduction:

The program makes use of the procedures given in chapter 2 and the first part of chapter 3. It is written in extended fortran to run on the ICL 1904 computer of the University. It is developed to be capable of doing the following types of analysis.

i   - Linear elastic analysis*

ii   - Nonlinear elastic analysis*

iii - Elastic-plastic analysis using the theorems of structural variation.

iv   - Elastic-plastic analysis of a derivative frame using the initial solution of the parent frame.

v   - Nonlinear moment-curvature analysis, using the theorems of structural variation.

vi   - The program also has the facility to carry out an iterative design of frames using the theorems of structural variation. This is given in the subroutine design, but since it is incomplete and also since it is out of the scope of this thesis, no further details of this will be given here.

The program consists of a master segment and a number of subroutines. Their functions are illustrated in the flow diagrams shown in figures (6.1), (6.2), (6.3), (6.4) and will be explained in detail in the following sections. The data presentation for this program will be given in appendix 1.

6.a.2 Description of the Program:

After data presentation the program starts constructing the compound load matrix [L C]. For the cases of linear and nonlinear

*The program was originally developed in atlas autocode by Majid[28] to carry out this type of analysis.

START

READ THE GENERAL DATA

Elastic Analysis? — YES

NO

CONSTRUCT THE COMPOUND LOAD MATRIX [L C]

SET THE AXIAL LOADS TO ZERO

CALL STIFMAT, CONSTRUCT K AND SOLVE L=KX OR [LC]=KX FOR X

CALCULATE THE MEMBER FORCES

LINEAR ELASTIC ANALYSIS? — YES → STOP

NO

NONLINEAR ELASTIC ANALYSIS? — YES → IS THE TOLERANCE TEST SATISFIED

NO

IS THE TOLERANCE TEST SATISFIED — NO

YES → STOP

DESIGN? — YES → CALL DESIGN → STOP

NO

ELASTIC PLASTIC ANALYSIS OF DERIVATIVE FRAME — NO

YES

READ THE NEW CROSS-SECTIONAL PROPERTIES OF CHANGING MEMBERS

CYCLE CHANGING MEMBERS

CALCULATE VARIATION RATIOS

CALL   CHANGE

LAST MEMBER? — NO

YES

NONLINEAR M-C ANALYSIS? — YES → CALL NONLINMC → STOP

NO → CARRY OUT ELASTIC-PLASTIC ANALYSIS → STOP

FIGURE 6.1 FLOW DIAGRAM OF THE MASTER SEGMENT

elastic analyses, this operation is not carried out, the following
paths can then be followed.

i - For the elastic-plastic analysis, the total number of load
cases are fed in as NCR=1. Where NCR is the number of expected
hinge locations. The first column of matrix $[\underline{L} \ \underline{C}]$ contains the
external loads $\underline{L}$ which are already read in. Each of the other
columns contains a unit load case corresponding to each hinge
location as given by equation (2.13).

ii - In the case of the elastic-plastic analysis of a derivative
frame, which is obtained by removing some of the members of a
parent frame or altering their cross-sectional or material
properties, the compound load matrix takes the form $[\underline{L} \ \underline{C} \ \underline{C}^{MR}]$.
Here the submatrix $\underline{C}^{MR}$ is the unit load matrix described by Saka[3]
and used when such alterations are carried out. The submatrix $\underline{C}^{MR}$
contains three columns for each member to be removed or altered.
The first deals with altering the member area. The other two are
the first and the second end unit load cases to alter the second
moment of area. If NMR is the number of members to be altered or
removed, the submatrix $\underline{C}^{MR}$ contains 3 NMR columns. The submatrix
$\underline{C}$ is similar to that described in case "i".

iii - In the nonlinear moment-curvature analysis, the unit load
matrix contains two columns for each member of the frame. The first
is given by equation (2.11) and the second by equation (2.12).

Having constructed the compound load matrix, the subroutine
stiffmat is entered. This constructs the overall stiffness matrix
$\underline{K}$ and solves the joint equilibrium equations $[LC] = \underline{K} \ \underline{X}$. The
control is then transferred to the main segment again and the
member forces are calculated from $\underline{P} = \underline{k} \ \underline{A} \ \underline{X}$. Where $\underline{P}$ is the

vector of member forces, $\underline{k}$ is the member stiffness matrix of the frame and $\underline{A}$ is the displacement transformation matrix of the whole frame.

Once the initial values of the member forces and deflections due to the working and the unit loads are calculated, the following operations are carried out, as required by the user:

1 - For the case of linear elastic analysis (the path counter I2 = 0), the process is already completed. The member forces and deflections are printed out and the analysis is terminated.

2 - In the nonlinear elastic analysis (I2 = -1), the resulting axial loads are used to reconstruct the overall stiffness matrix and solve for $\underline{X}$ again. This operation may be repeated until the values of the axial forces, for each member, in two successive cycles are within a specified tolerance.

3 - When an elastic-plastic analysis of the frame is required (I2 = -2), the bending moment matrix $\underline{M}$ and the axial force matrix $\underline{P}$ are constructed and used together with the deflection matrix $\underline{X}$ to carry out the elastic-plastic analysis within the corresponding block.

4 - I2 = -3 indicates that some members of the frame are to be removed or changed and an elastic-plastic analysis of the resulting frame is to be carried out. Each of the changing members is considered in turn and the variation ratios in its area and second moment of area are calculated. The subroutine "change" is then called to obtain the member forces and deflections of the resulting frame. Once the alteration in the topology of the frame is completed, the elastic-plastic analysis of the new frame is carried out in the manner given for case 3.

5 - For I2 = -4, the nonlinear moment-curvature analysis of the frame is required. The matrices $\underline{M}$ and $\underline{P}$ are constructed from the bending moments and the axial forces due to the working loads and unit load cases of each member. The first rows of these matrices correspond to the actual loading while each two of the other rows contain the bending moments and axial forces for the first and second end unit load cases of a member respectively. These matrices and the joint deflection matrix $\underline{X}$ are then used in "subroutine nonlinmc" to carry out the non-linear M-C analysis. The program is terminated after the control returns to the master segment.

6 - For I2 = -5 the program has the facility of carrying out an iterative design. This is done by entering the subroutine design.

6.a.3 The Elastic-Plastic Analysis Block:

The flow diagram of this block is shown in figure (6.2). After entering the block, the elastic-plastic analysis procedure is initiated by cycling the possible hinge locations. The lowest load factor at which the next plastic hinge develops in the frame is calculated from equation (2.24). The member to which this hinge belongs is singled out. The actual member forces and deflections are calculated by multiplying those due to working loads by the predicted load factor (block 2 of the flow diagram). The variation factor for each row of the matrix $\underline{M}$ is calculated from equation (2.15) in block 3. These factors are then used to modify the matrices $\underline{M}$, $\underline{P}$ and $\underline{X}$ to obtain the bending moments, axial forces and deflections of the frame with the new hinge due to the working loads and unit load cases by means of equations (2.16) and (2.17).
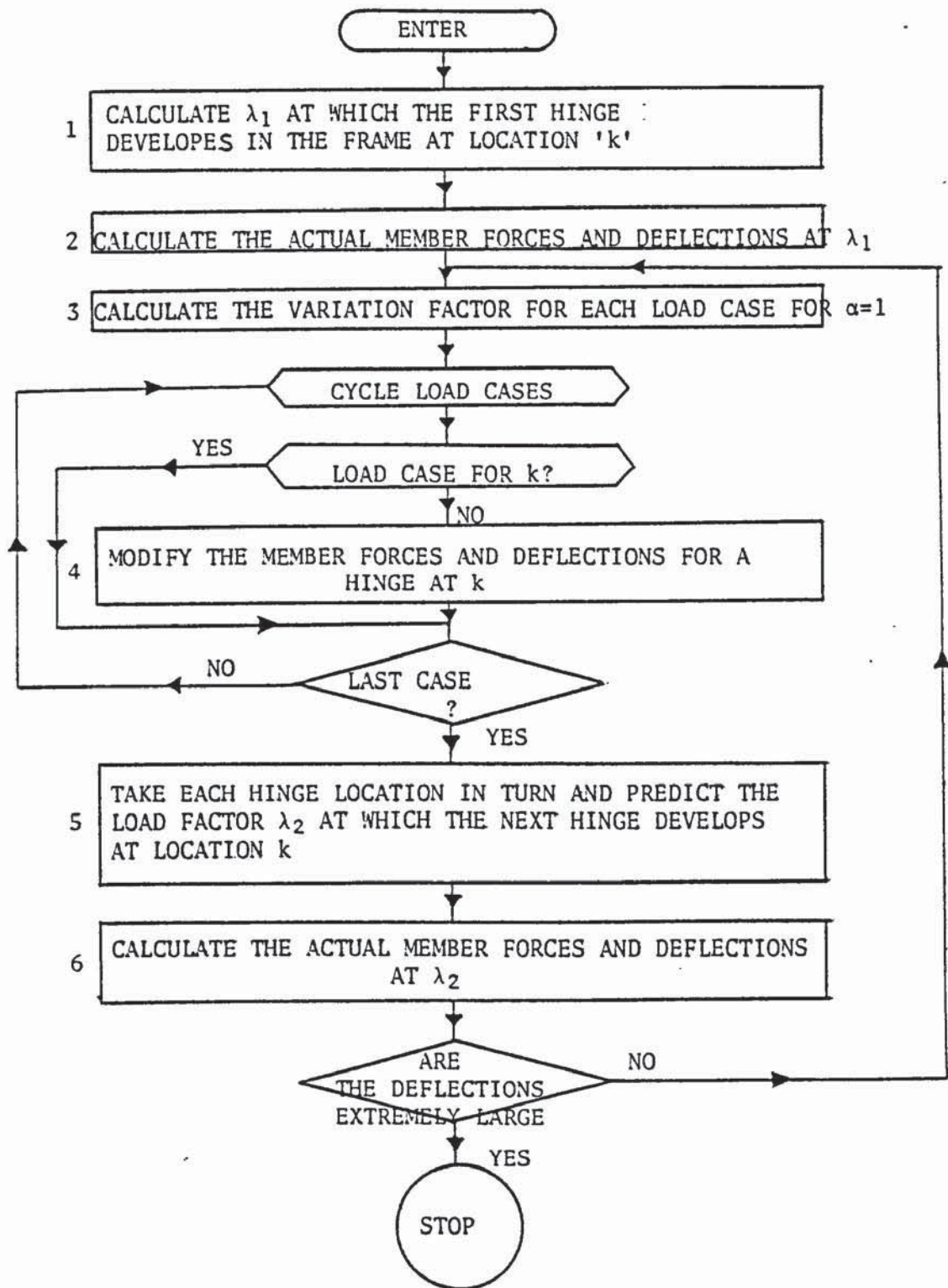
FIGURE 6.2   FLOW DIAGRAM OF THE ELASTIC-PLASTIC ANALYSIS BLOCK

Having inserted the new plastic hinge into the frame, the search is continued for the next plastic hinge. Each of the remaining locations at which a hinge has not yet developed, is considered in turn. The load factor for which a plastic hinge may develop in a location is calculated from equation (2.27). The critical location which gives the lowest load factor is singled out.

The actual member forces and deflections at this predicted load factor are calculated from equations (2.26). The control is then transferred back to block 3 to insert the new hinge into the frame and proceed further.

The whole process is continued until a sufficient number of plastic hinges develop in the frame to form a mechanism. Once this is reached, the displacements become extremely large and an overflow is recorded. If this is not reached, the program stops when the number of hinges becomes equal to the maximum permissible given in the data.

6.a.4 The Subroutine Nonlinmc:

The main function of this subroutine is to carry out a nonlinear moment-curvature analysis of the given frame. The moment-curvature diagrams of the members are presented as a series of successive linear portions. It makes use of the procedure given in the first part of chapter 3. As a special case, the program is also capable of carrying out strain hardening analysis, which is an extension of the elastic-plastic analysis procedure given in chapter 2. It takes into account the effect of strain hardening of the fully yielded sections including the spread of plasticity away from the initial hinge location.
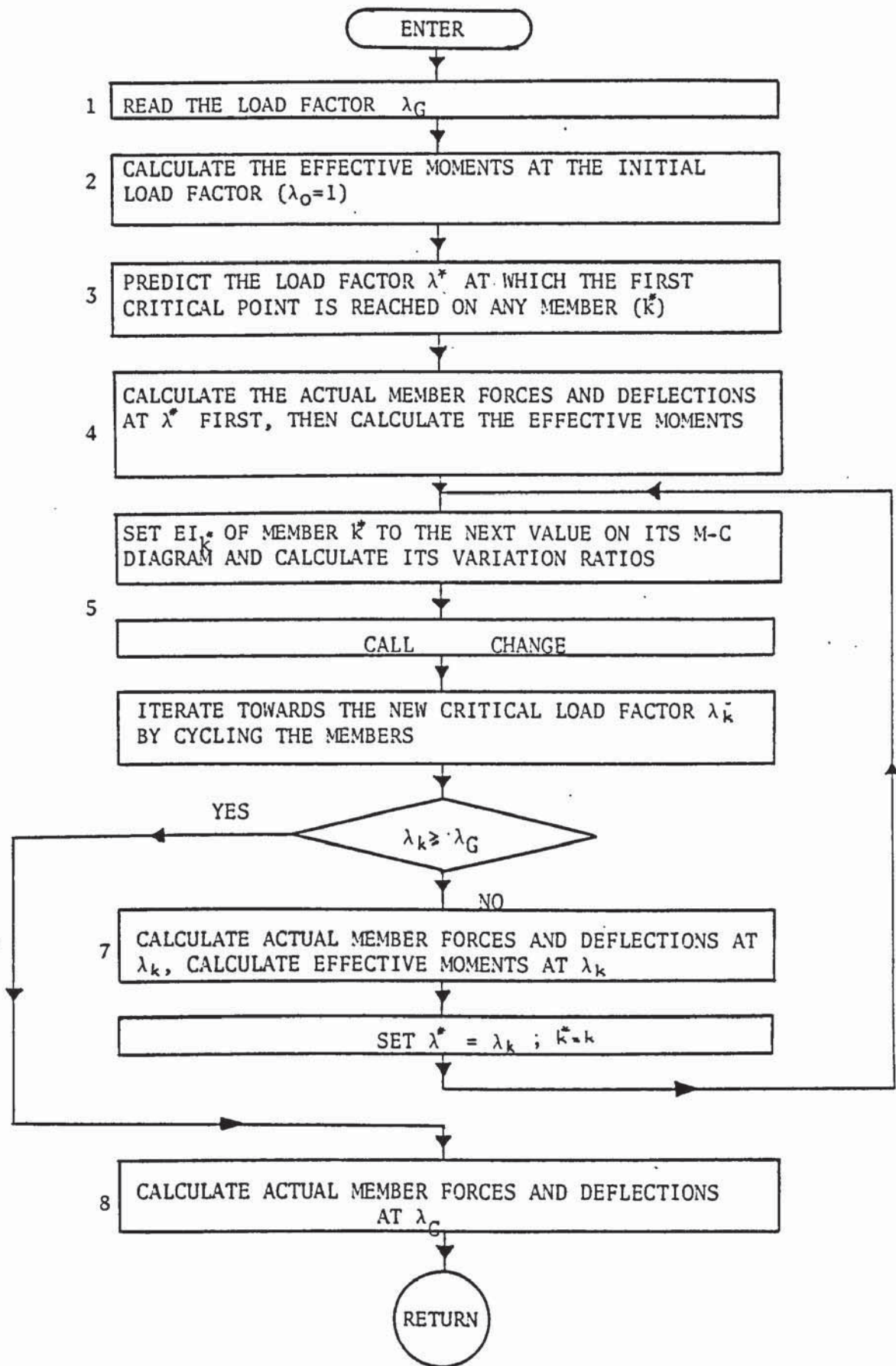
FIGURE 6.3 FLOW DIAGRAM OF SUBROUTINE NONLINMC

The flow diagram of this subroutine is given in figure (6.3). Its execution starts by reading the maximum load factor at which the analysis is to be terminated. If a failure load analysis is required, this load factor is set to a large number, (Block 1 of the flow diagram).

The initial effective moments are calculated from the bending moments at the initial load factor which is generally taken as unity (Block 2).

In block 3 each member is considered in turn. The load factor at which the next critical point is reached on the M-C diagram is calculated from equation (3.3). The lowest of these, λ^* is chosen. The member forces, the deflections and the effective moments due to the working loads are multiplied by the predicted load factor λ^* to obtain their up to date values.

The flexural rigidity of the critical member, k*, is then altered to the slope of the next transition region on its M-C diagram and the corresponding variation ratio is calculated from equation (2.3), (Block 5 of the flow diagram). This is to initiate the procedure of structural variation within the subroutine change and to obtain the member forces and deflections of the frame with the new flexural rigidity of the critical member, k*, due to the working loads and the unit load cases.

Once the new solution of the frame is obtained, the search is continued for the next critical point and the corresponding critical load factor. Again, each member is considered in turn and its critical load factor is calculated from equation (3.5). The member, which gives the lowest critical load factor, λ_k, is singled out.

This new predicted load factor λ_k is compared with the given load factor λ_G. If $\lambda_k < \lambda_G$, the actual member forces and deflections at λ_k are calculated from equation (2.26) and the effective moments from equation (3.4). The control is then transferred back to block 5 to alter the flexural rigidity of the present critical member and to continue searching for further critical points.

If on the other hand $\lambda_k \gtrless \lambda_G$ the actual member forces and deflections at λ_G are calculated, printed out and the program is terminated. For the failure load analysis, since λ_G is set to a large number, this condition can never be reached and the program is terminated when the deflections become extremely large and an overflow is recorded, indicating failure.

6.a.5 The Subroutine Change:

The member forces and the deflections of a parent frame are modified in this subroutine and the solution of one of its derivatives which is subject to the same loading is obtained. The derivative frame is obtained by changing or removing a member of the original frame. This is done by means of the theorems of structural variation[1,2] in the manner described by Saka[3]. All the operations are carried out within the matrices $\underline{M}$, $\underline{P}$ and $\underline{X}$ in a compact scheme and a considerable amount of computer storage is saved. The subroutine can be used for two different purposes given below.

1 - The second moment of area of a member, k, is altered while its area remains unchanged.

2 - Both the second moment of area and the area are changed by specified amounts or completely removed.
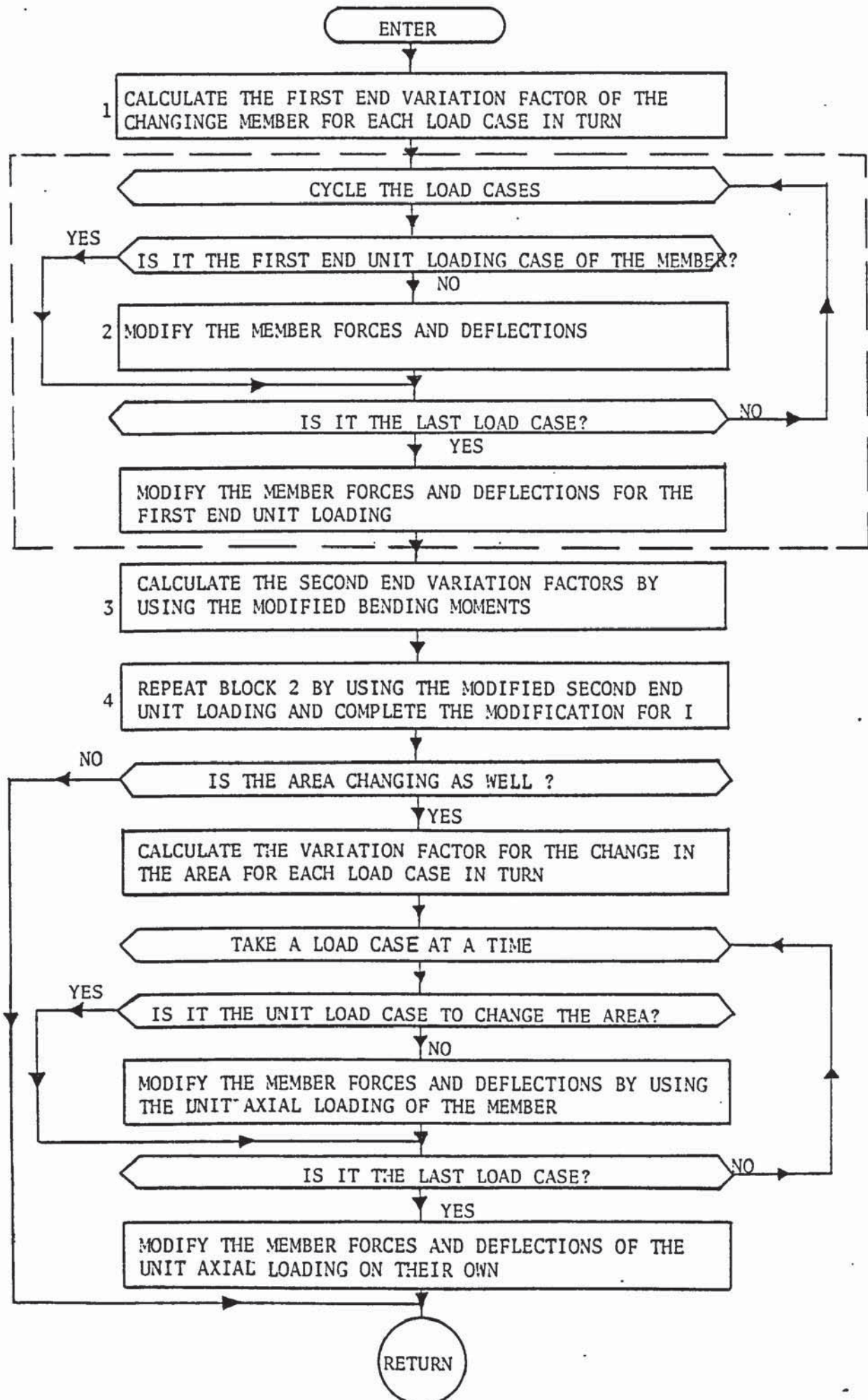
FIGURE 6:4   FLOW DIAGRAM OF THE SUBROUTINE CHANGE

The corresponding unit load matrices were previously discussed in the master segment of the program.

The flow diagram of this subroutine is given in figure (6.4). Its execution is commenced by calculating the first end variation factor of the second moment of area for each load case in turn (including the unit load cases), by means of equation (2.15). These factors are then used to modify the corresponding rows of the matrices $\underline{M}$, $\underline{P}$ and $\underline{X}$, by using equation (2.16). The bending moments, axial forces and the deflections due to the unit load case used in this modification lie on the $2k^{th}$ row of the matrices $\underline{M}$ and $\underline{P}$ and on the $2k^{th}$ column of matrix $\underline{X}$ for the first end unit load case. For the second end unit load case, the row or the column number is $2k-1$.

Once the modification of the member forces and deflections for the first end unit loading case is completed, the modified second end moments of the changing member due to each load case and due to its second end unit load case are used to calculate the second end variation factors. The matrices $\underline{M}$, $\underline{P}$ and $\underline{X}$ are remodified and the modification for the second moment of area is completed.

If the area of member k is also to be changed, the variation factor of area is calculated by using the axial forces in the member due to each load case and due to unit axial loads acting axially to the member, by means of equation (1.10). Again, equation (2.16) is used to complete the modification of the matrices $\underline{M}$, $\underline{P}$ and $\underline{X}$. These matrices now contain the member forces and deflections of the frame due to the working loads and all the unit load cases. This is either with member k removed or altered.

6.b.   A COMPUTER PROGRAM FOR THE FAILURE

      LOAD ANALYSIS OF COMPLETE STRUCTURES

6.b.1 Introduction:

As an application of the methods proposed in the second part of chapter 3, chapter 4 and chapter 5, a computer program for the nonlinear analysis of complete building structures up to and including failure was written in Fortran and run on the Aston I.C.L. 1904. The structures consist of slabs, shear walls and intermediate frames of any configuration, provided that they are arranged parallel to each other. The slabs may be made out of any homogeneous material or out of reinforced concrete. The frames can be made out of steel, reinforced concrete or any other material with a nonlinear stress-strain diagram (or a moment-curvature diagram). The program is arranged in such a way that the preparation of data is simple and its amount is as little as possible.

Considering the limitations of the available core store, the backing store facilities are used so that considerably large structures can be analysed. The magnetic tape facilities are preferred to the direct access files. This is to provide the facility of running the program on any other computer which has a fortran compiler.

The program consists of a main segment and five subroutines. Their functions will be described in the following sections and illustrated in the flow diagrams. Data preparation is also given in appendix 2.

```
                          ┌─────────────┐
                          │    BEGIN    │
                          └─────────────┘
                                 │
                                 ▼
   1 ┌───────────────────────────────────────────────────────┐
     │              READ THE GENERAL DATA                     │
     └───────────────────────────────────────────────────────┘
          NO                                          YES
       ◄───────< REINFORCED CONCRETE GRILLAGE? >────────►
       │                                                 │
       ▼                                                 ▼
   ┌────────────────────────────┐      ┌────────────────────────────┐
   │ READ THE CROSS-SECTIONAL   │      │ READ THE CROSS-SECTIONAL   │
 2 │ PROPERTIES AND CALCULATE   │      │ PROPERTIES AND CALCULATE   │
   │ THE LATERAL BUCKLING       │      │ $M_{ult}$, $M_{tult}$ AND  │
   │ PARAMETERS                 │      │ $S_{yult}$                 │
   └────────────────────────────┘      └────────────────────────────┘
       │                                                 │
       └────────────────►    ◄───────────────────────────┘
                                 │
                                 ▼
   3 ┌───────────────────────────────────────────────────────┐
     │              READ THE GRILLAGE DATA                    │
     └───────────────────────────────────────────────────────┘
                                 │
                                 ▼
     ┌───────────────────────────────────────────────────────┐
     │        PRINT THE GENERAL AND GRILLAGE DATA             │
     └───────────────────────────────────────────────────────┘
                                 │
                                 ▼
   4 ┌───────────────────────────────────────────────────────┐
     │                    CALL GRILL                          │
     │ CONSTRUCT $\underline{G}$, $\underline{a}$, $[\underline{G}\ P + \underline{a}]$ AND STORE $\underline{K}_G$ │
     └───────────────────────────────────────────────────────┘
                                 │
                                 ▼
   5 ┌───────────────────────────────────────────────────────┐
     │  READ THE GENERAL AND CROSS-SECTION DATA FOR FRAMES    │
     └───────────────────────────────────────────────────────┘
          NO
       ◄───────< REINFORCED CONC. FRAMES? >
       │                          │ YES
       │                          ▼
   6   │     ┌─────────────────────────────────────────────┐
       │     │       READ THE DATA FOR M-C DIAGRAMS         │
       │     └─────────────────────────────────────────────┘
       │                          │
       └────►    ◄─────< CYCLE FRAMES >
                                  │
                                  ▼
   7 ┌───────────────────────────────────────────────────────┐
     │            READ MEMBER AND LOAD DATA                   │
     └───────────────────────────────────────────────────────┘
                                  │
                                  ▼
   8 ┌───────────────────────────────────────────────────────┐
     │       CONSTRUCT THE ADDRESS SEQUENCE ARRAY             │
     └───────────────────────────────────────────────────────┘
                                  │
                                  ▼
   9 ┌───────────────────────────────────────────────────────┐
     │           SET THE MEMBER FORCES TO ZERO               │
     └───────────────────────────────────────────────────────┘
          NO                     │
       ◄───────<   LAST FRAME?   >
                                  │ YES
                                  ▼
                ◄─────< CYCLE FRAMES >
                                  │
                                  ▼
  10 ┌───────────────────────────────────────────────────────┐
     │          CONSTRUCT THE UNIT LOAD MATRIX                │
     └───────────────────────────────────────────────────────┘
                                  │
                                  ▼
  11 ┌───────────────────────────────────────────────────────┐
     │                  CALL STIFFMAT                         │
     │ AND CALCULATE THE CONTRIBUTIONS TO MATRIX $\underline{F}$ │
     └───────────────────────────────────────────────────────┘
          NO                     │
       ◄───────<   LAST FRAME?   >
                                  │ YES
                                  ▼
  12 ┌───────────────────────────────────────────────────────┐
     │                  CALL COMPACTDIV                       │
     │ SOLVE $(\underline{G}+\underline{F})\underline{f}=(\underline{G}\ P + \underline{a})$ for $\underline{f}$ AND EVALUATE │
     │ $\underline{g}$ FROM $\underline{g} = \underline{p}-\underline{f}$ │
     └───────────────────────────────────────────────────────┘
                                  │
                                  ▼
  13 ┌───────────────────────────────────────────────────────┐
     │   CALCULATE THE LOAD MATRIX FOR EACH FRAME AT $\lambda_o$ │
     └───────────────────────────────────────────────────────┘
                                  │
                                  ▼
                              ┌───────┐
                              │   A   │
                              └───────┘
```

CONTINUED

FIGURE 6.5   FLOW DIAGRAM OF THE MAIN SEGMENT
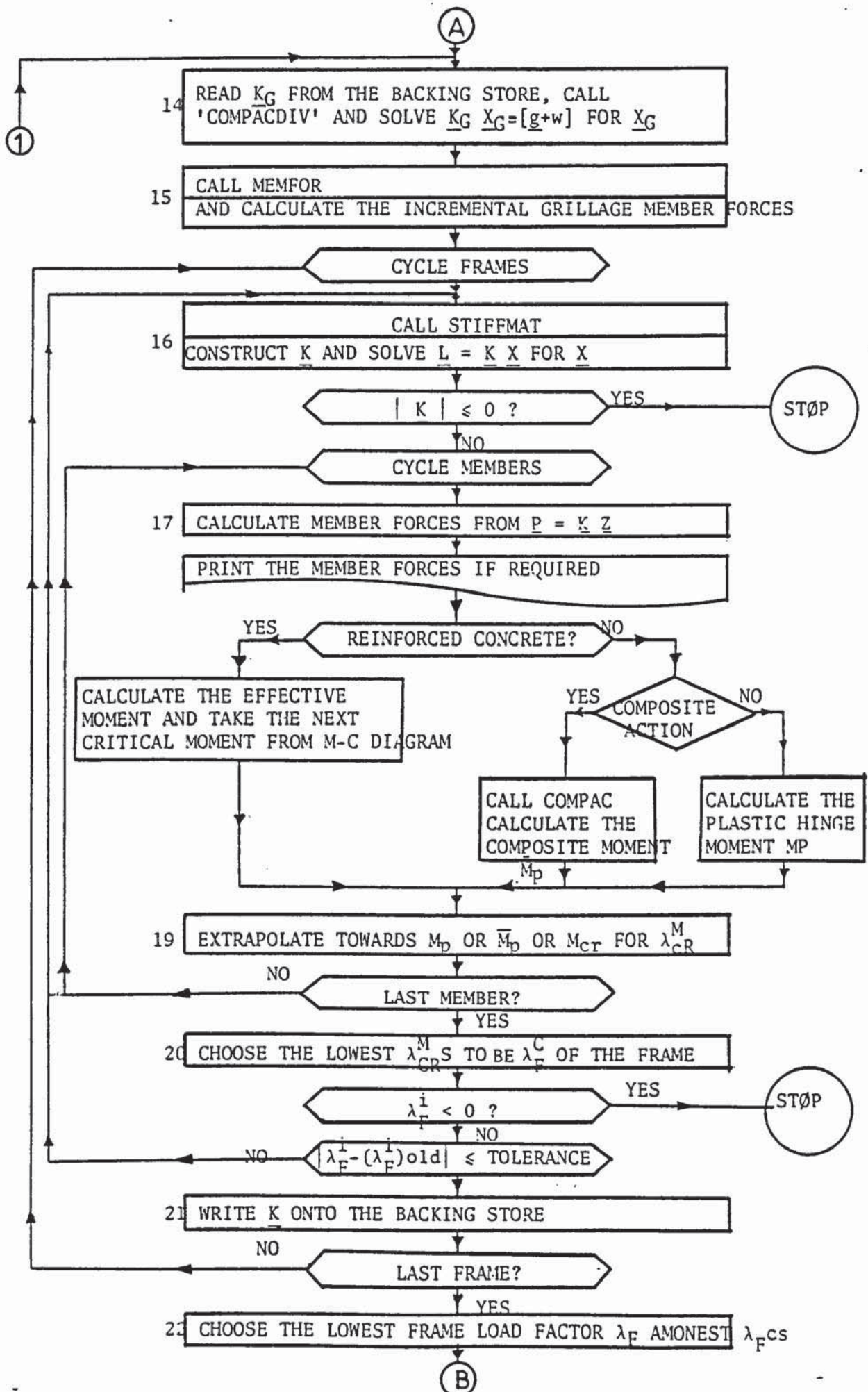
FIGURE 6.5 CONTINUED   FLOW DIAGRAM OF THE MAIN SEGMENT

Ⓑ

23 — CALL CHECK
TO CALCULATE THE LOWEST GRILLAGE LOAD FACTOR λ_G

$\lambda_F < \lambda_G$? —YES / NO

24 — $\lambda_{cr} = \lambda_F$ $\lambda_{cr} = \lambda_G$

25 — CALCULATE GRILLAGE FORCES AND DEFLECTIONS AT λ_{cr}

$\lambda_G > \lambda_{cr}$? —YES / NO

26 — SET THE EI AND GJ OF MEMBER k TO THE NEXT VALUE ON M-C curve

27 — CALL GRILL
CONSTRUCT AND STORE $\underline{K}_G$, $\underline{G}_n$, $\underline{a}_n$ AND $\underline{G}_n P + \underline{a}_n$

28 — CALCULATE THE LOADS ACTING ON THE FRAMES AT λ_{cr}

CYCLE   FRAMES

29 — READ $\underline{K}_F$ OF THE FRAME FROM THE BACKING STORE

$\lambda_F^i - \lambda_{cr} \leq$ TOLERANCE? —NO / YES

REINFORCED CONCRETE —YES / NO

30 — CHANGE THE EI OF THE CRITICAL MEMBER, CALCULATE THE VAR. RATIO

32 — CHECK HINGE ROTATIONS, CALCULATE $[-\underline{K}_{1h}\theta_h]$ FOR EVERY INACTIVE HINGE AND ADD IT TO THE LOAD MATRIX

31 — CALCULATE THE NEW COMPENSATING LOADS, ADD THEM TO THE LOAD MATRIX AND SUBTRACT THE OLD ONES

33 — INSERT A HINGE INTO THE FRAME

34 — CALCULATE THE MEMBER FORCES AND DEFLECTIONS AT λ_{cr} BY EXTRAPOLATION

35 — CONSTRUCT THE UNIT LOAD MATRIX

36 — CALL STIFFMAT, CALCULATE CONTRIBUTIONS TO $\underline{F}_n$

LAST FRAME? —NO

37 — CONSTRUCT $[\underline{G}_n + \underline{F}_n]$, CALL COMPACDIV AND SOLVE $[\underline{G}_n + \underline{F}_n]\underline{f}_n = [\underline{G}_n P + \underline{a}]$, THEN EVALUATE $\underline{g}_n = P - \underline{f}_n$

38 — SET $\lambda_{cr}^n = \lambda_{cr} + $ INCR. FO R THE NEXT CYCLE, CALCULATE THE FRAME LOADS AT λ_{cr}^n
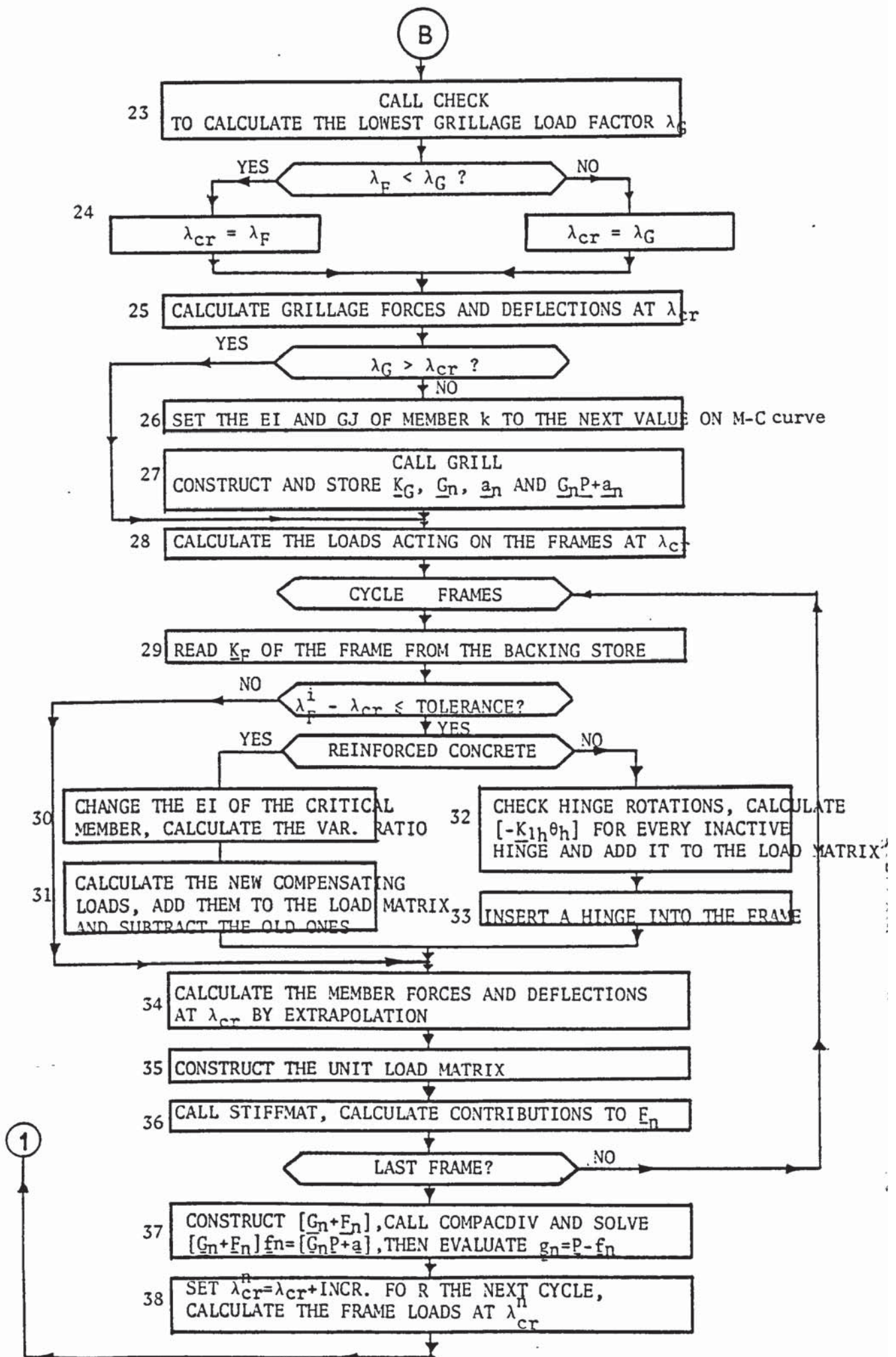
①

FIGURE 6.5 CONTINUED   FLOW DIAGRAM OF THE MAIN SEGMENT

6.b.2 Description of the Program:

After feeding the general and the grillage data, the execution of the program is commenced. The flexural rigidity array of the grillage members is filled with the initial EI values given by their M-C diagrams. Other auxiliary arrays are also constructed.

The "subroutine grill" is called to construct the initial stiffness matrix K_G of the grillage. The initial influence coefficient matrix $\underline{G}$ of the grillage and the column vector $(\underline{G}\ \underline{P} + a)$ of equation (4.2) are constructed. Matrix $\underline{G}$ is of order $(mxn)^2$ and the vector $(\underline{G}\ \underline{P} + \underline{a})$ contains (mxn) elements. Here m is the total number of frames and n is the total number of floors. These matrices are placed in the backing store for subsequent use. (block 4 of figure (6.5)).

Having constructed the above matrices the necessary arrays for the analysis of each frame are constructed. These include the lowest nonzero joints connected to each joint; the address sequence array which contains the number of elements on the leading diagonal of the stiffness matrix for each frame; the total number of plastic hinges which can possibly form in the vicinity of each joint in a steel frame.

The frame influence coefficient matrix $\underline{F}$ and therefore the matrix $(\underline{G} + \underline{F})$ of equation (4.2) is constructed in the following manner.

Each frame is considered in turn and a corresponding unit load matrix is constructed. Each column of this matrix contains entirely zero elements except a unit horizontal load at the lowest joint number at each floor level. The total number of columns is thus equal to the number of floors. The subroutine stiffmat is

called to construct and solve the equations $\underline{F} = \underline{K}^{-1} \underline{L}$. The resulting horizontal deflection of the joint with the lowest number at each floor level is the contribution of that floor to matrix F. This matrix has the same dimensions as matrix $\underline{G}$. Its non zero elements are those contributed by the frames. These elements are added to the elements in the corresponding locations of matrix $\underline{G}$ and the construction of (G + F) is completed, (block 10 of figure(6.5)).

It is well known from the reciprocal theorem that matrices $\underline{G}$ and $\underline{F}$ are both symmetrical. Because of this, matrix $[\underline{G} + \underline{F}]$ is also symmetrical. This nature makes it possible to employ the technique given by Jennings[72] to solve the influence coefficient equation (4.2). To do this half of matrix $[\underline{G} + \underline{F}]$ is stored in a one dimensional array and the address sequence array for the diagonal elements is constructed. The subroutine compacdiv[20] which uses the technique of Jennings is called. As a result of these operations the horizontal loads $\underline{f}$ transmitted to the frames are calculated. The loads transmitted to the grillage are then calculated from equation (4.1) (block 11 of figure (6.5)). The total loads acting on each frame are then calculated from equation (4.5).

Once the horizontal loads transmitted to the grillage and to the frames are calculated, each of these are treated separately under their own share of loads.

For the analysis of the grillage, the loads $\underline{w}$, acting on the shear walls, are picked from the backing store and added to matrix $\underline{g}$ and the load matrix of the grillage under the working loads is constructed. The stiffnes matrix $\underline{K}_G$ of the grillage has

already been constructed and stored in a form suitable for the subroutine compacdiv to solve the equations $\underline{L}_G = \underline{K}_G \, \underline{X}_G$ for the unknown deflections $\underline{X}_G$. These deflections are then used to calculate the member forces of the grillage within the subroutine ˙memfo r˙ (blocks 13 and 14 of figure (6.5)).

Each frame is taken in turn. The member forces are set to zero. The iteration process is then started either towards the first critical point or towards the first plastic hinge. With zero axial forces, the stiffness matrix of a frame is constructed and the joint equilibrium equations are solved for the joint displacements $\underline{X}$, within the subroutine stiffmat. Before leaving this stage the determinant of the stiffness matrix is checked. If it is zero the program is terminated, indicating the failure of the frame and thus the local failure of the complete structure. Otherwise, the resulting displacements are used to calculate the new member forces. For steel frames, the member forces are calculated in the usual manner. For reinforced concrete frames, the member forces due to the compensating loads for each member which became critical previously are added to the appropriate member forces calculated in the usual manner.

The iteration process towards the next critical load factor is basically similar for the cases of reinforced concrete and steel frames. However the following operations appear to be different.

i - Reinforced concrete frames: An equivalent moment is calculated from equation (3.2) and the next critical point is chosen on the M-C diagram of the member to iterate towards.

ii - Steel frames: It is first tested whether composite action

is to be considered between each member and slabs. If so, the composite moment is calculated[33].

Otherwise the value of the reduced plastic hinge moment of the section is calculated by using the updated axial load in the member.

The procedure described by Majid and Anderson[20] is then utilised to predict the load factor λ_F^i at which a plastic hinge will form in a steel frame, or a critical point will be reached in a reinforced concrete frame.

The value of the predicted load factor λ_F^i is

$$\lambda_F^i = \lambda_1 + \frac{(\lambda_2 - \lambda_1)\ (M'_{p1} - m_1)}{M'_{p1} - M'_{p2} + m_2 - m_1} \qquad 6.1$$

Where M'_{p1} and M'_{p2} are the reduced plastic moments of the section of a member at previous and current iterations. λ_1, m_1 and λ_2, m_2 are the load parameters and the bending moments at the previous and current iterations respectively. For the case of reinforced concrete frames, the plastic hinge moments M'_{p1} and M'_{p2} are replaced by the critical moment M^N_{cr} of the member. m_1 and m_2 are also replaced by the effective moments M^E_1 and M^E_2 of the member for previous and current iterations. Equation (6.1) thus becomes:

$$\lambda_F^i = \lambda_1 + (\lambda_2 - \lambda_1)(M^N_{cr} - M^E_1)/(M^E_2 - M^E_1) \qquad 6.2$$

The predicted load factor λ_F^i is compared with the current load factor λ_2. If they are within a specified tolerance the iteration is terminated. This indicates that a plastic hinge can be inserted into the steel frame or a critical point is reached in the reinforced concrete frame. Otherwise, the old load factor is replaced by the current one, while the current load factor is replaced by the predicted one. The current axial loads are also

replaced by the predicted ones and a further iteration is started. The actual loads acting on the frame at λ_F^i are calculated from equation (4.5). The stability functions $\phi_2 - \phi_5$ are calculated using the new axial loads. The overall stiffness matrix is constructed once again and the stiffness equations are solved for the new joint displacements. The iteration process is continued until the tolerance test is satisifed. Having predicted the critical load factor of the frame, the member forces, the joint deflections and the stiffness matrix are stored for further use and printed if required.

The above procedure is carried out for each frame in turn. The location of the expected plastic hinge or the critical member is printed out together with the predicted load factor. After each frame is analysed, the critical load factors are compared to each other and the smallest among them is chosen. This is the critical load factor λ_{FL} for all the frames (block 22 of figure (6.5)).

Subroutine check is then called to predict the critical load factor λ_G of the grillage. At this load factor, a critical point is reached on the M-C diagram of one of the panels.

The lower of λ_{FL} and λ_G is the next critical load factor λ_{cr} for the whole structure (block 24 of figure (6.1)). At λ_{cr}, the member forces and the deflections of the grillage are calculated from equation (5.g.1).

For $\lambda_G = \lambda_{cr}$, the EI and GJ values of the critical panel in the grillage, are replaced by those given by the next portion of the M-C diagram. If the panel fails completely, its EI and GJ values are set to a very small value and the panel is practically disregarded (block 27 of figure (6.5)). Subroutine grill is then

called and the new matrices $\underline{K}_G, \underline{a}_n, \underline{G}_n$ and $(\underline{G}_n\underline{P} + \underline{a}_n)$ are constructed and stored for further use.

The loads acting on each frame at λ_{cr} are calculated and stored for further use. Each frame is considered in turn. λ_{cr} is compared with the load factor of the frame. If they are within the stipulated tolerance , the following operations are carried out depending on the material of the frames:

i - For a reinforced concrete frame, the flexural rigidity of its critical member is set to the slope of the next transition region of its M-C diagram. The corresponding variation ratio is calculated from equation (3.23). The new compensating loads are calculated from equation (2.10) and added to the load matrix of the frame while the old ones are subtracted.

ii - For a steel frame, the hinge rotations are checked and the contribution - $[\underline{k}_{1h} \theta_h]$, (where $\underline{k}_{1h}$ is the column of the stiffness matrix which corresponds to the inactive hinge h and θ_h is the rotation of that hinge), is calculated for every hinge which has just become inactive, and added to the load matrix of the frame.

The new plastic hinge is then inserted into the frame and the plastic hinge moment is included in the load matrix of the frame.

A new hinge in a steel frame or the reduction of the flexural rigidity of a member in a reinforced concrete frame alters the relative stiffness of the frames and therefore the influence coefficient matrix $\underline{F}$ is altered. This matrix also changes when the axial forces in the members are increased. The member forces at λ_{cr} are calculated by multiplying their values at λ_F^i by the ratio of λ_{cr}/λ_F^i. Here λ_F^i is the predicted critical load factor

of the frame. The stiffness matrix of the frame is constructed

taking the axial loads into consideration. The inverse transformation

$\underline{F} = \underline{K}^{-1} \underline{L}$ is carried out to calculate the contributions of the

frame to the new influence coefficient matrix $\underline{F}_n$.

If $\lambda_{cr} = \lambda_G$, the matrix $[\underline{G}_n + \underline{F}_n]$, otherwise $[\underline{G} + \underline{F}_n]$, is

constructed. Matrix $\underline{G}$ is the previously constructed grillage

influence coefficient matrix while $\underline{G}_n$ is new, constructed at

$\lambda_{cr} = \lambda_G$ (block 37 of figure (6.5)).

The influence coefficient equations are now solved to

preserve the compatibility at the frame - slab junctions. The

new parts of the external loads $\underline{f}_n$ and $\underline{g}_n$ transmitted to the

frames and grillage for a unit increment in the overall load

factor, are calculated.

The overall load factor is increased by a small amount such

as 0.1 to prepare for the next cycle of analysis, the loads

acting on the frames at the new load factor are calculated and the

next cycle of iteration is initiated by transferring the control

back to block 13.

6.b.3 The Subroutine Stiffmat:

This subroutine was originally developed in atlas autocode

by Majid and Anderson[20] to construct the stiffness matrix of a

plane frame. It was later modified by Önen[32] to allow for the

analysis of complete building structures. For the present

program it was translated into "FORTRAN" and modified to be used

in the construction of the stiffness matrix of a grillage and to

allow for the analysis of reinforced concrete frames. The flow

diagram for this subroutine is shown in figure 6.6.

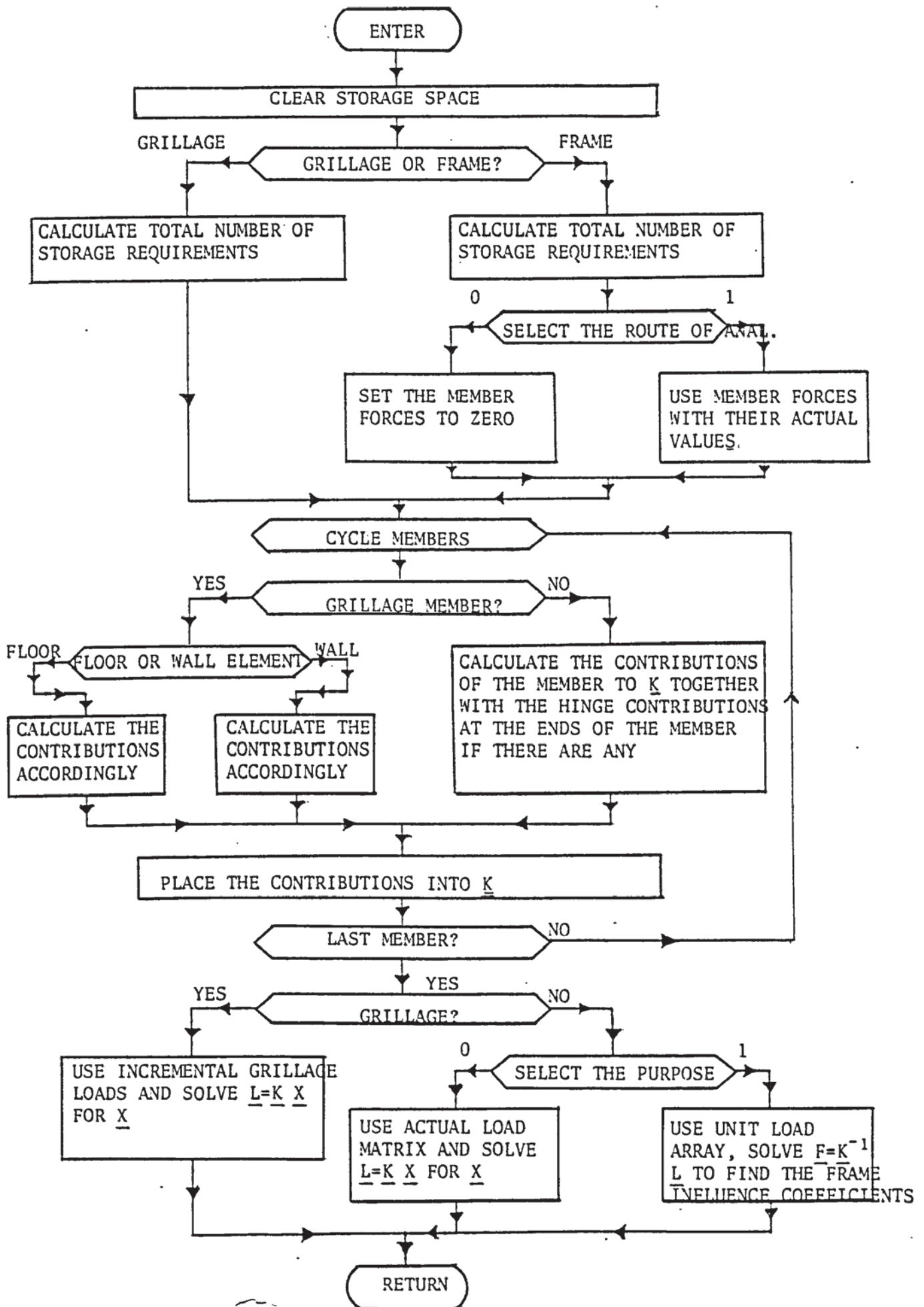Each joint of the grillage is assumed to have three degrees

FIGURE 6.6 FLOW DIAGRAM OF SUBROUTINE STIFFMAT

of freedom in Z, θ_x and θ_y directions while the linear deformations along x,y and the rotation about z axis are neglected (see figure (4.1)). Thus the problem becomes analogous to that of a plane frame. The storage requirements are calculated in the same way as for plane frames. The contributions of a panel to the overall stiffness matrix are calculated directly by considering, whether it is a wall element or a slab element, as given by Croxton[67]. The triple multiplication $\underline{A}'$ $\underline{k}$ $\underline{A}$ is avoided thus reducing the computer time. Because each joint of the grillage has three degrees of freedom the usual procedure[20] of constructing the stiffness matrix remains unaltered. The process for reinforced concrete frames is similar to that for steel frames, except for the fact that hinges do not occur.

6.b.4 The Subroutine Compacdiv:

This subroutine is in the form as it was originally developed by Majid[28] in atlas autocode. However it is translated into FORTRAN and slightly modified to cope with more than one load case.

6.b.5 Subroutine Grill:

In this subroutine, the load matrix $\underline{L}_G^u$ and the stiffness matrix $\underline{K}_G$ of grillage are constructed, the inverse transformation $[\underline{a}\ \underline{G}] = \underline{K}_G^{-1}\ [\underline{w}\ \underline{L}_G^u]$ is carried out. This transformation yields the vector $\underline{a}$ and grillage influence coefficient matrix $\underline{G}$ of equation (4.2). $\underline{a}$ contains the horizontal deflections of the grillage at the frame-slab junctions due to the action of all the wind forces $\underline{w}$ on the shear walls. The column vector $\underline{a}$ and matrix $\underline{G}$ are then used to construct the vector $[\underline{G}\ \underline{P} + \underline{a}]$ of equation (4.2). Here $\underline{P}$ is the horizontal load vector acting on frame-slab junctions. The limited storage capacity of the computer in use is taken into
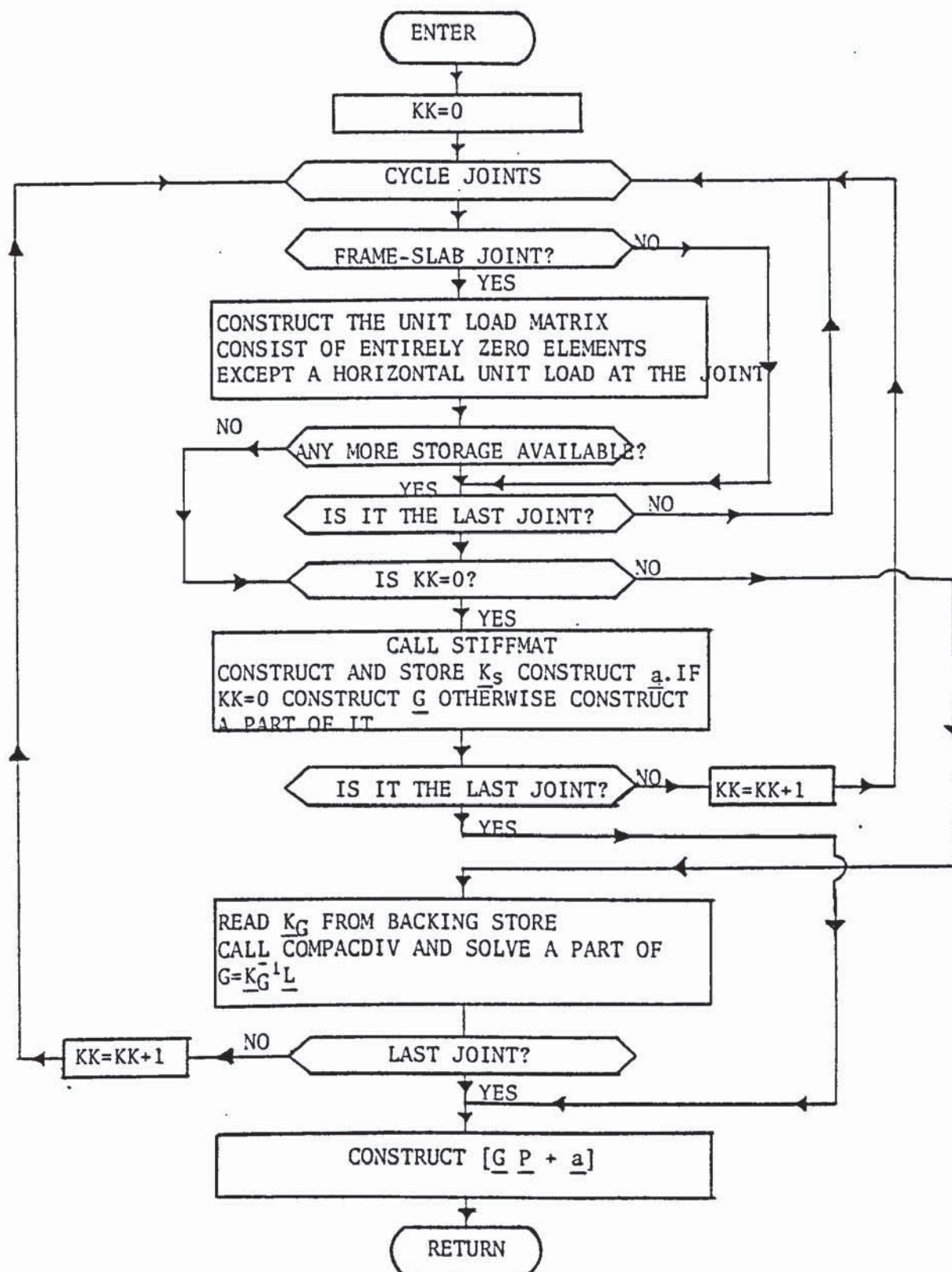
FIGURE 6.7   FLOW DIAGRAM FOR SUBROUTINE GRILL

account and the process is arranged in such a way that the inverse transformation is carried out step by step to confine itself within the allowed storage.

To begin with, the step counter kk is set to zero. The first column of the combined load matrix $[\underline{w}\ \underline{L}_G^u]$ is filled with the wall loads, picked from the backing store. Then every frame-slab joint is considered in turn and a column vector is constructed for this joint. This vector consists of zero elements except for a unit horizontal load acting on that joint. Before considering the next joint, the number of column vectors constructed so far, are compared with the maximum number of columns which can be stored. If the available store is exhausted and the step counter kk is zero, the subroutine stiffmat is called to construct $\underline{K}_G$. The joint equilibrium equations are solved for the first part of the load matrix. This yields the joint displacements of the grillage. The horizontal displacements of frame-slab junctions are collected and vector $\underline{a}$ is constructed. These displacements for each unit load matrix are also collected and the corresponding column of matrix $\underline{G}$ is constructed. The matrix $\underline{K}_G$ and the vector $\underline{a}$ are put into the backing store for future use.

If all the frame-slab junctions are not yet considered, the step counter is increased by one and the storage is cleared to construct the next part (kkth part) of matrix $\underline{L}_G^u$. After the kkth part of $\underline{L}_G^u$ has been constructed, the stiffness matrix $\underline{K}_G$ formed and stored in the backing store earlier, is brought into core and the joint equilibrium equations are solved for the current part of $\underline{L}_G^u$ and the corresponding horizontal displacements are placed in matrix $\underline{G}$. The step counter, kk, is again increased by one and
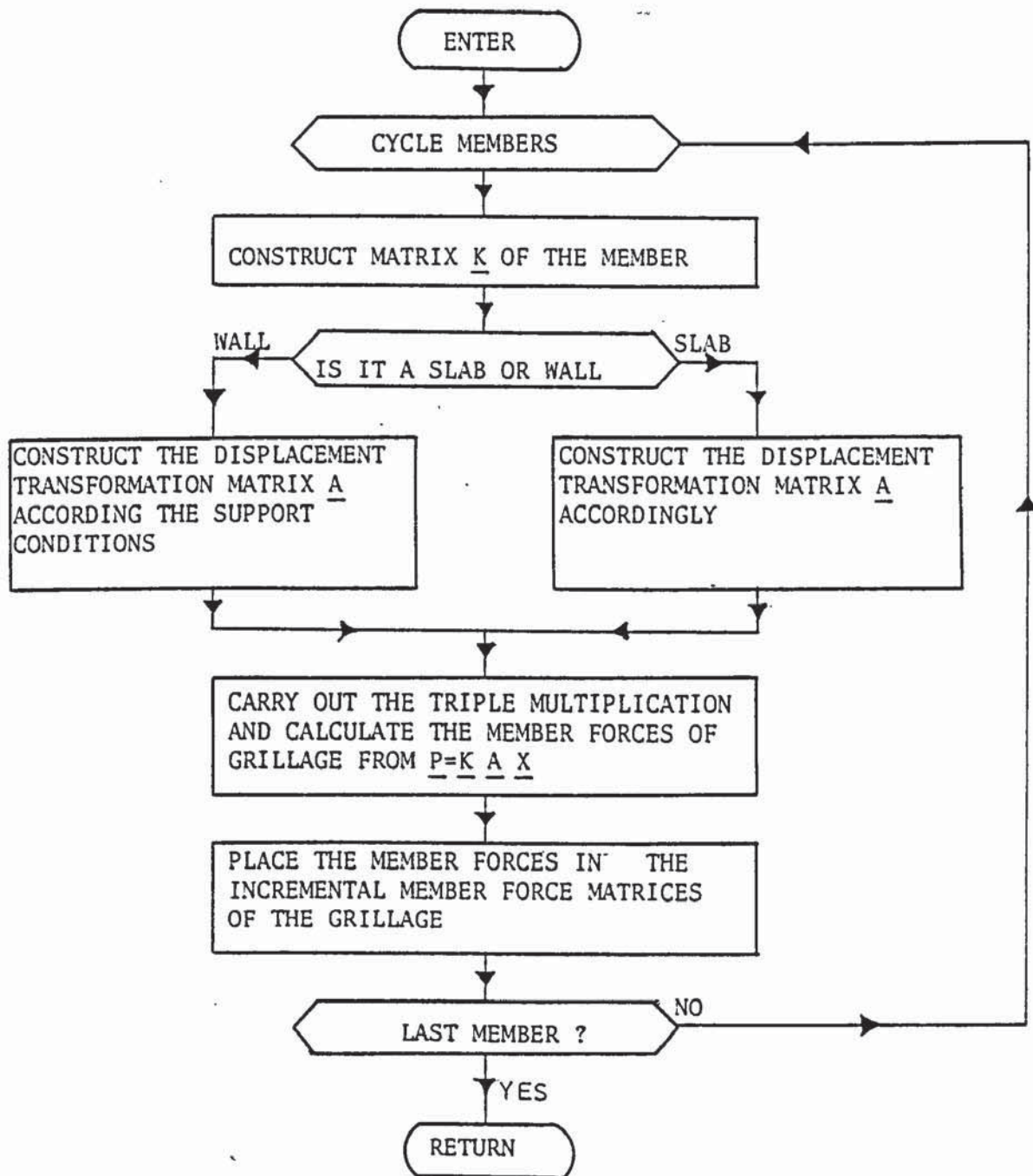
```
                    ┌─────────────┐
                    │    ENTER    │
                    └──────┬──────┘
                           ▼
           ◄──────────────────────────────────►◄──────────────────┐
           │         CYCLE MEMBERS             │                   │
           └──────────────────┬───────────────┘                   │
                              ▼                                    │
        ┌──────────────────────────────────────────┐              │
        │  CONSTRUCT MATRIX K OF THE MEMBER         │              │
        └──────────────────┬───────────────────────┘              │
                           ▼                                       │
   WALL ◄──────────────────────────────────────► SLAB             │
        │         IS IT A SLAB OR WALL          │                 │
        │                                        │                │
        ▼                                        ▼                │
┌────────────────────────┐          ┌────────────────────────┐    │
│ CONSTRUCT THE DISPLACE-│          │ CONSTRUCT THE DISPLACE-│    │
│ MENT TRANSFORMATION    │          │ MENT TRANSFORMATION    │    │
│ MATRIX A ACCORDING THE │          │ MATRIX A ACCORDINGLY   │    │
│ SUPPORT CONDITIONS     │          │                        │    │
└───────────┬────────────┘          └───────────┬────────────┘    │
            └──────────────────┬────────────────┘                 │
                               ▼                                   │
        ┌──────────────────────────────────────────┐              │
        │ CARRY OUT THE TRIPLE MULTIPLICATION       │              │
        │ AND CALCULATE THE MEMBER FORCES OF        │              │
        │ GRILLAGE FROM P=K A X                     │              │
        └──────────────────┬───────────────────────┘              │
                           ▼                                       │
        ┌──────────────────────────────────────────┐              │
        │ PLACE THE MEMBER FORCES IN  THE           │              │
        │ INCREMENTAL MEMBER FORCE MATRICES         │              │
        │ OF THE GRILLAGE                           │              │
        └──────────────────┬───────────────────────┘              │
                           ▼                              NO        │
           ◄──────────────────────────────────►──────────────────┘
           │          LAST MEMBER ?            │
           └──────────────────┬───────────────┘
                              ▼ YES
                    ┌─────────────┐
                    │   RETURN    │
                    └─────────────┘
```

FIGURE 6.8   FLOW DIAGRAM OF SUBROUTINE MEMFOR

the process is repeated until all the frame-slab junctions have been considered.

Having constructed vector $\underline{a}$ and matrix $\underline{G}$, the column vector $[\underline{G}\ \underline{P} + \underline{a}]$ is formed and control is transferred to the main segment. The flow diagram of this subroutine is presented in figure (6.7).

6.b.6 Subroutine Memfor:

This subroutine calculates the member forces of the grillage by using the incremental joint displacements X_G^i obtained from the joint equilibrium equations $[\underline{w} + \underline{g}] = K_G X_G^i$. Its flow diagram is given in figure (6.8).

Each member of the grillage is considered in turn, and the matrix $[k\ \underline{A}]$ is constructed directly according to whether the member is a wall element or a slab element. Then the member forces are obtained by multiplying this matrix by the vector of the displacements of the joints at which the member is connected. The resulting member forces are then placed in the incremental member force array of the grillage.

6.b.7 The Subroutine Check:

In this subroutine, the load factor, at which a critical point is reached in any member of the grillage is predicted together with the critical member itself. Its flow diagram is presented in figure (6.9). Two different paths are followed depending upon the material used, which may be reinforced concrete or a homogeneous brittle material.

After entering the subroutine, the incremental load factor $\Delta\lambda_G$ is set to a large figure such as 100. Each member is then considered in turn. The first check is to find out whether the member is made out of a homogeneous material or reinforced concrete.
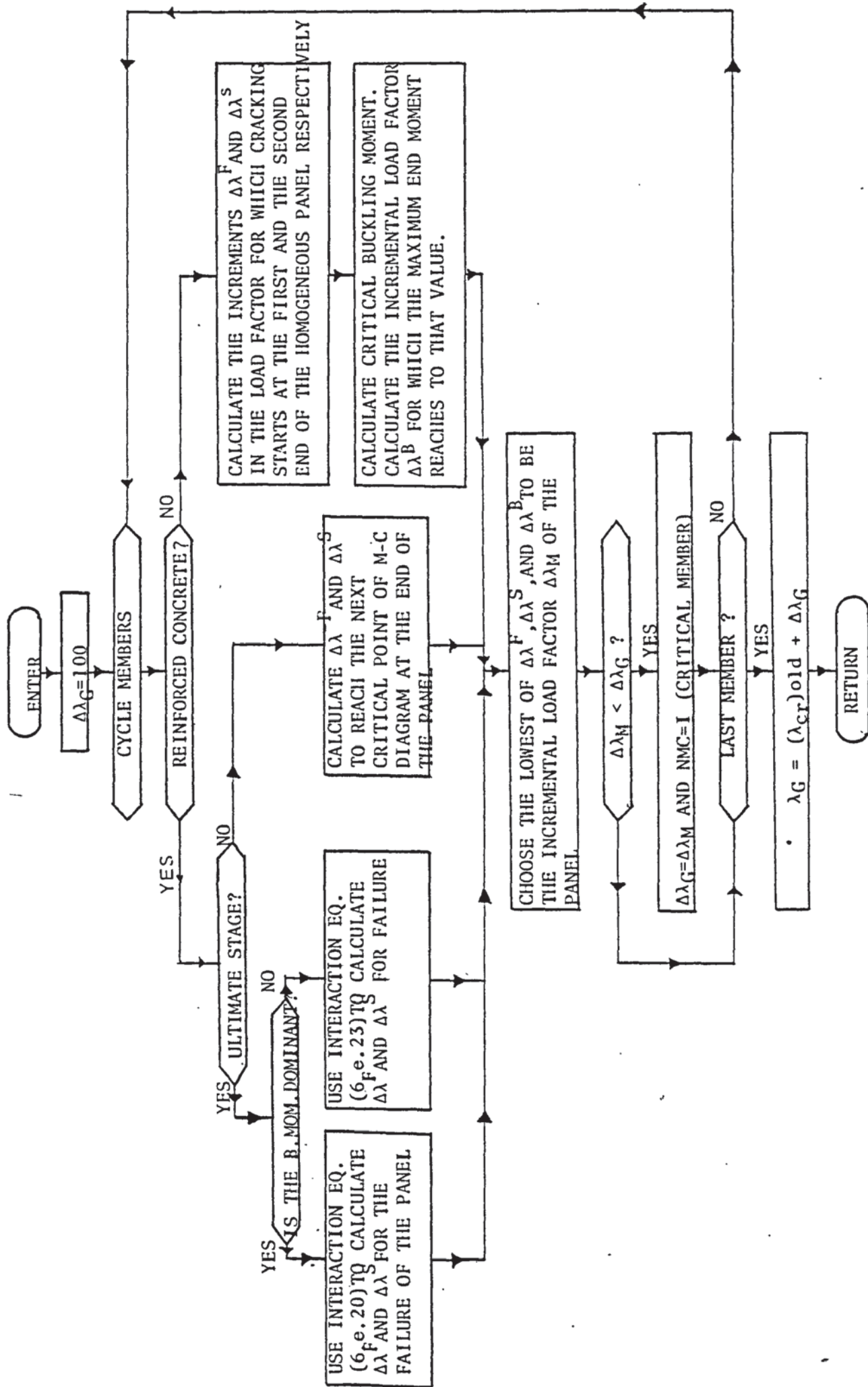
FIGURE 6.9 FLOW DIAGRAM OF SUBROUTINE CHECK

For the first case the following operations are carried out

i - The incremental load factors $\Delta\lambda^F$ and $\Delta\lambda^S$, at which cracking starts at the first or the second end of the panel, are calculated.. The method proposed in chapter 4, section g is used for this purpose.

ii - The critical value of the maximum end moment, which causes lateral instability in the panel, is calculated using the method given in chapter 4, section f. The incremental load factor $\Delta\lambda^\beta$ for which the maximum end moment reaches its critical value is then calculated by extrapolation.

If the panel is made out of reinforced concrete, the incremental load factors $\Delta\lambda_c^F$ and $\Delta\lambda_c^S$ are calculated. These are the increments in the load factor needed to reach the next critical point on the M-C diagram of a panel. When the panel not yet cracked and bending dominates torsion and shear, the last two are neglected. Each incremental load factor is calculated from

$$\Delta\lambda = \frac{M_{cr} - M^{\lambda cr}}{\overline{M}} \qquad\qquad 6.3$$

In this formulae, M_{cr} is the bending moment at the next critical point on the M-C diagram of the panel, $M^{\lambda cr}$ is the bending moment at either end of the panel at the former critical stage of the whole structure under λ_{cr} and $\overline{M}$ is the value of the bending moment at either end of the panel due to the loads ($\underline{w}+\underline{g}$) due to a unit increment in the load factor. If torsion and shear dominate bending, the method given in chapter 4, section g, is used to determine $\Delta\lambda$. In this case the rupture strength of the concrete is used to be the uniaxial cracking strength.

When the panel is already cracked and the effect of bending

dominates torsion, the interaction equation (5.e.20) is used to predict the ultimate stage, thus the incremental load factors $\Delta\lambda_c^F$ and $\Delta\lambda_c^S$. On the other hand, if torsion dominates, equation (5.e.23) replaces equation (5.e.20).

Once $\Delta\lambda^F$, $\Delta\lambda^S$, $\Delta\lambda^B$ or $\Delta\lambda_c^F$ and $\Delta\lambda_c^S$ are calculated, the lowest of these is chosen to be the critical incremental load factor, $\Delta\lambda^M$ of the member. $\Delta\lambda^M$ is compared with $\Delta\lambda_G$. If $\Delta\lambda^M < \Delta\lambda_G$, $\Delta\lambda^M$ replaces $\Delta\lambda_G$ i.e. $\Delta\lambda^M$ is chosen to be the critical incremental load factor of the grillage. Therefore the member is the critical member "NMC" unless any other member's critical incremental load factor is lower than $\Delta\lambda_G$. Once all the members are cycled and $\Delta\lambda_G$ is predicted, the next critical load factor of the grillage is calculated by adding $\Delta\lambda_G$ to the former critical load factor, λ_{cr}, of the whole structure. Hence $\lambda_G = \lambda_{cr} + \Delta\lambda_G$.

CHAPTER 7

EXPERIMENTAL WORK

7.a. Introduction:

To verify the theoretical work given in Chapters 4 and 5, a series of tests, carried out on complete structures, are described in this chapter. The size of the test structures were chosen to suit the facilities provided in the laboratories of the Department of Civil Engineering at the University. These sizes together with other particulars of structures tested are given in tables (7.1), (7.2), (7.3), (7.4) and figures (7.1), (7.2), (7.3), (7.4), (7.5) and (7.6).

The structures tested, can be classified into three groups as follows:

1 - Structures made of reinforced concrete panels with no intermediate frames. These are structures 1, 2, 3, 4 listed in table 7.1 and each one consists of a slab and two shear walls as shown in the table. Structures 1 and 2 were loaded at the slab-shear wall junctions A and B and at each third point of the slab, C and D. Structures 3 and 4 were loaded at every quarter point E, F and G of the slab only.

2 - Structures with reinforced concrete shear walls and slabs and with intermediate frames made out of steel. These are labelled 5, 6, 7, 8, 9 and 10. Details of these are given in table 7.2. Structures 5-9 were loaded at frame-slab and slab-wall junctions H, I, J, K. Structure 10, on the other hand, was loaded at frame-slab junctions M, N, P only.

3 - Structures with reinforced concrete panels and intermediate frames. These are labelled 11 to 16 and given in tables 7.3 and 7.4. All of these structures were loaded at frame-slab junctions only. Structures 11 and 12 were single storey. The rest were two
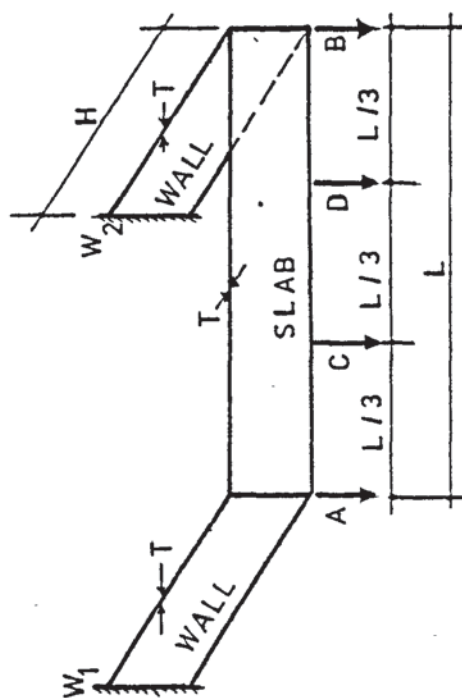
STRUCTURES 3 AND 4

STRUCTURES 1 AND 2
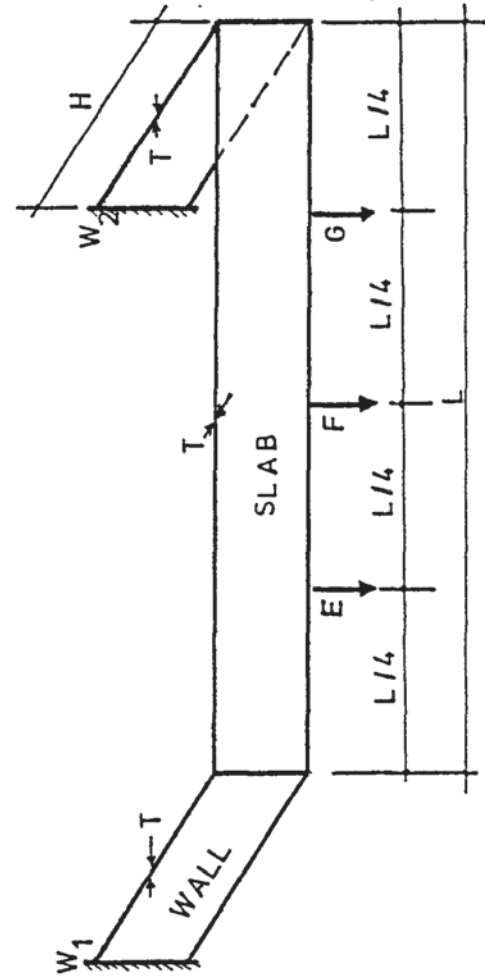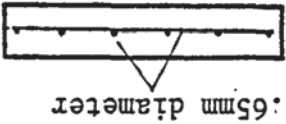
Structure No.	H Height (mm)	L Length (mm)	D Width (mm)	FLOOR SLAB – SHEAR WALL SPECIFICATIONS			REINFORCEMENT				
				Thickness (mm)	f_{cu} (kN/mm²)	E_c (kN/mm²)	σ_{ult} (kN/mm²)	E_s (kN/mm²)	ε_y	ε_H	DETAIL
1	605	1200	200	40	0.0276	20.5	0.635	0.635	0.003	0.009	2.65mm diameter, 25.4mm x 25.4mm square mesh
2	605	1200	200	"	0.0260	19.95	"	"	"	"	
3	580	2000	300	"	0.0200	19.60	0.761	209.0	0.00365	0.0066	
4	580	2000	300	"	0.0225	21.70	"	"	"	"	

TABLE 7.1 SPECIFICATIONS OF ONE STOREY R.C. STRUCTURES WITHOUT INTERMEDIATE FRAMES

TABLE 7.2: SPECIFICATIONS OF ONE STOREY R.C. STRUCTURES WITH STEEL FRAMES

STRUCTURE NO	H Height mm	L Length mm	D Width mm	FRAMES Number of frames	Frame width mm	cross section of bars mm²	σy kN/mm²	E kN/mm²	SHEAR WALLS–FLOOR SLABS T Thickness mm	D Depth mm	f_cu kN/mm²	E_c kN/mm²	REINFORCEMENT σu kN/mm²	E_s kN/mm²	ε_sy	ε_su	DETAIL
5	605	1200	200	2	187.3	12.7mm×12.7mm	0.285	211.0	40	200	0,0208	20,52	0,635	211.5	0,003	0,009	2.65mmØ 25.4mm×25.4mm square mesh
6	"	"	"	2	"	"	0,403	212.0	"	"	0,0249	23.49	"	"	"	"	
7	"	"	"	2	"	"	"	"	"	"	0,0254	24.08	0,761	209,0	0,00365	0,0066	
8	"	"	"	2	180,95	19,05×19,05	0,288	213,0	"	"	0,0241	24,60	"	"	"	"	
9	"	"	"	2	"	"	"	"	"	"	0,0261	26,30	"	"	"	"	
10	580	2000	300	3	280,95	"	"	"	"	300	0,0235	24.10	"	"	"	"	

STRUCTURE 10

STRUCTURES 5–9

STRUCTURE NO.		11	12
	Height (mm) (H)	580	580
	Length (mm) (L)	200	200
	WIDTH (mm) (D)	300	300
	No. of Frames	3	3
REINFORCED CONCRETE FRAMES	Frame width mm	280	280
	Cross section mm^2	50mmx50mm	50mmx50mm
	E_c kN/mm^2	21.67	20.50
	f_{cu} kN/mm^2	0.0036	0.0272
	Reinforcement steel	4.76mm ϕ black mild steel	
	E_s kN/mm^2	216.0	216.0
	f_{sy} kN/mm^2	0.212	0.212
SHEAR WALLS & SLABS	Slab thickness mm	40.0	40.0
	Wall thickness mm	40.0	40.0
	Depth of slabs and s. walls mm	300.0	300.0
	f_{cu} kN/mm^2	0.031	0.0292
	E_c kN/mm^2	24.50	24.0
GRILLAGE REINFORCEMENT	Detail	25.4mmx25.4mm square mesh with 2.65mmϕ bars	
	f_{su} kN/mm^2	0.591	0.656
	E_s kN/mm^2	200.27	200.3
	ε_y	0.00295	0.003
	ε_{ult}	0.006	0.0055

TABLE 7.3 : ONE STOREY STRUCTURES WITH REINFORCED CONCRETE FRAMES

Wall Cross Section Slab Cross Section

W_2 was singly reinforced in structure 15 and substituted by a frame for structure 16.
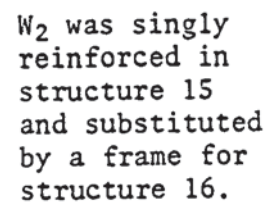
STRUCTURE NO.		13	14	15	16
	Height of first storey H_1 (mm)	300	300	300	300
	Height of second storey H_2 (mm)	300	300	300	300
	Length L (mm)	2000	2000	2000	2000
	Width (mm)	350	350	350	350
	No. of walls	2	2	2	1
	No. of Frames	2	2	2	3
REINFORCED CONCRETE FRAMES	Width of the frames W_1	330	330	330	330
	Cross section mmxmm	50x50	50x50	50x50	50x50 Inner frames 60x60 Outer frame
	E_c kN/mm^2	21.0	23.3	23.08	19.14
	f_{cu} kN/mm^2	0.03191	0.03305	0.03305	0.02546
	Reinforcement steel	4.75 mm	ϕ black mild steel		
	E_s kN/mm^2	216.0	216.0	200.0	196.0
	f_{sy} kN/mm^2	0.212	0.212	0.208	0.190
SHEAR WALLS AND SLABS	Slab thickness (mm) T_1	40	40	40	40
	Wall thickness (mm) T_2	60	60	60	60
	Depth of Slabs and Walls D (mm)	350	350	350	350
	f_{cu} kN/mm^2	0.02575	0.03203	0.03045	0.02823
	E_c kN/mm^2	21.0	25.45	24.80	27.50
GRILLAGE REINFORCEMENT	Detail	2.55 mm ϕ, 25.4x25.4 mm square mesh;shear walls are doubly, slabs are singly reinforced.			
	f_{su} kN/mm^2	0.509	0.509	0.556	0.625
	E_s kN/mm^2	203.3	203.3	200.0	196.0
	ε_y	0.0025	0.0025	0.00235	0.00228
	ε_{ult}	0.006	0.006	0.007	0.007

TABLE 7.4 : TWO STOREY STRUCTURES WITH REINFORCED CONCRETE FRAMES
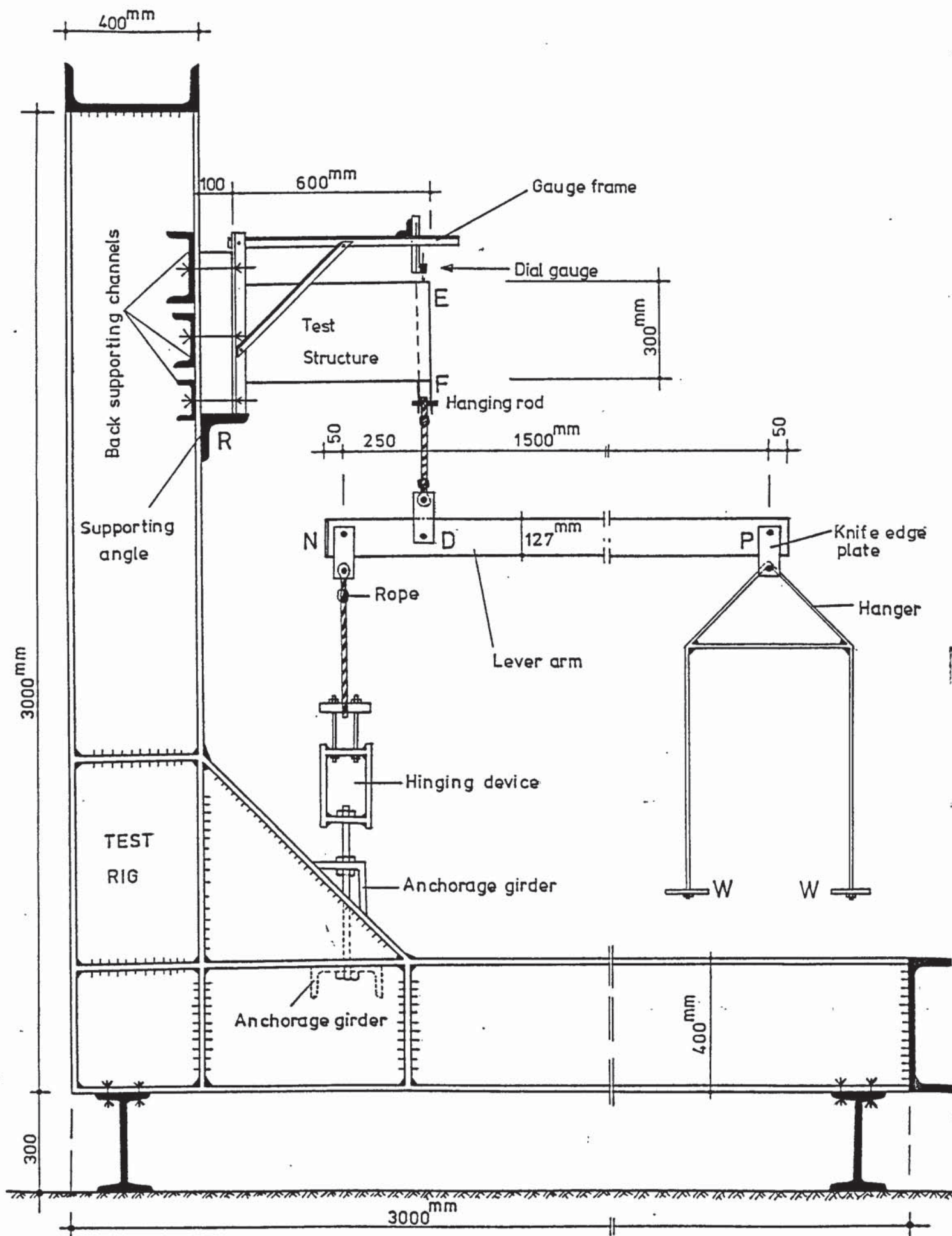
FIGURE 7.1: ANCHORAGE OF A TEST STRUCTURE TO THE TEST RIG
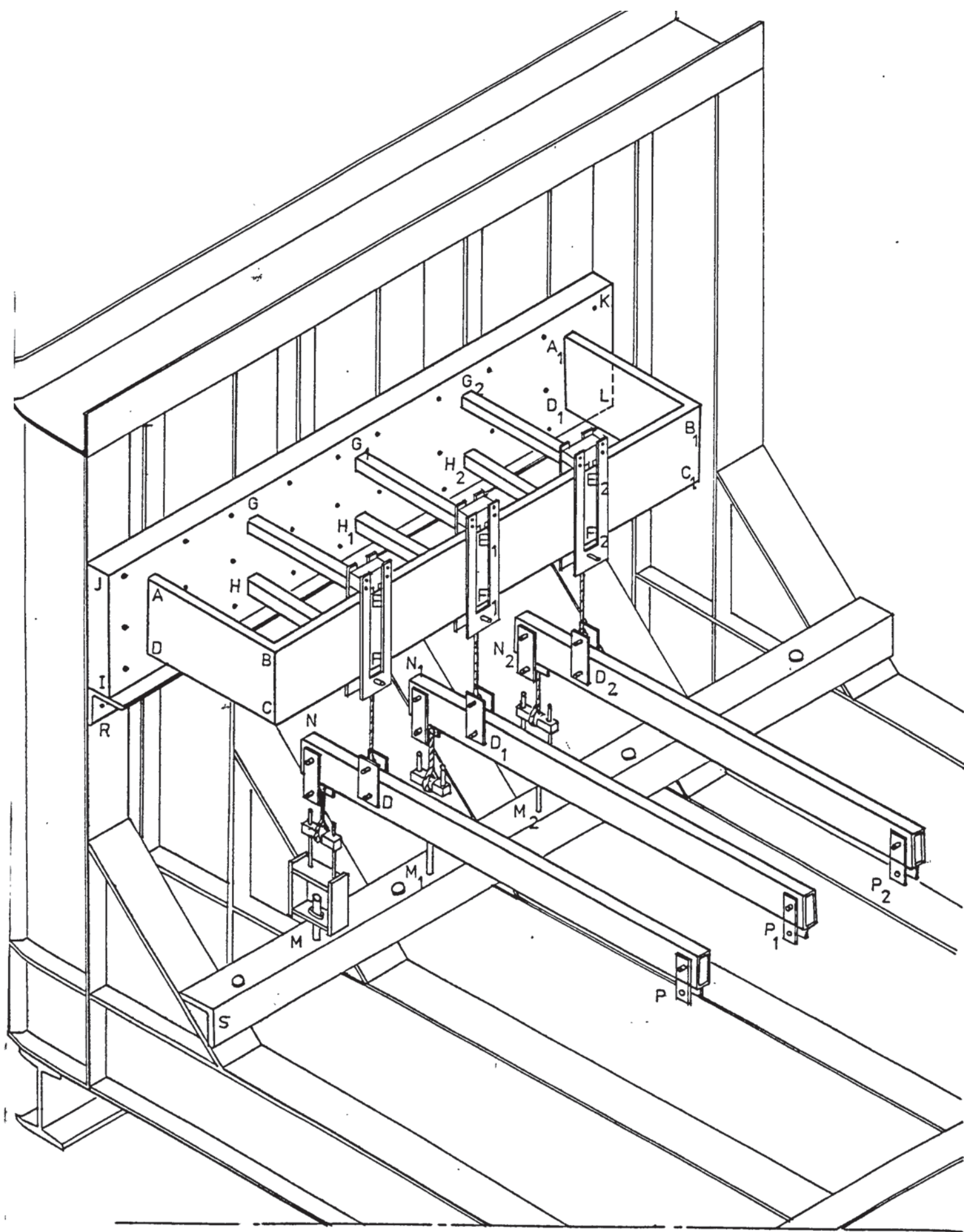
FIGURE 7.2: A STRUCTURE AND LOADING ARRANGEMENT
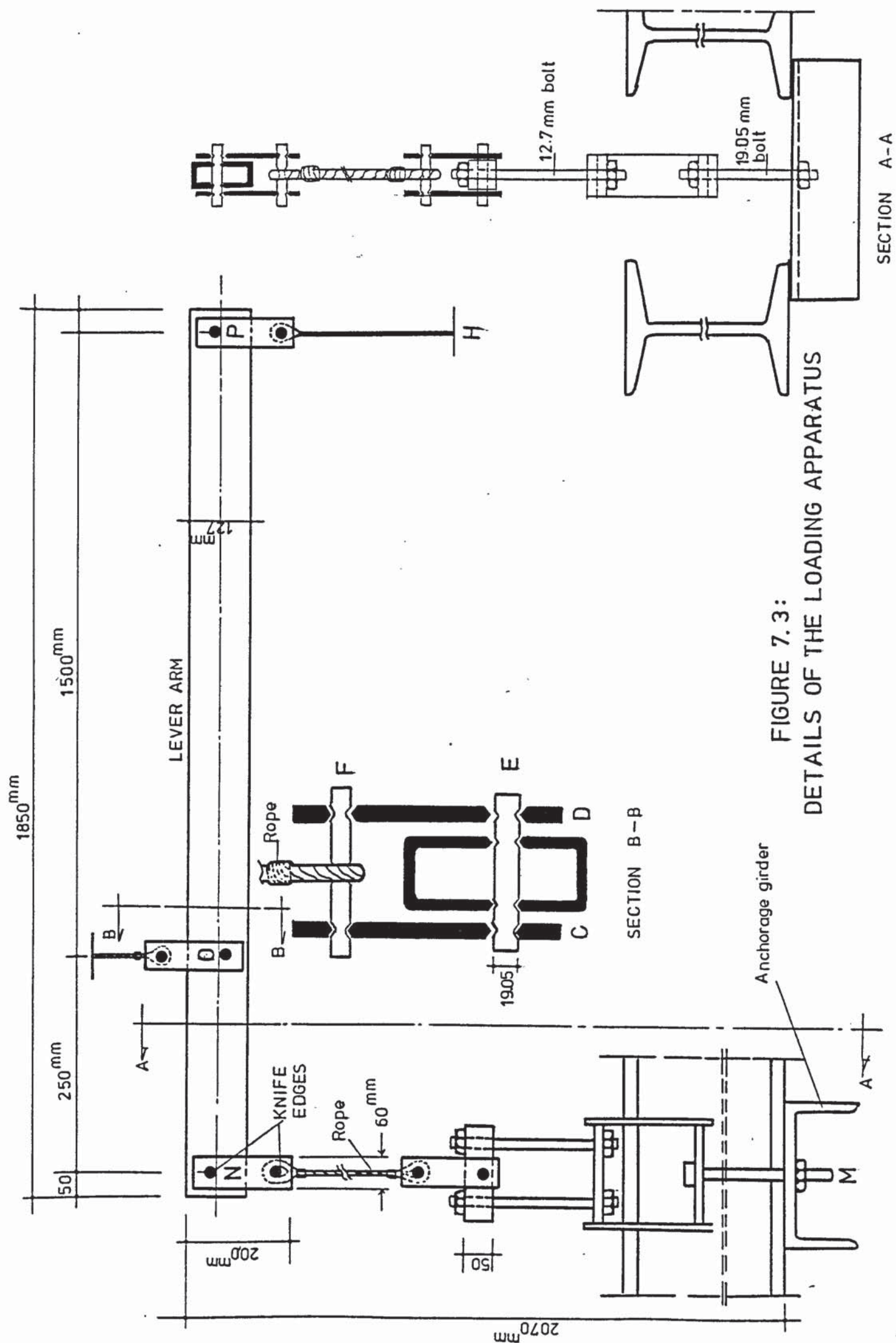
FIGURE 7.3 :
DETAILS OF THE LOADING APPARATUS

a-Elevation

1240mm

40 | 350 | 60 | 340 | 60 | 350 | 40

A

25.4mm×25.4mm
square mesh

Loading strap

Frames
12.7mm×12.7mm
square section
for structures
5,6,7. 19.05mm×
19.05mm for
structures 8,9.

Bolts

40

580

700 mm

80

A

120 | 400 | 400 | 400 | 120

60 | 120 | 160 | 150 | 160 | 140 | 160 | 150 | 160 | 120 | 60

1440 mm

b-Plan

120 | 400 | 400 | 400 | 120

1440mm
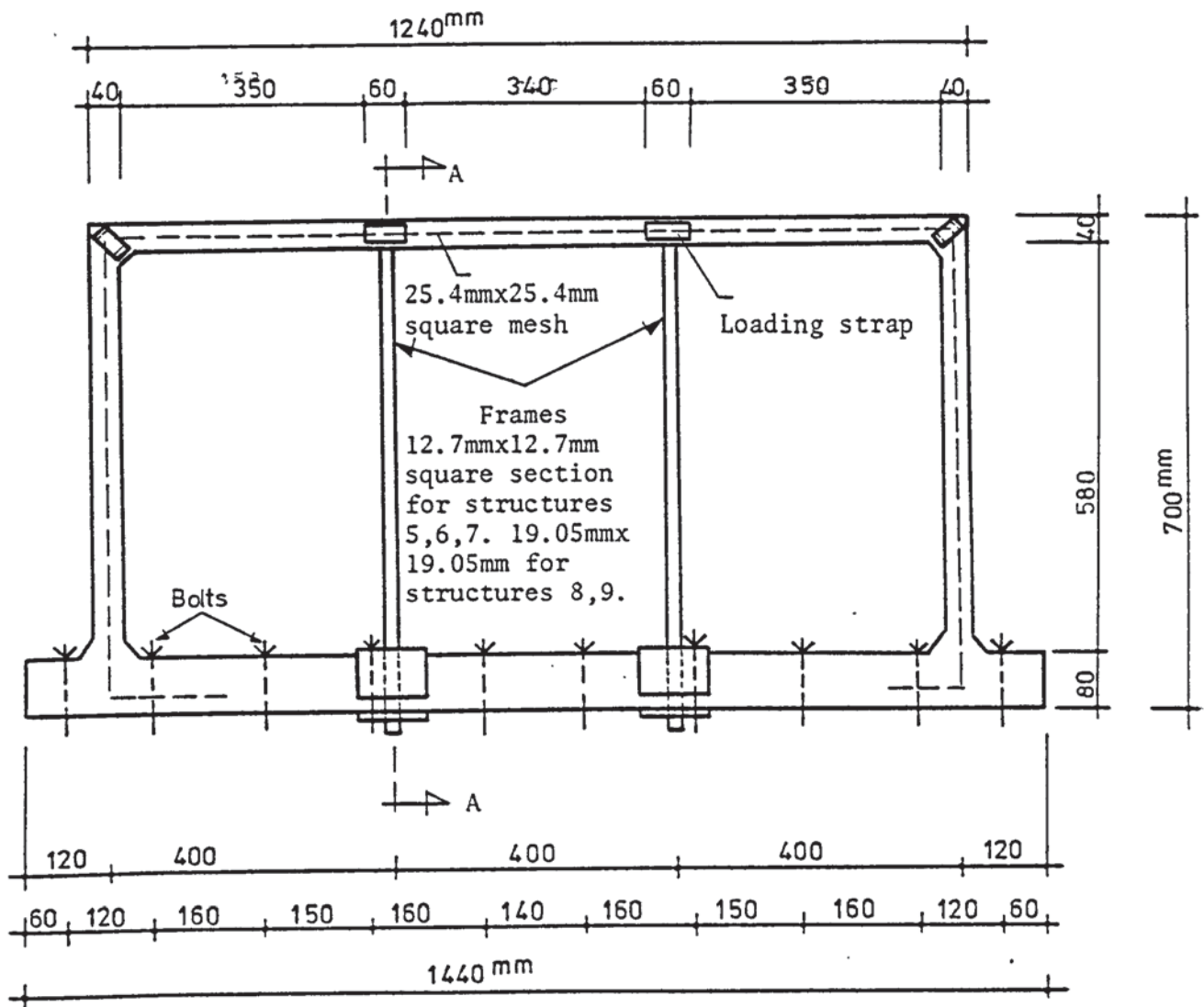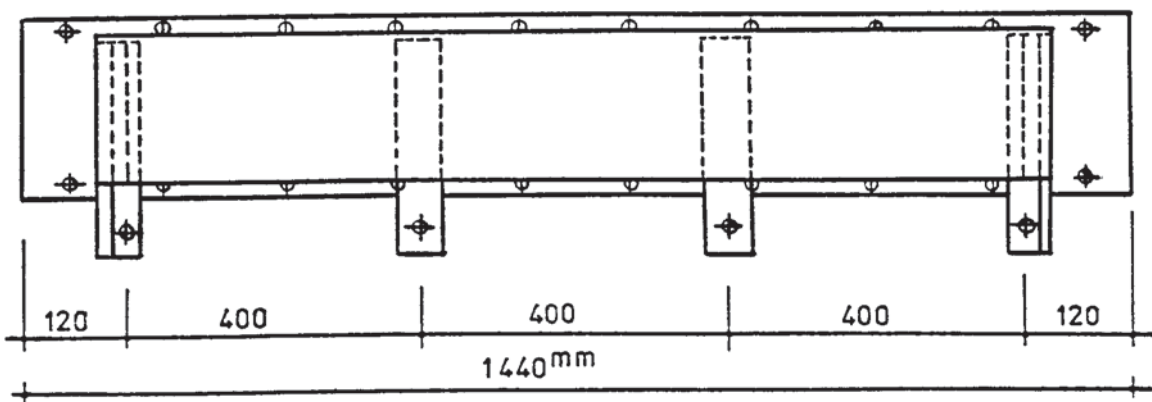
FIGURE 7.4 : DESIGN OF TEST STRUCTURES 1,2,5,6,7,8,9
(STRUCTURES 1,2 HAVE NO INTERMEDIATE FRAMES)
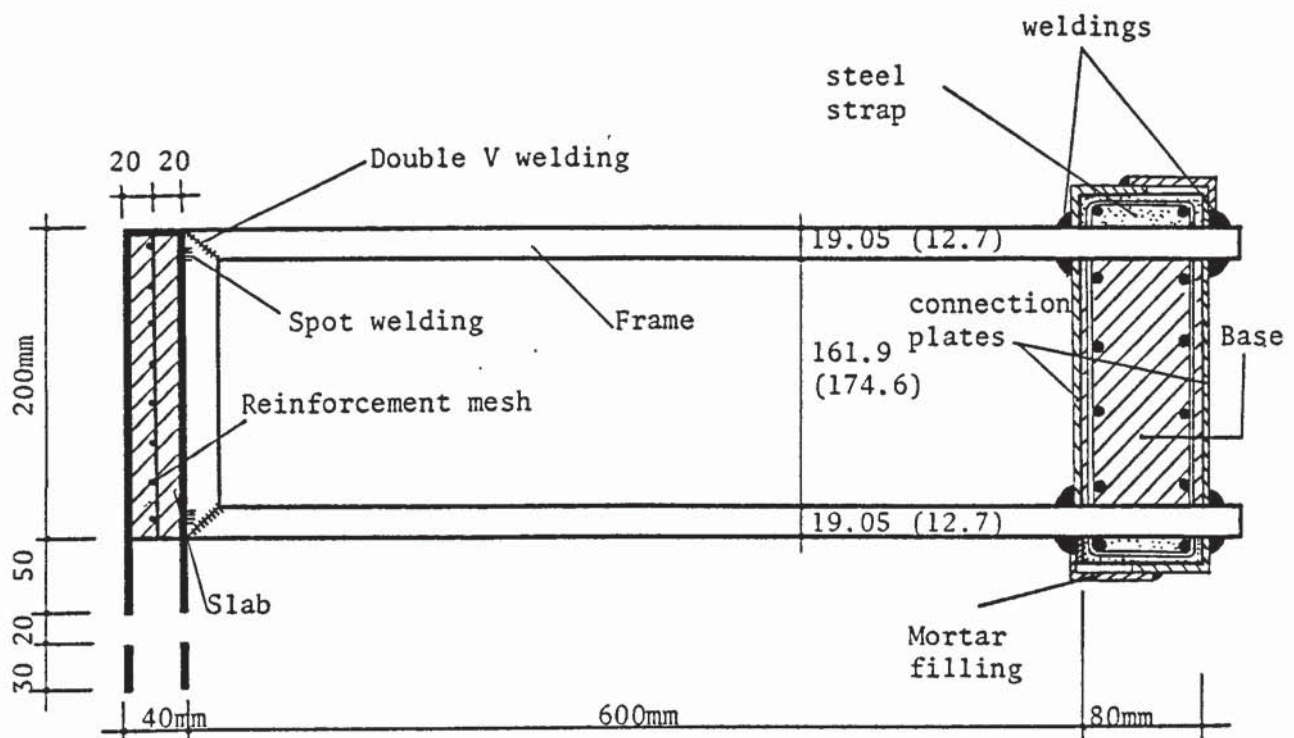
FIGURE 7.4.C : SECTION A-A FOR STRUCTURES 5-9
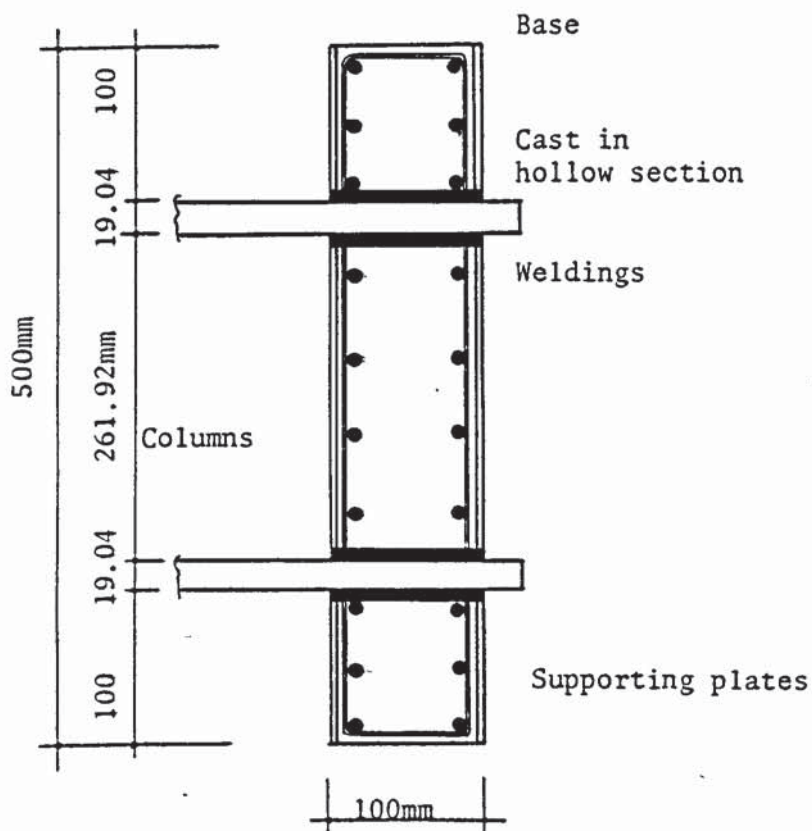
NOTE: Overall design of structure 10 is given in figure 7.5. The connection of the frames to the slab is similar to that shown in figure 7.4.C.

FIGURE 7.4.d ANCHORAGE OF A FRAME TO THE BASE PANEL
(STRUCTURE 10 ONLY)

a-PLAN
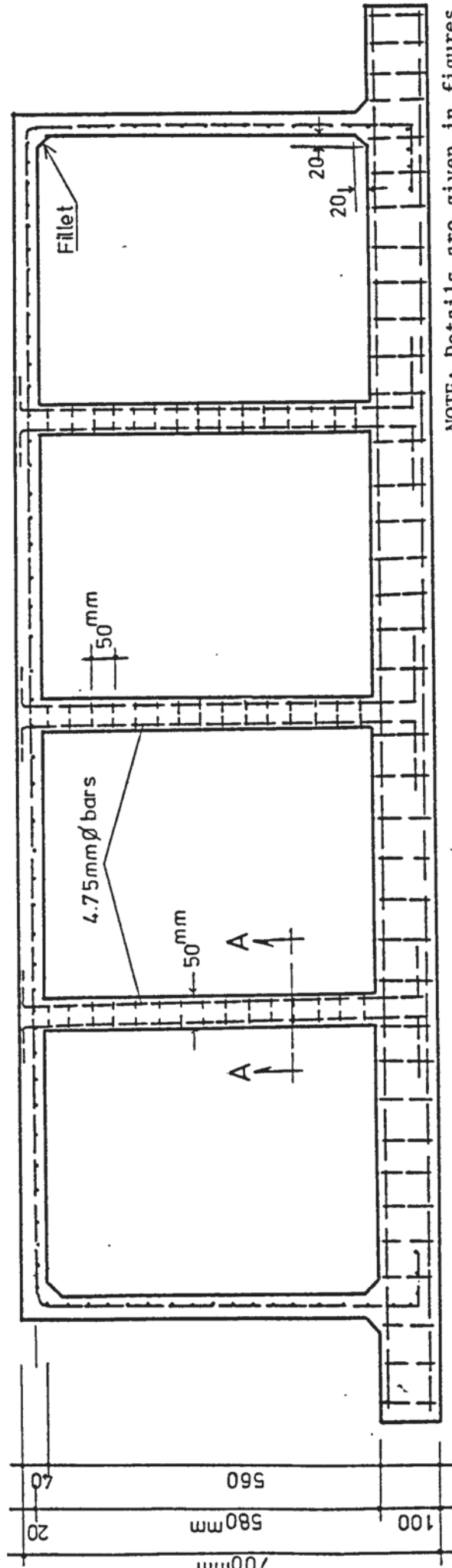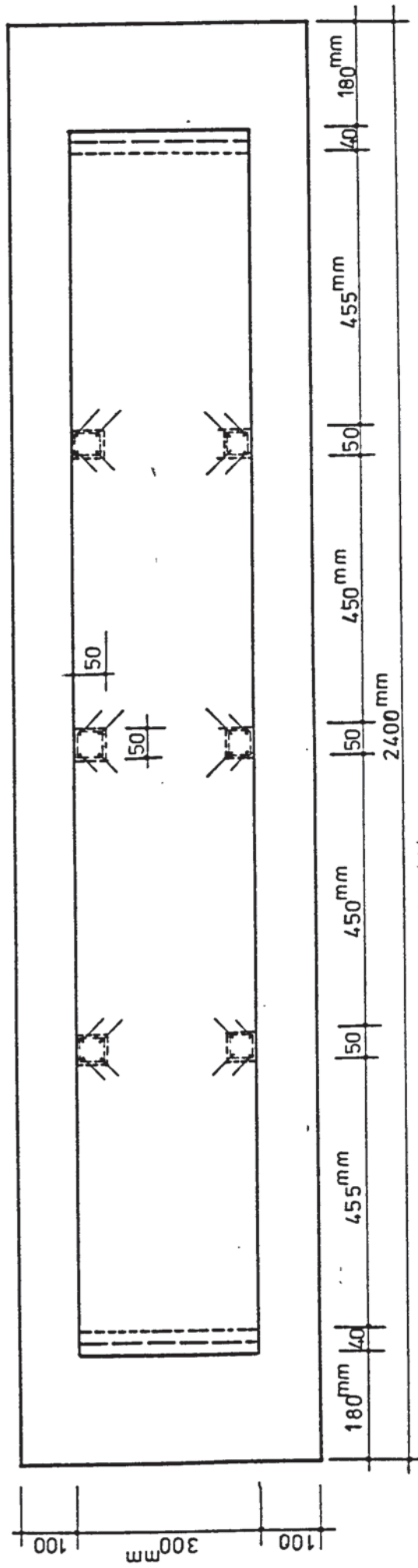
b-ELEVATION

NOTE: Details are given in figures (8.2)&(8.3)

FIGURE 7.5   DESIGN OF STRUCTURES 3,4,10,11,12
(STRUCTURES 3,4 HAVE NO FRAMES, STRUCTURE 10 HAS THREE STEEL FRAMES)

a-PLAN
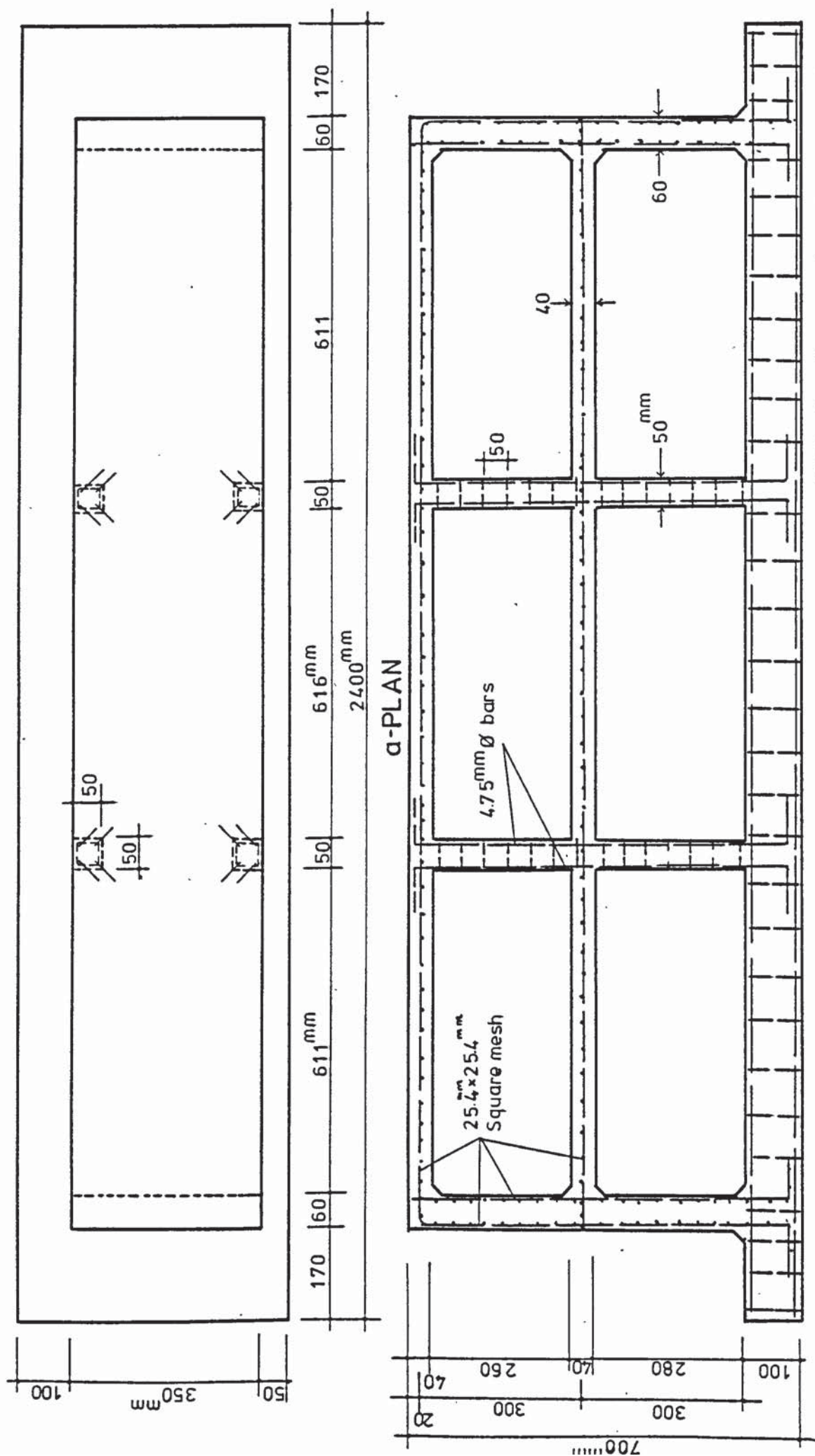
b-ELEVATION

NOTE: Details are given in figures (8.2) and (8.3)

FIGURE 7.6 DESIGN OF STRUCTURES 13,14

storey. Structure 16 had only one wall. The overall dimensions
of the structures, the number of intermediate frames and the
loading arrangements were varied to cover as many modes of
failure as possible. Because of the difficulties involved in
manufacturing and loading reinforced concrete structures, it was
decided to make most of these single storey. This is with the
exception of the last four.

7.b. Anchorage of Model and Loading Arrangement:

The testing rig consists of a system of horizontal and
vertical steel stanchions connected by bolts and welded as shown
in figures (7.1) and (7.2). The models were attached by their
base (IJKL in figure 7.2) to the vertical stanchions of the rig.
Thus the floor slabs were in fact subject to vertical loads in their plane.
A sufficient number of 11.1 mm diameter bolts were used to connect
the base to the rig by means of supporting channels fixed to the
flange of the stanchions as shown in figure 7.1. This fixed the
base firmly to the rig and toppling due to subsequent loading was
prevented. A supporting continuous angle (R) was also fixed to
the rig at the base of the model as shown in figures 7.1 and 7.2
by letter R. This type of anchorage was preferred to anchoring
the model, with its base horizontal, because it made it possible
to apply the loads by means of a simple system of horizontal lever
arms NOP.

The loads were applied to each load point by means of straps
lettered as EF, E_1F_1 etc. in figure (7.2). These were suspended
from each junction. Each strap was connected to a lever arm by a
system of hanging rods, cables and connection plates shown as
CDEF, in figure (7.3). The end, N, of the lever arm was anchored

to the test rig beneath by a system of rope and hinging device. This anchorage system, NM, is shown in figure (7.3). Dead weights were applied to the free end, P, of the levers by hangers W. In this manner constant loading was provided as creep took place. The lever arms NOP were made out of 50.8mm x 127mm hollow rectangular sections and had a magnification ratio of 1:7. Each lever arm contained three 20mm diameter knife edged holes at N,O and P. The outer holes N and P were situated just above the centre line of the lever while the middle hole, O, was just below this line. These holes are shown in figure 7.3 where it is noticed that the points of application of the loads at N,O and P all lie on a straight line. The lever ratio was thus kept constant irrespective of the inclination of the lever.

7.c. Construction of Structural Models:

7.c.1. The Base:

The shear walls and the slabs for each complete structure were cast together with a strong base panel to provide a strong fixity of the shear walls at the supports. The base panel IJKL was designed to simulate the properties of a rigid support and to transmit the forces due to the loads acting on the structure to the test rig. It was doubly reinforced with the longitudinal bars connected by stirrups which also sustained the bending moments in the transverse direction. A series of 12.7 mm diameter holes in the base enabled a structure to be fixed to the test rig by bolts. The thickness of a base varied between 80 mm and 100 mm and depended upon the size of the structure being tested.

7.c.2 The Shear Walls:

In the single storey structures the thickness of the shear walls were kept constant at 40 mm while their depth was varied

between 200 mm and 300 mm. The walls were reinforced by 25.4^{mm} x 25.4^{mm} square mesh which was made out of 2.65^{mm} diameter steel bars and placed in the middle of the cross section as shown in figures (7.4) and (7.5).

The shear walls of the two storey structures were 60 mm thick, 350 mm deep and doubly reinforced by two parallel layers of 25.4^{mm} x 25.4^{mm} square mesh. This provided sufficient resistance against torsion as well as in-plane bending and shear. For structure 15, one of the shear walls was singly reinforced as in the case of single storey structures. One of the shear walls was altogether removed from structure 16 and replaced by a reinforced concrete frame. Tests on structures 15 and 16 were carried out to examine the computer program given in chapter 6 section b for the asymmetric modes of failure, in which the torsional moment plays an important part.

7.c.3 The Slabs:

The depth of slabs was the same as the shear walls which also varied between 200 mm and 300mm for the single storey structures and kept at 350 mm for two storey ones. Their thickness was 40 mm. A single mesh of reinforcement was placed in the centre plane of the slabs. For structures (1-4) and (5-10) the loading straps were cast in at the specified loading points. For structures 5-10, these straps were also used to connect the steel frames to the slabs.

For structures 11-16, polystrene blocks were placed at the junctions of the slabs and the frames and cast in as the reinforced concrete frames were to be cast at a later stage. These blocks were then removed once the concrete grillage was hardened. The

spaces left behind were cleaned thoroughly and then roughened to provide sufficient bond between the concrete of the grillage and that of the frames. At about a week later the frames were cast.

7.c.4 The Steel Frames:

For the test structures 5, 6 and 7, these were manufactured out of 12.7 mm x 12.7 mm square black mild steel bars while those for structures 8, 9 and 10 were made out of 19.05 mm x 19.05 mm square section. The beams and columns were welded together with double V velding and the beams were spot welded to the loading straps at the joints as shown in figure (7.4.c).

For structures 5-9, wooden blocks were placed in the positions at the junctions of the columns at the base panel. After the concrete had hardened, these blocks were removed and replaced by the columns. L shaped connection plates were used to hold the ends of the columns in position (see figure 7.4.c). The remaining spaces in the holes were then filled by mortar and the connection plates were welded to each other and to the columns. This arrangement insured that the columns were perfectly fixed to the base and virtually no rotation of the support was possible. This arrangement, however, was not suitable for the large base panel of structure 10. It was not possible to slide a ready made frame through the deep holes in the base. It was also considered that such holes weaken the base itself. For this structure it was decided to use 20^{mm} x 20^{mm} hollow sections cast in at the column positions together with supporting plates at either side of the base. The columns of the frames were pushed into these sections and then welded to the beams to form the frames. These were then adjusted in their positions and welded to the hangers.

Finally the columns were welded to the hollow sections and the supporting plates at the back and front faces of the base panel. Details of this arrangement is shown in figure (7.4.d).

7.c.5 Reinforced Concrete Columns:

Reinforced concrete columns were used in structures 11 to 16. They were made out of 50 mm x 50 mm square sections with the same reinforcing arrangements. In structure 16, the cross section of the outer columns, replacing one of the shear walls was 60 mm x 60 mm. The reason for this, was to avoid the constructional difficulties. Four 4.75 mm diameter bars were placed in the corners of each column. The stirrups were made out of 2.65 mm diameter bars placed at 50 mm spacing as shown in figure (7.5.b). The columns were connected to the floors, which were assumed to be acting as large beams against out of plane bending.

7.d. Manufacturing Process:

The cement used throughout the test series was ordinary portland. The aggregate used was 3/8" crushed gravel and zone III sand. The concrete mix was 1:2:3 with a water-cement ratio of 0.6. However, the secondary casting mixture, which was used to cast the columns was a 1:2 mortar with 0.6 water-cement ratio. The reason for using this was to obtain a fairly compact, easy filling and a relatively strong mixture compared to the concrete used in the grillage. This was particularly necessary to prevent premature failure at the frame-slab junctions.

The overall mould was assembled and screwed onto a thick panel which prevented excessive deformation during the casting process. The reinforcement mesh was cut to size and placed in the mould. The joining on the reinforcement was avoided at the junctions.

When necessary, the junctions were strengthened by extra reinforcement to prevent premature failure.

Having assembled the grillage reinforcement, the base reinforcement was placed in and the free arms of the mesh were bent over the base reinforcement, thus sufficient bond was provided between the base concrete and the mesh. The outer panels of the overall mould were then fixed to cover the reinforcement. Three strips were cut out of the original mesh and tested to determine their physical properties.

Once the overall mould and the reinforcement was set, the whole structure was put on two table vibrators and made ready for casting. This was carried out in one operation except for the columns which were cast separately at a later stage. Shrinkage cracks were checked by the use of fillets at the junctions of the shear walls with the base and with the slabs.

Two capped and two uncapped 150 mm x 300 mm cylinders and two 100 mm x 100 mm x 500 mm standard rupture test specimens were taken from each mixture. These specimens were tested to find the ultimate crushing strength, the modulus of elasticity and the rupture strength of the grillage concrete. After a few days the mould was stripped off and the concrete left to cure in a humid place for at least 21 days.

In the case of structures with steel frames, the frames were fixed a week before testing. The surface of the frames were cleaned by emery cloth and covered by hot resin in order to detect the formation of plastic hinges during the testing process. Three tensile specimens were prepared from the steel bars and used to determine the stress-strain diagram, the modulus of elasticity

and the yield stress.

For structures with reinforced concrete frames, the polystrene blocks were cleared after stripping the mould, the frame moulds were then fixed and secondary casting was carried out. Provision was made in this phase to prevent local failure at the frame-slab junctions as explained in section (7.c.3). Again capped and uncapped 150 mm x 300 mm cylinders and rupture test specimens were taken from secondary mixture to determine its crushing strength, young's modulus and the rupture strength. The physical properties of the frame reinforcement was determined from three specimens cut out of the original material.

Altogether three different moulds were used to manufacture the test structures. The first was used to cast structures 1,2 without frames; structures 5, 6, 7, with two steel frames of 12.7 mm x 12.7 mm square steel bars, and structures 8 and 9 with two 19.05 mm x 19.05 mm steel frames.

The second mould was also used to generate another series of single storey structures 3, 4, 10, 11 and 12.

Finally the third mould was used to generate structures, 13, 14, 15 and 16.

7.e. Instrumentation:

Measurement of deflection and strain was carried out using mechanical dial gauges and electrical strain gauges.

The sway deflections of the joints were measured by Baty dial gauges of 0.001" (0.0254 mm) per division and 2" (50.8 mm) range. These were situated at each joint and carried by a dexian frame (see figure 7.1). This frame was supported on the base of the structure. Therefore errors in deflections due to bending of

supporting channels and the extension of the bolts were excluded.

The strains in the models were measured by using Tokyo Sakki Kenyujo PL-60 strain gauges. The purpose of using these gauges and their arrangement were discussed in chapter 5. The marked gauge positions were sanded and cleaned. A thin film of bonding cement was applied and the strain gauges were lightly pressed into position. When the cement had dried, electric wires were soldered to the gauge leads. These wires were then connected to the junction box of the compulog Alpha 16 data logger. A typical arrangement of the strain gauges at a critical section G is shown in plate 7.2 while a structure under test is shown in plate 7.1.

7.f. Test Procedure:

Once a model was manufactured, it was set up and clamped onto the test rig. The gauge frame was adjusted into position and the strain gauges were connected to the data logger's junction box.

The test commenced by recording the initial readings of the dial and strain gauges. The model was then loaded by the lever arms. The dial gauge readings were recorded while the strain gauge readings were automatically taken by the data logger. The loads applied due to the self weight of the lever arms and other loading instruments were predetermined and considered as the initial loading. These loads were about 0.6 kN for structures 1, 2, 5, 6, 7, 8; 0.7 kN for structures 3, 4 and 1.0 kN for structures 10, 16.

The first increment of weights were determined from a rough calculation of the load carrying capacity of the structure and applied onto the hangers W at the free ends of the lever arms. Dial and strain gauge readings were recorded after allowing
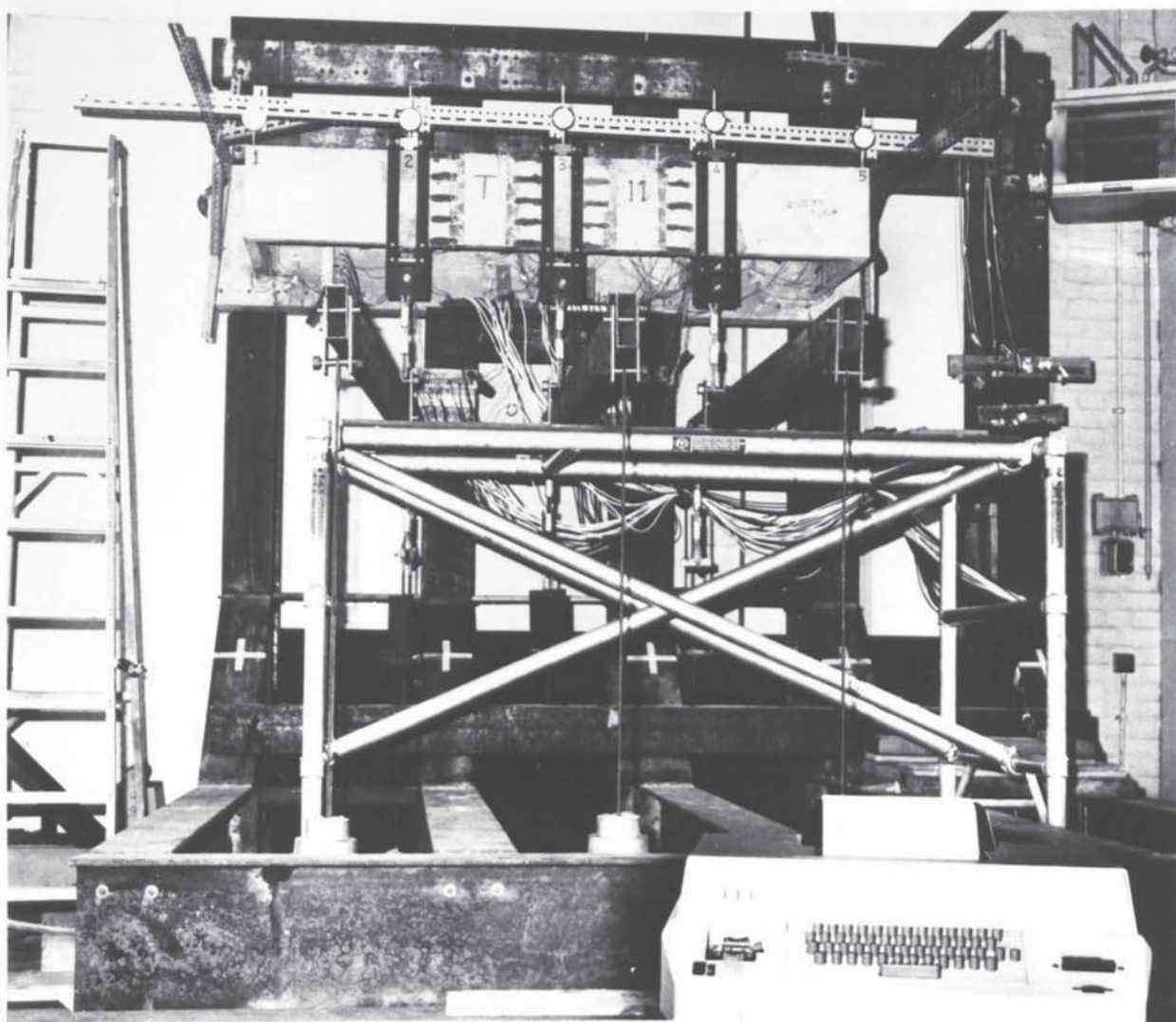
PLATE 7·1: A STRUCTURE ON TEST
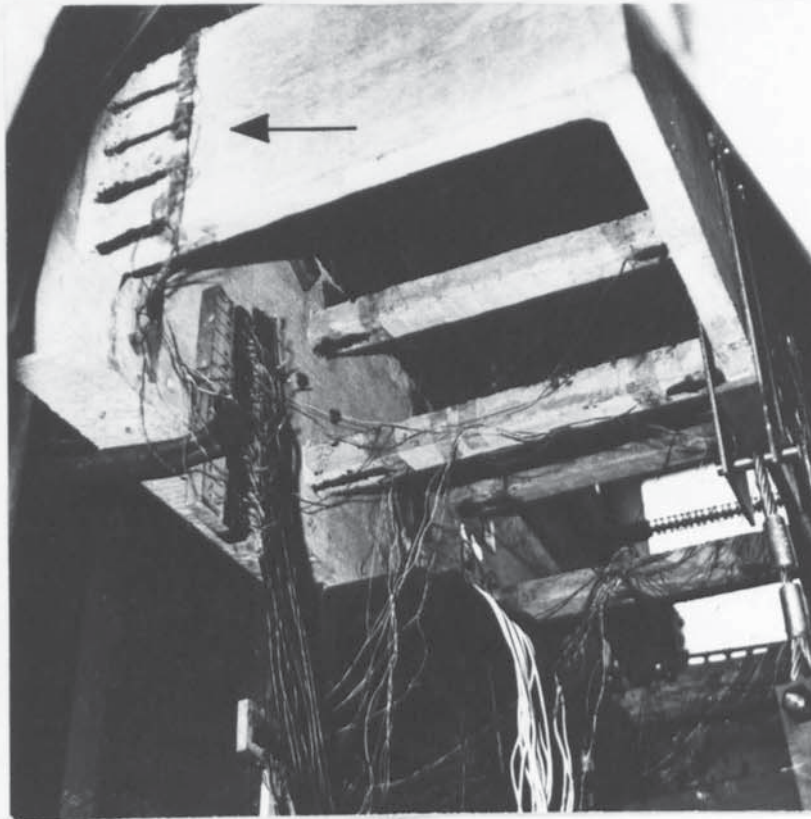
PLATE 7.2: POSITION OF STRAIN GAUGES
AT THE BASE OF A SHEAR WALL
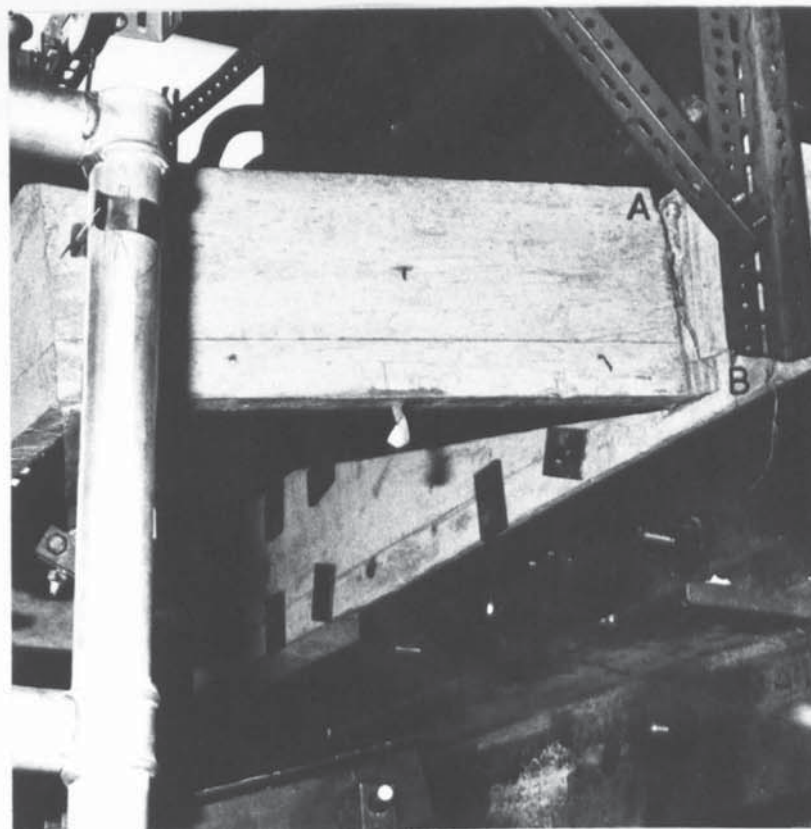
PLATE 7.3: FAILURE OF TEST STRUCTURE 2

sufficient time for the gauges to settle. This waiting time was gradually increased as failure was approached. During the test, the deflection of a critical joint in the structure was plotted against the applied load. The graph obtained gave an indication of the behaviour of the structure and was used to decide the magnitude of each subsequent loading increment. Every time the readings were recorded, the structure was carefully examined for crack formation and propogation and also to detect the formation of any plastic hinges in the steel frames. The whole process was continued until failure took place.

The concrete control specimens were tested on the same day using the Dennison compression and three point bending machine, in accordance to British Standard 1881. The control specimens of the reinforcement and the steel frames were tested using the Dennison universal tensile testing machine in a standard manner. The results of the control specimens are given in tables 7.1, 7.2, 7.3 and 7.4 together with the specifications of the test structures.

7.g. Failure Patterns

7.g.1. Failure of Structures without Intermediate Frames:

This series contained single storey structures 1, 2, 3, 4. They were primarily designed for a direct justification of the interaction equation (5.e.20). The first two structures were constructed to be identical. However, the mechanical properties of the concrete as obtained by the control specimens, were found to be slightly different. Both structures failed by propogation of cracks at the base of the shear walls. The failure loads were 1.577 kN for structure 1 and 1.727 kN for structure 2. It was noticed in structure 1 that the reinforcing bars slipped from the

base panel and the whole structure collapsed by a complete breaking off. Structure 2, however, failed by cracks developing in one of the shear walls where yielding and plastic flow of the reinforcements were visible. The failure pattern was that due to combined bending and shear. In this pattern, it was observed that failure was due to excessive straining of the outermost tensile reinforcements and no crushing was observed in the concrete at the compression zone. The crack developed is shown by letters A B in plate 7.3.

Structures 3 and 4 were similar and consisted of a single storey with a slab and two parallel shear walls. Structure 3 failed due to bending. At about half way through the loading process cracks developed in the middle portion of the slab and also at the supports. These cracks then propogated and failure was due to extensive straining of the outermost tensile reinforcements within the major crack in the middle of the slab. This was a vertical crack. The behaviour of structure 4 was similar to that of structure 3. However, at the final stage of loading a sudden failure at the support of one of the shear walls was observed. This was followed by the catastrophic failure of the slab at its midspan. The failure load of structure 4 was 6.362 kN which is 6.27% higher than that of structure 3.

7.g.2 Failure of the Structures with Steel Frames:

This series contained structures 5-10. The overall dimensions, loading arrangements and the cross-sections of the frames of structures 5, 6 and 7 were similar. However, the frames of structures 6 and 7 were manufactured from harder steel while the reinforcement mesh of the grillage of structure 7 was relatively stronger than those of structures 5 and 6. The concrete for
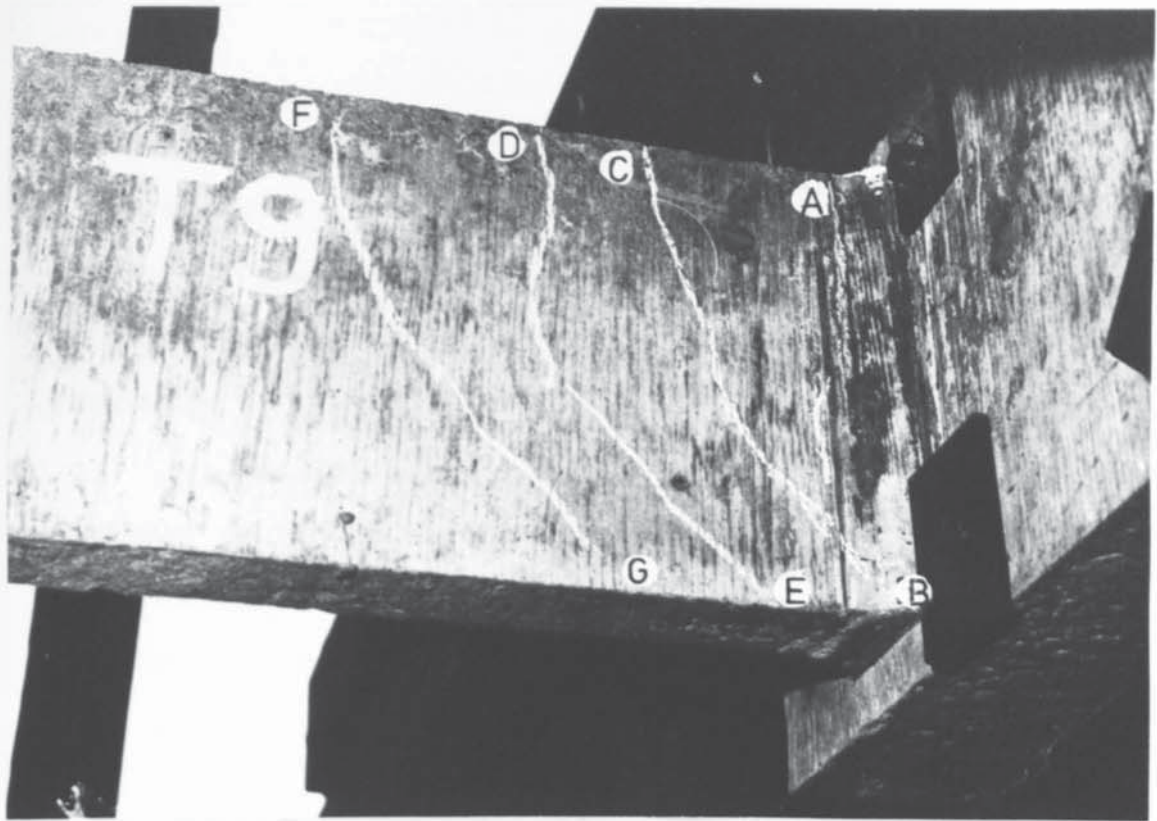
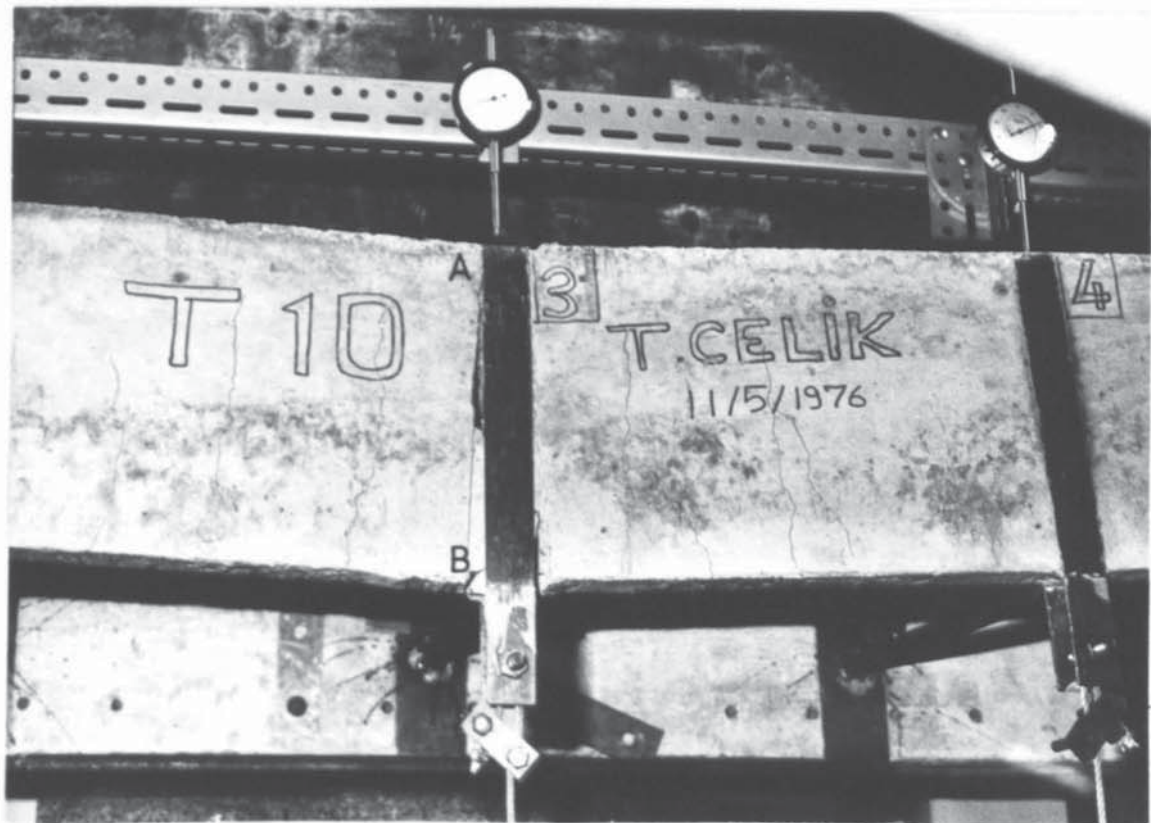PLATE 7.4: CRACKS IN A SHEAR WALL OF STRUCTURE 9

PLATE 7.5: FAILURE OF STRUCTURE 10

structure 5 was weaker than those of structures 6 and 7. The
failure loads were 2.4 kN, 2.61 kN and 3.023 kN for structure 5,
6 and 7 respectively. These variations in material properties
caused a maximum discrepancy of 20.6% in the load-carrying
capacity.

All the structures failed by propogation of cracks at the
base of the shear walls. Only in structure 3, the development of
plastic hinges were observed at the column bases just before
failure. In structures 8 and 9 the cross section of the frames
was increased from 12.7 mm x 12.7 mm to 19.05 mm x 19.05 mm. The
rest of the properties were kept the same as 5, 6 and 7. The cracks
developed in a shear wall of structure 9 are shown as lines AB,
CB, DE and FG in plate (7.4). The failure load of structure 8
was 4.052 kN and structure 9 failed at a load of 3.919 kN. Some
diagonal cracks also developed in the shear walls but not prior
to failure. The properties of structure 10 were different from
those of structures 5-9. The former was larger in size and had
three intermediate frames. It was designed to make the slab
fail before the walls and as expected, failure did take place in
the middle of the slab. This was due to bending, at a load of
9.794 kN. This failure pattern is shown as AB in plate (7.5).

7.g.3 Failure of Reinforced Concrete Structures:

In this series, structures 11 and 12 were identical single
storey structures consisting of a slab and two shear walls with
three intermediate reinforced concrete frames. Both structures
showed bending cracks in the slabs and frames, and diagonal cracks
were observed in the shear walls. The actual failure took place
in the middle of the panels. This is shown as AB in plate (7.6).
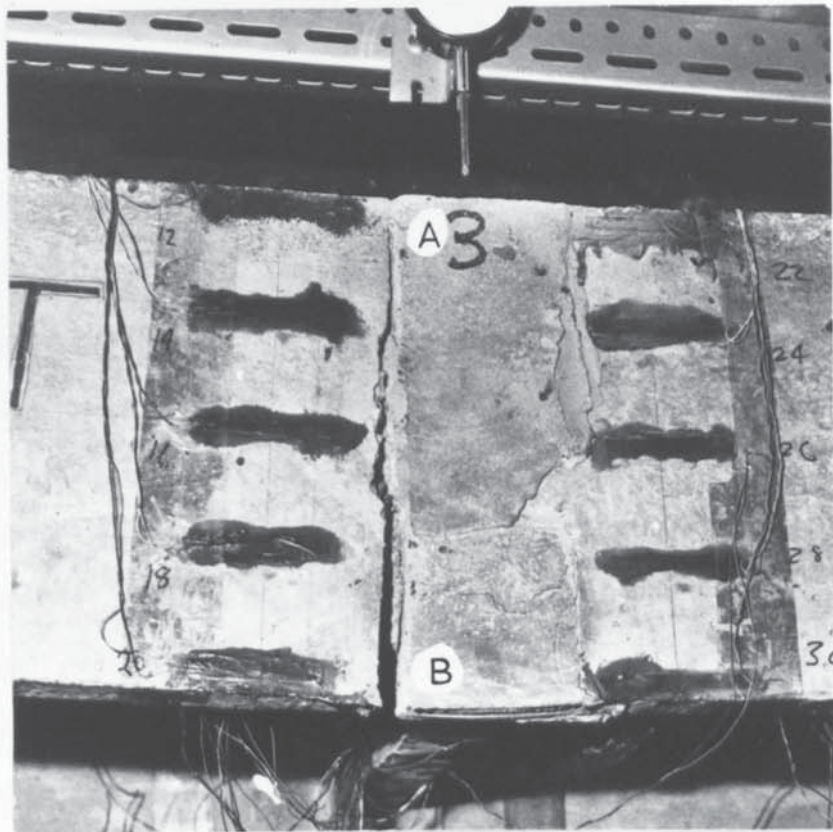
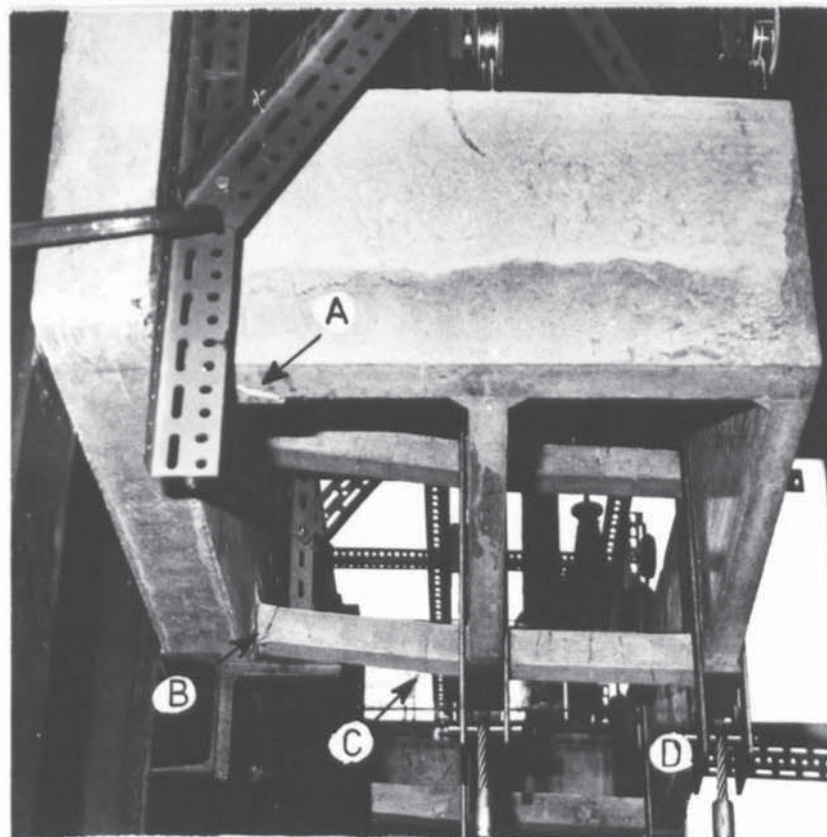PLATE 7.6: FAILURE OF STRUCTURE 11 IN THE
SLAB

PLATE 7.7: STRUCTURE 13 AFTER FAILURE

This was at loads 13.292 kN and 14.590 kN for structures 11 and 12 respectively. Structures 13 and 14 were similar and failed in the same manner at loads of 13.292 kN and 14.580 kN respectively. As the failure of each structure was approached, bending cracks in the frames and the slabs became visible. Diagonal cracks of shear walls also propogated rapidly. The top floor panel failed first and was followed by the failure of the first floor slab. A sway mechanism developed in the frames as failure took place along the diagonal cracks in the shear walls. The complete failure patterns can clearly be seen in plates (7.7), (7.8) and (7.9). In plate (7.7), the diagonal failure pattern of a shear wall of structure 13 can be seen at point A. The inside view of this pattern is also shown in plate (7.8) as AEF. The cracks in a first storey column are shown as B and C in plate (7.7). "D" refers to the failure pattern of the top floor slab in the same plate. This pattern, however is not clearly seen. A similar failure pattern also took place in structure 14 as shown by AB in plate (7.9), while CDEF refers to the bottom storey sway mechanism of one of the frames.

A typical bending/shear failure was observed in the singly reinforced shear wall of structure 15, with the floor slabs and doubly reinforced shear wall having diagonal cracks. The intermediate frames failed in the usual sway mechanism. The failure load of this structure was 10.14 kN. In structure 16, the outermost frame substituting one of the shear walls failed first by a sway mechanism. The other components of this structure showed a failure pattern similar to structure 15 and the ultimate failure took place at a load of 6.16 kN.
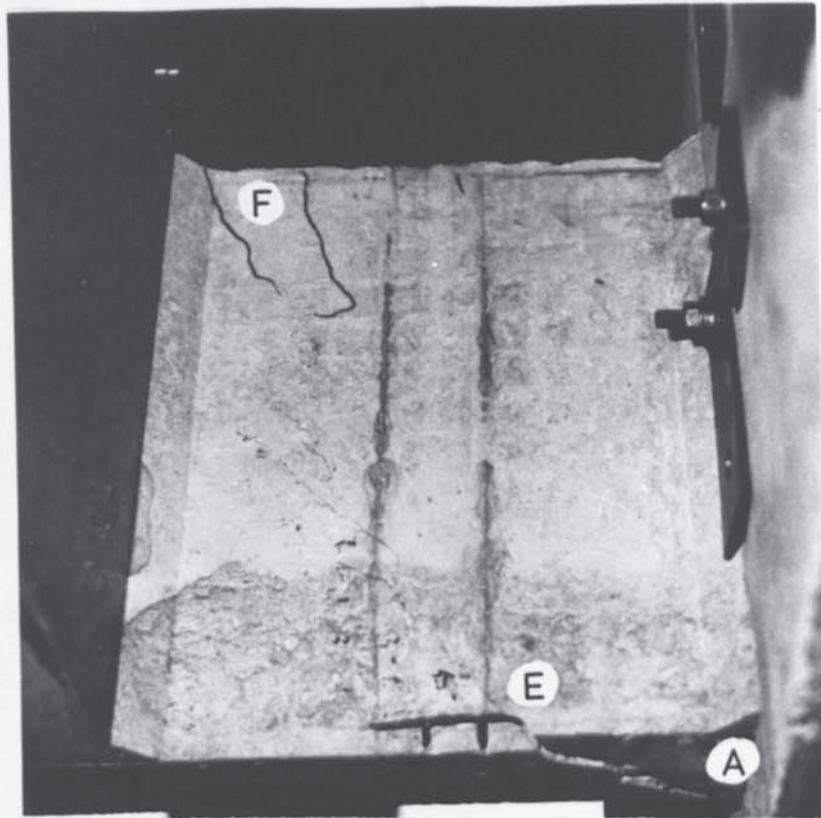
PLATE 7.8: DIAGONAL FAILURE PATTERN
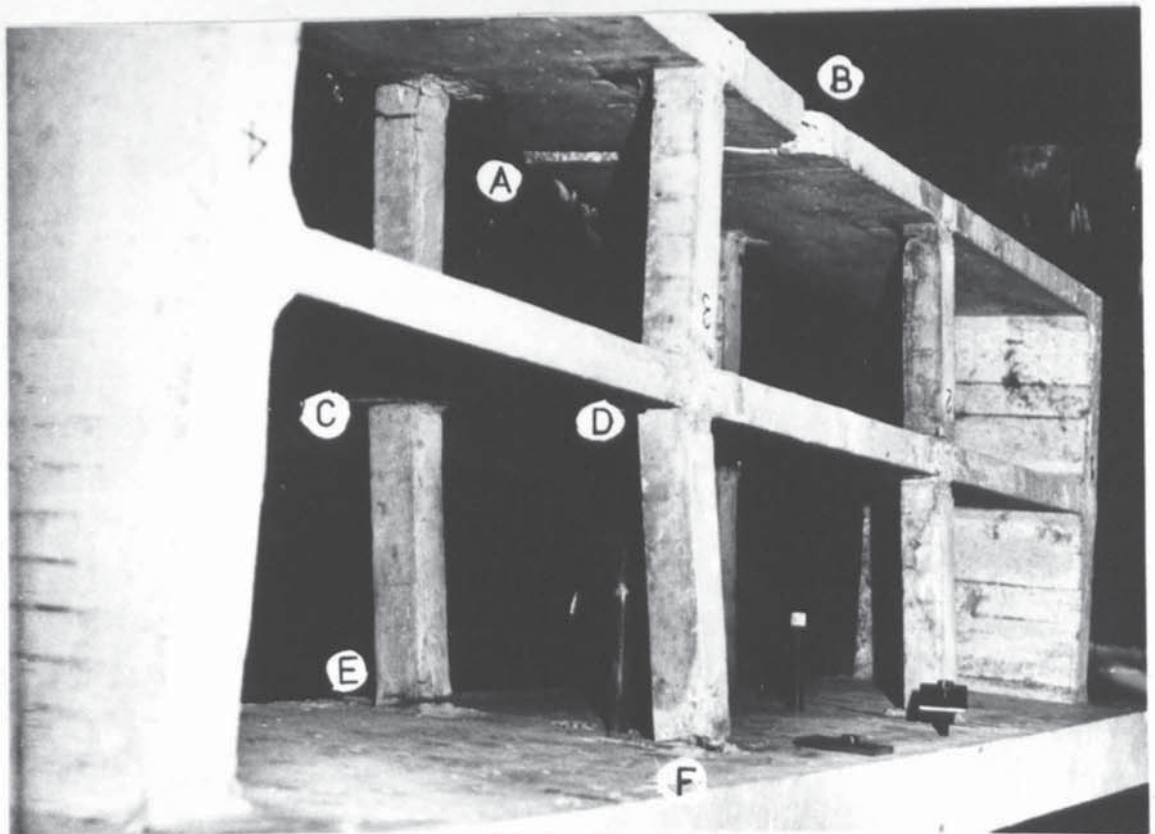IN A SHEAR WALL OF STRUCTURE 13

PLATE 7.9: STRUCTURE 14 AFTER FAILURE

CHAPTER 8

COMPARISON OF EXPERIMENTAL AND ANALYTICAL

RESULTS AND ANALYSIS OF PRACTICAL STRUCTURES

8.a   Introduction

A number of experiments carried out to test the computer
program for the analysis of complete structures, described in
chapter 6 were discussed in chapter 7. The results of the test
structures with no intermediate frames are given in chapter 5 and
compared with the analytical results there. The rest of the
results are discussed here in this chapter. Once the validity of
the analytical approach is established this chapter is concluded
by the analysis of a number of complete practical type structures.
These are either four storey or six storey structures. The effect
of composite action on the load carrying capacity and on the order
of formation of plastic hinges and cracks is also studied and
conclusions are drawn.

8.b   Analysis of Single Storey Structures with Intermediate
       Steel Frames:

Details of these structures are given in table (7.2). The
theoretical and experimental failure loads are compared in table
(8.1). The structures were analysed by the computer program
given in chapter 6 section b. Two different types of analysis
were carried out for most of the structures. The first assumed
bilinear moment-curvature relationship for the grillage while
the second assumed a trilinear relationship. In the bilinear
approximation, it was assumed that a panel of the grillage keeps
its initial stiffness constant; until the ultimate stage is
detected by the use of the interaction equations (5.e.20) or (5.e.23).

Structure No.	Experimental failure load (kN)	Theoretical Failure Loads				Remarks
		Bilinear Moment-Curvature Approx.		Trilinear Moment-Curvature Approx.		
		Result (kN)	% difference	Result (kN)	% difference	
5	2.400	2.475	+3.03%	2.622	+8.46%	two steel frame
6	2.610	2.732	+4.46%	-	-	"
7	3.023	2.992	-1.05%	3.205	+5.68%	"
8	4.052	3.927	-3.10%	4.025	-0.72%	"
9	3.919	3.937	+0.35%	4.041	+3.00%	"
10	9.794	9.641	-1.56%	9.641	-1.56%	three steel frames

TABLE 8.1 : EXPERIMENTAL AND THEORETICAL FAILURE LOADS FOR ONE STOREY STRUCTURES WITH STEEL INTERMEDIATE FRAMES

In the trilinear approximation, the initial flexural rigidity remains constant until the stress at the outermost fibres of a section reaches the rupture strength of the concrete and cracks begin to develop. After that the stiffness of the section reduces considerably and the new flexural rigidity $(EI)_c$ of the cracked section does not change until ultimate failure is detected by one of the above interaction equations. The method for calculating $(EI)_c$ is given in chapter 3. As the ultimate stage is reached, the value of EI is again reduced drastically.

A maximum discrepancy of 8.46% was obtained between the theoretical and the experimental failure loads. This was for structure 5 with a trilinear M-C curve. The rest of the analytical results are even closer to the experimental values. These results show that the method for the failure load analysis of complete structures presented in chapter 4 and the interaction equations of bending, torsion and shear, given in chapter 5 predict the actual behaviour of complete structures in a realistic manner.

As an example, the analysis of structure 9 will be discussed here in detail. The structure and loading are both symmetrical as shown in figure (8.1). The experimental and the theoretical load-deflection curves for this structure are also shown in this figure. The floor and the shear walls are 40mm thick. They are 605mm high and 200mm deep, the reinforcement is a 25.4mm square steel mesh placed in the middle of the cross section. The yield stress, the yield strain and the ultimate strain of this mesh were found experimentally to be 0.761 kN/mm², 0.00365 and 0.0066 respectively. The two intermediate frames are made from 19.05mm

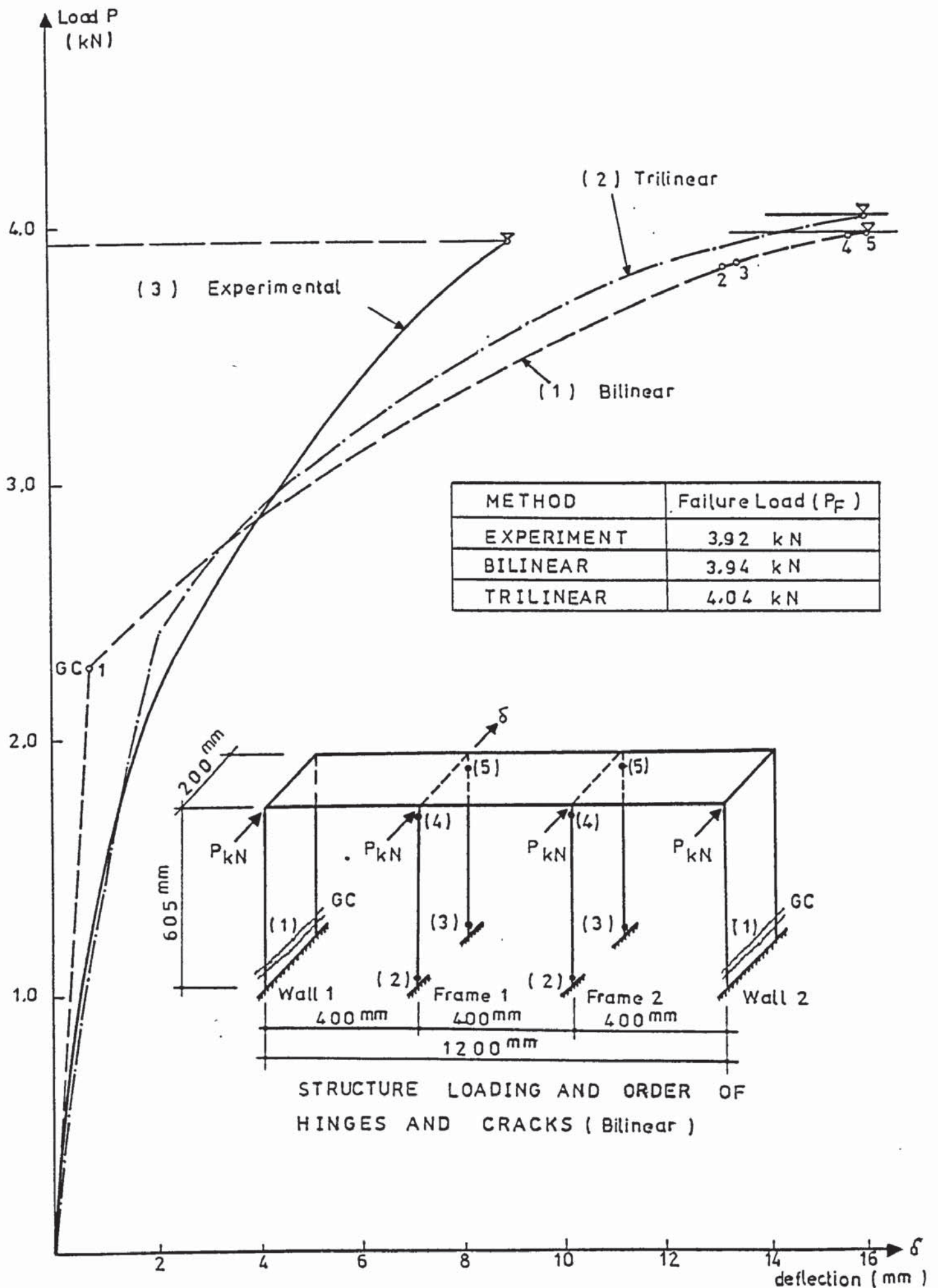| METHOD	Failure Load (P_F)
EXPERIMENT	3.92 kN
BILINEAR	3.94 kN
TRILINEAR	4.04 kN

FIGURE 8.1- COMPARISON OF THEORETICAL AND
EXPERIMENTAL LOAD-DEFLECTION
GRAPHS OF TEST STRUCTURE 9

x 19.05mm square black mild steel bars. The modulus of elasticity
and the yield stress for these bars are 213 kN/mm^2 and 0.28kN/mm^2
respectively. The concrete used in the construction of the
grillage had a modulus of elasticity E_c = 26.32 kN/mm^2 and 150mm
diameter cylinder crushing strength fcu = 0.0261 kN/mm^2.

There are three load-deflection curves in figure (8.1).
Curve 1 was obtained theoretically by assuming that the moment-
curvature diagram of the panels is bilinear. Curve 2 was also
obtained theoretically by employing a trilinear representation of
the M-C diagram of the panels while curve 3 was obtained
experimentally.

In the analysis assuming the bilinear M-C relationship, the
shear walls failed first at their base at a load P_1 = 2.28 kN.
The points were P are applied are shown in the figure. The
stiffness of these walls were then reduced to 1% of their initial
value but the overall failure of the structure did not take place.
For the applied load P > 2.28 kN, large loads were transmitted to
the frames and plastic hinges 2, 3, 4 and 5 developed in both
frames at loads P_2 = 3.84 kN, P_3 = 3.86 kN, P_4 = 3.93 kN and
P_5 = 3.937 kN respectively. Every time a hinge developed, the
loads transmitted to the frames and the grillage were recalculated.
As soon as the last hinge developed in the frames, the structure
failed by sway mechanism in the frames.

The analysis assuming trilinear M-C relationship need not be
discussed in great detail. However it can be seen from figure
(8.1) that this slightly improves the theoretical load-deflection
diagram but not the predicted value of the failure load. The
experimental failure load was 3.92 kN; the bilinear approach gave
$P_{bilinear}$ = 3.937 kN with a relative difference of only 0.35% over

the experimental. On the other hand the trilinear failure load was 4.04 kN and a difference of 3% with the experimental.

Notice, in the diagram shown in figure (8.1) and on the theoretical curves, the numbers (1), (2), (3) etc., refer to various critical stages obtained analytically during the loading process. Thus the number (1) indicates that the grillages failed by crack development. The numbers (2), (3), (4) and (5) indicate the order of the plastic hinges in the steel frames.

8.c Single Storey Structures with Reinforced Concrete Frames:

As a second group of examples, the single storey test structures 11 and 12, which contained three reinforced concrete intermediate frames, are discussed. The general dimensions of these structures are shown in figure (8.2). The shear walls and the floor slabs are 40mm thick. The reinforcement is 25.4mm x 25.4mm square mesh which is made out of 2.55mm diameter steel bars and placed in the middle of the cross section. A typical cross-section of the columns is shown in figure (8.3). The columns are directly connected to the floor slabs, which are acting as large beams against out of plane bending. The maximum breadth of such a beam was considered to be the distance between two neighbouring frames. The effect of this assumption will be discussed later and some conclusions will be drawn. The moment-curvature diagrams of the shear walls, slabs and frame sections were calculated by means of the method given in chapter 3, section h, in conjunction with the method described in chapter 5.

As an example, the analysis of structure 12 will be given here in detail. The data obtained from the control tests is as follows:
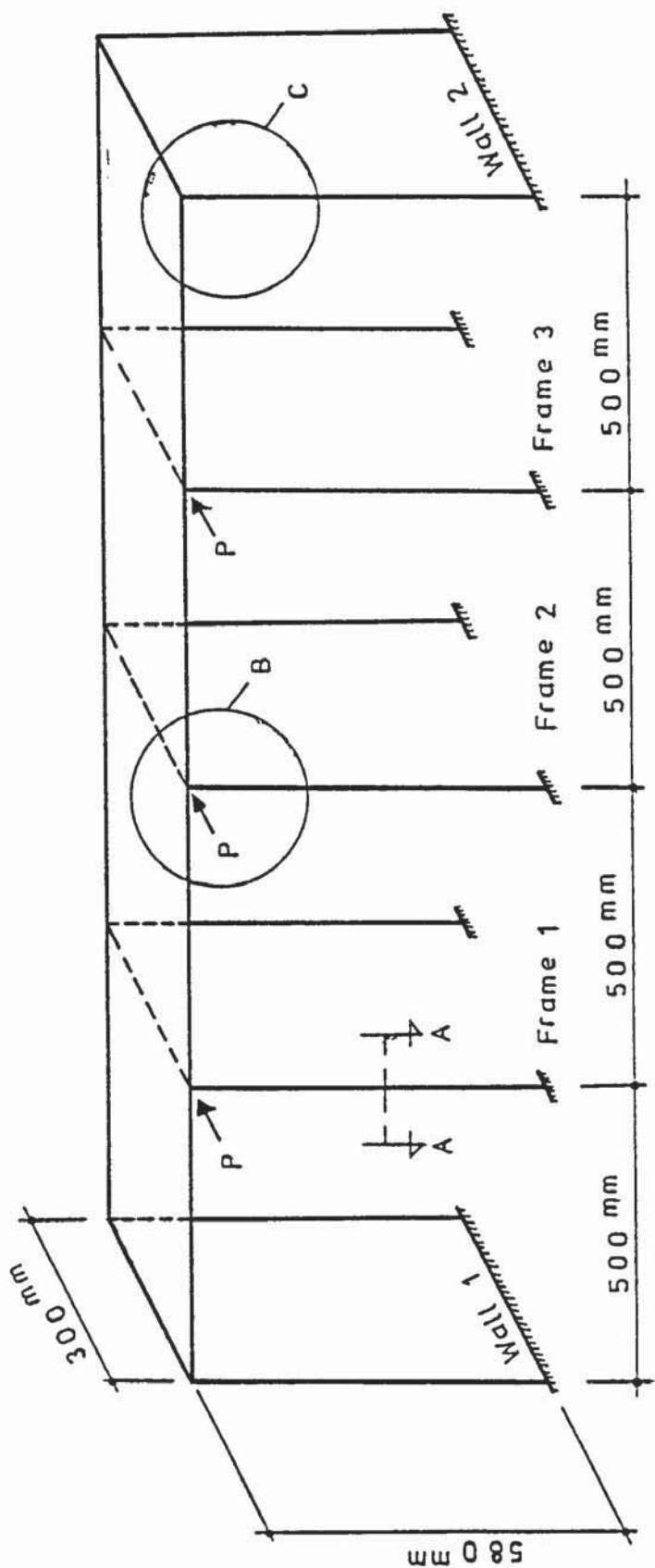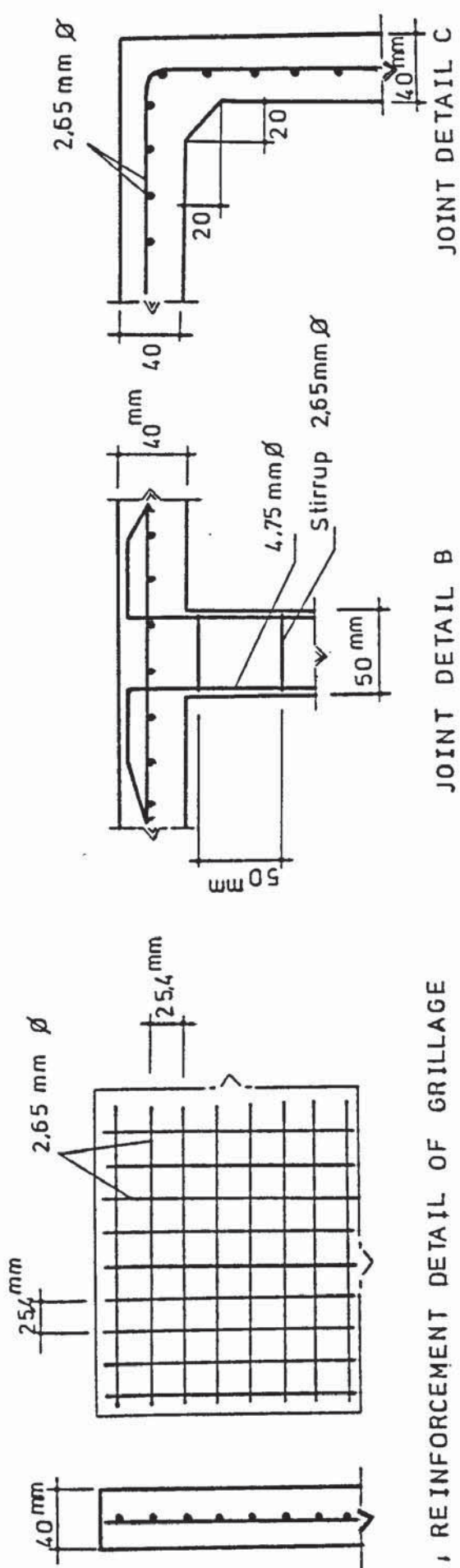
2,65 mm ⌀

JOINT DETAIL C

40 mm

20

20

40

40 mm

4,75 mm ⌀

Stirrup 2,65mm ⌀

50 mm

50 mm

JOINT DETAIL B

2,65 mm ⌀

25,4 mm

25,4 mm

40 mm

REINFORCEMENT DETAIL OF GRILLAGE

C

Wall 2

Frame 3

500 mm

P

Frame 2

500 mm

B

P

P

Frame 1

500 mm

A

A

P

500 mm

Wall 1

500 mm

300 mm

580 mm

FIGURE 8.2: A SINGLE STOREY REINFORCED CONCRETE STRUCTURE
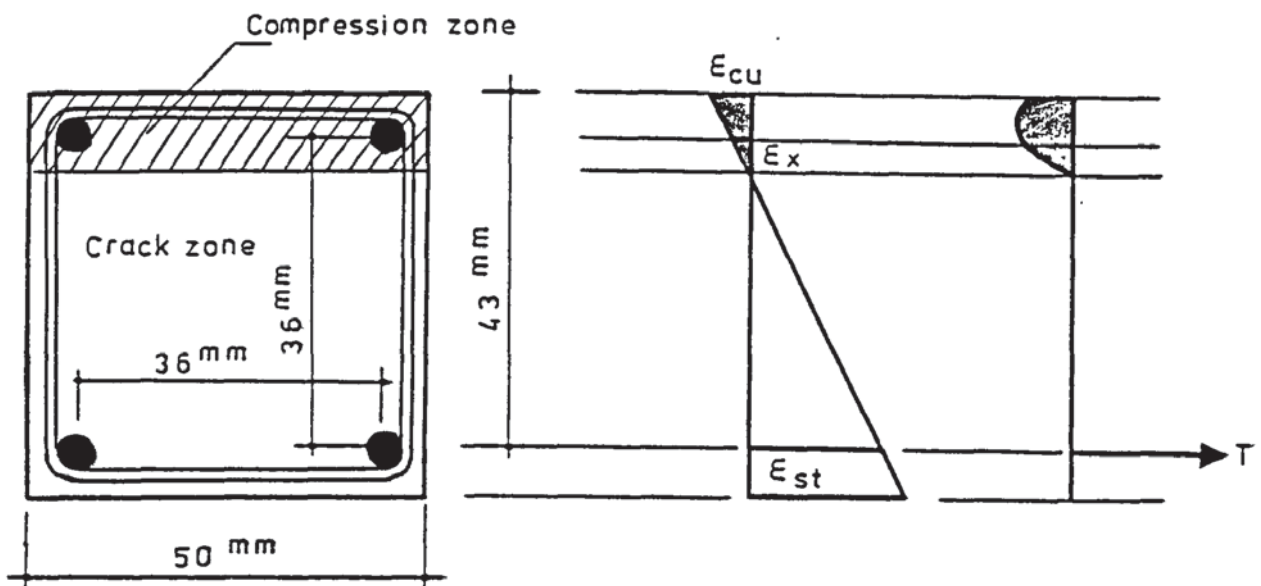
FIGURE 8.3- A TYPICAL REINFORCED CONCRETE
FRAME CROSS SECTION A-A

A - Frame data:-

E_c = 20.5 kN/mm^2

f_{cu} (cylinder) = 0.0272 kN/mm^2

f_{cu} (cube) = 1.25 f_{cu} (cylinder) = 0.0340 kN/mm^2

$f_{rupture}$ = 0.00272 kN/mm^2

E_s = 216 kN/mm^2

Reinforcement: 4.75mm diameter bars at each corner.

The stress-strain diagram of the reinforcement is given in figure (8.4).

B - Grillage data:-

E_c = 24.0 kN/mm^2

f_{cu} (cylinder) = 0.0292 kN/mm^2

f_{cu} (cube) = 0.0365 kN/mm^2

Although the rupture strength of the concrete was obtained to be 0.003809 kN/mm^2 from the standard rupture tests, the empirical formulae given below[97] may be used more efficiently.

$$fr_{(N/mm^2)} = 0.87 \ (1 + \frac{6450}{d^2})^3 \ \sqrt{f_{cu}(cube)} \qquad 8.1$$

This formulae for f_r relates empirically the rupture strength to the ultimate crushing strength with respect to beam depth. For the grillage panels used in this structure d = 300 mm.

Thus f_r = 3.09 N/mm^2 = 0.00309 kN/mm^2

The moment-curvature diagram of the column cross-section in figure (8.3), is shown in figure (8.5) and constructed as follows. The initial flexural rigidity $(EI)_i$:

$$I_i = \frac{50 \times 50^{-3}}{12} + 4 \times \frac{216}{20.5} \times \frac{4.75^{-2} \times \pi}{4} \times (\frac{36}{2})^2 = 762814.7 \ mm^4$$

and therefore $(EI)_i$ = 15627702.12 kN×mm^2

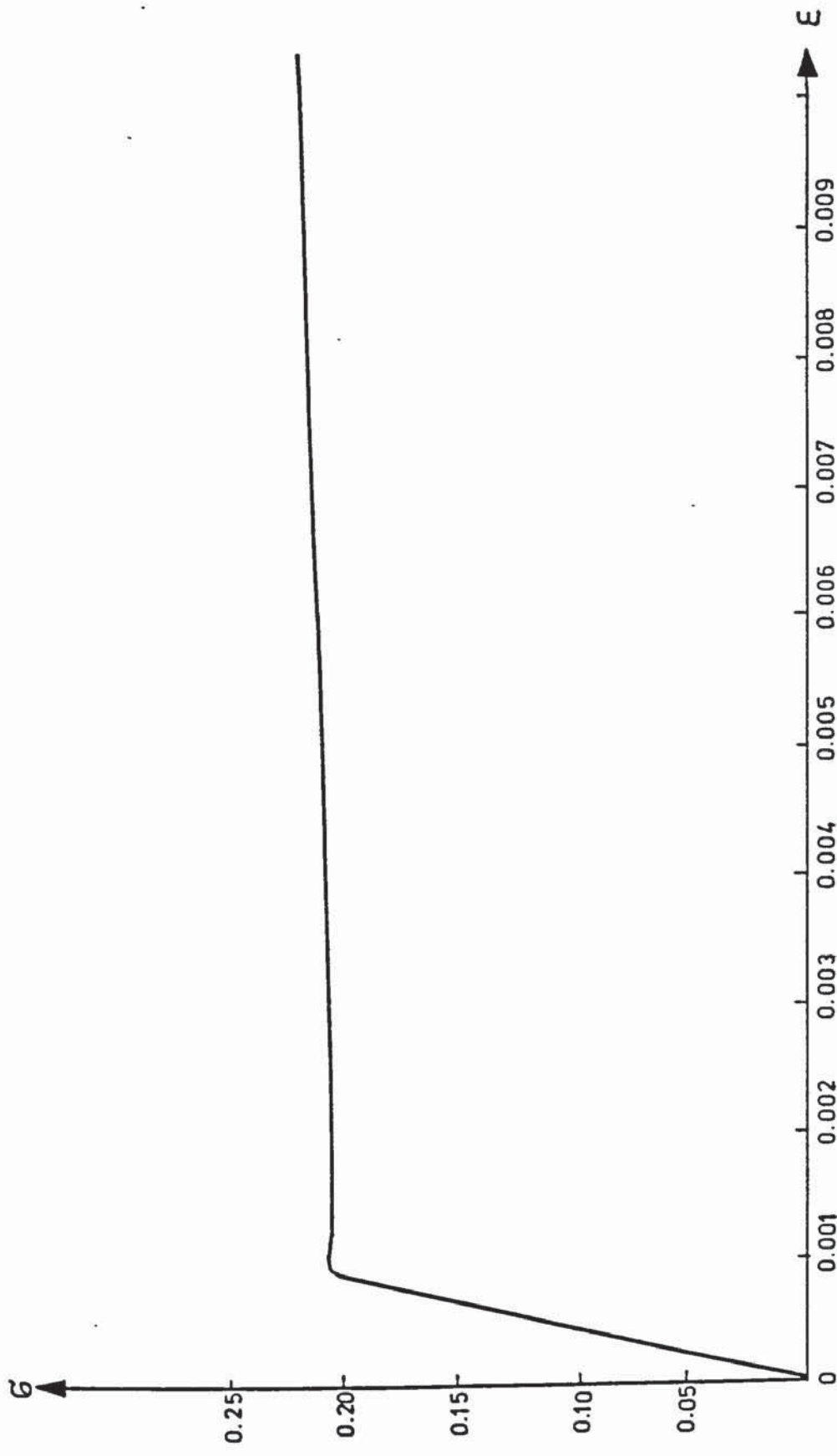The percentage tensile reinforcement = r = 1.4176%.

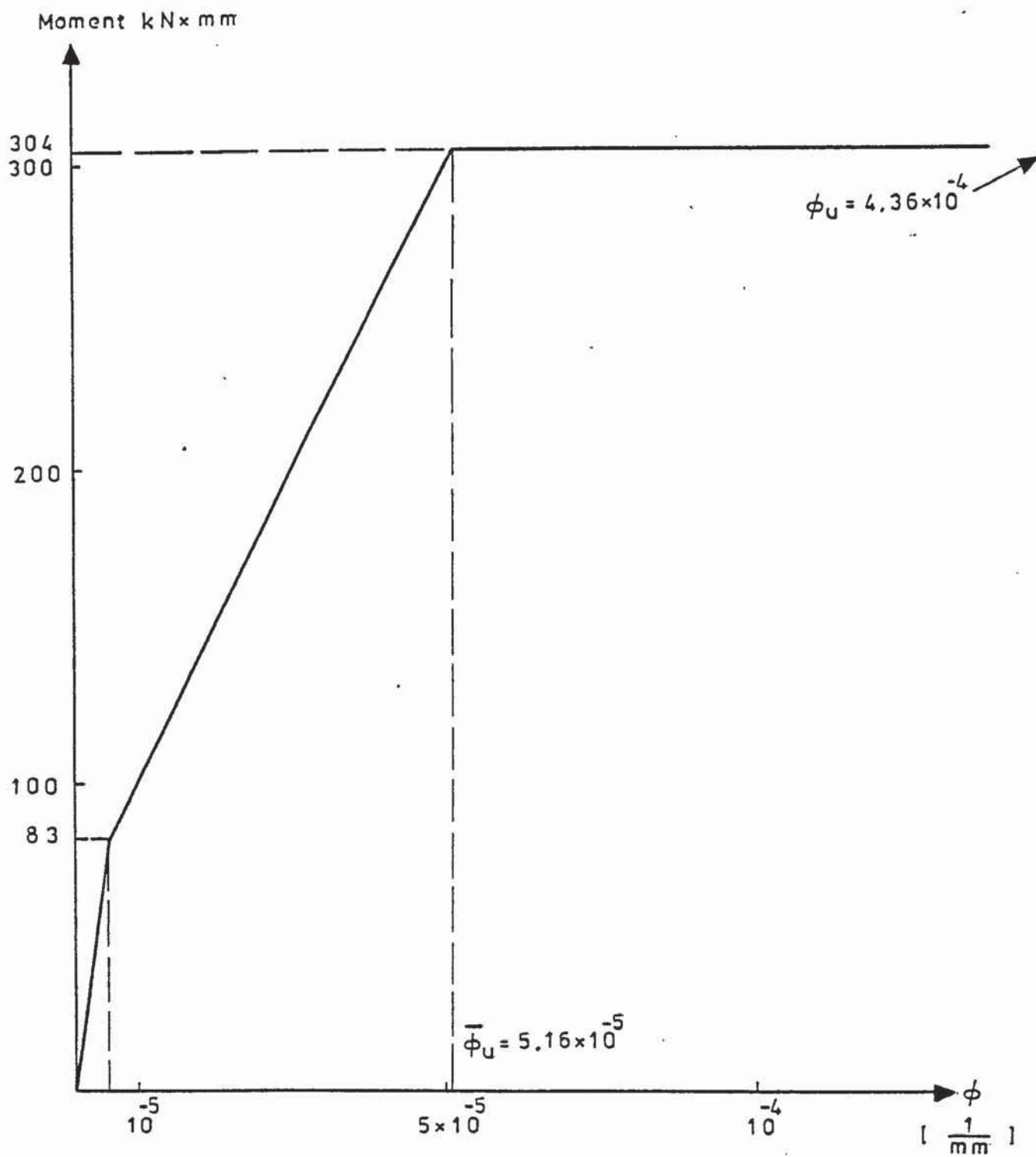FIGURE 8.4: STRESS STRAIN DIAGRAM FOR FRAME REINFORCEMENT
FOR TEST STRUCTURE 12

FIGURE 8·5: M–C DIAGRAM FOR THE COLUMNS OF
TEST STRUCTURE 12

The flexural rigidity $(EI)_c$ was obtained from equation (3.10)

as $(EI)_c = 4776051.0$ kNxmm^2.

The cracking moment was obtained from equation (3.8)

as $M_c = 83$ kNmm.

Calculation of ultimate moment:

From equations (3.12), (3.13) and (3.14) the properties of concrete compressive stress distribution at the ultimate state were obtained as

$$\beta_1 = 0.451, \beta_2 = 0.581 \text{ and } \varepsilon_{cu} = 0.0034$$

Using equations (3.16) and (3.18) the depth of the neutral axis and the strain at the outermost compression fibre were obtained iteratively as follows:

$$X = \frac{2 \times 17.72 \times A_S \ f_m}{0.581 \times 34 \times 50}$$

and

$$\varepsilon_S = 0.0034 \ \frac{43-x}{x}$$

Assume $X_{(1)} = 20$mm $\therefore \varepsilon_S = 0.00391$
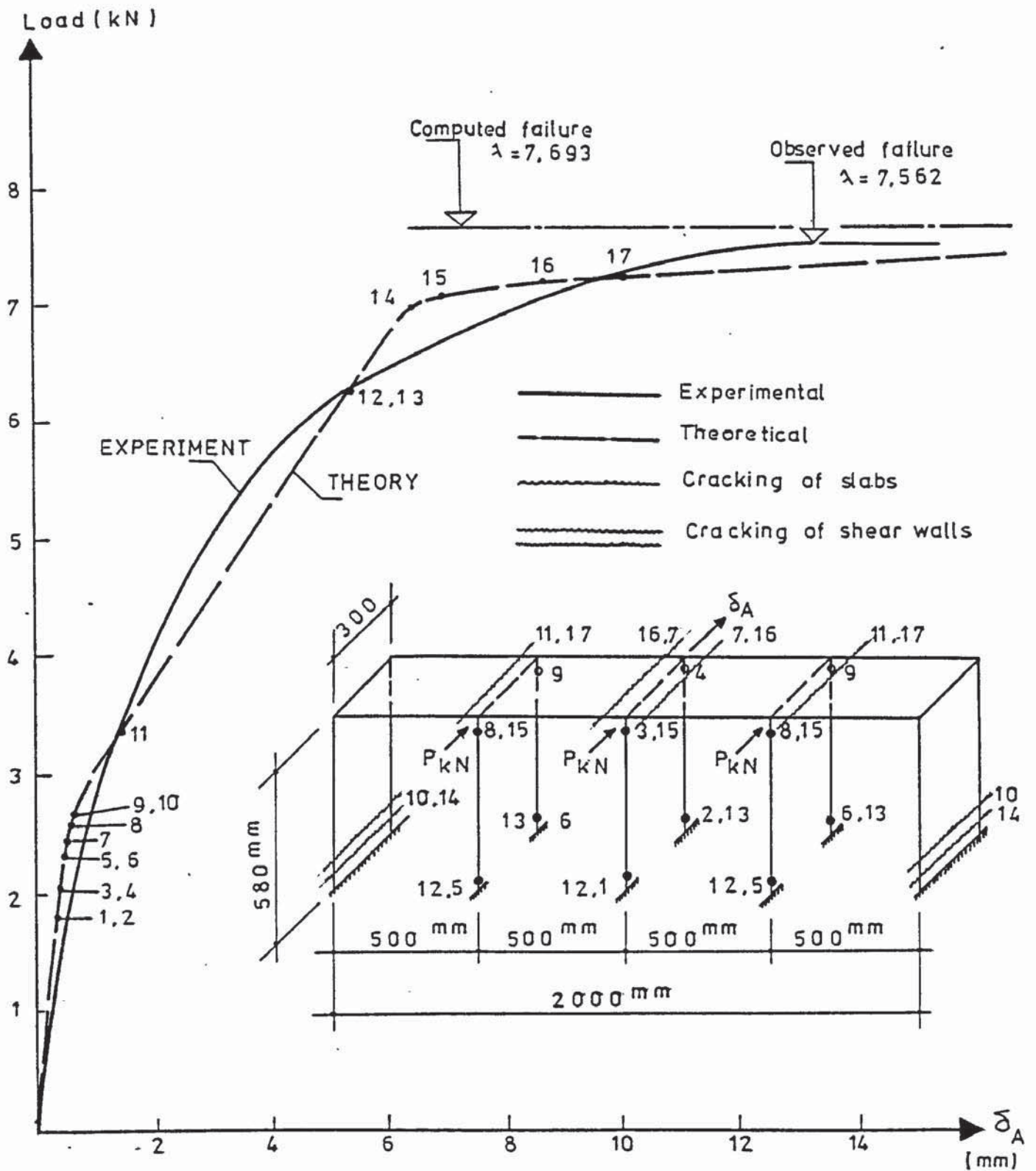
The corresponding force in steel was obtained from the stress-strain graph of figure (8.4) as $A_S f_m = 7320$ N. Hence $X_{(2)} = 7.411$mm. This value was then used to calculate the strain in the tensile reinforcement as $\varepsilon_S = 0.016327$, thus $A_S \ f_m = 7700$ N. Using equation (3.16)

$X_{(3)} = 7.796$mm $\therefore \varepsilon_S = 0.01535$ and $A_S \ f_S = 7700$ N which gives $X_{(4)} = 7796$mm. Because $X_{(4)} = X_{(3)} = 7.796$mm the iteration was stopped and the ultimate moment was obtained from equation (3.19) as:

$$M_u = 7.700 \ (43-7.8 \times 0.451) = 304.0 \text{ kNmm}.$$

The curvatures ϕ_c, $\overline{\phi}$ and ϕ_u were obtained from equations (3.9), (3.22) and (3.20) as:

FIGURE 8·6: EXPERIMENTAL AND THEORETICAL
LOAD-DEFLECTION DIAGRAMS OF
TEST STRUCTURE 12

$\phi_c = 5.31 \times 10^{-6} (1/\text{mm})$; $\overline{\phi}_u = 5.16 \times 10^{-5} (1/\text{mm})$ and $\phi_u = 4.36 \times 10^{-4} (1/\text{mm})$. The moment-curvature diagram of the effective parts of the slab acting as beams was also constructed similarly.

The moment-curvature diagram for the shear walls and the slab was automatically constructed within the computer program. However the value of "γ" was calculated by the use of equations (5.b.15), (5.b.16) and (5.c.4) to be 0.865 and fed into the computer. The cracking moment and the flexural rigidity were also precalculated from equations (3 . 8) and (3. 10) as 1722.6 kNxmm and 243618524.0 kNmm and fed in. Using this information, the M-C diagram of each panel was constructed by the computer according to the state of loads acting on the panel. Each time the forces acting on the members were calculated, the corresponding M-C diagrams were constructed and used in the current iteration.

Having prepared the necessary data, the structure was analysed by the computer program of chapter 6, section b. The analytical and the experimental load-deflection curves are shown in figure (8.6) together with a sketch of the structure indicating the locations and the order of the critical points.

The structure has failed theoretically at a load of 7.693 kN which is 1.7% higher than the observed failure load of 7.562 kN, obtained experimentally.

To investigate the influence of the effective width of the beams on the value of the theoretical failure load, structure 11 was analysed for various assumed beam widths. These varied between 80mm and 400mm. The value of 80mm was calculated according to the draft unified code of practice CP110 1972. The results of this investigation are presented in figure (8.7) where it can be
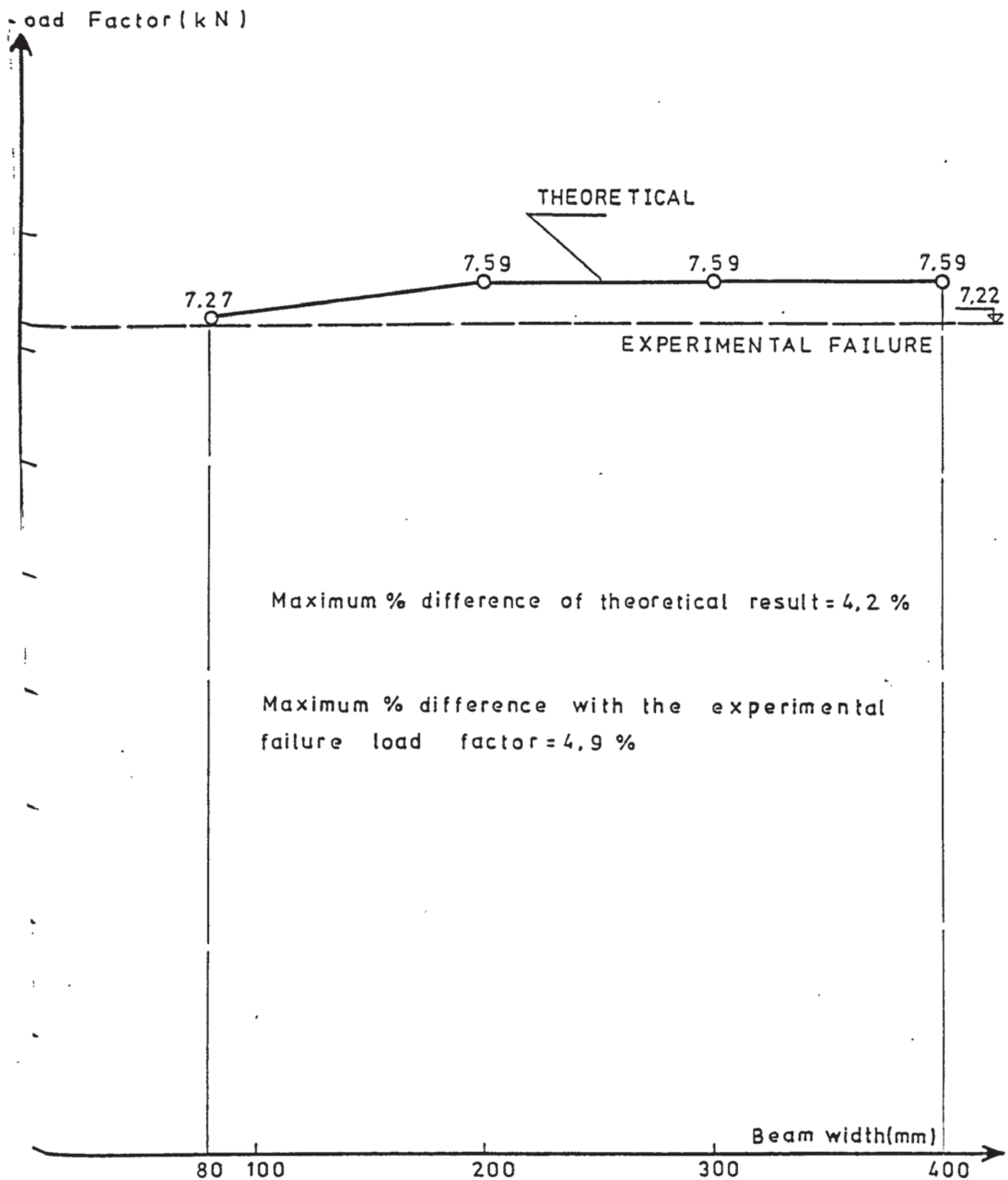
FIGURE 8·7 : VARIATION OF FAILURE LOAD OF TEST
STRUCTURE 11 WITH VARIOUS ASSUMED
BEAM WIDTHS

Theoretical Failure
$\lambda = 7,270$ kN

Experimental Failure
P = 7,223 kN

Theoretical Curve

Experimental Curve

δ_A

A

P   P   P
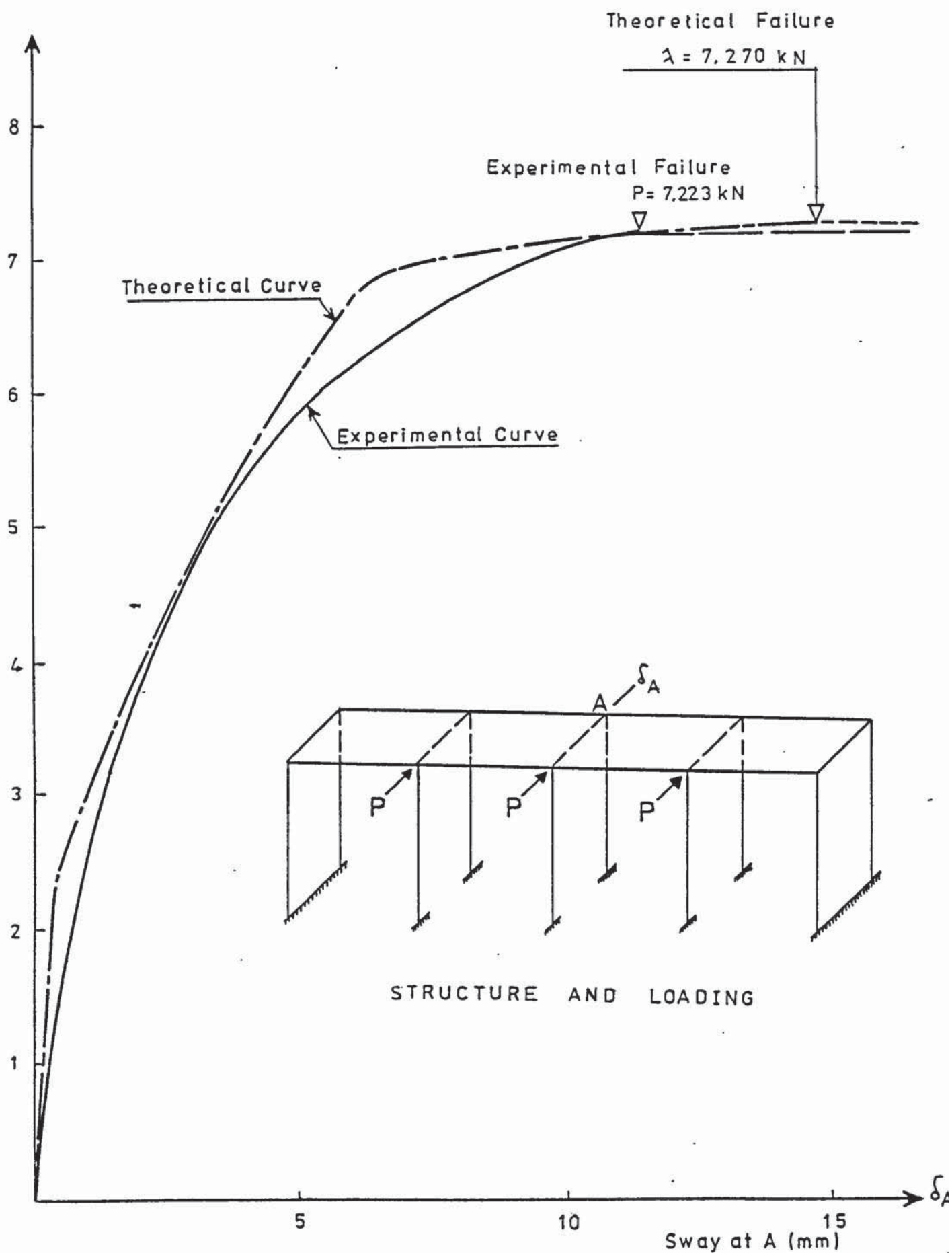
STRUCTURE   AND   LOADING

Sway at A (mm)

δ_A

FIGURE 8.8: COMPARISON OF THEORETICAL AND
EXPERIMENTAL LOAD-DEFLECTION
CURVES FOR TEST STRUCTURE 11

seen that the failure load is not very sensitive to the variations
in the beam width. A maximum discrepancy of 4.2% was obtained
between the two extreme cases. The load-deflection diagrams did
not show any significant change and were almost matching on each
other. The load-deflection diagram obtained for the beam width
of 80mm and that obtained experimentally, are shown in figure (8.8).
The theoretical failure load was predicted to be 7.270 kN, being
0.65% higher than the experimental failure load of 7.223 kN.

8.d Two Storey Structures:

The computer program of chapter 6, section b was further
tested by two storey experimental structures 13, 14, 15 and 16.
These consisted of 40mm thick slabs, 60mm thick shear walls and
reinforced concrete frames with the same cross-section as in
structures 11 and 12. The general dimensions and specifications
for these structures are given in figure (8.9) and table (7.4)
respectively. During the computer analysis, each member of a
frame was divided into three submembers in order to improve the
accuracy of the analysis. The M-C diagrams for these structures
were obtained in the same manner as that for structures 11 and 12.
The theoretical and experimental load-deflection curves of structures
13 and 14 are shown in figures (8.10) and (8.11). The order of
development of various critical points in the structures are shown
by numbers at the locations where they develop and on the graphs.

It can be seen in figure (8.10) that the theoretical load-
deflection curve of structure 13 is steeper than the experimental
curve, up to a load of 11.95 kN. The curve then bends, flattens
considerably and is fairly linear until the structure fails
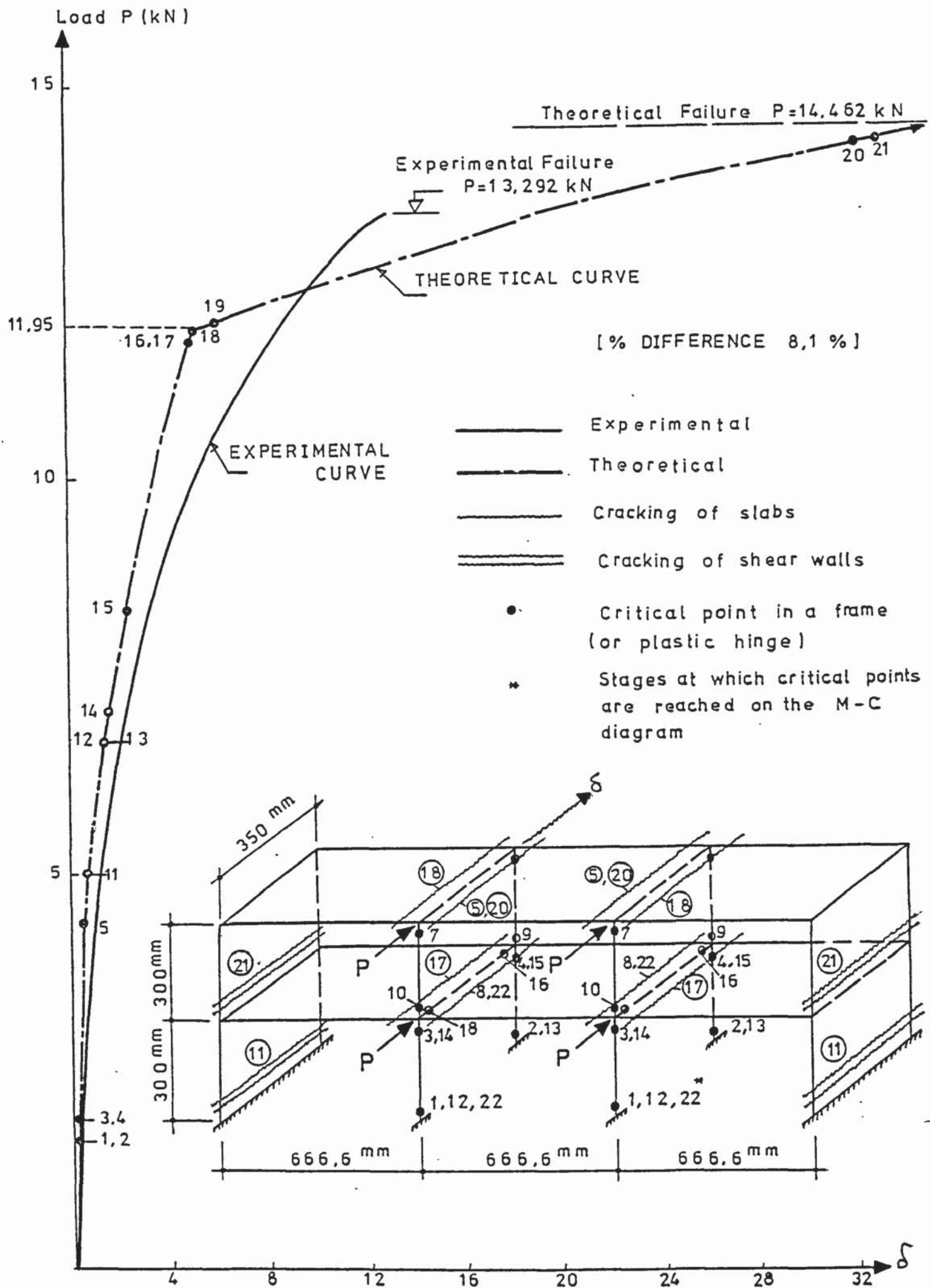theoretically at a load P = 14.462 kN per junction. This is 8.1%

FIGURE 8.9: GENERAL DIMENSIONS OF TWO STOREY STRUCTURES

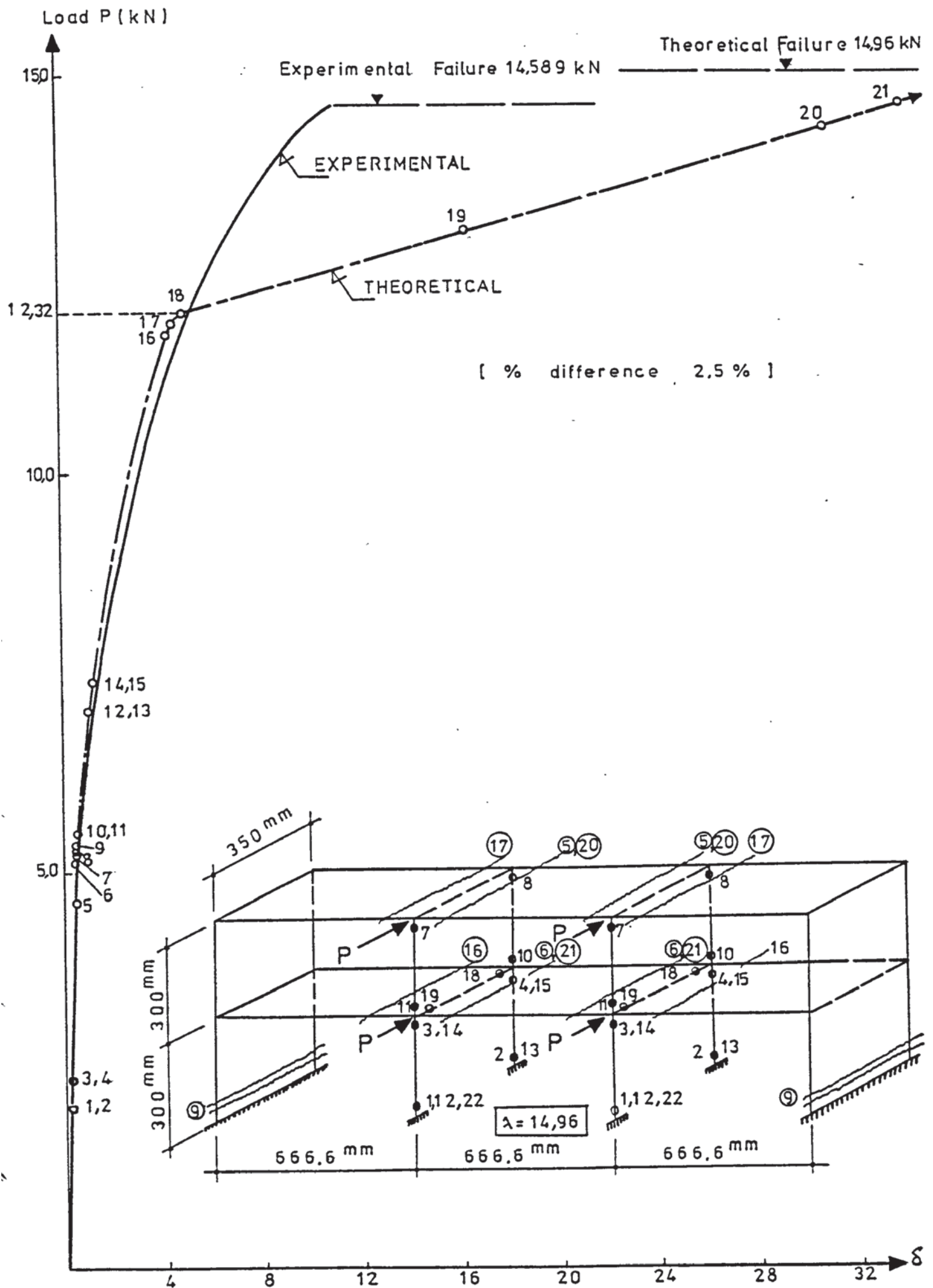FIGURE 8.10: EXPERIMENTAL AND THEORETICAL LOAD-DEFLECTION CURVES FOR STRUCTURE 13

FIGURE 8.11: THEORETICAL AND EXPERIMENTAL LOAD-DEF_
LECTION CURVES OF STRUCTURE 14

higher than the experimental failure load of 13.292 kN.

In figure 8.11, the theoretical and the experimental load deflection diagrams for structure 14 are shown together with the order in which critical points developed in this structure. Theoretically, the first development was the formation of cracks at the top and bottom of all the columns of the ground floor. These are numbered 1 to 4 in figure 8.11. The middle slab panels cracked next. That in the top floor cracked at either end at a load P = 4.59 kN. The position of the cracks are marked in figure 8.11. That in the first floor (No.6) cracked at P = 5.16 kN. Soon after at P = 5.229 kN the shear walls cracked at their supports (critical point No.8) and later at P = 7.36 kN the top and bottom ends of the columns of the ground floor reached their ultimate moments. Nevertheless, theoretically the structure was nowhere near failure. The analytical results indicated that the top storey columns continued to transmit the loads, not to the base, but from one floor slab to another. Eventually at stage 16 the side panels of the first floor slabs cracked and this was followed by cracks in the second floor at P = 11.75 kN and stage 17.

Up to this stage the theoretical and the experimental load deflection curves almost matched each other. Beyond this stage the theoretical curve lost its steepness, recording excessive deflections as shown in figure 8.11. The dramatic deterioration of the carrying capacity of the structure was exhibited by the development of longitudinal cracks at first floor panels, thus cracks developed due to out of plane bending in these panels which were considered to be acting as the beams of the frames (see stages 18 and 19 in figure 8.11). At stages 20 and 21 the

failure of the top and first floor slabs took place at P = 14.28 kN and 14.53 kN respectively. Soon after, at a load of P = 14.96 kN the ultimate failure of the whole structure took place at stage 22, the "last straw" causing the fracture of the ground floor columns at their fixed ends. The theoretical failure load was 2.5% higher than the experimental value of 14.589 kN.

In the experimental process, the cracks of the floor panels became visible at a load of 9.16 kN. This was followed by the cracking of the shear walls at the bases at P = 10.59 kN. As the loads were further increased to a value of 11.71 kN the cracks at the bases of the columns became visible. Further increments in the loads caused secondary cracks developing in the middle panels of the floors and diagonal cracks in the shear walls. When the last increment of loads was applied (P = 14.589 kN), the rate of creep increased rapidly and some sudden, noisy settlements took place. These were followed by the failure of the top floor panel in the middle. Then, the first floor panel failed. These resulted in an immediate sway failure of the intermediate frames and the failure of the shear walls along inclined cracks indicating that these walls failed by the combined effect of bending, torsion and shear.

In the analysis of structure 15, the top floor slab was the first to crack, at a load of 5.92 kN. The bottom portion of the weaker shear wall was next to crack at a load of 7.55 kN. Then the first storey slab cracked at P = 9.09 this was followed by cracks in the frames and the structure failed when the weaker shear wall reached its ultimate stage at a load of 11.32 kN. The experimental failure load of this structure was recorded as 10.14, being 10.42% lower than the theoretical.

In the case of structure 16, the experimental failure was observed at P = 6.16 kN, due to the failure of the outer frame which replaced one of the shear walls. The single remaining shear wall failing along an inclined crack due to excessive torsion. The theoretical analysis also showed the same failure pattern, indicating the failure load to be 5.36 kN which is 13.1% lower than the experimental value.

8.e Analysis of Practical Structures:

A comparison of the theoretical and the experimental results indicate that the computer program can trace, with sufficient accuracy, the load deflection behaviour of structures up to and including the stage of failure. This is in spite of the fact that reinforced concrete is a material difficult to control. The results were sufficiently encouraging to give the author the confidence to move into the analysis of complete practical structures.

Two groups of such structures were selected. The first were four storey single bay and the second were six storey with two unequal bays. Details of these are now given.

8.e.1 Analysis of Four Storey Structures:

The first group of structures analysed, had 3, 5 and 7 four storey, single bay steel frames. Their grillage consisted of 152.4mm thick reinforced concrete slabs and two 304.8mm thick reinforced concrete shear walls placed at either end. The dimensions, cross sectional properties and the external loads applied to the frames were the same for all the structures. The frames were spaced equally at 9.144mm C-C. As a typical example, the structure with 7 intermediate frames will be discussed here.
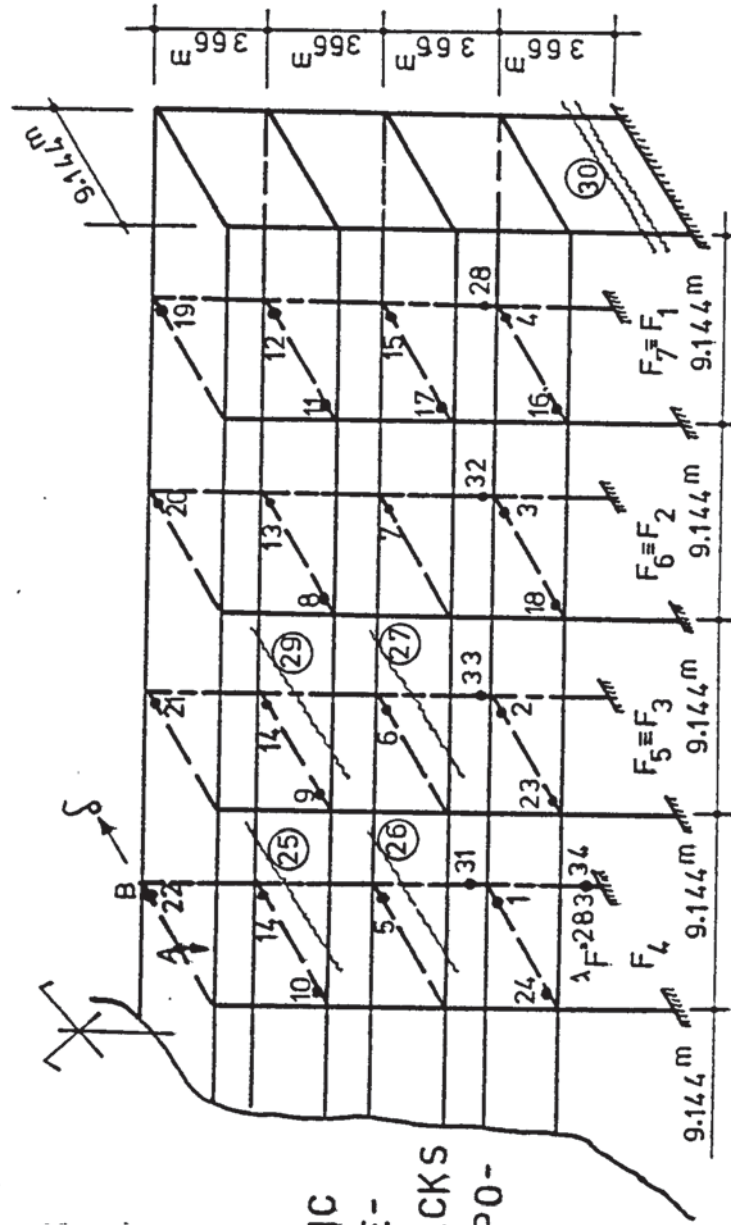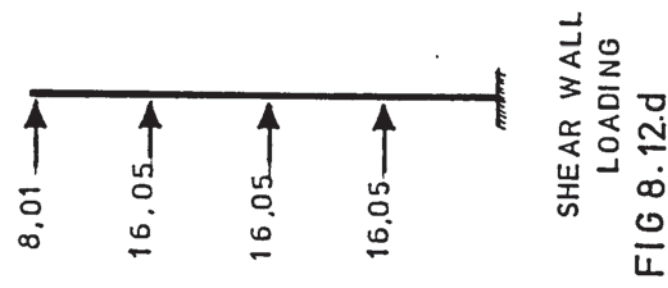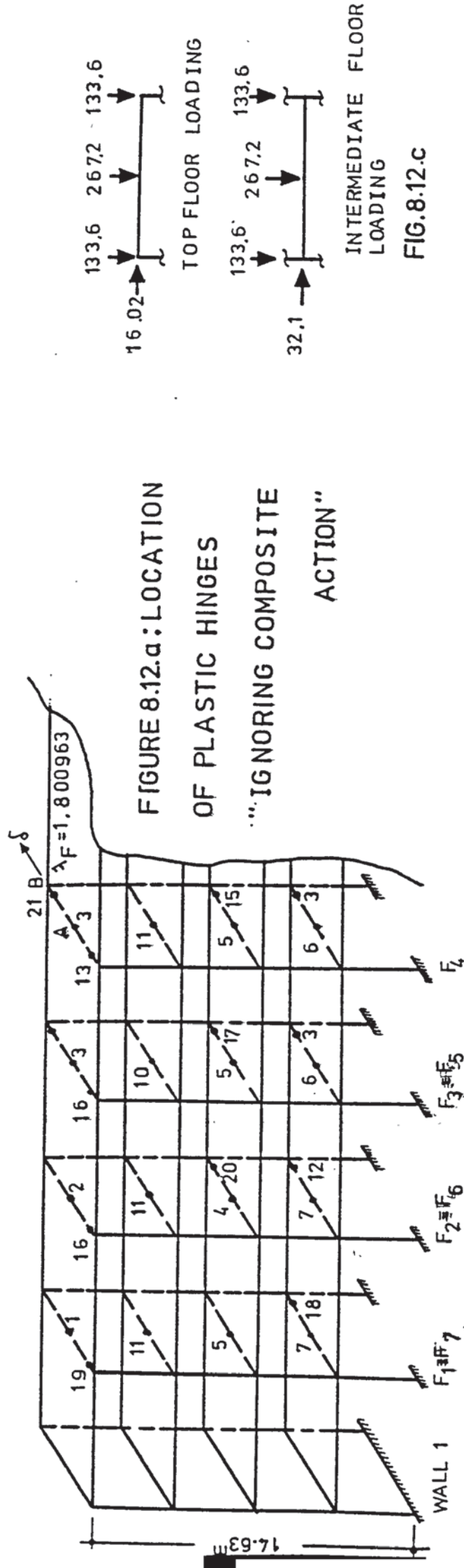
FIGURE 8.12.a: LOCATION OF PLASTIC HINGES "IGNORING COMPOSITE ACTION"

FIGURE 8.12.b: ORDER OF PLASTIC HINGES AND DEVELOPMENT OF CRACKS "CONSIDERING COMPOSITE ACTION"

TOP FLOOR LOADING
FIG. 8.12.c

INTERMEDIATE FLOOR LOADING
FIG. 8.12.c

SHEAR WALL LOADING
FIG 8.12.d

FIGURE 8.12: FOUR STOREY STRUCTURE WITH SEVEN INTERMEDIATE FRAMES

MEMBERS	SECTIONS
BEAMS	406x178x60 UB
GROUND FLOOR COLUMNS	305x305x118 UC
OTHER COLUMNS	254x254x89 UC

TABLE 8.2 : SECTIONS USED FOR THE FRAMES OF THE
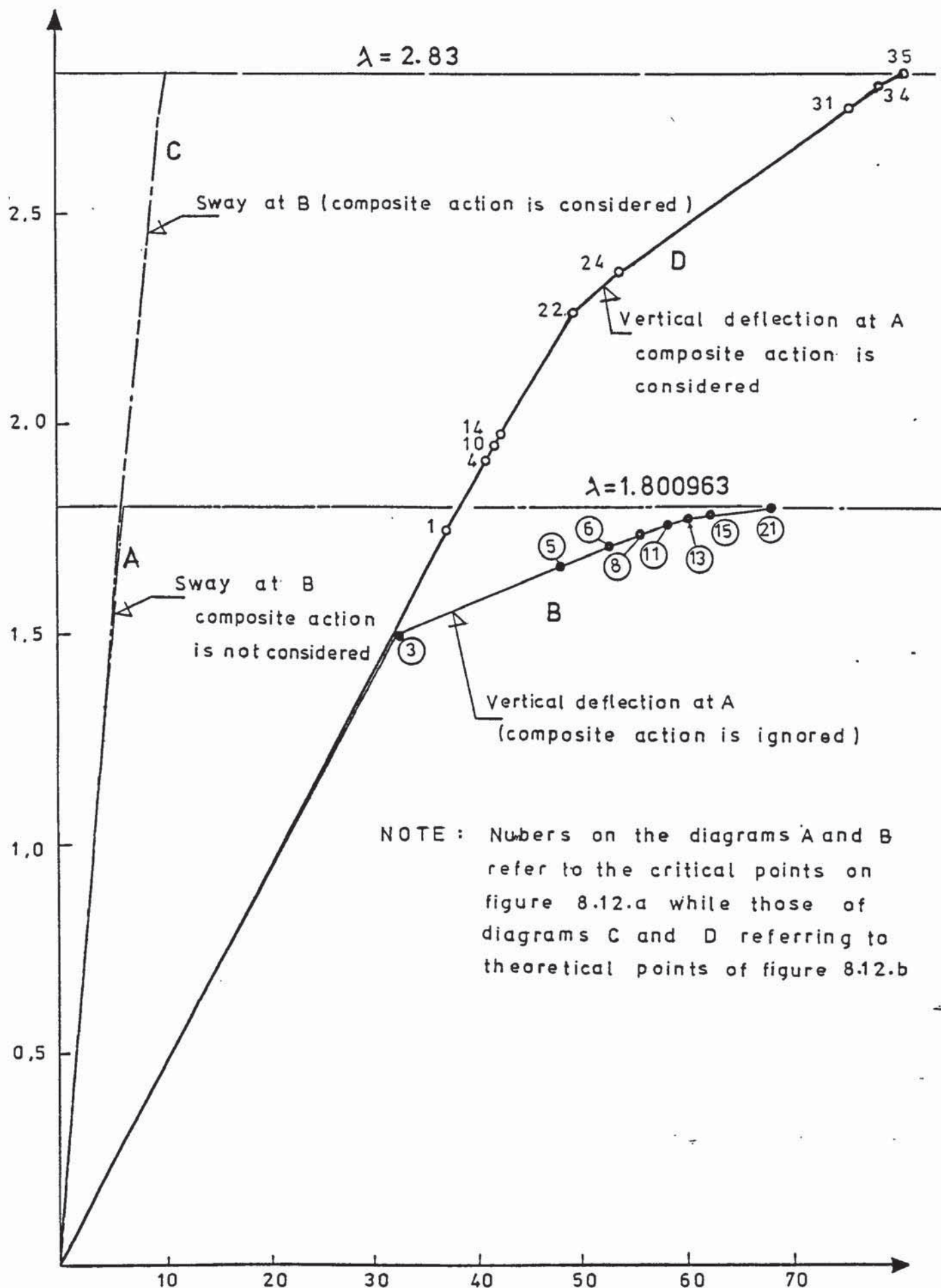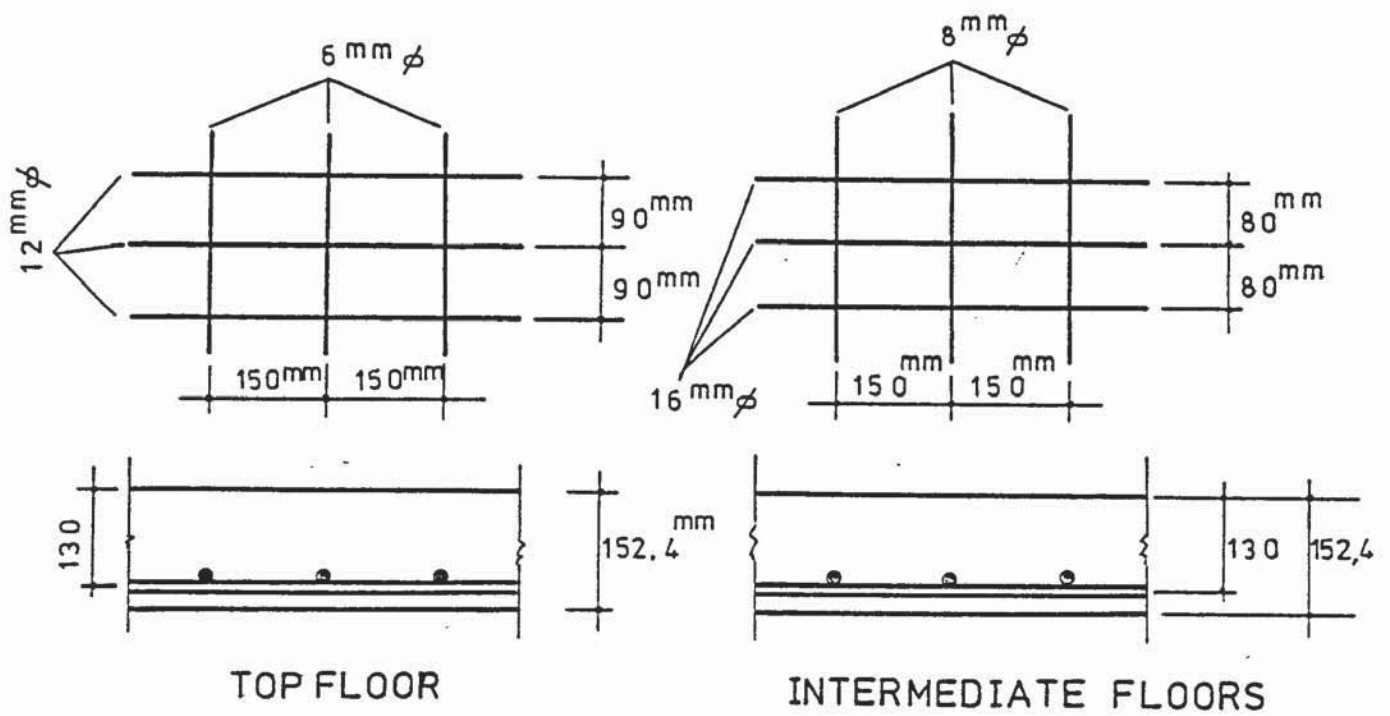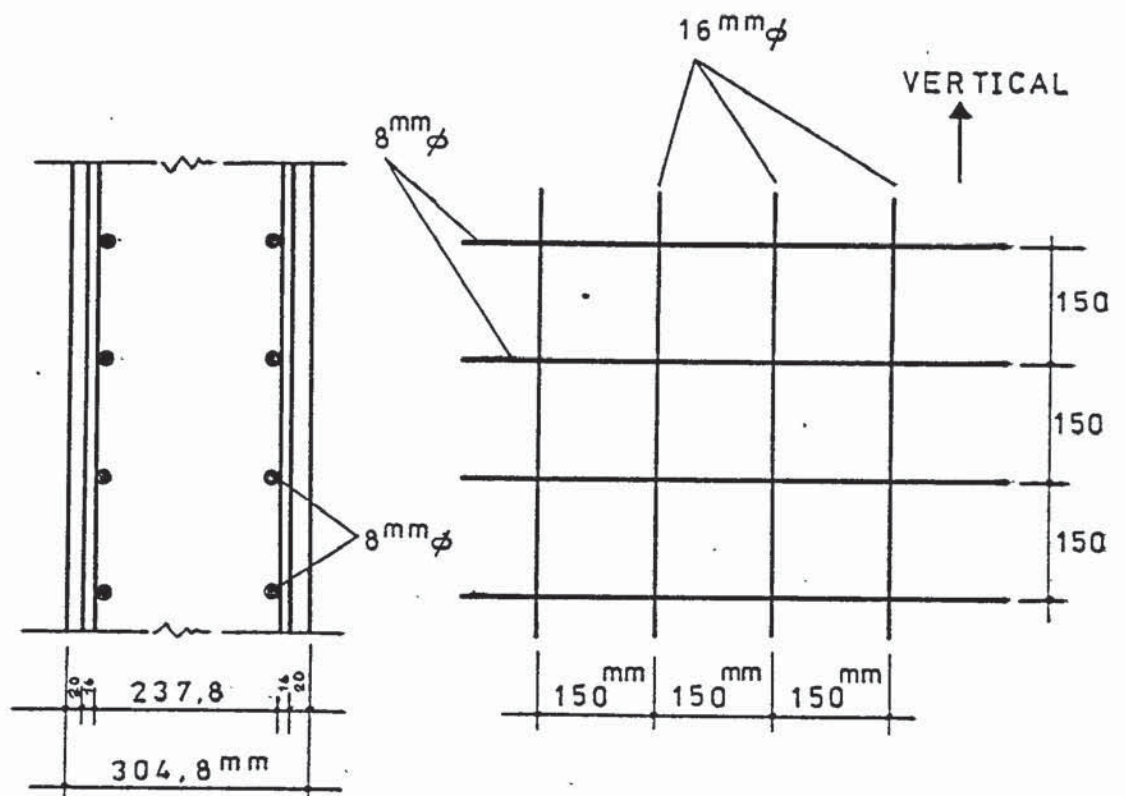FOUR STOREY STRUCTURES

FIGURE 8.13: COMPARISON OF THE LOAD DEFLECTION DIAGRAMS
OBTAINED BY CONSIDERING AND IGNORING THE
COMPOSITE ACTION FOR THE FOUR STOREY
STRUCTURE WITH 7 FRAMES

a-Floor Slabs Reinforcement Design

b-Shear Wall Reinforcement Design

FIGURE 8.14: REINFORCEMENT DESIGN OF FLOORS
AND SHEAR WALLS FOR LARGE
STRUCTURES

This structure is shown in figure (8.12). The slabs and shear walls were designed according to the requirements of CP114. Details of these are shown in figure (8.14).

The ultimate strength f_{cu} and the modulus of elasticity E_c for concrete were taken as 0.0214 kn/mm^2 and 26.3 kN/mm^2. The values of f_y, E, ε_y and ε_u for the reinforcement were 0.25 kN/mm^2, 207.0 kN/mm^2, 0.002 and 0.045 respectively. The frames were made out of universal beams and columns with E = 207.0 kN/mm^2 and f_y = 0.234 kN/mm^2. The cross sectional properties of the sections used to construct the frames are given in table (8.2).

The shear walls and the slabs are deep and lateral loads applied to the structure are comparatively small. To begin with, neglecting the composite action of the slabs, the theoretical analysis showed that failure takes place due to vertical loads causing beam type mechanisms of the frames. This is in spite of the fact that the structure was subjected to wind loads as shown in figure 8.12. Altogether 50 plastic hinges developed in the frames. All of them in the beams. The shear walls and slabs of the grillage all remained elastic. The horizontal and vertical load deflection curves for the top storey of the middle frame (Points B and A in figure 8.12.a) are shown in figure 8.13 as the curves A and B respectively. The order and locations of the plastic hinges are given in figure (8.12.a). The load deflection curves show that the effect of vertical loads dominated the effect of horizontal loads. In fact the horizontal loads were mostly transmitted to the grillage while the frames carried the vertical loads. The loading pattern is shown in figures (8.12.c) and (8.12.d). The structure failed due to simultaneous beam mechanisms

developing at the top storeys of frames 3, 4 and 5 at a combined
load factor of 1.80. This combined load factor is, in fact,
slightly below the failure load factor of a bare frame subject
only to vertical loads. It appears that, if composite action of
the slabs are neglected, it may be fair to design the frames to
carry the vertical loads while the grillage sustains the
horizontal loads only.

The results obtained by the present method are similar to
those obtained by Majid and Önen[31]. This reveals that the
assumption, made by Majid and Önen, that the grillage remained
elastic throughout was correct for these structures. However,
it will be shown later that when the composite action is taken
into account, this state of affairs changes dramatically and
cracking of the grillage plays an important part in the overall
behaviour of complete structures. The results obtained from the
analyses of the four storey structures are summarised in table
(8.3) together with those obtained by Majid and Önen. It appears
that the number of intermediate frames in a structure does not
alter the carrying capacity of the structure considerably.
However, intuition suggests that as the number of frames increase,
the shear walls become less effective and thus failure at lower
loads due to sway may take place.

8.e.2 Analysis with Slab Composite Action:

To study the effect of composite action on the overall
behaviour of these structures, the one with seven intermediate
frames was analysed by considering this effect. The order of
hinges and cracks in the shear walls and slabs are given in
figure (8.12.b). The horizontal and vertical load-deflection

	Type of Analysis	Type of Loading	Failure Load Factor	Type of Failure
	Bare frame	Combined	1.420	sway
	Bare frame	Vertical	1.802	beam mechanism
COMPLETE STRUCTURE	with 3 frames no composite action	Combined	1.80265	beam
	with 5 frames no composite action	Combined	1.80235	beam
	with 7 frames no composite action	Combined	1.80096	beam
	with 7 frames composite action	Combined	2.83	Cracks in slabs and shear walls

TABLE 8.3 : Analysis of Four Storey Structures

curves for the top storey of the middle frame are shown by the curves C and D in figure (8.13) and the ultimate failure load obtained from this analysis is also given in table (8.3). Because the composite plastic moment is very high, no hinge developed in the sagging portions of the beams where the slab and the beam have composite action. In the hogging parts where concrete is in torsion the composite action is neglected and hinges did develop at these parts in the beam. These were followed by the development of cracks in the slabs and walls. The resulting flexible grillage, rejecting the loads, caused more lateral loads to be transmitted to the frames. Nonetheless, this did not increase the lateral sway of the structure in any significant manner. At a load factor of 2.68 hinges started developing in the columns and at a load factor of 2.83 frame 4 failed due to instability.

A comparison of figures (8.12.a) and (8.12.b); graphs A, C and B, D of figure 8.13 indicates that the effect of composite action changes the whole pattern of progressive failure of the complete structure and alters the failure load considerably. Taking composite action into consideration prevented the formation of beam mechanisms in the frames and aggravated instability and plasticity in the columns. The middle frame collapses without the development of a mechanism. It is evident that failure takes place in a manner totally unpredictable by plane frame idealisation. It is clear that methods suggested by the plastic theory or the elasto-plastic theory of frames under estimates the carrying capacity of complete structures by an unacceptable margin.

	MEMBERS	SECTIONS
BEAMS UB	2,7,12,17,22	305x165x40
	4	254x146x31
	9	254x146x37
	14,27	203x133x30
	19,24,29	203x133x25
COLUMNS UC	1,8,13	254x254x73
	3	305x305x97
	5,6	203x203x60
	10,11,18	203x203x52
	15,20,21,23,25,26,28,30	152x152x37
	16	203x203x146

TABLE 8.4 : SECTIONS USED FOR THE FRAMES
OF SIX STOREY STRUCTURES

8.f Analysis of Six Storey Structures

8.f.1 A Six Storey Symmetrical Structure:

As the first example of this series, the six storey structure shown in figure (8.15) was analysed. This had two 304.8mm thick shear walls, six 152.4mm thick slabs and three similar frames with two unequal bays. Bay one is 6.098m while bay 2 is 3.049m. The dimensions and the applied loads are shown in the figure. The reinforcement for the shear walls and the floor slabs were the same as for the four storey structures and shown in figure (8.14). The cross sectional properties of the frames are given in table (8.4). The material properties of the materials used in the structure are also the same as in four storey structures, except that the yield stress f_y of the steel used in the frames is 0.252 kN/mm^2 in this case.

The analysis was carried out neglecting the effect of composite action. As the load factor was increased, six successive plastic hinges developed in the beams as shown in figure (8.15). As soon as the sixth hinge developed at a load factor λ = 1.699, the first plastic hinge reversed the direction of its rotation and became inactive. This hinge was situated at the midspan of member 22 on the fifth floor and originally took place at λ_1 = 1.492. Altogether 12 plastic hinges occurred in each frame until failure took place at λ = 1.801. This was due to a beam mechanism on the longer span of the top floor of frame 1. It should be stressed that the structure was subject to vertical loads as well as wind loads as shown in figure (8.15). With these loads a bare frame analysis suggests collapse due to sway instability. Under vertical loading only the bare frame failed at λ = 1.802.
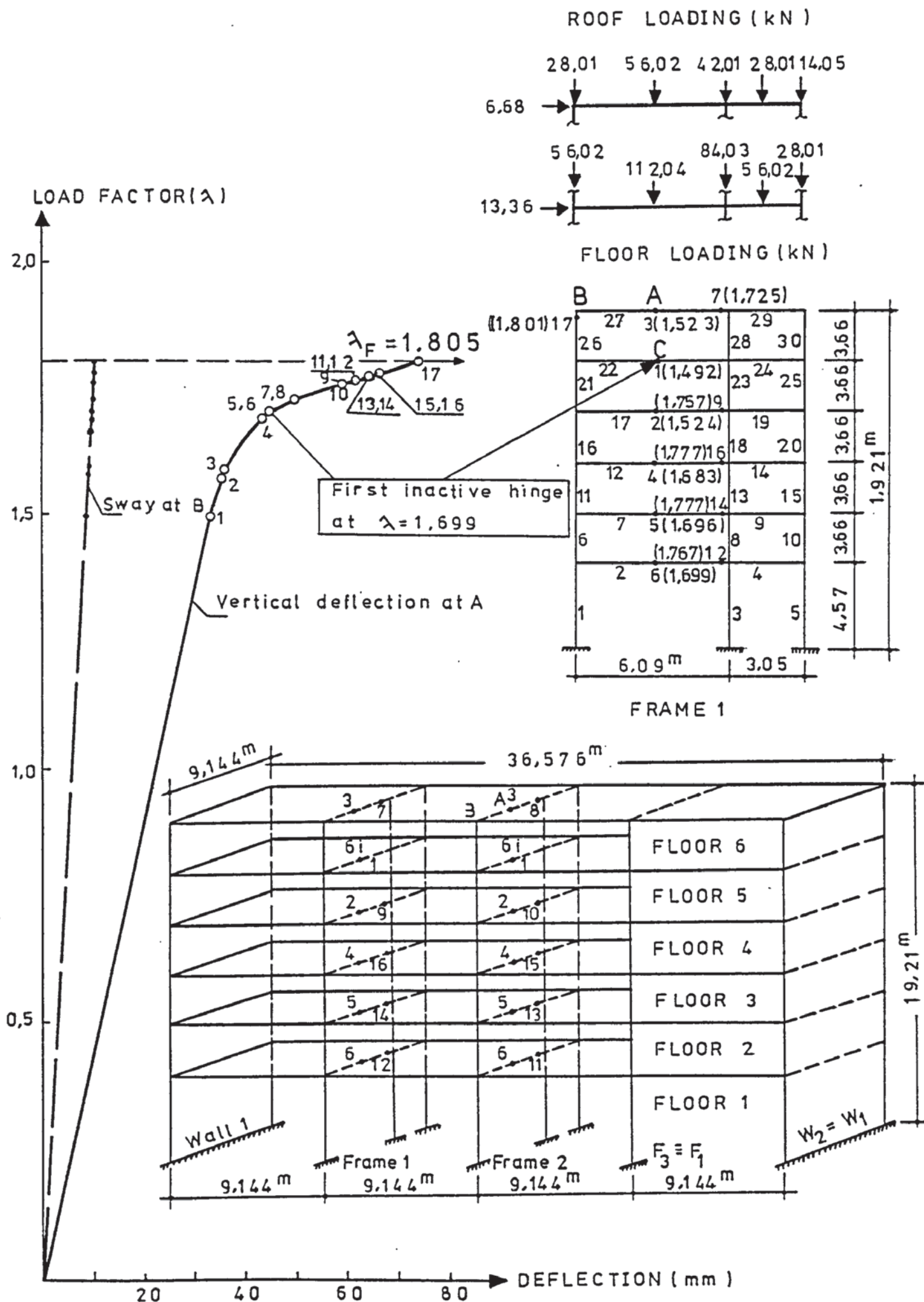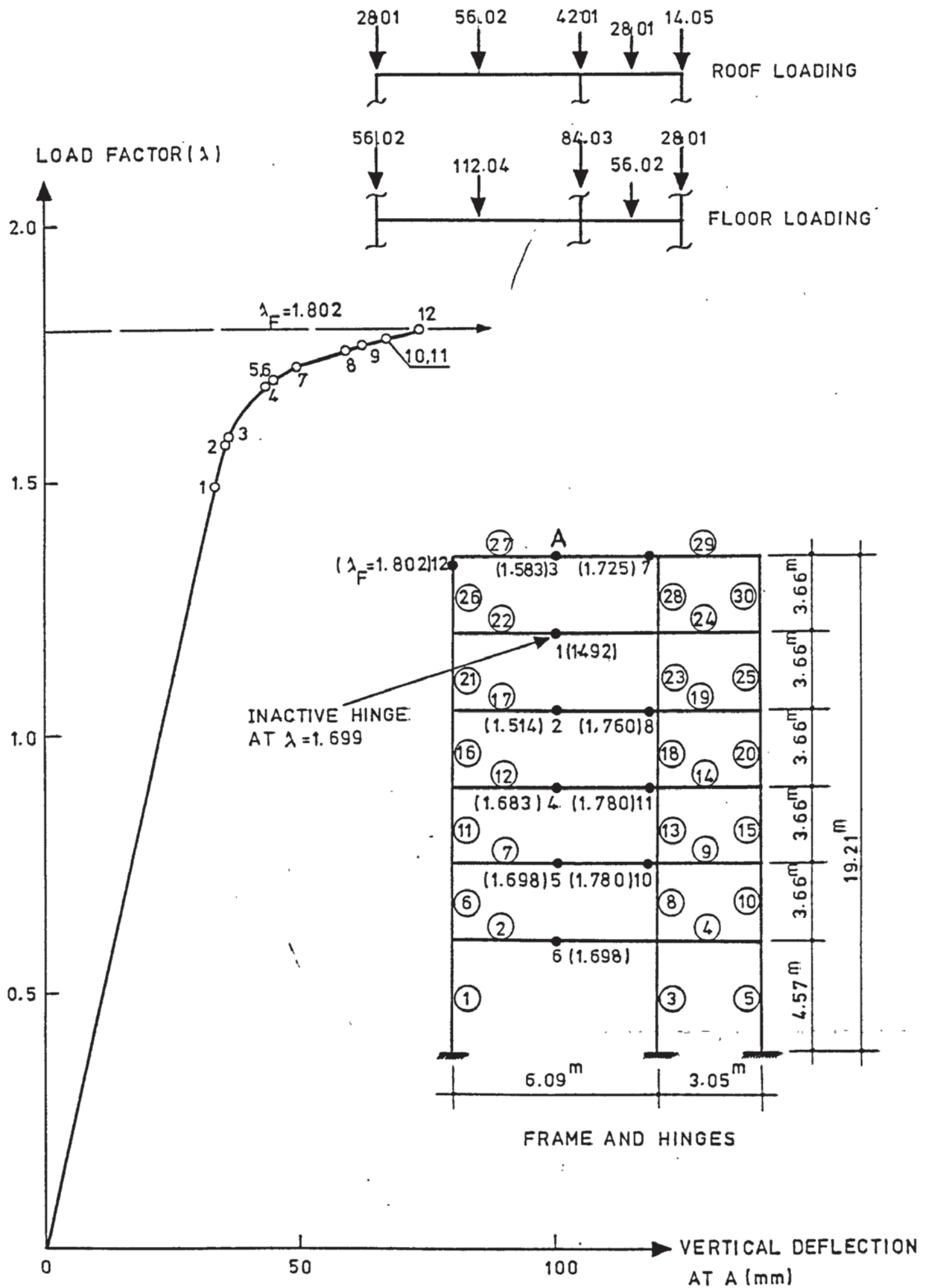
FIGURE 8.15 : SIX STOREY SYMMETRICAL STRUCTURE

FIGURE 8.16:A SIX STOREY BARE FRAME

This structure was also analysed by Majid and Önen[31]. The failure load factor obtained by them was 1.767 slightly lower than that obtained here. The vertical and the horizontal load-deflection curves are presented in figure (8.15). In this structure too, the effect of vertical loading dominates that of horizontal loads. All the plastic hinges form in the beams and the grillage remained elastic. The vertical load-deflection curve of the bare frame is presented in figure (8.16). A comparison of this figure and figure (8.15) shows that the load deflection curves are matching almost exactly while the hinge patterns are slightly different. The ultimate failure was due to beam mechanisms in both cases.

8.f.2 Six Storey Structure with One Shear Wall:

The other six storey structure analysed, was unsymmetrical and is shown in figure (8.17). The loads and the other specifications for its frames, shear wall and slabs are similar to those of the symmetrical six storey structure of the last section. The structure had two similar frames but a single shear wall. The spacing was 9.144m as shown in the figure. The structure was analysed twice. In the first analysis the effect of composite action was ignored. In the second this effect was included. The resulting patterns of hinges and cracks and the load-deflection diagrams are shown in figures (8.17) and (8.18).

In the first analysis altogether 34 hinges developed in the structure, until failure took place at a load factor of 1.778. Most of these hinges developed in the beams and only a few in the columns. No cracks developed in the grillage. Hinge number 9 developed in member 23, which is the longer beam at the fourth floor of the outer frame. Once this hinge occurred, hinges 1,2,3

b-Crack and hinges (Composite action considered)

$\lambda_F = 1.974$

$\lambda_F = 1.778$

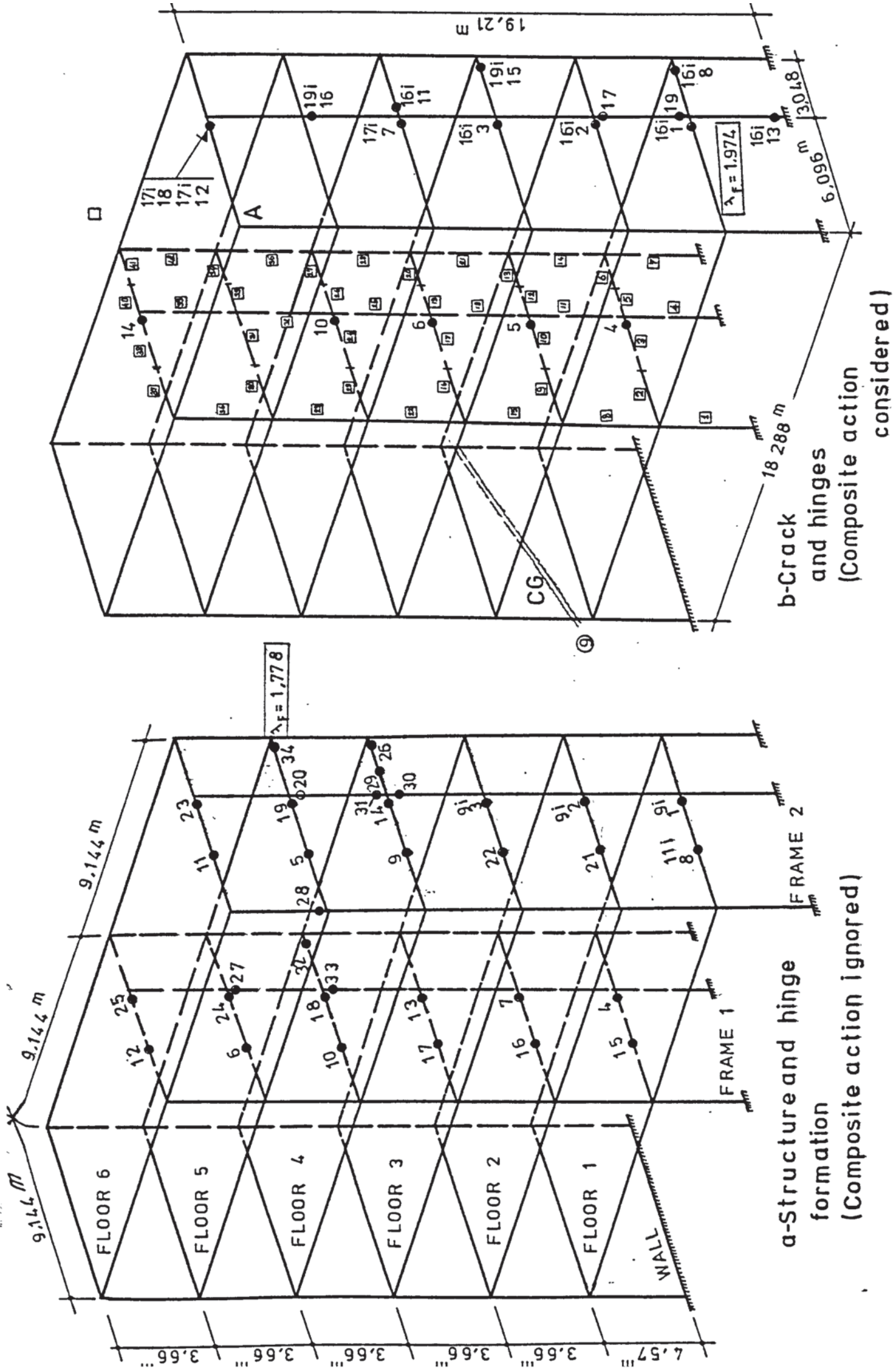a-Structure and hinge formation (Composite action ignored)

FIGURE 8.17: SIX STOREY STRUCTURE WITH ONE SHEAR WALL

all became inactive. These had formed earlier at the second end of members 3, 10 and 17 near to the interior columns. Notice in figure (8.17.a) these positions are marked "9i" to indicate the stage at which the hinges became inactive. None of these hinges were reactivated during the loading process. Hinge 8 in the middle of the first floor beam in the large span of frame 2 also became inactive when hinge 11 developed. After this stage, several hinges started developing within very small increments in the load factor. This was especially the case nearer failure when 5 hinges developed in the structure almost at the same load factor. Notice that initially hinges formed in the outer frame but nearer failure many of the hinges also occurred in the inner frame.

In the analysis considering the composite action, the first four hinges developed in the structure at the same locations and the same load factors as in the analysis ignoring this effect. Later, however, the similarity disappeared. Hinges in the present analysis, developed at the ends of the floor beams. At load factor $\lambda_{cG} = 1.784$ a diagonal crack was recorded in the second storey shear wall panel as shown in figure (8.17.b). This was followed by the development of hinges 10-16 in the frames. As the 16th hinge developed at the first end of interior column 32 of the outer frame, the previously developed hinges 1,2,3,8,11 and 13 became inactive. This was followed by the development of the 17th hinge in member 11, which is also an interior column, but at a lower load factor of $\lambda = 1.894$. With the formation of hinge 17, hinges 7 and 12 became inactive. Hinge 12 however, was soon reactivated at stage 18 at $\lambda = 1.897$. The final hinge 19 then developed at the second end of column 11 of this outer frame, at
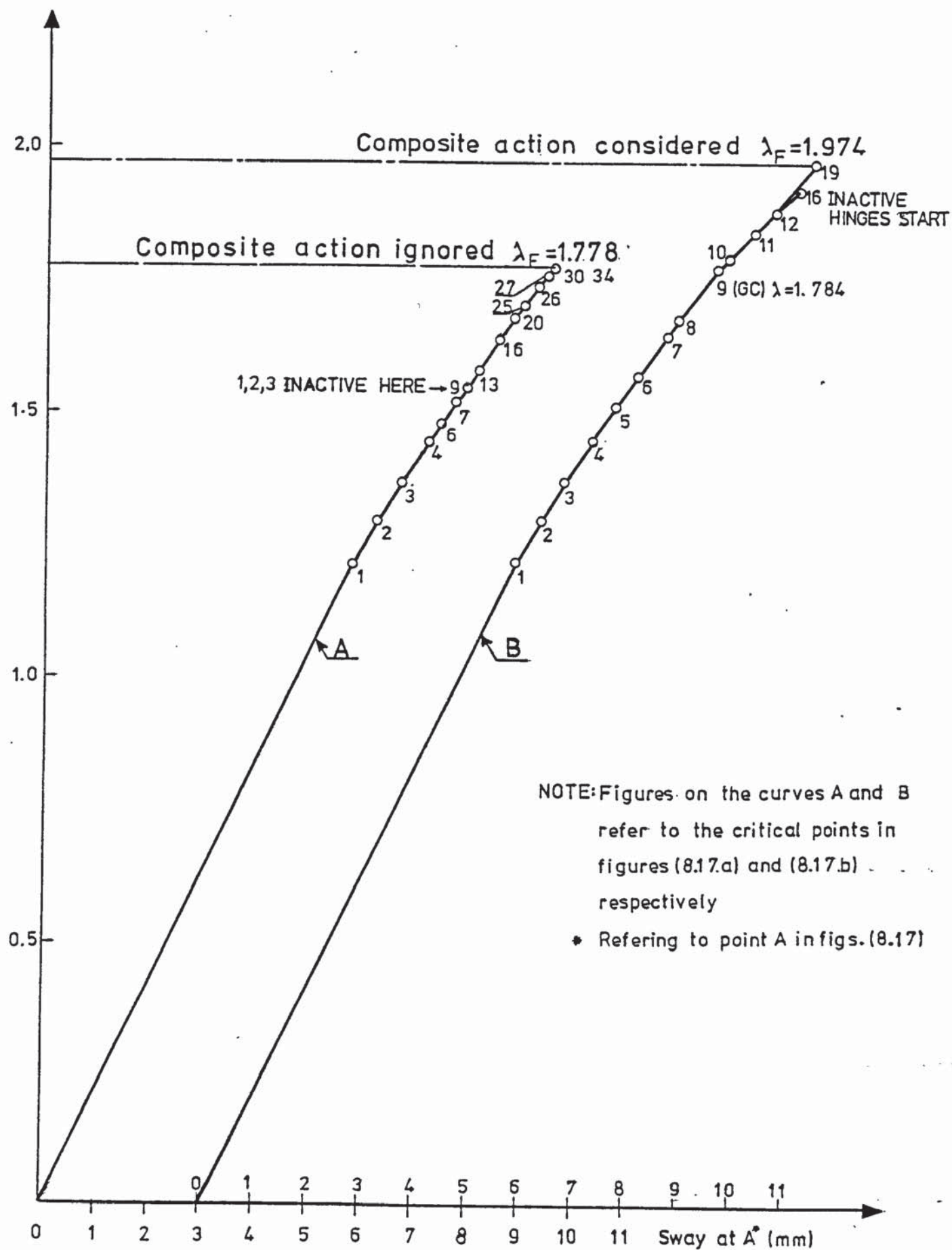
FIGURE 8.18: LOAD-DEFLECTION DIAGRAMS FOR
THE SIX STOREY STRUCTURE WITH
ONE SHEAR WALL

$\lambda_F = 1.974$. Failure was recorded to be due to loss of stiffness of the outer frame. The failure load factor is 9.92% higher than the failure load factor of 1.778 predicted by ignoring the effect of composite action. Again it can be seen in figure 8.18 that the lateral displacements of both structures are virtually the same. This is due to the fact that even in this case, when the grillage is much weaker, most of the lateral loads are indeed transmitted to it.

The results obtained for this structure also support the conclusion that the failure of a complete structure is due to a combined effect of crack development, hinge formation and frame instability. Therefore, an analysis considering the frames or the grillage separately to represent the overall behaviour of a complete structure may yield erroneous results, while a complete analysis ignoring some of the above effects can perhaps be more useful. It is again clear that the plane frame analysis under-estimate the failure load considerably.

CHAPTER 9

General Conclusions and Suggestions for Future Work

As a result of the investigations in chapters 2 and 3, the theorems of structural variation were found to be useful (i) - in carrying out a piecewise linear elastic-plastic analysis, (ii) A strain hardening analysis for a steel frame and (iii) - A nonlinear M-C analysis of a frame, made out of a nonlinear material.

A single initial analysis of the frame under the working loads and the unit load cases, is sufficient to trace the whole load-deflection curve of a frame upto and including failure. It was also found that, by the use of these theorems, a linear elastic analysis of a ground frame can be used to predict the nonlinear behaviour of a variety of derivative frames obtained by removing or altering some of its members. However, so far, only the stiffness parameters (A,I,E), that are linearly related to the stiffness matrix of a structural member can be changed. The second order effect of axial loads, on the stability functions, are not considered in these theorems. It appears that, if this problem is also solved, then the rigorous nonlinear analysis of frames will be simplified. The time consuming operation of constructing the stiffness equations repeatedly will be avoided altogether.

The theorems may also be extended to be applied to space frames, plates and shells in conjunction with the finite element method. The concept of compensation loads driven out of these theorems, was used in developing a rigorous nonlinear analysis for reinforced concrete frames which can also be extended to analyse reinforced concrete space frames. This analysis considers the effect of axial loads and the nonlinear property of moment-curvature relationships. The concept of plastic hinges, in the elastic-plastic analysis of steelframes is substituted here by the

concept of critical points at which the stiffness of an element changes from one linear form to another. The loads applied to a frame during such an analysis may increase either proportionally or otherwise. The load deflection curve can thus be traced up to a given load factor or upto and including the stage of failure. However some local drifting was encountered during the analyses of plane frames. It was found that drifting happens when a number of critical points are about to be reached at the same load factor and only one of these can be considered at a time. Drifting in the analysis lasts until all of these points are dealt with. It was also found that this drifting may be and in fact can be overcome selecting a suitable subdivision of the members. However, further research is needed to improve this procedure. The moment-curvature diagrams are assumed to be the functions of the bending moment only. This may only be reasonable for small frames. In tall frames, heavy axial loads, present in the columns can change the moment-curvature properties considerably. Although this effect can approximately be taken into account, the present method of analysis should also be extended to consider this effect in a rational manner.

A method for the failure load analysis of complete structures was proposed in chapter 4. These structures consisted of a number of parallel frames and shear walls connected by floor slabs. The frames may be made out of steel or reinforced concrete while the grillage of slabs and shear walls, may be manufactured from reinforced concrete or any homogenous material. The latter being manufactured for laboratory purposes only. The method traces the load-deflection behaviour of these complete

structures up to and including the stage of failure. Again the loading procedure may or may not be proportional. As the loads are increased, a number of qualitative 'critical changes' such as plastic hinges develop ins steel frames, critical M-C changes also take place in reinforced concrete frames. Furthermore, lateral instability or cracks can develop in the shear walls or the slabs. Any one of these changes alters the relative stiffness of the various components of the complete structure. With it, the loads transmitted to the grillage or to any one of the frames alter drastically. Therefore, contrary to assumptions made by the advocates of the plastic theory, a failure load analysis of a frame carried out under proportional loads cannot be altogether realistic. This is the case even if the complete structure itself is loaded proportionally. In the same chapter, an approximate method was given to estimate the critical value of the bending moment which causes lateral instability. Failure criterions of panels made out of brittle,homogenous material under the combined action of bending torsion and shear, were also discussed. Together with these, the proposed method was applied to the two storey structures tested by Önen[32]. The analytical results were found to be reasonably close to those obtained by Önen's experiements. This is in spite of the fact that the method used to detect lateral instability was approximate. Önen's analytical results did not however agree with his experimental results. This was because the grillage was assumed by Önen to be elastic throughout. This assumption was removed in the work presented in this thesis and improved the analysis considerably.

In chapter 5, failure of deep reinforced concrete panels
under the combined action of bending, torsion and shear, was studied.
The interaction equations were derived to predict the stage of
failure. It was found that a realistic prediction of the depth
of the neutral axis is necessary for an accurate estimation of
the stage of failure for these deep panels. The significance of
this was illustrated theoretically, on a single storey structure
tested by the author. As a result of the investigation carried
out in this respect, an iterative approach was proposed to calculate
the depth of the neutral axis for such deep panels. This approach
was then verified by the data obtained from the tests described
in chapter 7.

The proposed interaction equations were then tested by the
experimental results obtained from single storey reinforced concrete
structures, without frames. Reasonably close agreement was obtained
between theoretical and experimental failure loads. It was then
found that, although these interaction equations can be successfully
used in the analysis described in chapter 4, the nonlinear M-C
property of the panels should also be taken into account for a better
estimation of the deflections. The failure load analysis procedure
of chapter 4 was then altered to allow for this effect.

The single storey symmetrical test structures consisting of
reinforced concrete grillage and steel frames were analysed by the
help of the computer program given in chapter 6 section b. Two types
of analysis were carried out for most of these structures.

In the first analysis, it was assumed that a panel of the grillage holds its initial flexural and torsional rigidities until its failure is detected by the interaction equations given in chapter 5. These were then reduced drastically, so that the panel was practically disregarded in the subsequent steps of the analysis. This resulted in the load deflection curve being steeper than the experimental curve, at the earlier stages of loading. At stages closer to failure, the deflections were over estimated. The theoretical failure loads, on the other hand were found to be very close to the experimental failure loads.

In the second type of analysis, a trilinear moment-curvature relationship was assumed for each panel. This relationship was theoretically constructed by means of the method described in chapter 3, while its failure was, again, to be detected by the interaction equations of chapter 5. The initial flexural and torsional rigidities were kept until cracks started developing in the panel. The flexural rigidity at the cracked stage was calculated by empirical formulae given by Mannier[18]. To avoid further complications, the torsional rigidity of a panel was reduced by the ratio of the cracked flexural rigidity to the initial. This treatment improved the load-deflection curves slightly.

The single storey structures with reinforced concrete frames were then analysed. Trilinear M-C diagrams were assumed for the frames as well as for the grillage. Close agreements were obtained between the theoretical and the experimental load-deflection curves and failure loads respectively. The slabs were assumed to be acting as large beams against the out of plane bending in the transverse direction. The effective beam width was however unpredictable. It was first assumed that this is equal to the distance between two neighbouring frames.

To study the validity of this assumption, the analysis of one of the structures was repeated for various assumed beam widths. It was then found that the failure load is not very sensitive to the variations in the beam width. The load deflection diagrams on the other hand did not show any significant change. However, the results obtained for the effective width, calculated according to CP110 1972, was found to agree most with the experiment.

Further analyses were carried out for two storey experimental structures with reinforced concrete frames. Both the predicted failure loads and the load-deflection diagrams were found to be in good agreement with the experiments for the symmetrical structures. The discrepancies were however larger in the case of assymmetrical structures, but still within acceptable limits. A maximum relative difference of 13.1% was obtained between the theoretical and the experimental failure loads in this case.

These results obtained from the analyses of the experimental structures indicate that the computer program can trace, with sufficient accuracy, the load-deflection behaviour of structures upto and including failure.

Having demonstrated this, a number of practical type of structures were analysed. The following conclusions were then drawn concerning the behaviour of actual structures.

1. -Because the loads transmitted to the individual frames are not proportional, some of the plastic hinges develop during the loading process may stop rotating and become inactive. These may be reactivated at later stages of loading.

2. -Most of the lateral loads are carried by the grillage not the frames.

3. -The effect of composite action changes the whole pattern of progressive failure and alters the failure load considerably.

4. -Failure of a complete structure takes place in a manner totally unpredictable by plane frame idealisation.

5. -Methods suggested by the plastic theory or elastic-plastic theory of frames underestimate the carrying capacity of a complete structure by an unacceptable margin. In the work presented in this thesis the difference was as high as 16.5%.

6. -Failure of a complete structure is not due to individual effects of crack development, hinge formation and frame instability but, a combination of these effects.

It was already mentioned that the method of analysis given in chapter 4, is restricted to a class of structures consisting only of parallel shear walls and frames. The shear walls and the slabs were assumed to be monolithic and only the sway in the direction of the wind was taken into account. It is desirable to extend the present method to deal with the longitudinal beam-slab systems and coupled shear walls by considering the grillage as a space frame.

It was also assumed that the bases of the frames and the shear walls are rigid, even at the stage of failure. It was shown [67] however, that even a small elastic rotation at the base of a wall may alter the lateral forces transmitted to the frames and to the grillage considerably. It is also possible that the soil underneath a column or a shear wall may fail before the ultimate failure of the structure takes place. Although these effects can be idealised by including a fictitious member, which simulates the behaviour of the

soil, its validity should extensively be studied by a general
finite element program dealing with the interaction of the soil and
the structure.

Failure of slabs was considered due to the combined action
of in-plane bending, torsion and shear only. The effect of out of
plane bending due to vertical loads was ignored. In reality, since
the vertical loads are applied through the slabs, this effect should
also be taken into account and the interaction equations given in
chapter 5 have to be extended to deal with the interaction of torsion,
biaxial bending and shear. These out of plane forces may be obtained
from the analysis of an idealised frame in the plane perpendicular to
the wind direaction, under vertical loads, each joint will then have
three degrees of freedom in the directions of x, y and θ_z. This
can be seen in Frame ABCDEFGHIJ in the x,y plane shown in figure 8.9.
In the present approach, the bending moment-curvature diagram of a
panel was only described for the in-plane bending. Its torque-rotation
diagram was assumed to have the same properties as the in-plane
M-C diagram. This may be reasonable for the case considered in this
thesis. When, on the other hand, the effect of out of plane bending
is taken into account, the corresponding M-C diagram should be
described. The interaction of this and the in plane M-C diagram and
the torque rotation diagram should also be considered in the suggested
analysis.

APPENDIX 1

PRESENTATION OF DATA FOR THE COMPUTER PROGRAM

GIVEN IN CHAPTER 6, SECTION A

The information concerning the geometry of the frame, type of analysis, material properties and loading are read in as follows:

i - The first input card contains three integers referring to the number of different cross-sections in the frame, output requirement and requirement for strain hardening analysis respectively. The values '0' and '1' specify the printing of the most necessary results and all of the useful information respectively. On the other hand the third figure is only meaningful when the nonlinear M-C analysis is carried out. 'Zero' specifies ordinary nonlinear M-C analysis while 'One' describes the slightly modified procedure of M-C analysis to carry out an elastic-plastic analysis including the effect of strain hardening.

ii -The second deck of cards contains the information about the cross-sectional properties. Each of these cards has the following information for each cross section. There are four real numbers on the card the first two are the area and the second moment of area in all the cases. The last two are dummy figures for the cases of linear,nonlinear elastic analysis and nonlinear M-C analysis. The third one is the plastic moment 'Mp' of the section while the last one is still dummy. In the case of design the third figure is the permissible stress for bending and the last one is the permissible stress for axial loads.

iii -The third card contains eight figures which are:
number of cases, number of members, number of joints, number of real hinges, if any, modulus of elasticity, type of analysis, number

of load cases and a specified tolerance which has meaning for the case of nonlinear elastic analysis only.

The following values are given for the sixth figure to indicate the type of analysis:

   0 refers to the elastic analysis

  -1 refers to the nonlinear elastic analysis

  -2 refers to the elastic-plastic analysis

  -3 refers to the elastic-plastic analysis of a derivative frame

  -4 refers to the nonlinear M-C analysis

  -5 refers to the iterative design

iv - The member data is given by the fourth group of cards. Each card contains the length, the first joint number, the second joint number, the inclination and the cross-section number of each member.

v - If there are any real hinges in the frame, these hinges are read in. Each member is considered in turn and the number of hinges at each end of the member are read from the card. If there is no hinge at an end, zero value is given as the hinge number. The numbering of the hinges starts from 3M[1 in increasing manner, where m is the total number of joints.

vi - If the type of analysis is -3 the total number of members to be altered or removed is read from a card. Then, the number of members to be altered are read in. A maximum of 12 figures are read from each card.

vii - Having finished the general and member data, the externally applied loads are read in the following manner:
The external loads applied on each joint in turn are given on a card. These are the loads in X and Y directions and the bending moment. For the cases of linear elastic analysis and design, there maybe more than one load case externally applied to the frame. These loads are also read in the same manner as the first load case.

viii - When the type of analysis is '-3', the new area and the second
moment of area of the changing members are read in. Each card
contains these values of each changing member.

ix - Finally, when the nonlinear M-C analysis is required (case
no. -4) the maximum load factor at which the analysis is to
be terminated is read in.

If the elastic-plastic analysis is required, the maximum number of
hinges to form a mechanism in the frame is read in.

APPENDIX 2

PRESENTATION OF DATA FOR THE COMPUTER PROGRAM

GIVEN IN CHAPTER 6, SECTION B

The data to be read into the computer concerns the geometry of the
complete structure, type of analysis required, the material properties
and the applied loads. The information regarding the grillage is read in
first, followed by frame data.

1. - In the first card the general information about the grillage is fed
   in. These are:

   The number of members

   The number of joints

   The number of floors

   The number of frames

   The number of walls

   The number of different type of sections

   The symmetry identifier (zero indicates that the structure is
   symmetrical, otherwise the opposite is true).

   The modulus of elasticity

   The shear modulus of elasticity

   The material identifier (zero indicates that the panels are made out
   of a homogenous material, otherwise they are reinforced concrete).

2. - The second deck of cards specify the properties of each type of cross
   section. If the cross section is homogenous, only its thickness and
   depth are read in on a card. If on the other hand it is reinforced
   concrete, two cards are spared for its properties. The first of these
   cards contains the following:-

   The thickness

   The depth

   The location of neutral axis at failure

The area of each longitudinal reinforcement layer

The modulus of elasticity of the longitudinal reinforcement

The yield strain of the longitudinal reinforcement

The ultimate strain of the longitudinal reinforcement

The area of stirrups

The spacing of longitudinal reinforcement

The spacing of stirrups

An integer specifying the type of stirrups (1 indicates the reinforcement placed in the middle of the cross section; 2 indicates stirrups without horizontal stirrup legs; 3 indicates closed stirrup loops).

The second card contains the value of the rupture moment and the ratio of the cracked flexural rigidity to the initial.

3. - The next set of cards contains the following for each member:

The length of member

The first joint number

The second joint number

The inclination

The section reference number

4. - The following information is then given to specify the type of junction at each joint, the integer 1 indicating a shear wall-slab junction and integer 0 indicating a slab-frame junction.

5- - The horizontal loads applied at the frame-slab junctions are then read in.

6. - The next set of cards require the loads applied to the grillage joints. Each card contains the loads on each joint, in z, θ_x, and θ_y directions (The horizontal loads acting on the frame-slab joints are set to zero).

7. - Having completed the grillage data, the general information about
   the frames is read in by 4 cards.

The first card contains the following:-

   The symmetry of the structure (as for grillage)

   The output channel (this will be 0 or 1 according to the amount
   of information required).

   The next integer concerns about the composite action of the slabs
   and beams. Zero value ignores this effect and 1 takes it into account.

The second card contains the type of section used and the number of different
sections used in all the frames. Where type 1 indicates universal sections
and type 2 indicates rectangular sections.

The third card is read in when the composite action is required.

This contains:-

   The thickness of slab

   The effective width of slab

   The yield stress of the slab reinforcement

   The yield stress of the steel beam

   The amount of reinforcement per unit run

   The cube strength of concrete

   The concrete cover of the slab reinforcement.

In the fourth card the following information about the frames are given:

   The maximum number of members in any of the frames

   The maximum number of joints in any of the frames

   The number of frames

   The number of floors

   The modulus of elasticity for the frames

   The stipulated tolerance (0.001)

   The load factor, after which more than one plastic hinge can be
inserted in a frame at a time.

The specified increment to initiate the next cycle of iteration when a critical point is detected in the structure (0.1). The type of frames, zero, indicates steel frames and 1 indicates reinforced concrete frames.

The number of critical points on the M-C diagrams for the frame members.

8. - Each of the next deck of cards contains the information about each type of section. These are:

a - For a rectangular section :-

The area

The second moment of area

The plastic section modulus

The breadth of the section

The depth of the section

b - For a universal section, a total of 7 properties are needed. Apart from the first three mentioned above the rest of the properties are taken from the safe load tables (96) to calculate the reduced plastic section modulus.

c - Further four properties about the geometry of the section is needed for the case when the composite action is considered. These are:

The height of the section

The width of the flanges

The thickness of the flanges

The thickness of the web

9. - If the frames are made out of reinforced concrete, the values of the discontinuity moments and the ratios of the slopes of the transition regions to the slope of the initial transition region of the M-C diagram for each type of section are given by two different cards.

Each frame is then considered in turn and the following data is read in:-

10. - The number of joints, the number of members and the number of real hinges are given on a card.

11. - If there are any real hinges in the frame, the hinge numbers at the first end and at the second end of each member are given on a card. The absence of hinge at any end is specified by the integer 0.

12. - The member data is then read in. The following specifications of each member are given on a card:-

The length of the member

The first end joint number

The second end joint number

The inclination of the member in degrees

13. - The section reference numbers of the members are read in as twelve values on a card.

14. - The loads in z, y and θ_x directions, acting on each joint of the frame are given on a card. Because the horizontal load acting on the z direction is already given, this is specified by a dummy figure 0.0.

15. - For the case when the composite action is considered. The members which are attached to the slabs are read in as twelve values on a card.

16. - The next set of cards give the yield stresses of the members.

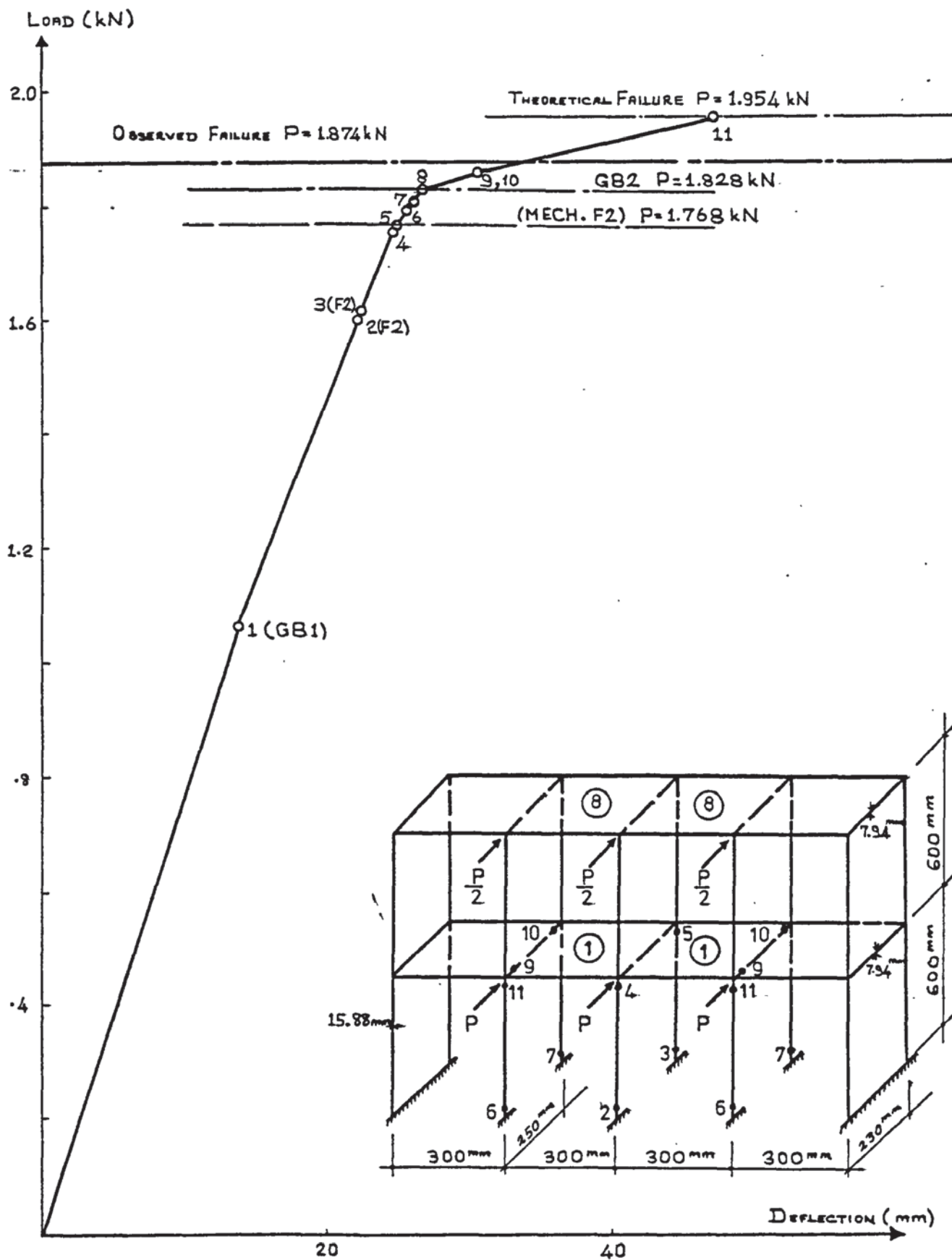17. - The final deck of cards give the joint numbers of the frame, which are attached to the grillage.

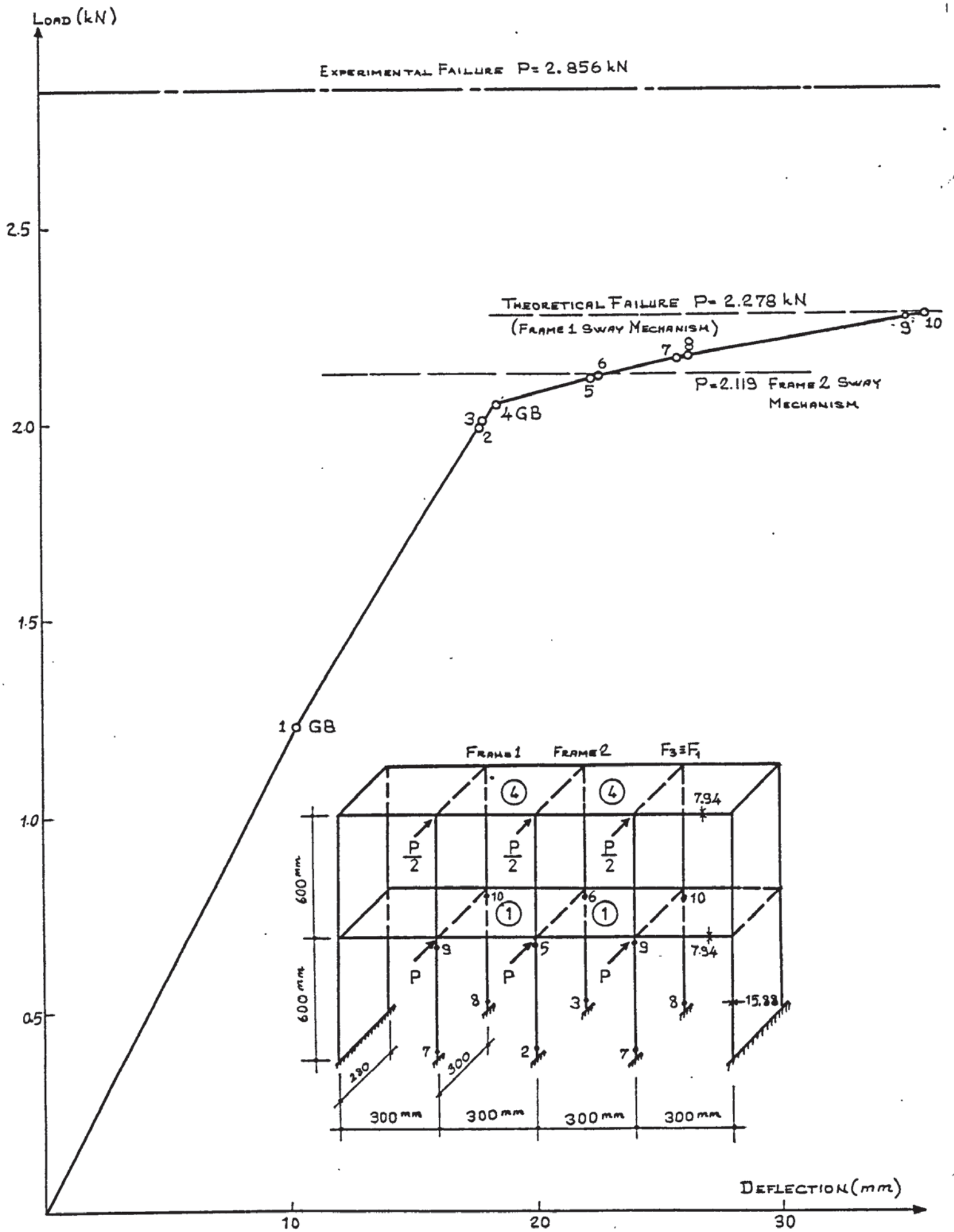This concludes the data requirements for the program.

APPENDIX 3

THEORETICAL LOAD-DEFLECTION
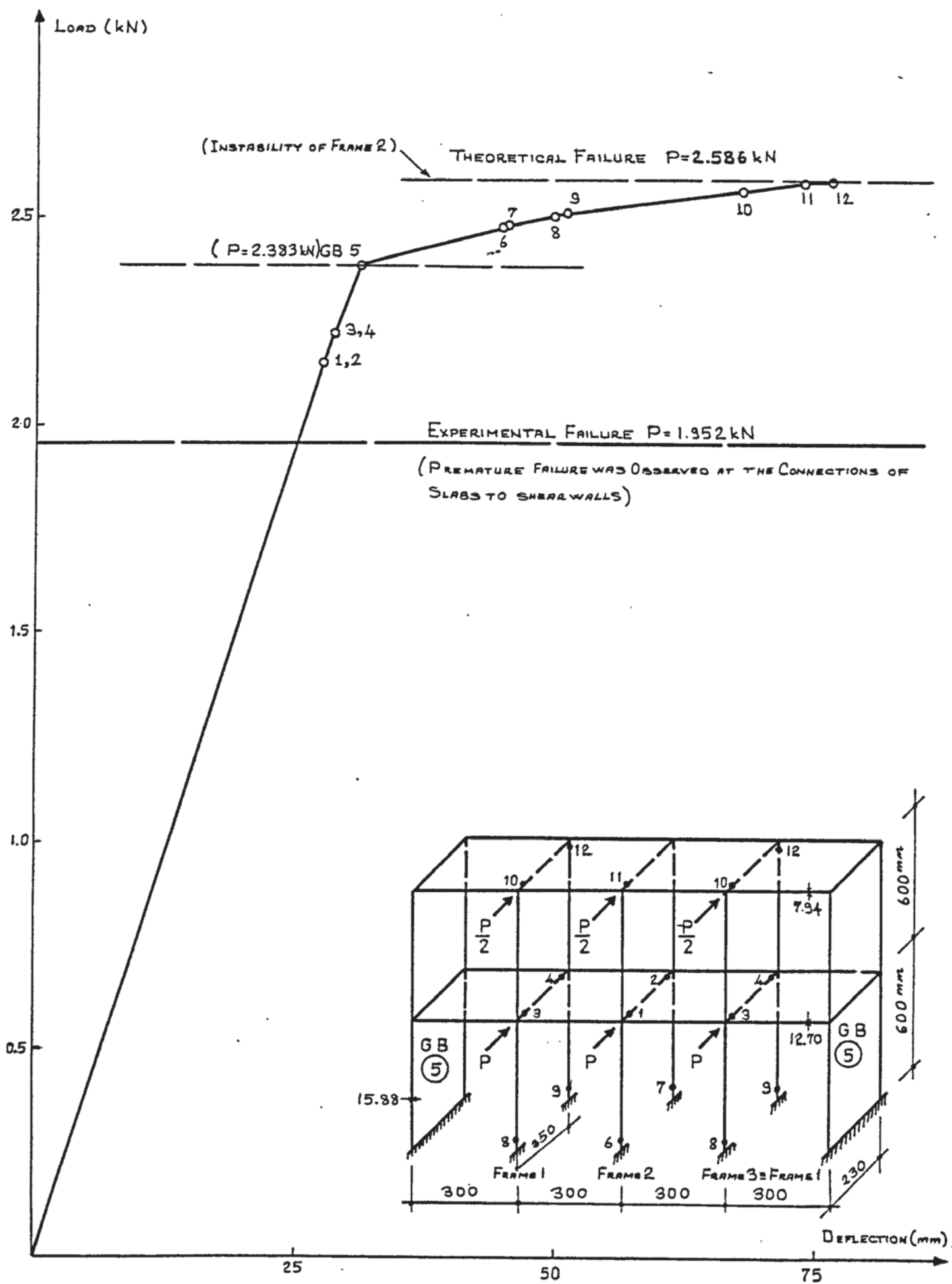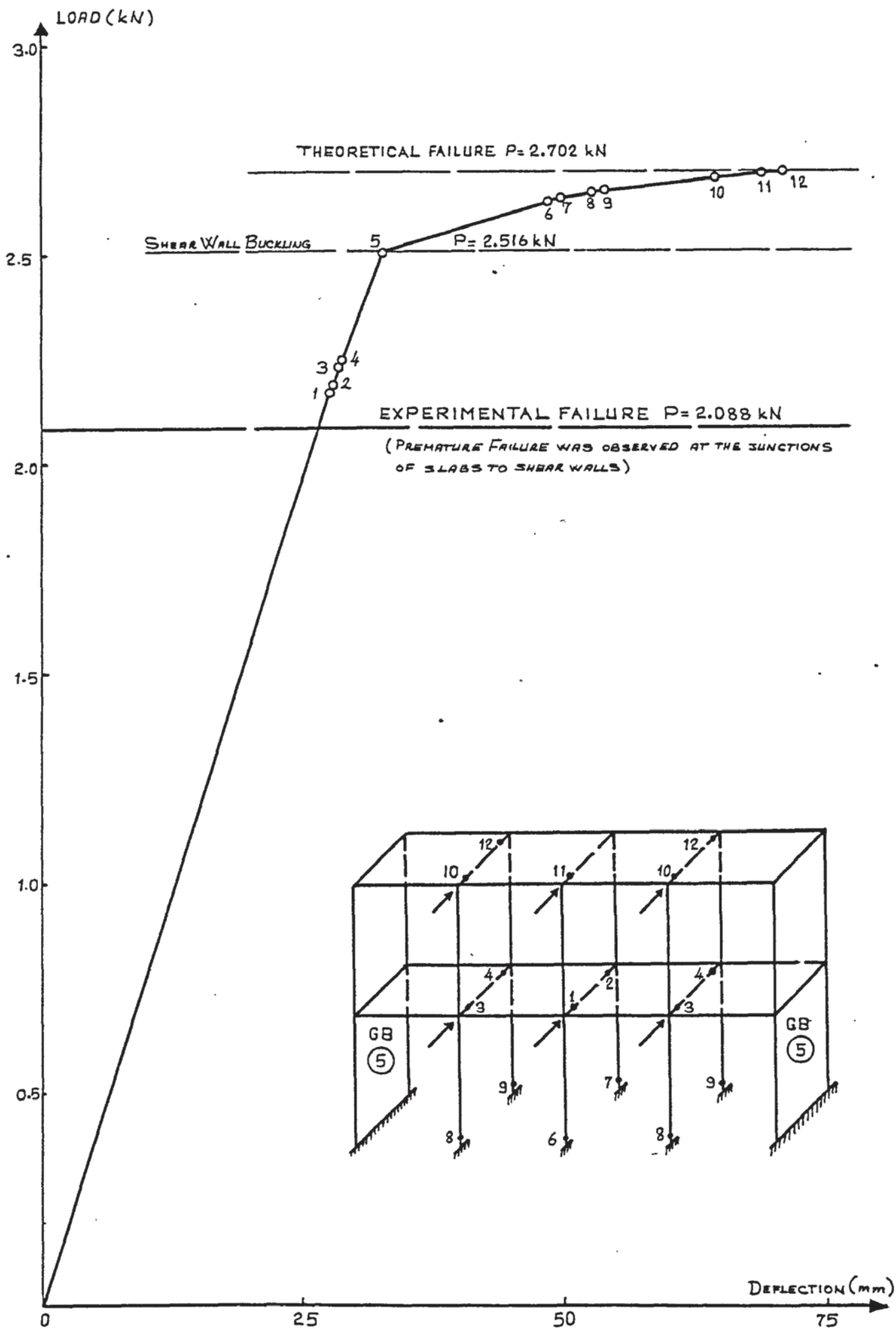
DIAGRAMS FOR ONEN'S TWO STOREY

STRUCTURES

ÖNEN'S SECOND TWO STOREY STRUCTURE

ÖNEN'S THIRD TWO STOREY STRUCTURE

ÖNEN'S FOURTH TWO STOREY STRUCTURE

ÖNEN'S FIFTH TWO STOREY STRUCTURE

Load kN

THEORETICAL FAILURE P=3.277 kN

SHEAR WALL CRACKING P= 3.197 kN

6 (GC)

7 8 9

(CRACKS DEVELOPED AT THE BASES OF THE SHEAR WALLS)
EXPERIMENTAL FAILURE P= 2.746 kN

(GB) 5 BUCKLING OF SECOND FLOOR SLAB P=2.644 kN

3 4

1 2
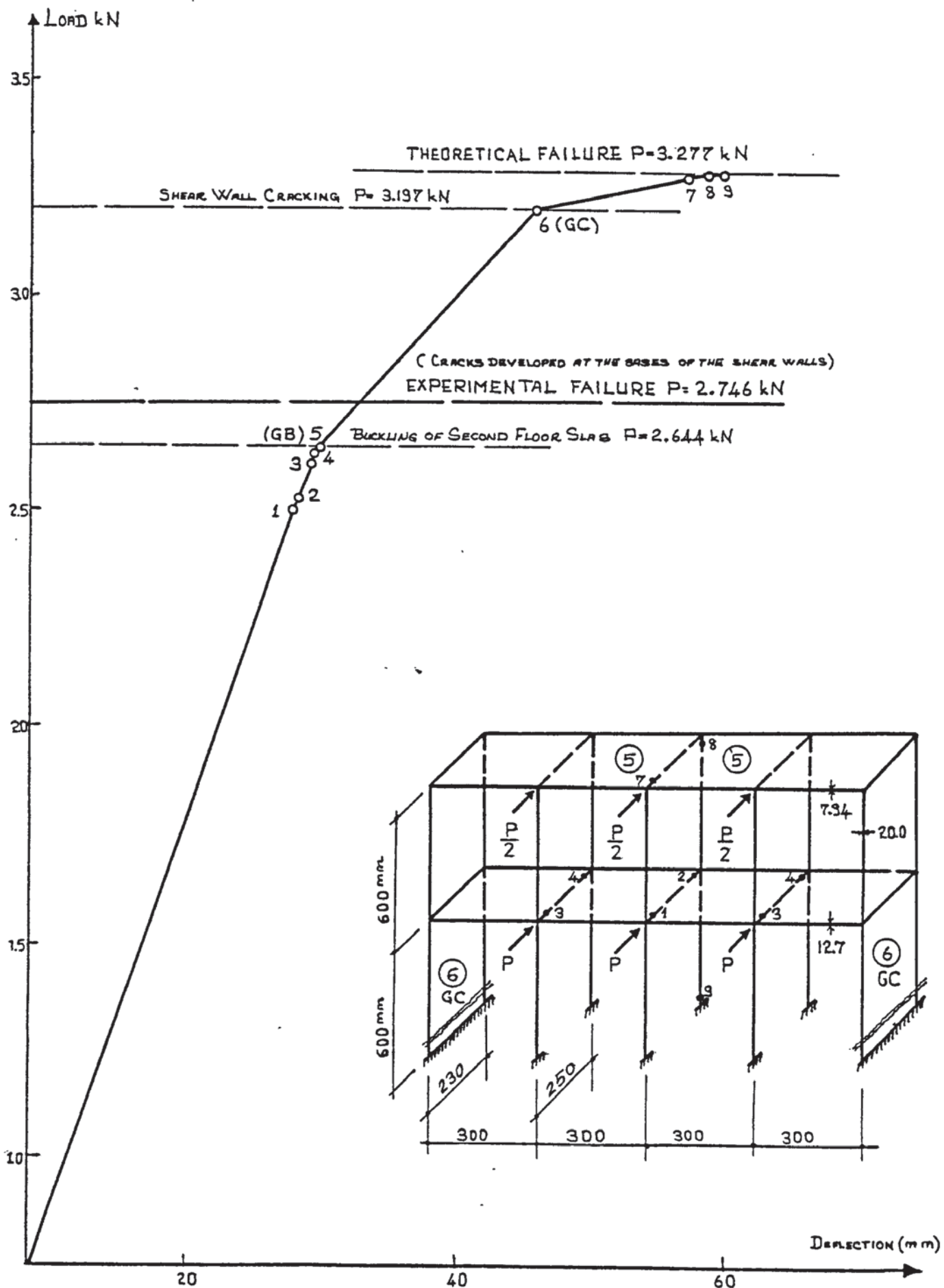
DEFLECTION (m m)

ÖNEN'S SIXTH TWO STOREY STRUCTURE
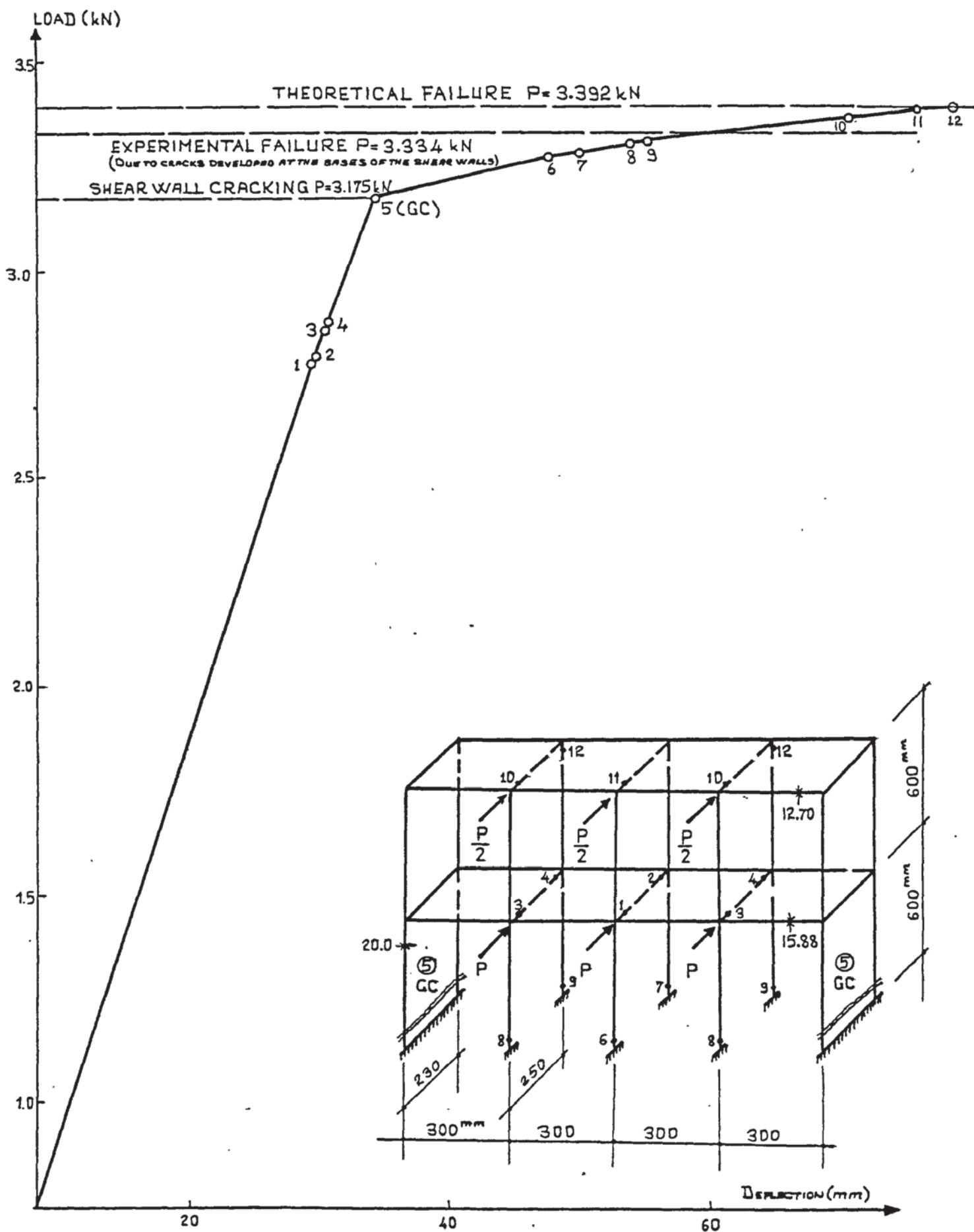
ÖNEN'S SEVENTH TWO STOREY STRUCTURE

APPENDIX 4

EXPERIMENTAL AND THEORETICAL

LOAD-DEFLECTION DIAGRAMS FOR

SINGLE STOREY TEST STRUCTURES WITH

STEEL FRAMES

LOAD (kN)

P = 2.62 kN
6,7

P = 2.47 kN

EXPERIMENTAL FAILURE P = 2.40 kN
4,5

TRILINEAR M-C DIAGRAM ASSUMED

BILINEAR M-C DIAGRAM ASSUMED

EXPERIMENTAL CURVE

CRACKING

2   2   2   2

P   P   P   P

(CRACKING)1
(ULT. STAGE)3

1,3

DEFLECTION (mm)

TEST STRUCTURE 5

TEST STRUCTURE 6

LOAD (kN)

Experimental Failure P=3.029 kN

Trilinear Failure P=3.205 kN

Trilinear M-C Diagram For Grillage

P=2.992 k

Bilinear M-C Diagram is Assumed For Grillage

STRUCTURE 7 AND LOADING

Deflection (mm)

TEST STRUCTURE 7

TEST STRUCTURE 8

LOAD (kN)

P=9.79kN (EXPERIMENTAL FAILURE)

P=9.64kN

8 9

TRILINEAR M-C CURVE ASSUMED

6 7

BILINEAR M-C CURVE ASSUMED

5

4

EXPERIMENTAL CURVE

3

2

1

4 (ULT. STAGE)

3 (CRACKED)

1 (CRACKED)

3 (CRACKED)

P   P   P

2 (CRACKED)

2 (CRACKED)

(ULT. STAGE) 5

(ULT. STAGE) 5

STRUCTURE AND LOADING

DEFLECTION (mm)

5   10   15
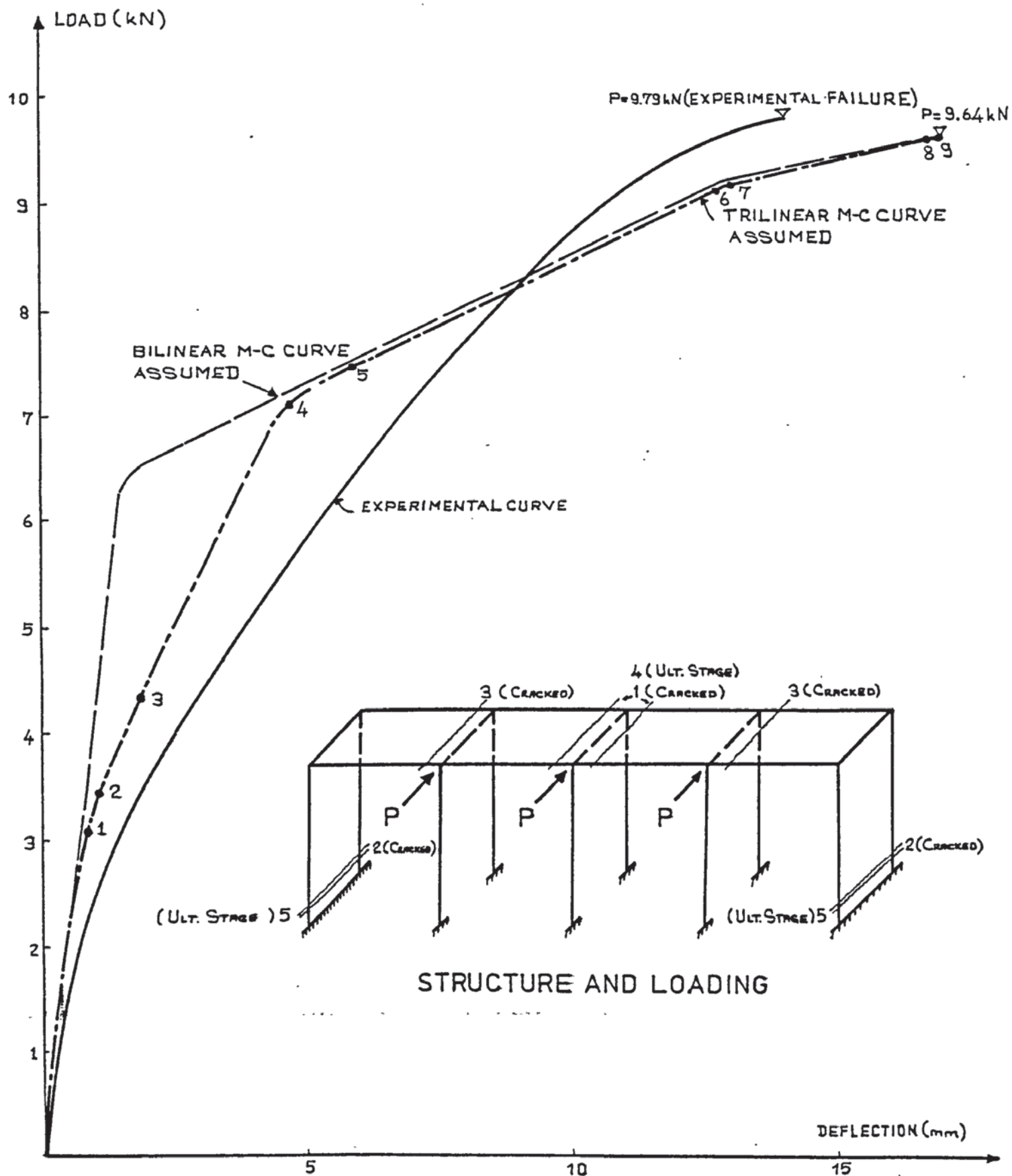
TEST STRUCTURE 10

REFERENCES

1 - Majid, K.I. and Elliott, D.W.C., "Forces and deflections in changing structures", The Structural Engineer, March 1973, Volume 51, Number 3.

2 - Majid, K.I., "Optimum design of structures", London, Butterworths, 1974.

3 - Saka, M.P., "Optimum design of structures", Ph.D thesis The University of Aston in Birmingham 1975.

4 - Majid, K.I., "Nonlinear structures", London, Butterworths, 1972.

5 - Horne, M.R., Majid, K.I., "Elastic-plastic design of rigid jointed sway frames by computer", Research report No.1, Department of Civil Engineering, University of Manchester, March 1966.

6. - Elliott, D.W.C., "Optimum design of structures", Ph.D thesis The University of Aston in Birmingham 1971.

7 - Hrennikoff, A., "Theory of -nelastic bending with reference to limit design", A.S.C.E., Transactions, March 1947, Paper No. 2334.

8 - Roderick, J.W. and Heyman, J., "Extension of simple plastic theory to take account of strain-hardening range", The Structural Engineer.

9 - Matheson, J.A.L., "Hyperstatic structures", London, Butterworths, 1970.

10 - Cakiroglu, A. and Cetmeli, E., "Yapi Statigi", cilt 2, Istanbul, Ari Kitabevi, 1970.

11 - Horne, M.R., "Instability and the Plastic theory of structures", Transactions of the engineering institute of Canada, Vol. 4, No. 2, 1960.

12 - Davies, J.M., "Frame instability and strain hardening in plastic theory", Journal of The Structural Division, A.S.C.E., Vol. 92, No. ST3, June 1966.

13 - Timoshenko, S.P., "Strength of Materials Part 1", Second Edition. D. Vand Nostrand Co. Inc., New York, 1940.

14 - Baker, J.F., and Charlton, T.M., " A Test on a Two-Storey, Single Bay Portal Structure", Report No. FE.1/53/57, British Welding Research Association, London, England, 1957.

15 - Charlton, T.M., "A test on a pitched roof portal structure with short stanchions", British Welding Journal, London, England, Vol. 7, 1960.

16 - Deeble, R.H., "Nonlinear analysis of reinforced concrete frames", Ph.D thesis, Department of Civil Engineering, University of Aston in Birmingham 1973.

17 - Hoegnestad, E., Hanson N.W., and McHenry D., "Concrete Stress Distribution in Ultimate Strength Design". Journ. Amer. Conc. Inst., Vol. 27, No. 4, (Dec. 1955).

18 - Monnier Th., "The Moment Curvature Relation of Reinforced Concrete", Heron (Netherlands), Vol. 17, No. 2, 1970.

19 - Cranston W.B., "Determing the Relation Between Moment, Axial Load and Curvatures for Structural Members". C & C.A. Tech. Report TRA/395, (1966).

20 - Majid, K.I., and Anderson D., "Elastic-Plastic Design of Sway Frames by Computer", Proc. Inst. Civ. Engrs. December 1968.

21 - Anderson, D., "Ph.D Thesis", Manchester University, 1969.

22 - Leone Corradi, Oswaldo De Donato and Guilio Maier "Inelastic Analysis of Reinforced Concrete Frames". ASCE Journal of the Structural Division, Vol. 100, No. ST 9, Sep. 1974, P.P. 1925 - 1942.

23 - Macchi, G., et al, "Nonlinear Analysis and Limit Design", presented at the ASCEIABSE International conference on planning and Design of Tall Buildings, held at Lehigh University, Bethlehem, Pa., Aug. 1972.

24 - Merchant, W., "The Failure Load of Rigid Jointed Frameworks as Influenced by Stability", The Struct. Engr., July 1954.

25 - Livesley, R.K., "The Application of an Electronic Computer to some Problem of Structural Analysis", The Struct. Engr. Vol. 34, 1956.

26 - Livesley, R.K. "The Application of Computers to Problems Involving Plasticity", Symposium on the use of Electronic Computers in Structural Engr. September 1959.

27 - Horne M.R. and Medland I.C., "The Collapse Loads of Steel Frameworks, Allowing for the Effect of Strain Hardening", Proc. Inst., of Civil Engrs., London, Vol. 33, March 1966.

28 - Majid, K.I., "Elastic-Plastic Structural Analysis", Ph.D thesis, Manchester University 1963.

29 - Jennings, A. and Majid, K.I., "An Elastic-Plastic Analysis by Computer up to Collapse", The Struct. Engr., December 1965.

30 - Davies J.M., "The Response of Frameworks to Static and Variable Repeated Loading in the Elastic-Plastic Range", The Structural Engineer, Vol. 44, No. 8, Aug. 1966.

31. - Majid, K.I., and Önen Y.H., "The Elasto-Plastic Failure Load Analysis of Complete Building Structures", Proc. Instn Civ. Engrs, Vol. 55, Sept. 1973.

32 - Önen, Y.H., "Elastic-Plastic Analysis of Complete Building Structures", Ph.D Thesis, University of Aston in Birmingham 1973.

33 - Holmes, M., Majid, R.I., "The Desing of a Beam and Slab Floor System by Computer", International Symposium on the "Composite Desing of Structures by Computer", University of Warwick, 1972.

34 - Glanville W.H., and Thomas, F.G., "Moment Redistribution in Reinforced Concrete", London, H.M. Stationary Office, Building Research Technical Paper No. 22, (1939).

35. - Baker A.L.L., "A Plastic Theory of Desing for Ordinary Reinforced and Prestressed Concrete Including Moment Redistribution in Continuous Members", Mag. of Conc. Research, Vol. 1, No. 2, (June 1949).

36 - Baker, A.L.L., "The Ultimate Load Theory Applied to the Desing of Reinforced and Prestressed Concrete Frames", Concrete Publications, (1956).

37 - Baker, A.L.L., "Ultimate Load Theory for Concrete Frame Analysis", Trans. of Amer. Soc. of Civ. Engrs., Paper No. 3386, Vol. 127, Part II, (1962).

38 - Report of the Research Committee. "Ultimate Load Design of Concrete Structures", Report with Discussion, Instn. of Civ. Engrs., (1962).

39 - Committee European de Beton. "Recommendations of an International Code of Practice for Reinforced Concrete". English translation Cement and Concrete Association (C.&C.A.)

40 - Cranston, W.B., "A Computer Method for the Inelastic Analysis of Plane Frames", C. & C.A., Tech. Report TRA/386, (1965).

41 - Baker, A.L., "Frame Instability". Concrete, (Feb. 1967).

42 - Nahhas, U, and Yu, C.W. "The Elastic-Plastic Design of Reinforced Concrete Sway Franes against Instability". Proc. Inst. Civ. Engrs., Vol. 53, (June 1972).

43 - Chin, M.W., "The Failure Loads of High Tensile Steel Structures", Ph.D. Thesis, Manchester University, (1966).

44 - Majid, K.I., Williamson, M., "Linear Analysis of Complete Structures by Computers", Proc. Inst. Civ. Engrs., Oct. 1967.

45 - Majid, K.I., Williamson, M., Discussion on the paper "Linear Analysis of Complete Structures by Computers". Proc. Inst. Civ. Engrs., Vol. 43, 1969.

46 - Whitney, C.S., Anderson, B.G., Cohen, E., "Design of Blast Resistant Construction for Atomic Explosions". Jnl. A.C.I. Vol. 51, 1955.

47 - Rosenblueth, E., Holtz, I., "Elastic Analysis of Shear Walls in Tall Buildings". Jnl. A.C.I., Vol. 56, 1960.

48 - Rosman, R., "An Approximate Analysis of Shear Walls Subject to Lateral Loads". Jnl. A.C.I., Vol. 56, 1960.

49 - Rosman, R., "An Approximate Method of Walls of Multi-Storey Buildings". Proc. Inst. Civ. Engrs. Vol. 59, 1964.

50 - Coull, A., and Chantaksinopas, B., "Design Curves for Coupled Shear Walls on Flexible Bases", Proc. Instn. Civ. Engrs. Part 2, 1974, 57, Dec.

51 - Coull, A. and Stafford Smith, B., "Analysis of Shear Wall Structures", Tall Buildings, Pergamon Press 1967, pp.139-155.

52 - Heidebrecht, C.A., and Stafford Smith, B., "Approximate Analysis of Tall Wall - Frame Structures", Journal of Struct. Div. proc. ASCE. Vol. 99, No. ST 2, Feb. 1973.

53 - Coull, A et al, "Numberical Elastic Analysis of Coupled Shear Walls", proc. instn. Civ. Engrs., May 1972 Part 2.

54 - Gluck, J., "Elasto-Plastic Analysis of Coupled Shear Walls", Journal of the Str. Div. ASCE, Vol. 99, No. ST 8, Aug. 1973.

55 - Mee, A.L. et al, "Wall-Beam Frames under Static Lateral Load", Journal of the Str. Div. ASCE, Vol. 101, No. ST 2, Feb. 1975.

56 - MacGregor, J.G. et al, "Approximate inelastic Analysis of Shear Wall-Frame Structures", Journal of the Str. Div., ASCE, Vol. 98, No. ST 11, Nov. 1972.

57 - Macleod, I.A., "Analysis of Shear Wall Buildings by the Frame Method", Proc. Instn. of Civ. Engrs. 1973.

58 - Winokur, A., and Gluck, J., "Lateral Loads in Asymmetric Multi Storey Structures", Journal of the Struct. Div., ASCE, Vol. 94, No. ST3, March 1968.

59 - Rosman, R., "Dynamics and Stability of Shear Wall Building Structures", Proc. Instn. Civ. Engrs., 1973.

60 - Prato, C., "Wall-Frame Interaction by Numerical Integration", Journal of Struc. Div. ASCE, Vol. 101, No. ST 7, July 1975.

61 - Bryan, E.R., EL Dakhakhni, W.M., "Behaviour of Sheeted Portal Frame Sheds; Theory and Experiments". Proc. Inst. Civ. Engrs., December 1964.

62 - Bryan, E.R., El Dakhakhni, W.M., Discussion on the paper "Behaviour of Sheeted Portal Frame Sheds: Theory and Experiments". Proc. Inst. Civ. Engrs., Vol. 1, 1965.

63 - Clough, R.W., King, I.P., and Wilson, E.L., "Structural Analysis of Multi Storey Buildings", J. Struct. Div. ASCE, 1964, Vol. 90, ST 3, June, 16-34.

64 - Goldberg, J.E. "Analysis of Multi-Storey Buildings Considering Shear Wall and Floor Deformations", Tall Buildings, Proc. Symposium on Tall Buildings, Univ. of Southampton, April 1966. Pergamon Press, Oxford, 1967.

65 - Jennings, A, Majid, K.I., "The Computer Analysis of Space Frames Using Sparce Matrix Technique", Univ. of Surrey, C4, 1966.

66 - Majid, K.I., and Croxton, P.C.L., "Wind Load Analysis of Complete Building Structures by Influence Coefficients", Proc. Instn. Civ. Engrs., 1970, 47 (October).

67 - Croxton, P.C.L., "The Analysis of Complete Structures Consisting of Bare Frames, Shear Walls and Plate Components", Ph.D. Thesis, The University of Aston in Birmingham, 1974.

68 - Majid, K.I., "The Effect of Composite Action on the Elasto Plastic Analysis of Complete Building Structures", Finite Element Methods in Engineering, The University of New South Wales, 1974.

69 - Wood, R.H., "The Stability of Tall Buildings", Proc. Instn. Civ. Engrs., September, 1958.

70 - Neal, B.G., "The Plastic Methods of Structural Analysis", Chapman and Hall, 1963.

71 - Timoshenko, S.P. and Goodier, J.N., "Theory of Elasticity", Third Edition, McGraw-Hill, Kogakusha 1970.

72 - Jennings, A., "A Compact Storage Scheme for the Solution of Symmetrical Linear Simultaneous Equations", The Comp. Journ., November 1966.

73 - Horne, M.R., "The Flexural-Torsional Buckling of Members of Symmetrical I-Section under Combined Thrust and Unequal Terminal Moments", Quart, Journ. and Applied Math., Vol. VII, Pt. 4 (1954).

74 - Salvadori, M.G., "Lateral Buckling of Eccentrically Loaded I Columns", A.S.C.E. Transactions, January 1955. Paper No.2836.

75 - Trahair, N.S., "Stability of I-Beams with Elastic End Restraints", The Journ. of the Instn. of Engrs, Australia, June 1965.

76 - Massey, C., "Lateral Instability of Reinforced Concrete Beams under Uniform Bending Moments", A.C.I. Journal, March 1967.

77 - Nethercot, D.A. and Rockey, K.C., "A Unified Approach to the Elastic Lateral Buckling of Beams", The Struct. Engineer, July 1971, No. 7, Vol. 49.

78 - Vacharajittiphan, P., and Trahair, N.S., "Analysis of Lateral Buckling in Plane Frames", Journ. of the Struct Div. Proc. ASCE, Vol. 101, No. ST7, July 1975.

79 - Venkataraman, B. and Sharad A. Patel, "Structural Mechanics with Introductions to Elasticity and Plasticity", McGraw Hill 1970.

80 - Inan, M., "Cisimlerin Mukavemeti", Istanbul, Ari Kitabevi, 1967.

81 - "Analysis of Structural Systems for Torsion", Publication SP - 35 American Concrete Institute, Detroit, Mich., 1972, 438 pp.

82 - Collins, M.P. et al, "Reinforced Concrete in Torsion", UNICIV Report No. R-31, School of Civil Eng., University of New South Wales, Kensington, Australia, Mar. 1968, 328 pp.

83 - Elfren, L., "Reinforced Concrete Beams Loaded in Combined Torsion, Bending and Shear. A study of the Ultimate Load-Carrying Capacity", Ph.D. Chalmers University of Technology. (Division of Concrete Structures Publication 71:3).

84 - Elfren, L., and Karlsson, I., "Torsion of Structural Concrete. A State of the Art Review", Report 69.2, Division of Concrete Structures, Chalmers University of Technology, Göteberg, Sweden, Dec. 1969, 179 pp.

85 - Goode, C.D., and Helmy, M.A., "Ultimate Strength of Reinforced Concrete Beams in Bending and Torsion", Torsion of Structural Concrete, Publication SP-18, American Concrete Institute, Detroit, Mich. 1968, pp 357-377.

86 - Gvozdev, A.A., Lessig, N.N. and Rulle, L.K. "Research on Reinforced Concrete Beams under Combined Bending and Torsion in Soviet Union", Torsion of Structural Concrete, Publication SP-18, American Concrete Institute, Detroit, Mich. 1968, pp. 307-336.

87 - McMullen, A.E., Warwaruk, J., "Concrete Beams in Bending, Torsion and Shear", Journal of the Structural Division, ASCE, Vol. 96, No. ST5, Proc. Paper 7270, May 1970, pp. 885-903.

88 - Elfren, L., Karlsson, I., and Losberg, A., "Torsion-Bending-Shear Interaction for concrete Beams", Journal of the Structural Division ASCE. Vol. 100, No. ST8, August 1974, pp. 1659-1676.

89 - Timoshenko, S.P., "Theory of Elastic Stability". (McGraw-Hill, 1936), Chapter 5.

90 - Michell, A.G.M., "Elastic Stability of Long Beams under Transverse Forces", Phylosophical Magazine, Vol. 48, 1899, p.208.

91 - Hoegnestad, E., "Fundamental Concepts in Ultimate Load Design of Reinforced Concrete Members", Journal of American Concrete Institute Title No. 48.53, Vol. 23, No. 10, June 1952.

92 - Kani, G.N.J., "How Safe are our Large Reinforced Concrete Beams?". ACI Journal, March 1967.

93 - M.A. Sheikh, H.A.R. Paiva, A.M. Neville, "Flexure-Shear Strength of Reinforced Concrete Deep Beams", The Structural Engineer, August 1971, No. 8, Vol. 49.

94 - Reusch, "Analysis of Torsion and Shear in Reinforced Concrete" Julius Springer, Berlin Germany, 1929, pp.53.

95 - Lamperth, P., "Ultimate Strength of Reinforced Concrete Beams Loaded in Torsion and Bending". Bericht No. 26, Institut fur Baustatik, Eidgenössiche Technische Hochschule, Zurich, Switzerland, Jan. 1970, pp. 189.

96 - "Handbook of Structural Steelwork", Publication of the British Const. Steelwork Assoc. Ltd., 1971.

97 - A. E. Allos, Ph.D. Department of Civil Engineering, University of Aston in Birmingham, 1977.